Lessons from snake venom: new insights into the structural and functional aspects of factor V and factor X

Verhoef, D.

Citation
Verhoef, D. (2021, September 22). *Lessons from snake venom: new insights into the structural and functional aspects of factor V and factor X*. Retrieved from https://hdl.handle.net/1887/3213580

Version:	Publisher's Version
License:	Licence agreement concerning inclusion of doctoral thesis in the Institutional Repository of the University of Leiden
Downloaded from:	https://hdl.handle.net/1887/3213580

Note: To cite this publication please use the final published version (if applicable).

Lessons from snake venom:

New insights into the structural and functional aspects of factor V and factor X

Daniël Verhoef

ISBN: 978-94-6416-600-2
Provided by thesis specialist Ridderprint, ridderprint.nl
Printing: Ridderprint
Layout and design by: Camiel Lemmens, persoonlijkproefschrift.nl
Cover Art: Marjolein Verhoef-Fontijn; etch of a vintage snake based on an illustration by LittleAirplane.

© Daniël Verhoef, 2021. All rights reserved. No part of this book may be reproduced or transmitted in any form or by any means without prior written consent of the author or publisher of the included scientific papers.

Lessons from snake venom:

New insights into the structural and functional aspects of factor V and factor X.

Proefschrift

ter verkrijging van

de graad van doctor aan de Universiteit Leiden

op gezag van de rector magnificus prof.dr.ir. H. Bijl,

volgens besluit van het college voor promoties

te verdedigen op woensdag 22 september 2021

klokke 15 : 00 uur

door

Daniël Verhoef

Geboren te Haarlemmermeer in 1984

Promotor	Prof. dr. P.H. Reitsma
Co-promotor	Dr. M.H.A Bos
Promotiecommissie	Prof. dr. H.H. Versteeg Prof. dr. A.B. Meijer (Universiteit Utrecht) Dr. E. Castoldi (Universiteit van Maastricht

The research described in this thesis was funded by the European Union FP7 People Program, the National Blood Foundation, the Trombosestichting Nederland and the Bayer Hemophilia Awards Program. The research was performed at the Einthoven Laboratory for Vascular and Regenerative Medicine of the Leiden University Medical Center, Leiden, The Netherlands.

Financial support by VarmX. B.V. for the publication of this thesis is gratefully acknowledged.

Machtig zijn de werken van de Heer, wie ze liefheeft, onderzoekt ze.
(Psalm 111:2)

Preamble

Hemostasis

It's late at night and you are walking home after a good evening among friends. You are very tired and as you are strolling along you fail to notice that your shoestring has come untied. The outcome is inevitable: you stumble and hit the pavement, hard. The fall has badly hurt your knee, and to make matters worse there is a nasty cut in the palm of your hand that starts to bleed instantly. Fortunately, you are just ten minutes away from home and your fully stocked first-aid kit. However, by the time you reach home the cut in your hand has stopped bleeding completely and so therefore bandages are not required. Alas, your bruised knee is not so lucky. There's a burning sensation that seems to get worse and the site of injury has turned into a blaze of purple and red. Surely, that will be sore for quite a while.

Hemostasis seems to be straightforward: upon vascular injury blood congeals to form a protective barrier that prevents further blood loss. In fact, hemostasis is a delicately organized and intrinsically complex process which can easily become disrupted by genetic defects, use of medication, infections, detrimental lifestyle, and natural toxins like snake venom. So, while the painful narrative above may appear harmless, it can have dire consequences to individuals with genetic bleeding disorders such as hemophilia or to individuals that are being treated with anticoagulant drugs.

Contents

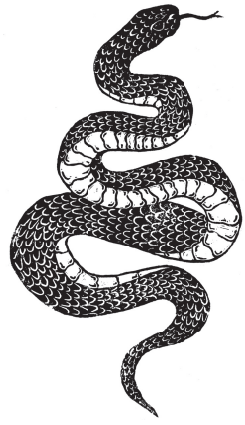

Chapter 1

General introduction

The coagulation cascade

Initiation of coagulation

On a molecular level, hemostasis is characterized by the formation of a key regulatory enzyme in blood coagulation: thrombin. This clotting enzyme is typically generated upon vascular damage in a timely and localized manner through an intricate network of enzymatic reactions governed by (pro)enzymes, (pro)cofactors, and inhibitors, collectively known as the coagulation cascade (**Figure 1**). Thrombin converts, among others, soluble fibrinogen to insoluble fibrin strands that serve to stabilize the primary platelet-based blood clot [1]. Insufficient thrombin generation therefore results in poor clot stability, which is at the basis of recurrent bleeding in patients suffering from bleeding disorders such as hemophilia [2]. On the other hand, thrombin formation at the wrong time and place can lead to a pathologic condition known as thrombosis. Thrombin is generated through a complex series of enzymatic reactions. Under normal circumstances, vascular damage results in exposure of membrane bound tissue factor (TF) to the bloodstream where it encounters its ligand, coagulation factor VIIa (FVIIa), to form the 'extrinsic' tenase complex (**Figure 1**) [3]. The interaction between TF and FVIIa occurs exclusively on membranes that present negatively charged phosphatidylserine on their outer membrane leaflet, such as activated platelets or damaged vascular endothelium, and requires the presence of calcium ions. Once the extrinsic tenase complex has been assembled, it converts the zymogen form of coagulation factor X (FX) into the protease FXa (the suffix "a" indicates the activated form) by proteolytic removal of the FX activation peptide. The newly formed N-terminus subsequently folds back into the serine protease (SP)-domain of FX. This results in a molecular rearrangement of the serine protease domain that primes the protease active site and enables FXa to cleave peptide bonds in other proteins. Once activated, FXa performs a central role in hemostasis as it is the only endogenous enzyme capable of converting prothrombin (factor II) into thrombin (factor IIa). However, efficient prothrombin conversion is only achieved upon assembly of FXa into the prothrombinase complex together with its cofactor Va (FVa). Once thrombin has been generated it is able to further propagate coagulation as detailed in the next section.

Propagation of coagulation

Hemophilia is a hereditary bleeding disorder that is characterized by varying degrees of hemorrhagic tendencies that usually require immediate specialized medical attention, especially when combined with trauma. On a molecular level, hemophilia is characterized by a (functional) deficiency in coagulation factor VIII (FVIII) or factor IX (FIX). These two 'anti-hemophilic' clotting factors are essential components of the intrinsic coagulation system, which participates both in the so-called contact activation pathway, as well as the TF-FVIIa-mediated pathway

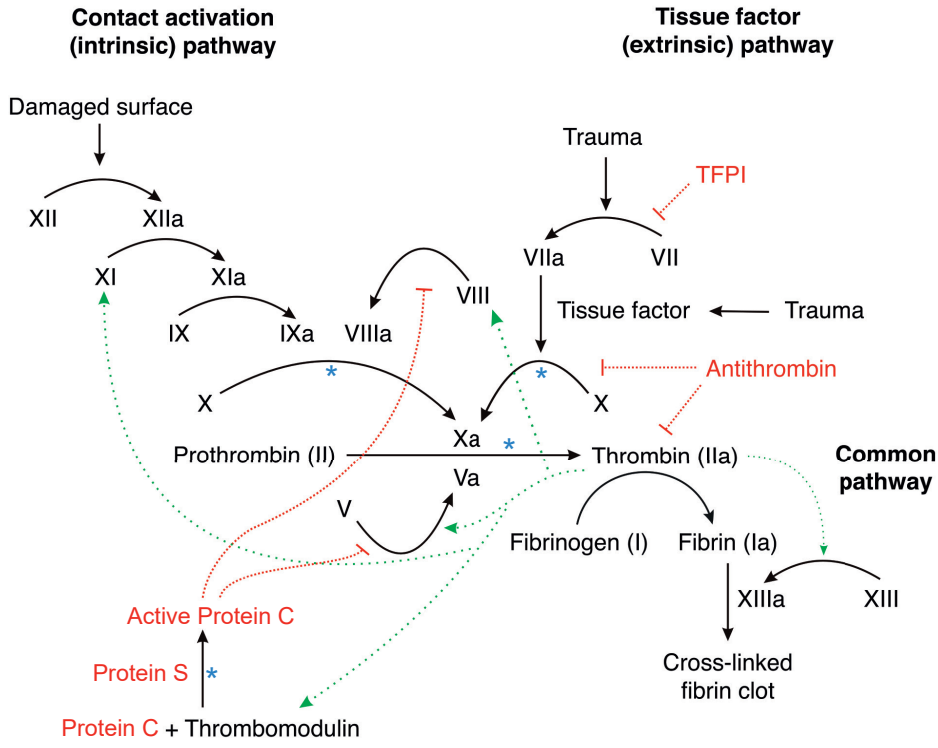

Figure 1. The coagulation cascade. Trauma is the major initiator of the coagulation cascade, resulting in activation of thrombin via tissue factor/factor VIIa and factor Xa/Va. Thrombin is then able to further propagate coagulation by additional activation of factor V and by enhancing factor X activation via the contact activation pathway through factors VIII and XI. Thrombin also mediates downregulation of the coagulation cascade through activation of protein C. Major inhibitors of the tissue factor pathway are TFPI (Tissue Factor Pathway Inhibitor) and antithrombin (which are highlighted in red). Roman numerals are used as numbering system for coagulation factors. Arrows denote negative (red) and positive (green) feedback loops. Blue asterisks indicate phospholipid-dependent reactions. Image scourced from Wikimedia [4].

[5] (**Figure 1**). The intrinsic system is traditionally regarded as a positive feedback loop to thrombin generation and is directly engaged by thrombin itself through proteolytic activation of the procofactor FVIII and zymogen FXI. Following activation, the serine protease FXIa directly converts FIX to FIXa. In addition, FIX may also be activated by FVIIa on activated platelets [6]. Once FVIII and FIX have been activated, these are able to interact on a negatively charged phospholipid surface in the presence of calcium ions to form the intrinsic tenase complex and to cooperatively activate FX. Intriguingly, the contact pathway may also be engaged upon exposure of the blood to negatively charged surfaces, such as by polyphosphates from invading pathogens [7]. This results in the generation of the serine protease FXIIa, which in turn leads to activation of FXI and FIX. However, the physiological relevance of this activation route in normal hemostasis remains contentious [8]. Accumulating evidence indicates that FXIIa-mediated FXI activation may be important in pathologic thrombus formation [9, 10]. In addition, a deficiency in FXI (hemophilia C) is not commonly associated with bleeding and is only linked to excessive hemorrhage upon trauma or surgery [11]. On the other hand, deficiencies in either FVIII (hemophilia A) or FIX (hemophilia B) are most commonly associated with recurrent bleeding episodes and treatment typically requires factor replacement therapy. The societal impact of these forms of hemophilia is extensive. For example, in the US alone, annual treatment costs may be as high as 300.000 dollar per individual, with up to 94% of the costs related to factor replacement products [12].

The prothrombinase complex

While activation of FX is prerequisite to the propagation of thrombin generation, physiologically relevant rates of thrombin generation are only achieved in the presence of activated coagulation factor V (FVa), which is an essential cofactor to FXa. FV circulates in blood as an inactive procofactor, and its domain organization (A1-A2-B-A3-C1-C2) is homologous to that of blood coagulation FVIII [13]. Activation of FV proceeds via limited proteolysis by either thrombin or FXa, which results in removal of its central B-domain that contains auto-inhibitory sequences [14-17]. Like the extrinsic and intrinsic tenase complexes, FVa and FXa exclusively associate on anionic membrane surfaces and in the presence of calcium ions, thereby forming 'the prothrombinase complex'. In FVa, membrane binding is governed by its lipid-binding C-domains, while the three A domains are involved in interactions with the protease FXa and physiological substrate prothrombin [18]. In FXa (domain organization: GLA-EGF1-EGF2-SP), membrane binding is governed by its N-terminal GLA-domain. This domain binds calcium ions which enables FX to interact with phosphatidylserine in the membrane via ionic interactions. Membrane binding GLA-domains are also found in homologous clotting factors such as prothrombin, FVII, FIX, protein C (PC), and protein S. Suggestions as to how the membrane surface propagates the coagulation reactions include increased local

reactant concentrations, induced conformational changes, or restricted protein movement. However, molecular details adequately describing this process are incomplete. Once FXa and FVa have assembled into the prothrombinase complex on a membrane surface, FVa is able to radically increase the catalytic rate of FXa towards prothrombin by serving as a platform to which FXa and prothrombin are able to bind [18, 19]. The prothrombinase complex forms the starting point of the so-called 'common pathway' which governs all thrombin-mediated clotting processes including: fibrin deposition, platelet and cell activation, and the activation of FV, FVIII, FXI, FXIII, and protein C (**Figure 1**).

Inhibition of coagulation

The progressive activation of clotting factors in the coagulation cascade creates a potent positive feedback loop that can rapidly produce a sustained burst of thrombin activity. In order to prevent runaway coagulation, several molecular mechanisms are in place that contain the thrombin burst to the site of injury. First and foremost, formation of the FX- and prothrombin-activating complexes each require the presence of negatively charged membrane surfaces, which effectively localizes the conversion of FX and prothrombin to activated platelets and damaged endothelium. In addition, naturally occurring inhibitors of coagulation present in blood tightly control the proteolytic activity of procoagulant serine proteases such as thrombin and FXa. The largest group of inhibitors are the serine protease inhibitors (serpins) [20]. These inhibitors prevent clotting enzymes from cleaving peptide bonds by occupying the region (active site) where substrates would normally bind and undergo proteolysis. Antithrombin (AT) is the main active site inhibitor of FXa, FIXa, and thrombin [21]. AT binds irreversibly and traps the enzyme in an inactive conformation, which is then cleared from the circulation and degraded. Another important anticoagulant protein is tissue factor pathway inhibitor (TFPI), which reversibly inhibits the active site of FXa. In addition, TFPI is able to inhibit the extrinsic tenase complex, both independently and when complexed with FXa. Furthermore, it is able to suppress FV activation and can associate with FV to suppress prothrombinase activity [22, 23]. Finally, thrombin also mediates downregulation of prothrombinase and intrinsic tenase through proteolytic activation of protein C, which is mediated by the cofactor thrombomodulin. Together with its cofactor protein S, activated protein C can proteolytically degrade FVa and FVIIIa, thereby limiting their cofactor activities [24] (**Figure 1**).

Thrombosis and anticoagulant drugs

Thrombosis is defined as unwanted clot formation (thrombus) within the vasculature that may obstruct the flow of blood through the vessel, or become dislodged and enter the circulation as an embolus, resulting in thromboembolism [25]. Thrombotic disorders are generally sub-defined by the type of blood vessel

that is affected (arterial or venous) and the exact location of the blood vessel or the organ it supplies. Common risk factors for arterial and venous thrombosis include (among others): advanced age, cardiovascular health (atherosclerosis, smoking, hypertension), atrial fibrillation, cancer, surgery, fractures, prolonged immobilization and oral contraceptive use [26, 27]. In addition, many genetic predispositions to venous thrombosis have been documented relating to mutations in genes encoding coagulation factors [28].

Thrombosis represents a major public health concern; it is estimated that one out of ten individuals world-wide will suffer from a thrombotic disorder during his or her lifetime. For example, in the United States up to 600.000 individuals per year are affected by venous thromboembolism alone [29]. Millions of patients worldwide therefore require anticoagulant drugs for the prophylactic management of thrombotic disorders. Over the past decades, warfarin and other vitamin K antagonists have been prescribed as anticoagulants. These anticoagulant drugs inhibit the turn-over of vitamin K (K=Koagulation) during post-translational ɣ-carboxylation of glutamic acid residues (Glu) to Gla residues. Clotting factors that comprise a GLA-domain, such as FX and prothrombin, typically require this post-translational modification in order to bind calcium ions and engage negatively charged membranes. While the effectiveness of vitamin K antagonists has been well established, their use has been implicated in many bleeding-related adverse events [30, 31].

Since 2013, new oral anticoagulant therapies have become available which directly inhibit either thrombin (dabigatran) or FXa (apixaban, rivaroxaban, edoxaban). The advantage of these so-called direct oral anticoagulants (DOACs) over the traditional vitamin K antagonists is their rapid therapeutic effectiveness, ease of dosing, and lack of monitoring requirements. Importantly, a worldwide-approved specific reversal strategy to prevent and stop potential life-threatening bleeding complications associated with anticoagulant therapy should be available. This is particularly important considering that annually 1-3% of the patients treated with DOACs suffer an adverse severe bleeding event, of which up to 1 in 5 are fatal [32]. For dabigatran, idarucizumab was succesfully introduced as specific reversal agent [33]. Nevertheless, specific reversal strategies are not available for all patients taking the FXa-inhibiting DOACs. Prothrombin complex concentrates (PCCs) are nonetheless regularly used in clinic in case of bleeding or acute surgery [34, 35]. Even so, recent studies have shown that PCCs are not able to fully restore hemostasis in all patients [36]. In addition, a recombinant modified factor Xa protein known as Andexanet-alfa has recently been approved in both the US and EU as antidote for FXa-DOACs [37]. However, the use of Andexanet-alpha carries an elevated thrombogenic risk due to sequestering of TFPI by the FXa-like molecule [38].

Factors V and X from snake venom

Over the past decade, significant scientific effort has been put into studying venom-derived toxins in order to harness their potential as drug discovery platform [39-41]. Snake venoms are widely recognized as an exceptional source of biologically active proteins and peptides that interact with the hemostatic system [42]. This is best exemplified by a family of Australian Elapid snakes, in which the blood coagulation proteins FV and FX have been converted into potent biological weapons to support envenomation of prey [43]. Pseutarin C, a powerful prothrombin activator that is found in the venom of the Australian elapid *Pseudonaja textilis*, or common brown snake, has been studied most extensively so far [44-46]. This unique prothrombin activator consists of a FVa-FXa complex and can efficiently generate thrombin in the absence of a negatively charged phospholipid surface [47], unlike any other FVa-FXa complex known to date. In addition, several unique gain-of-function modifications have been identified in both *P. textilis* venom FV and FX that serve to enhance their procoagulant potential. For example, venom FV is constitutively active due to the absence of a regulatory B-domain sequence [44, 47]. Moreover, it is functionally resistant to proteolytic inactivation by the enzymatic regulator of FV, APC [47]. Venom FX is hallmarked by a significantly shortened activation peptide, which possibly reflects the need for a more protease-like venom protein [48]. Additional modifications can be identified in the antithrombin binding site, which were shown to result in an impaired inhibition of venom FXa by antithrombin [49]. The venom FXa substrate binding pocket has also been structurally modified through an extended 99-loop (His91-Asp102), which is a surface-exposed loop that borders the active site in serine proteases [48, 50, 51]. These combined alterations enable the *P. textilis* 'venom prothrombinase' to escape hemostatic regulation and initiate indiscriminate clotting throughout the vasculature. The venom FVa-FXa complex is therefore an attractive model for prospective protein engineering strategies.

Outline of the thesis

The aim of this thesis was to uncover the unique structural and functional relationships that govern venom FXa-FVa complex assembly and function, with the intention to harness its potent procoagulant potential. In addition, by studying these venom-derived clotting factors we intend to better our understanding of the molecular mechanisms that drive prothrombinase assembly and function in humans.

In the first part of this thesis, we studied the genomic, structural, and functional implications of several molecular modifications found in the *P. textilis* venom FV molecule. In **chapter 2**, we have aimed to shed more light on the absence of the regulatory B-domain in the venom FV molecule by studying liver-expressed FV transcripts in snakes from the Elapid family and in various other snakes. In **chapter 3**, we have studied the functional implications of a disulfide bond that is exclusively found in the venom FV molecule with respect to APC inactivation of FV and lipid-independent cofactor function. In **chapter 4** of this thesis we investigated the functional relationship between cofactor stability and phospholipid binding in FV by exchanging the C-domains between human FV and *P. textilis* venom FV.

The second part of this thesis is focused on the structural and functional aspects of venom FX. In **chapter 5**, we studied the functional implications of the extended 99-loop that is unique to venom FXa. This study was partly carried out in silico through analysis of the molecular dynamics that goven venom FXa, and partly through biochemical characterization of human-snake FXa chimeras in which the snake 99-loop element was introduced. In **chapter 6**, we aimed to identify a suitable non-human plasma model system for the preclinical development of our new FX molecule. Using routine and specialty coagulation assays we established global clotting parameters in mouse, rat, rabbit, porcine, and goat plasma.

References

1. Riddel, J.P., Jr., et al., *Theories of blood coagulation.* J Pediatr Oncol Nurs, 2007. **24**(3): p. 123-31.
2. Dargaud, Y., et al., *Evaluation of thrombin generating capacity in plasma from patients with haemophilia A and B.* Thromb Haemost, 2005. **93**(3): p. 475-80.
3. Mackman, N., R.E. Tilley, and N.S. Key, *Role of the extrinsic pathway of blood coagulation in hemostasis and thrombosis.* Arterioscler Thromb Vasc Biol, 2007. **27**(8): p. 1687-93.
4. Wikimedia, *The coagulation cascade.* wikimedia.org/wiki/File:Coagulation_full.svg
5. Wu, Y., *Contact pathway of coagulation and inflammation.* Thromb J, 2015. **13**: p. 17.
6. Gabriel, D.A., et al., *Recombinant human factor VIIa (rFVIIa) can activate factor FIX on activated platelets.* J Thromb Haemost, 2004. **2**(10): p. 1816-22.
7. Baker, C.J., S.A. Smith, and J.H. Morrissey, *Polyphosphate in thrombosis, hemostasis, and inflammation.* Res Pract Thromb Haemost, 2019. **3**(1): p. 18-25.
8. Kravtsov, D.V., et al., *Factor XI contributes to thrombin generation in the absence of factor XII.* Blood, 2009. **114**(2): p. 452-8.
9. Cheng, Q., et al., *A role for factor XIIa-mediated factor XI activation in thrombus formation in vivo.* Blood, 2010. **116**(19): p. 3981-9.
10. He, R., D. Chen, and S. He, *Factor XI: hemostasis, thrombosis, and antithrombosis.* Thromb Res, 2012. **129**(5): p. 541-50.
11. Seligsohn, U., *Factor XI deficiency in humans.* J Thromb Haemost, 2009. **7 Suppl 1**: p. 84-7.
12. Zhou, Z.Y., et al., *Burden of illness: direct and indirect costs among persons with hemophilia A in the United States.* J Med Econ, 2015. **18**(6): p. 457-65.
13. Kane, W.H. and E.W. Davie, *Blood coagulation factors V and VIII: structural and functional similarities and their relationship to hemorrhagic and thrombotic disorders.* Blood, 1988. **71**(3): p. 539-55.
14. Bos, M.H. and R.M. Camire, *A bipartite autoinhibitory region within the B-domain suppresses function in factor V.* J Biol Chem, 2012. **287**(31): p. 26342-51.
15. Schuijt, T.J., et al., *Factor Xa activation of factor V is of paramount importance in initiating the coagulation system: lessons from a tick salivary protein.* Circulation, 2013. **128**(3): p. 254-66.
16. Camire, R.M. and M.H. Bos, *The molecular basis of factor V and VIII procofactor activation.* J Thromb Haemost, 2009. **7**(12): p. 1951-61.
17. Suzuki, K., B. Dahlback, and J. Stenflo, *Thrombin-catalyzed activation of human coagulation factor V.* J Biol Chem, 1982. **257**(11): p. 6556-64.
18. Schreuder, M., P.H. Reitsma, and M.H.A. Bos, *Blood coagulation factor Va's key interactive residues and regions for prothrombinase assembly and prothrombin binding.* J Thromb Haemost, 2019. **17**(8): p. 1229-1239.
19. Mann, K.G., et al., *Surface-dependent reactions of the vitamin K-dependent enzyme complexes.* Blood, 1990. **76**(1): p. 1-16.

20. Rau, J.C., et al., *Serpins in thrombosis, hemostasis and fibrinolysis.* J Thromb Haemost, 2007. **5 Suppl 1**: p. 102-15.
21. Bjork, I. and S.T. Olson, *Antithrombin. A bloody important serpin.* Adv Exp Med Biol, 1997. **425**: p. 17-33.
22. Broze, G.J., Jr., T.J. Girard, and W.F. Novotny, *Regulation of coagulation by a multivalent Kunitz-type inhibitor.* Biochemistry, 1990. **29**(33): p. 7539-46.
23. Wood, J.P., et al., *Tissue factor pathway inhibitor-alpha inhibits prothrombinase during the initiation of blood coagulation.* Proc Natl Acad Sci U S A, 2013. **110**(44): p. 17838-43.
24. Kisiel, W., et al., *Anticoagulant properties of bovine plasma protein C following activation by thrombin.* Biochemistry, 1977. **16**(26): p. 5824-31.
25. Furie, B. and B.C. Furie, *Mechanisms of thrombus formation.* N Engl J Med, 2008. **359**(9): p. 938-49.
26. Reiner, A.P., D.S. Siscovick, and F.R. Rosendaal, *Hemostatic risk factors and arterial thrombotic disease.* Thrombosis and Haemostasis, 2001. **85**(4): p. 584-595.
27. Previtali, E., et al., *Risk factors for venous and arterial thrombosis.* Blood Transfusion, 2011. **9**(2): p. 120-138.
28. Franco, R.F. and P.H. Reitsma, *Genetic risk factors of venous thrombosis.* Hum Genet, 2001. **109**(4): p. 369-84.
29. Beckman, M.G., et al., *Venous thromboembolism: a public health concern.* Am J Prev Med, 2010. **38**(4 Suppl): p. S495-501.
30. Budnitz, D.S., et al., *Emergency hospitalizations for adverse drug events in older Americans.* N Engl J Med, 2011. **365**(21): p. 2002-12.
31. Wysowski, D.K., P. Nourjah, and L. Swartz, *Bleeding complications with warfarin use: a prevalent adverse effect resulting in regulatory action.* Arch Intern Med, 2007. **167**(13): p. 1414-9.
32. Sardar, P., et al., *Risk of major bleeding in different indications for new oral anticoagulants: insights from a meta-analysis of approved dosages from 50 randomized trials.* Int J Cardiol, 2015. **179**: p. 279-87.
33. Pollack, C.V., Jr., et al., *Idarucizumab for Dabigatran Reversal - Full Cohort Analysis.* N Engl J Med, 2017. **377**(5): p. 431-441.
34. Arachchillage, D.R.J., et al., *Efficacy and safety of prothrombin complex concentrate in patients treated with rivaroxaban or apixaban compared to warfarin presenting with major bleeding.* Br J Haematol, 2019. **184**(5): p. 808-816.
35. Schulman, S., et al., *Prothrombin Complex Concentrate for Major Bleeding on Factor Xa Inhibitors: A Prospective Cohort Study.* Thromb Haemost, 2018. **118**(5): p. 842-851.
36. Gerner, S.T., et al., *Association of prothrombin complex concentrate administration and hematoma enlargement in non-vitamin K antagonist oral anticoagulant-related intracerebral hemorrhage.* Ann Neurol, 2018. **83**(1): p. 186-196.
37. Lu, G., et al., *A specific antidote for reversal of anticoagulation by direct and indirect inhibitors of coagulation factor Xa.* Nat Med, 2013. **19**(4): p. 446-51.
38. Favresse, J., et al., *Andexanet alfa for the reversal of factor Xa inhibitors.* Expert Opin Biol Ther, 2019. **19**(5): p. 387-397.

39. Vetter, I., et al., *Venomics: a new paradigm for natural products-based drug discovery.* Amino Acids, 2011. **40**(1): p. 15-28.
40. Vonk, F.J., et al., *Snake venom: From fieldwork to the clinic: Recent insights into snake biology, together with new technology allowing high-throughput screening of venom, bring new hope for drug discovery.* Bioessays, 2011. **33**(4): p. 269-79.
41. Koh, C.Y., et al., *Toxins Are an Excellent Source of Therapeutic Agents against Cardiovascular Diseases.* Semin Thromb Hemost, 2018. **44**(7): p. 691-706.
42. Markland, F.S., *Snake venoms and the hemostatic system.* Toxicon, 1998. **36**(12): p. 1749-800.
43. St Pierre, L., et al., *Comparative analysis of prothrombin activators from the venom of Australian elapids.* Mol Biol Evol, 2005. **22**(9): p. 1853-64.
44. Rao, V.S., S. Swarup, and R.M. Kini, *The nonenzymatic subunit of pseutarin C, a prothrombin activator from eastern brown snake (Pseudonaja textilis) venom, shows structural similarity to mammalian coagulation factor V.* Blood, 2003. **102**(4): p. 1347-54.
45. Rao, V.S., S. Swarup, and R. Manjunatha Kini, *The catalytic subunit of pseutarin C, a group C prothrombin activator from the venom of Pseudonaja textilis, is structurally similar to mammalian blood coagulation factor Xa.* Thromb Haemost, 2004. **92**(3): p. 509-21.
46. Masci, P.P., A.N. Whitaker, and J. de Jersey, *Purification and characterization of a prothrombin activator from the venom of the Australian brown snake, Pseudonaja textilis textilis.* Biochem Int, 1988. **17**(5): p. 825-35.
47. Bos, M.H., et al., *Venom factor V from the common brown snake escapes hemostatic regulation through procoagulant adaptations.* Blood, 2009. **114**(3): p. 686-92.
48. Bos, M.H. and R.M. Camire, *Procoagulant adaptation of a blood coagulation prothrombinase-like enzyme complex in australian elapid venom.* Toxins (Basel), 2010. **2**(6): p. 1554-67.
49. Johnson DJ, H.J., *Pseudonaja textilis venom FXa is poorly inhibited by human antithrombin.* Abstracts of the XXIV congress of the International Society on Thrombosis and Haemostasis, 2013: p. PB 4.58-2.
50. Lechtenberg, B.C., et al., *Crystal structure of the prothrombinase complex from the venom of Pseudonaja textilis.* Blood, 2013. **122**(16): p. 2777-83.
51. Hedstrom, L., *Serine protease mechanism and specificity.* Chem Rev, 2002. **102**(12): p. 4501-24.

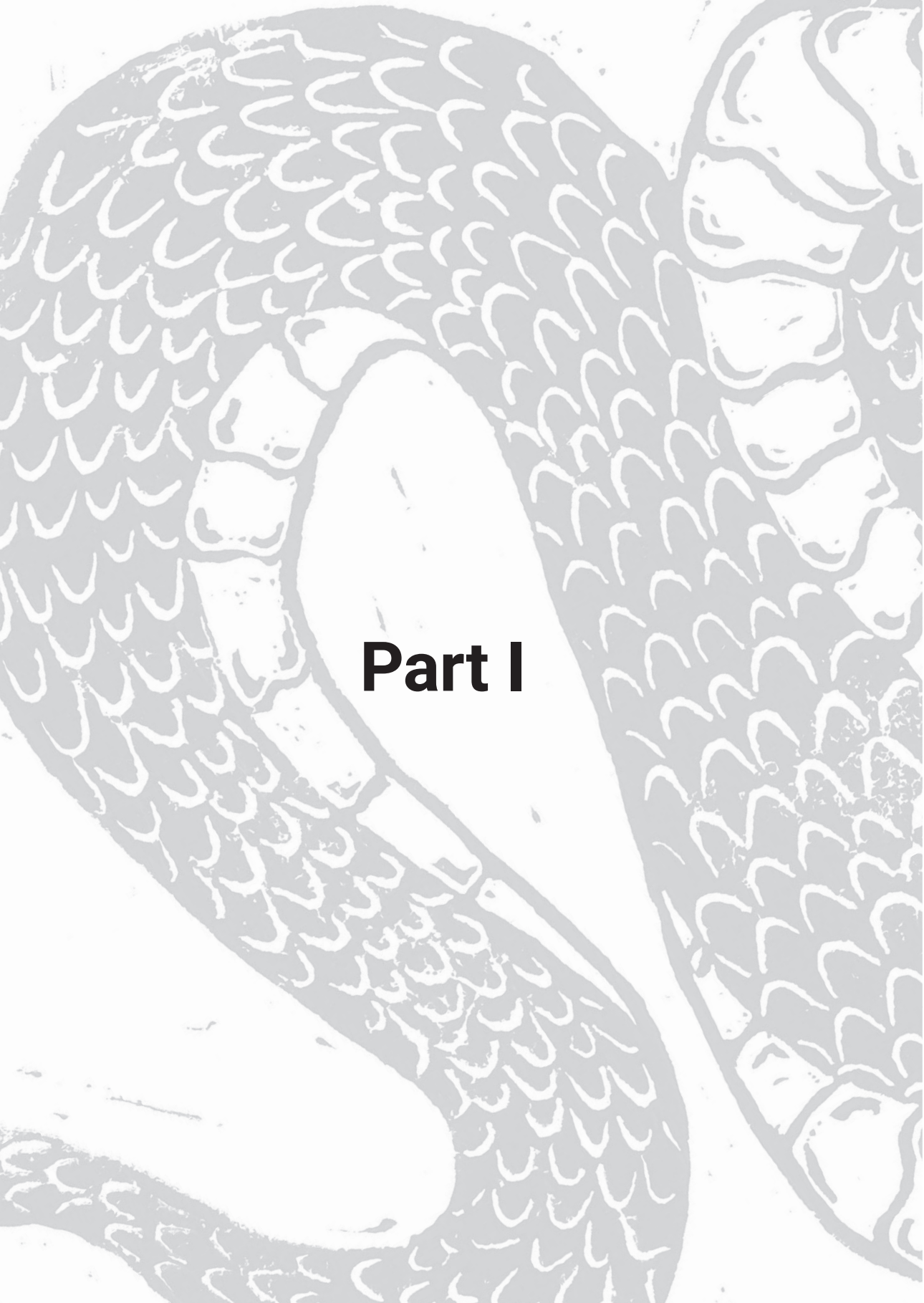

Part I

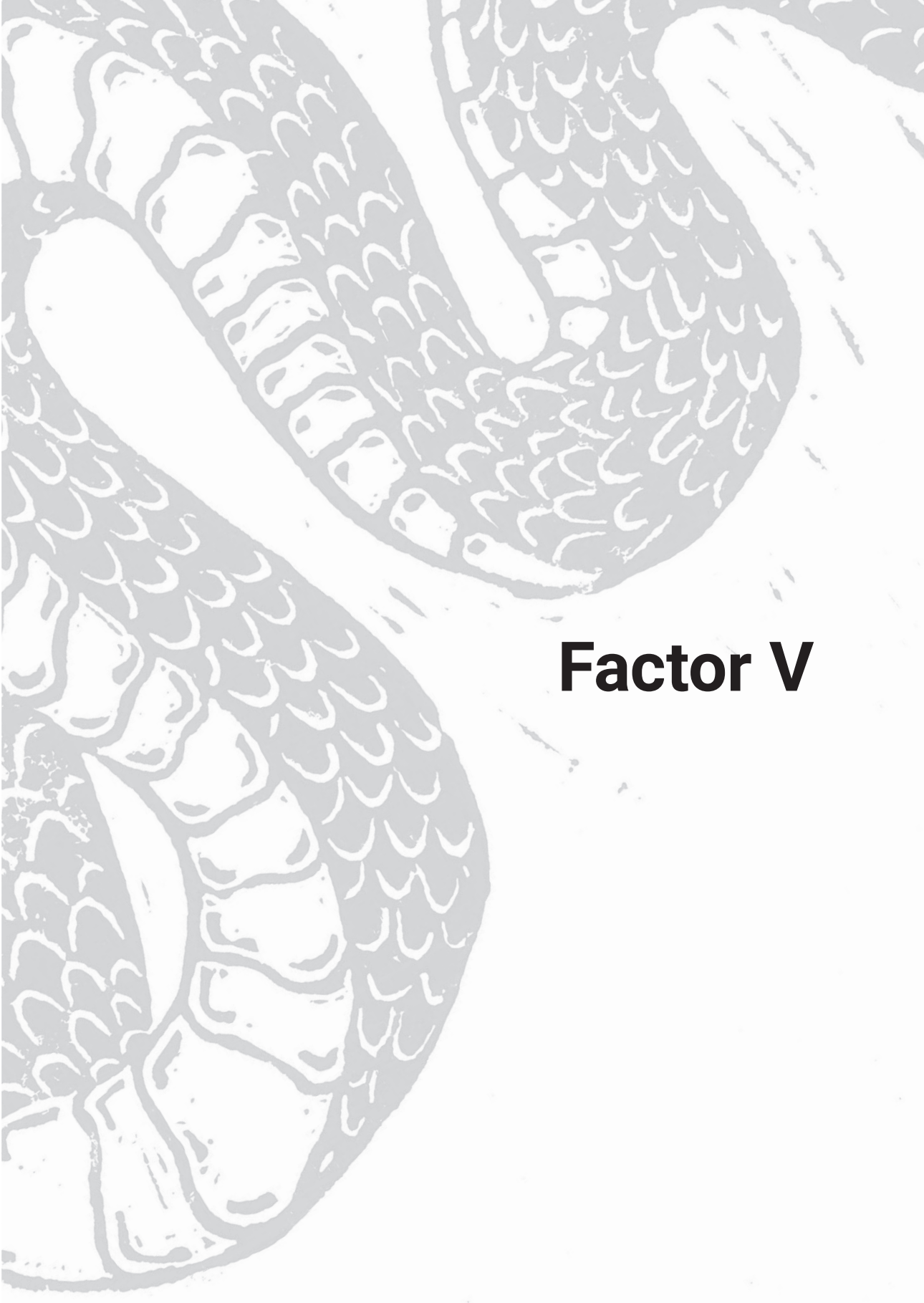

Factor V

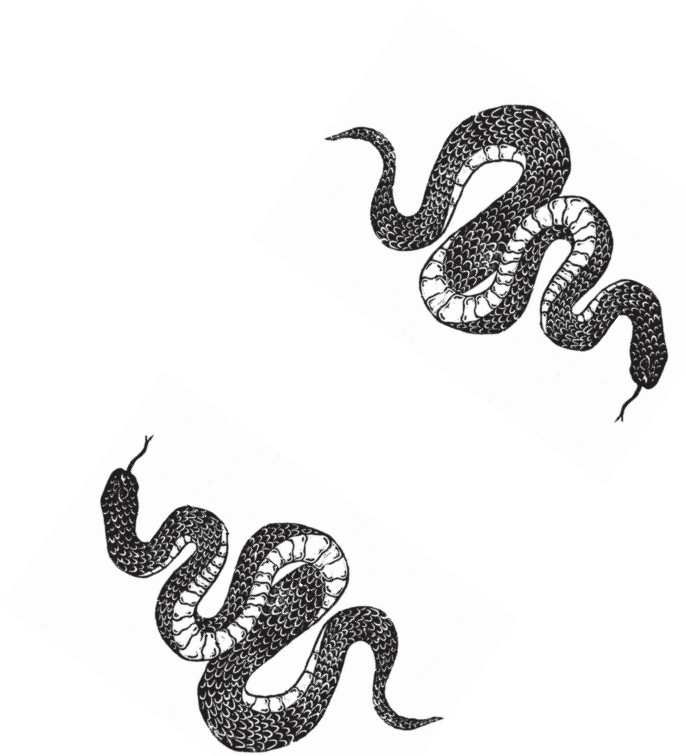

Chapter 2

Evolutionary conservation of regulatory B-domain elements in blood coagulation factor V in snakes

Daniël Verhoef, Ka Lei Cheung, Hans L. Vos, Ryan J.R. McCleary, R. Manjunatha Kini, Pieter H. Reitsma, Mettine H.A. Bos.

Manuscript in preparation

Abstract

The B-domain of blood coagulation factor V (FV) is an essential element that negatively regulates FV activity through conserved auto-inhibitory regions. Interestingly, a FV sequence lacking the B-domain has previously been identified in an elapid snake, suggesting a divergent molecular mechanism of FV regulation. To investigate whether this unique feature hallmarks the entire Serpentes suborder, we uncovered the identity of the FV B-domain from twelve distinct snake species. To do so, cDNAs were generated from fresh-frozen liver tissue, and B-domain fragments were amplified employing oligonucleotides complementary to conserved FV-specific sequences. Sequence analysis revealed that auto-inhibitory B-domain regions were preserved with high sequence identity in all snake species. In addition, amplification reactions also generated a truncated B-domain fragment that corresponded to a shorter B-domain that lacked the auto-inhibitory regions. Alignment of the compiled snake FV transcripts uncovered two conserved pre-RNA splice sites within the B-domain-encoding exon that may be at the basis of the truncated B-domain transcript. Additional quantitative analysis by qPCR and capillary electrophoresis showed that while in most snakes the regular B-domain is more abundant (20-1000-fold) than the truncated version, the latter are almost equally expressed in snake venom FV-comprising elapids and highly abundant in viperid species. Taken together this indicates that, while the B-domain has been preserved as a potential regulator of FV activity in all members of the suborder Serpentes, alternative splicing of the B-domain may play a role as a disparate mechanism of FV regulation in some snake species.

Introduction

Blood coagulation factor V (FV) is an essential and highly conserved protein component of the vertebrate blood coagulation system [1, 2]. FV normally circulates in blood as an inactive procofactor (domain organization A1-A2-B-A3-C1-C2) and is only converted to its active cofactor form (FVa) in the event of vascular damage. Conversion of FV to FVa proceeds upon limited thrombin- or factor Xa (FXa)-mediated proteolysis of three peptide bonds (Arg^{709}, Arg^{1018}, and Arg^{1545}) that either flank or are within the B-domain sequence, resulting in removal of the central auto-inhibitory B-domain and expression of cofactor activity [3-6]. The auto-inhibitory B-domain normally maintains the procofactor state through a dedicated procofactor regulatory region (PRR), which is generally well conserved among vertebrate B-domain sequences unlike the remainder of the B-domain sequence. The PRR typically constitutes a basic region (BR) and an acidic region (AR) that cooperatively stabilize the procofactor state [7, 8]. Removal of the PRR is required for the expression of FVa cofactor activity. Once removed, FVa is able to assemble into the prothrombinase complex by binding to FXa on a negatively charged phospholipid surface in the presence of calcium ions [7, 8]. This is an essential step during hemostasis, as FVa effectively enhances the conversion of prothrombin into thrombin to physiologically relevant catalytic rates [9, 10].

The venom of the Australian common brown snake *Pseudonaja textilis* contains a powerful prothrombin activator (pseutarin C) that is structurally and functionally similar to the human FVa-FXa complex [11, 12]. The non-enzymatic subunit of pseutarin C (venom FV) is a unique FVa cofactor analogue that is constitutively active upon translation/secretion due to the absence of a regulatory B-domain sequence within its mRNA [13, 14]. Interestingly, a highly similar FV transcript comprising a truncated B-domain lacking the PRR has also been identified in liver tissue of *P. textilis* [15], suggesting a divergent molecular mechanism of FV regulation in hemostasis. On the other hand, whole genome sequencing of the venomous king cobra, *Ophiophagus hannah*, revealed the presence of a single full-length FV gene that included all putative auto-inhibitory B-domain elements [7, 8, 16]. It is therefore uncertain whether the absence of a regulatory B-domain sequence in liver FV is unique to *P. textilis* physiology or whether this trait is shared among other snakes. We have therefore aimed to uncover the identity of the FV B-domain in liver-derived transcripts from snakes belonging to various lineages and geographic regions, as well as venomous vs non-venomous species. By doing so, we have revealed that all investigated snakes include both full-length and truncated FV B-domain transcripts in their liver transcriptome. These findings suggest functional diversification of the FV gene in the suborder Serpentes.

Material and Methods

Materials and Reagents

Fordonia leucobalia tissue was collected locally through permits in Singapore by Ryan McCleary and Vic Toh under Singapore National Parks permit NP/RP10-095. Liver tissues from *Bungarus candidus*, *Oligodon octolineatus*, and *Sistrurus catenatus* were kindly gifted by drs. F.J. Vonk (Naturalis Biodiversity Center/ Amsterdam Institute of Molecular and Life Sciences, The Netherlands), M.A. Reza Tuhin (University of Rajshahi, Bangladesh), and S.J. Mackessy (University of Northern Colorado, USA). All other snake liver tissues were purchased from Venom Supplies Pty Ltd (Tanunda, Australia). RNA-Bee was obtained from Tel-Test Inc (Friendswood, TX, USA). Phusion high-fidelity DNA polymerase was obtained from New England Biolabs (Ipswich, MA, USA). HOT FIREPol DNA polymerase was obtained from Solis BioDyne (Tartu, Estonia). The Wizard SV gel and PCR clean up system was obtained from Promega (Madison, WI, USA). RNAse-free DNAse and RNeasy DNA removal columns were obtained from Qiagen (Hilden, Germany). Oligo-dT primers and Superscript II reverse transcriptase was obtained from Invitrogen (Thermo Scientific, Waltham, MA, USA). SYBR select qPCR master mix was from Applied Biosystems (Foster City, CA, USA). The Agilent DNA 1000 kit was from Agilent Technologies (Santa Clara, CA, USA).

Liver RNA isolation and cDNA synthesis

Liver samples (± 20 – 40 mg) from single individuals were stored at -80°C in RNAlater solution. Upon thawing, the samples were homogenized in RNA-Bee, and total RNA was isolated from homogenates using guanidium-phenol-chloroform extraction and isopropanol precipitation, after which RNA was dissolved in Tris-EDTA-RNAse inhibitor buffer. Spectrophotometric quantification and quality analysis of the sample was performed, and the integrity of the RNA was confirmed by agarose gel electrophoresis. Following genomic DNA removal, first-strand cDNA synthesis was performed using Superscript II reverse transcriptase according the manufacturer's guidelines.

cDNA amplification and Sanger sequencing

The cDNA templates were amplified using Phusion high-fidelity DNA polymerase. Primer annealing temperatures were separately optimized by Touchdown PCR for each cDNA template from individual snake species. Individual cDNA amplicons were isolated by agarose gel electrophoresis and purified using the Wizard SV gel and PCR clean up kit. Sanger sequencing was performed at BaseClear B.V. (Leiden, the Netherlands). Primer design and DNA/Protein sequence analysis was performed employing the Vector NTI 11.5 Advance software suite (Thermo Scientific, Waltham, MA, USA). An overview of all PCR and Sanger sequencing primers is provided (**Table 1**).

Table 1. Overview of primer sequences

cDNA amplification		
A2-F1	forward	5′ CTACTGTAACAATGGACAATC 3′
A3-R1	reverse	5′ GTAGTCCCAGAAAACTTCTTC 3′
Sanger sequencing		
Sanger-F1	forward	5′ CAGGAAACAGCTATGACCCATCTTGCTGGTCACAC 3′
Sanger-F2	forward	5′ CAGGAAACAGCTATGACCCTACTGTAACAATGGACAATC 3′
Sanger-F3	forward	5′ CAGGAAACAGCTATGACCCTAATGATAGCTTCCATGCTTGGGC 3′
Sanger-F4	forward	5′ CTAATGATAGCTTCCATGCTTGGGC 3′
Sanger-F5	forward	5′ CTACTGTAACAATGGACAATC 3′
Sanger-F6	forward	5′ GCTTCAATGCTTGGGCTTCG 3′
Sanger-F7	forward	5′ TTTTAATTTCAAATATCACTGC 3′
Sanger-F8	forward	5′ CAGAACAGCAGCAGAAATGCCTC 3′
Sanger-F9	forward	5′ CCAACCACACAAAATTG 3′
Sanger-F10	forward	5′ CCAGAAAGATGAGAACTGCACTAT 3′
Sanger-F11	forward	5′ GATAATCCATATACCACAAG 3′
Sanger-R1	reverse	5′ TGTAAAACGACGGCCAGTGTAGTCCCAGAAAACTTCTTC 3′
Sanger-R2	reverse	5′ TGTAAAACGACGGCCAGTCTCCTCATCAAAGACC 3′
Sanger-R3	reverse	5′ TGTAAAACGACGGCCAGTCCTGATAGTCACCATCTTC 3′
Sanger-R4	reverse	5′ CCTGATAGTCACCATCTTC 3′
Sanger-R5	reverse	5′ GTAGTCCCAGAAAACTTCTTC 3′
Sanger-R6	reverse	5′ GCTATGTCATCAGGATTACGTGCAC 3′
Sanger-R7	reverse	5′ TGTAAAACGACGGCCAGTGCAGTGATATTTGAAATTAAAA 3′
Sanger-R8	reverse	5′ GAGGCATTTCTGCTGCTGTTCTG 3′
Sanger-R9	reverse	5′ ATAGTGCAGTTCTCATCTTTCTGG 3′
RT-qPCR		
qPCR-F1	forward	5′ GGGTCAGTTGCTGAAGAAGAA′3
qPCR-F2	forward	5′ GGATCAGTTGCTGAAGAAGAA′3
qPCR-R1	reverse	5′ ACTGTCAATTCGAGGATCAGAAG 3′
qPCR-R2	reverse	5′ ACTGTCAAGTCGAGAATCAGAAG 3′
Multiplex-PCR		
A2-F2	forward	5′ GGGTCAGTTGCTGA 3′
AR*-R1	reverse	5′ GTCAAGTCGAGAATCAGA 3′
AR*-R2	reverse	5′ GTCAATTCGAGGATCAGA 3′
BR-R1	reverse	5′ TCCCAATTCTTCATTACC 3′

Real-time quantitative PCR (RT-qPCR)

Snake species-specific RT-qPCR primers were designed with the PRIMER EXPRESS software (Applied Biosystems, Foster City, CA, USA) (**Table 1**). RT-qPCR was performed using the SYBR select qPCR master mix and primer pair qPCR-F1/-R1 for *P. textilis*, *Oxyuranus scutellatus*, *Oligodon octolineatus*, *Psammophis schokari*, and *Bungarus candidus*; primer pair qPCR-F2/-R1 for *Tropidechis carinatus*, *Drysdalia coronoides*, *Fordonia leucobalia*, *Furina diadema*, and *Vermicella annulata;* and primer pair qPCR-F1/R2 for *Sistrurus catenatus* and *Echis carinatus*. RT-qPCR was performed on the Viia 7 real-time PCR system, and analysis of relative gene expression was carried out using the 2-ΔΔCT method according to the manufacturer's guidelines [17].

Multiplex PCR and automated capillary electrophoresis

Both the 2000 bp and 600 bp snake FV B-domain templates were amplified in a single reaction mixture using HOT FIREPol DNA polymerase and primers A2-F2/BR-R1/AR*-R1 for *P. textilis*, *O. scutellatus*, *D. coronoides* and *F. diadema* cDNA, and primers A2-F2/BR-R1/AR*-R2 for *P. schokari* and *S. catenatus* cDNA (**Table 1**). The reaction was performed with 200 nM of forward primer and 100 nM of both reverse primers at 57.1°C annealing temperature. Automated capillary electrophoresis was performed on the Agilent 2100 Bioanalyzer (Agilent Technologies, Santa Clara, CA, USA) using the Agilent DNA 1000 Kit, and relative ratios were calculated based on a 25-1000 bp DNA standard (Agilent Technologies, Santa Clara, CA, USA) using the Bioanalyzer software package.

Bioinformatics

For the pre-RNA spliceosome analysis of full-length snake B-domain DNA sequences, the Human Splicing Finder (HSF) software version 3.1 (http://www.umd.be/HSF3/index.html) was employed making use of a transcription database based on Ensembl release number 70 - January 2013 [18, 19]. The theoretical isoelectric point (pI) of snake specific sequences was calculated with the ProtParam tool on the ExPASy server (https://web.expasy.org/compute_pi/) [20]

Results

Evolutionary and geographic snake origins

To investigate the nature of the B-domain of liver-expressed snake FV, fresh-frozen liver tissues from twelve distinct snake species were obtained (**Table 2**). The collection included two elapid species known to produce venom analogues of FVa and FXa (*Pseu. textilis*—pseutarin C and *O. scutellanus*—scutarin C) [21, 22], and another elapid known to produce a venom analogue of FXa only (*T. carinatus*—trocarin D) [23]. Four additional elapid species that have not been reported to produce venom analogues of FVa or FXa were also included: three species that inhabit the same geographic region as *P. textilis* (*D. coronoides*, *F. diadema*, and *V. annulata*), and one species that is native to Southeast Asia and Indonesia (*B. candidus*). Evolutionarily distinct species of snakes (last shared ancestor >50 million years ago [24]) from different geographic regions were also included: a non-venomous colubrid species (*O. octolineatus*); a mildly venomous species of the family Psammophiidae (*P. schokari*); a potentially venomous species of the family Homalopsidae (*F. leucobalia*); and two venomous viperid species (*S. catenatus* and *E. carinatus*). Of the latter, *E. carinatus* is well known for its venom-derived metalloprotease ecarin, which catalyzes the conversion of prothrombin into thrombin independent from FVa and FXa [25].

Table 2. Names, family, and geographic distribution of the studied snakes

	Common name	Latin name	Family	Range
1	Common brown snake	Pseudonaja textilis	Elapidae	Eastern Australia
2	Coastal taipan	Oxyuranus scutellatus	Elapidae	Northern Australia and New Guinea
3	Rough-scaled snake	Tropidechis carinatus	Elapidae	Eastern Australia
4	White-lipped snake	Drysdalia coronoides	Elapidae	Wider Australia
5	Red-naped snake	Furina diadema	Elapidae	Eastern Australia
6	Bandy-bandy	Vermicella annulata	Elapidae	Eastern Australia
7	Malayan krait	Bungarus candidus	Elapidae	Southeast Asia to Indonesia.
8	Striped kukri snake	Oligodon octolineatus	Colubridae	Indonesia
9	Schokari sand racer	Psammophis schokari	Colubridae	Africa, Southwest Asia
10	Crab-eating water snake	Fordonia leucobalia	Colubridae	Southeast Asia to Northern Australia
11	Massasauga	Sistrurus catenatus	Viperidae	North America
12	Saw-scaled viper	Echis carinatus	Viperidae	Middle East and Central Asia

Multiple factor V B-domain amplicons with varying lengths are generated from snake cDNA

Fresh frozen liver tissue samples were individually processed for RNA extraction and cDNA generation. PCR amplification of the FV B-domain was enabled by designing primers based on sequence conservation between the known FV sequences from the anole lizard (*Anolis carolinensis*, uniprot: G1KK71) [26] and the elapid king cobra (*O. hannah*, uniprot: V8P243) [16]. For cDNA amplification, the forward primer was designed to bind a conserved stretch within the *A. carolinensis* and snake FV A2 domains, and similarly designed reverse primers targeted the FV A3-domain. Interestingly, PCR amplification of *P. textilis* and *O. scutellanus* cDNA using one primer set consistently produced two 'long' (~2000 bp) B-domain amplicons and one 'short' (600 bp) B-domain amplicon, irrespective of annealing temperature (**Figure 1**). Furthermore, a less abundant semi-long amplicon of approximately 1600 bp was generated. From all cDNA samples of the other snakes similarly sized B-domain amplicons were generated using the same primer pairs

Next, the relative ratio between the 600 bp and 2000 bp B-domain amplicons was examined in more detail employing multiplex PCR and automated capillary electrophoresis (Bioanalyzer). By doing so, we were able to confirm that the long amplicon was more abundant in most of the elapid species as well as the colubrid, psammophiid, and homalopsid species assessed (**Figure 2A,B**). However, considerable differences were noted in the ratio between the short and long amplicons among species belonging to the family Elapidae. For instance, the long B-domain transcript was only 2-fold more abundant in *P. textilis* and *O. scutellatus*, whereas it was 26-fold and 76-fold more expressed in *D. coronoides* and *F. diadema*, respectively. In contrast, in viperid snakes the short B-domain transcript was 12 to 30-fold more abundant relative to the long B-domain. Similar trends among species and between snake families were also observed employing RT-qPCR using specifically designed primer pairs (**Figure 2B**).

The full-length B-domain of snake FV contains conserved auto-inhibitory regions

Sanger sequencing of the 2000 bp and 600 bp B-domain amplicons demonstrated that each long B-domain transcript contained an open reading frame that encoded an amino acid sequence that was highly similar (>90% identity) between snakes. Interestingly, each of these B-domain sequences contained three putative thrombin/FXa cleavage motifs that were similar to the human FV Arg^{709}, Arg^{1018}, and Arg^{1545} motifs (**Figure 3**) [4]. In addition, each individual B-domain sequence contained two discrete regions that were rich in either basic residues (KRK…PKV; theoretical pI: 9.9; **Figure 3** Basic Region (BR)) or acidic residues (DYQ…PDD; theoretical pI: 3.7; **Figure 3** Acidic Region (AR)). The order of these elements was also similar to that of the human FV B-domain, suggesting functional

relevance as auto-inhibitory B-domain elements (**Figure 3**). Collectively, these data demonstrate that the *P. textilis* genome comprises a gene encoding for full-length FV. However, considerable differences were noted in the relative spacing of these elements along the snake FV polypeptide chain when compared to human FV. For example, the snake BR is located 100 residues further downstream from the Arg^{709} cleavage motif when aligned with the human BR. On the other hand, the spacer sequence that separates the Arg^{1018} cleavage motif from the snake AR is nearly 410 residues shorter in the snake B-domain (**Figure 3**). The full-length snake B-domain sequence (504 ± 4 residues) is thus considerably shorter than that of the human B-domain (834 residues) and resembles the B-domain sequence identified in the king cobra [16].

Similar to the large B-domain transcript, we uncovered that the short B-domain transcript contained an open reading frame. Following amino acid sequence alignment, all short B-domain transcripts were shown to encode B-domain sequences that were highly similar (>90% identity) to the truncated B-domain sequence that was previously identified in the *P. textilis* venom gland and liver tissues [13, 15]. The short B-domain sequence features only the Arg^{709} and Arg^{1545} cleavage motifs and a short 45-residue linker separating these two motifs (**Figure 4**). Notably, the first part of this linker is formed by a distinct stretch of residues that lies adjacent to the putative Arg^{709} cleavage motif (*P. textilis;* EEE…AHAS; **Figure 4**). The second part is formed by the last 14 residues from the putative snake AR sequence (*P. textilis;* DPR…PDD; **Figure 4**), the latter being over 500 amino acids downstream from the Arg^{709} motif in the full-length B-domain sequence (**Figure 3**). The complete linker sequence is negatively charged (theoretical pI: 3.9) and is therefore labeled 'alternative' Acidic Region (AR*).

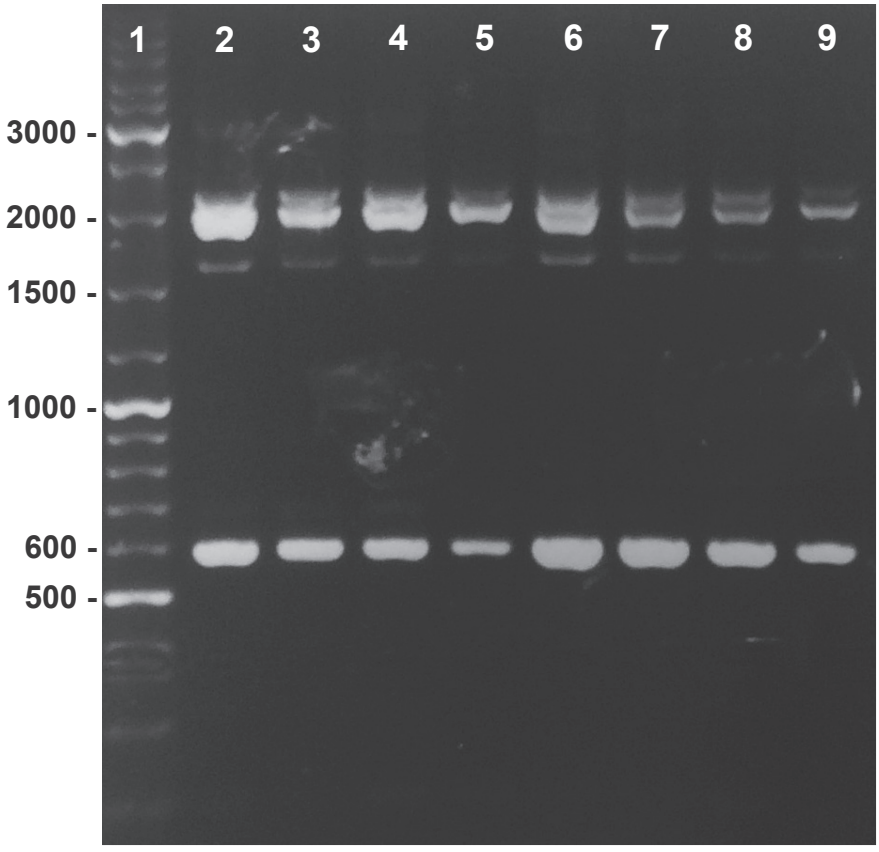

Figure 1. FV B-domain amplicons from *P. textilis* and *O. scutellanus*. Touchdown PCR amplicons from *P. textilis* and *O. scutellatus* liver-derived cDNA were amplified with forward primer A2-F1 and reverse primer A3-R1 at annealing temperatures (Ta) ranging between 57.9°C and 69.6°C and were subsequently run on a 1.0% Agarose gel. Lane 1: 1 kb GeneRuler Plus DNA Ladder, lanes 2-5: *P. textilis* amplicons, lanes 6-9: *O. scutellatus* amplicons, lanes 2,6: Ta 57.9°C, lanes 3,7: Ta 58.2°C °C, lane 4,8: Ta 63.0°C, and lane 5,9: Ta 64.5°C. The apparent bp lengths of the DNA standards are indicated.

A

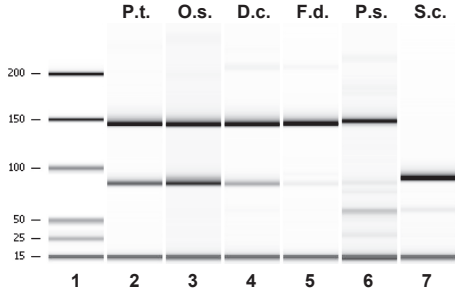

B

	Snake	Bioanalyzer	RT-qPCR
1	*P. textilis*	1:2	1:3
2	*O. scutellatus*	1:2	1:4
3	*T. carinatus* *	-	1:197
4	*D. coronoides*	1:26	1:38
5	*F. diadema*	1:76	1:207
6	*V. annulata* *	1:4	1:17
7	*B. candidus* *	-	1:615
8	*O. octolineatus* *	1:7	1:636
9	*P. schokari*	1:8	1:453
10	*F. leucobalia* *	-	1:1032
11	*S. catenatus*	30:1	14:1
12	*E. carinatus* *	12:1	2:1

Figure 2. Ratios of 600 and 2000 bp cDNA amplicons. (***A***) Electropherogram of multiplex-PCR derived B-domain amplicons from six representative snake species as analyzed by automated capillary electrophoresis. The ratio of the short over the long snake FV B-domain transcript was quantified using a predefined standard (lane 1) and PCR samples were analyzed in parallel (lanes 2 – 7); The ~150 bp band corresponds to the full-length B-domain and the ~90 bp band corresponds to the truncated B-domain. The long and short B-domain templates were amplified using a forward primer that bound the snake A2-domain (A2-F2) and a pair of reverse primers that targeted either the full-length snake B-domain BR (BR-R1) or the truncated B-domain AR* (AR*-R1/AR*-R2), respectively (**Table 1**). Lane 1: 25-1000 bp DNA standard, lane 2: *P. textilis* (P.t.), lane 3: *O. scutellatus* (O.s.), lane 4: *D. coronoides* (D.s.), lane 5: *F. diadema* (F.d.), lane 6: *P. schokari* (P.s.), lane 7: *S. catenatus* (S.c.). (***B***) Summary of automated capillary electrophoresis ('Bioanalyzer') and RT-qPCR experiments showing the ratio between truncated and full-length B-domain transcripts. The data are representative for two experiments; the asterisk indicates cDNA species that have been tested once.

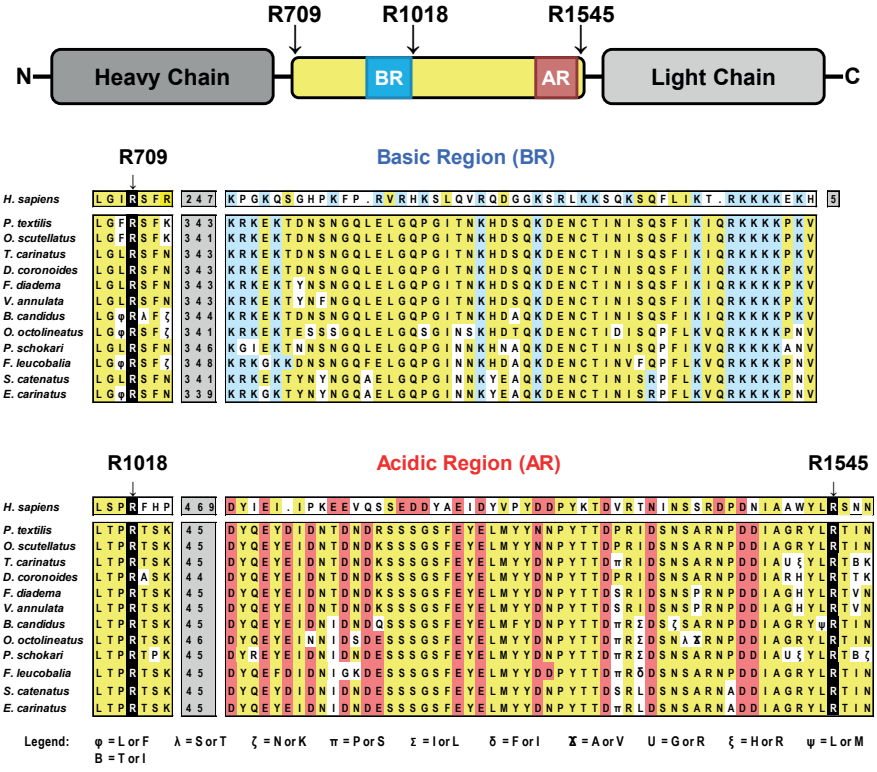

Figure 3. Conservation of regulatory B-domain elements within the full-length snake FV B-domain. ***Top:*** The human FV polypeptide chain is defined by an N-terminal heavy chain (A1-A2 domains; dark grey), a central regulatory B-domain (yellow) and a C-terminal light chain (A3-C1-C2 domains; light grey). The B-domain is removed after thrombin/FXa-mediated proteolysis; human cleavage sites are indicated above the B-domain. The blue box represents the Basic Region (BR; a.a. 963–1008) and the red box represents the Acidic Region (AR; a.a. 1493–1537). ***Middle:*** Amino acid alignment of the first cleavage motif (R709) and putative BR in full-length snake FV as identified through sequencing of 2000 bp cDNA amplicons from twelve snake species. The human sequence is shown for reference purposes, and the numbers within the grey boxes denote the number of amino acids between the regulatory elements. ***Bottom:*** Amino acid alignment of the second (R1018) and third (R1545) cleavage motifs and (putative) AR in human and snake FV, for which the mature human FV residue numbering is used. Greek letters represent amino acid discrepancies between a regular B-domain sequence (this figure) and a truncated B-domain sequence (**Figure 4)** of the same species, which are defined in the legend below the figure. Highlighted residues (yellow, red, or blue) represent identical or highly homologous amino acids at a particular location. Red highlighted residues are acidic and blue are basic. *P. textilis* refers to *P. textilis*.

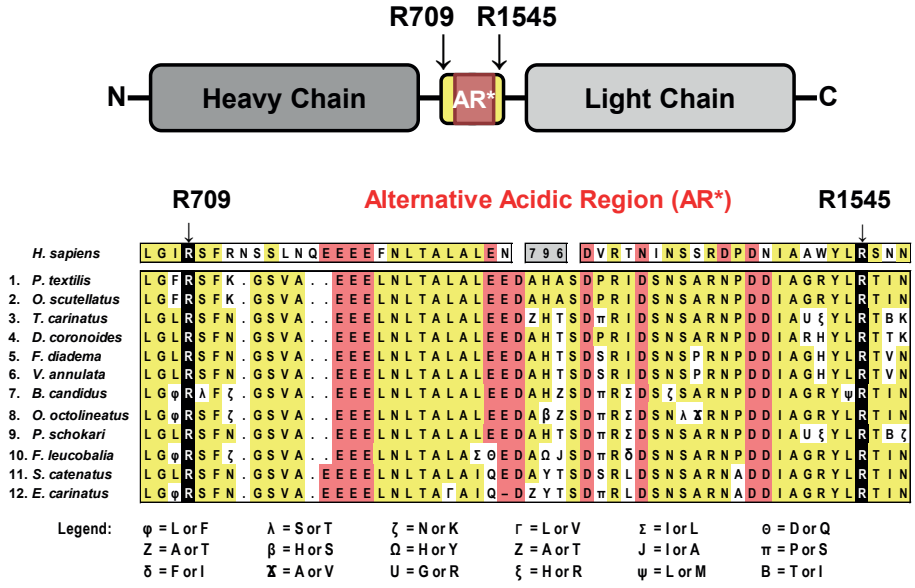

Figure 4. Sequence conservation within the truncated snake FV B-domains. ***Top:*** The truncated snake FV polypeptide chain is defined by an N-terminal heavy chain (A1-A2 domains; dark grey), a short central B-domain (± 46 residues; yellow) and a C-terminal light chain (A3-C1-C2 domains; light grey). The short B-domain retains the first (R709) and third (R1545) thrombin/FXa cleavage motifs and an alternative Acidic Region (AR*) that is represented by a red box. ***Bottom:*** Amino acid alignment of the R709 and R1545 thrombin cleavage motifs, for which the mature human FV residue numbering is used, and the putative AR* in truncated snake FV sequences as identified through sequencing of the ±600 bp amplicons from twelve snake species. The human FV B-domain sequence is shown for reference purposes, and the number within the grey box denotes the number of amino acids of the full-length human B-domain sequence that are not shown here. Greek letters represent amino acid discrepancies between the truncated B-domain sequence (this figure) and the regular B-domain sequence (**Figure 3)** of the same species, which are defined in the legend below the figure. Highlighted residues (yellow, red, or blue) represent identical or highly homologous amino acids at a particular location. Red highlighted residues are acidic and blue are basic. *P. textilis* refers to *P. textilis*.

Putative splice sites enable alternative splicing of the snake factor V B-domain

In order to investigate whether alternative splicing might account for the generation of a truncated B-domain transcript, we performed spliceosome analysis using the online splice site finder tool HSF [18]. Splice site analysis annotated several pre-mRNA exonic splicing enhancer motifs within the full-length snake B-domain transcripts. One such motif included a sequence that is typical for splicing in which the SRp40 protein assists, which was conserved in most of the species. Importantly, we observed that the precise location of the donor-acceptor sites was similar in each snake full-length B-domain transcript (**Figure 5**) and corresponded exactly with the sequence of the 600 bp fragments. Specifically, the snake FV sequence that is retained after putative splicing at the donor splice site precisely overlapped with the first part of the AR* sequence (AHAS, **Figure 4**). Similarly, the sequence that was retained after putative splicing at the acceptor splice site exactly matched the second part of the AR* sequence (DPRI, **Figure 4**). These findings suggest evolutionary conservation of the donor-acceptor motif in the B-domain of snake FV. Of note, this specifc donor-acceptor motif was not conserved in *O. octolineatus* and *E. carinatus* (**Figure 5**). Given that the truncated B-domain transcript was clearly identified in both of these snakes (**Figure 2A,B**), additional verification of these two B-domain sequences is required. Finally, as SR proteins involved in splicing are generally conserved among vertebrates [27, 28], spliceosome analysis was also performed on human, mouse, and anole lizard FV B-domain sequences. However, analogous exonic splicing enhancer motifs were not found within these sequences (data not shown).

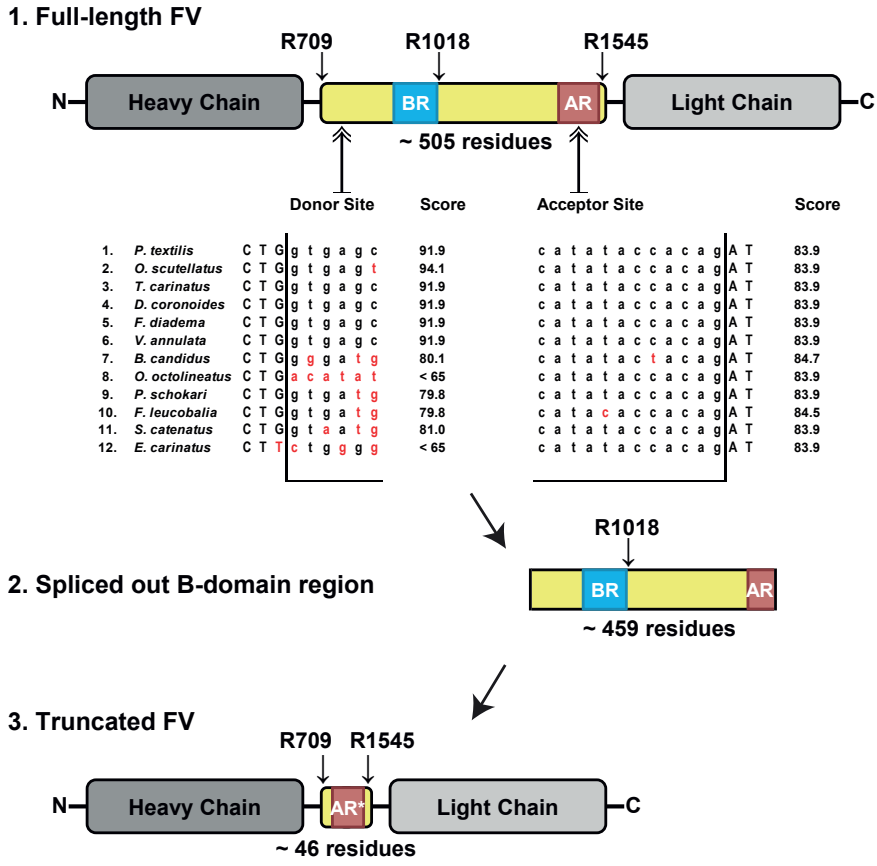

Figure 5. Putative SRp40-assisted donor and acceptor splices in the B-domain of snake FV. ***1:*** Splice site analysis of the full-length snake FV B-domain cDNA sequence revealed a putative donor site splice located C-terminal to the R709 cleavage site and a putative acceptor splice site located within the AR. The donor and acceptor splice sites are shown in the sequence alignment, dissimilar nucleotides are highlighted in red, and capital letters indicate sequences retained after splicing. Splice site probability scores assigned by HSF are specified, with the threshold for a putative donor or acceptor splice site being defined at 65; each HSF score above the threshold is considered a splice site. ***2:*** The regulatory B-domain elements that are lost after splicing of the snake FV transcript include the complete BR, the R1018 cleavage site, and part of the AR. ***3:*** The truncated snake FV transcript contains the R709 and R1545 cleavage consensus sites and an alternative acidic region (AR*) formed by a stretch of ±22 amino acids C-terminal to the R709 site and the last ±13 amino acid of the consensus AR (see **Figure 4)**. The mature human FV residue numbering is used to denote the thrombin/FXa cleavage motifs. *P. textilis* refers to *P. textilis*.

Discussion

In this study we have uncovered that the liver transcriptome of the Australian snake *P. textilis* contains two unique transcripts of FV. One transcript comprises a newly identified (full-length) FV sequence that includes a B-domain which contains all of the essential auto-inhibitory elements that comprise the FV PRR [7, 8]. Similar full-length FV B-domain transcripts were also identified in snakes from separate families, geographic regions, and venomous vs. non-venomous states, which suggest that the B-domain has been preserved as potential regulator of FV activity in all members of the suborder Serpentes. Similarly structured FV cDNAs have been found in all vertebrates, from fish to mammals. The other transcript incorporated a small ~46 amino acid B-domain sequence that is similar to the truncated B-domain FV sequence previously described for liver-expressed *P. textilis* FV [13, 15]. Remarkably, these small B-domain species share high sequence homology with the truncated B-domain from the FV-like component that is found in the venom of *P. textilis*, *O. scutellatus*, and *Oxyuranus microlepidotus* [13, 29, 30].

Through the use of bioinformatics we were able to identify the SRp40 pre-RNA splicing protein as a potential candidate for mediating the alternative splicing of the full-length snake FV B-domain sequence. Importantly, the location of the associated splice junction was similar in each B-domain sequence and corresponded to the exact sequence of the truncated B-domain. From these results we infer that the truncated FV B-domain transcript was generated through an alternative splicing event. Interestingly, apart from the full-length and truncated FV sequence, we also detected a B-domain amplicon of approximately 1600 bp in PCR reactions on *P. textilis* and *O. scutellanus* cDNA (**Figure 1**). While these amplicons might be the result of primer promiscuity or heteroduplex formation between the 2000 and 600 bp amplicon, they could alternatively represent less abundant FV splicing variants. Interestingly, a *P. textilis* venom gland transcriptome analysis performed by Viala et al. identified another splice variant of venom FV [31]. This splice variant was also detected at the protein level and comprised a unique A3-domain insertion of 34 residues upstream from the annealing site of our reverse primer (A3-R1; Table 1) used in cDNA amplification (**Figure 1**). The fact that this FV variant was not identified in the current study is not unexpected as we studied liver transcripts. In addition, it may be related to the general notion that venom genes undergo alternative splicing and accelerated evolution to give rise to a diverse toxin repertoire [32].

Quantitative analyses have shown that the full-length FV transcripts were more abundant than the truncated versions in most snake liver tissues. However, both transcripts were expressed at almost equal ratios in *P. textilis* and *O. scutellatus* (**Table 2**), which are those elapids that comprise truncated FV in their venom.

These results may be indicative of a link between the expression levels of truncated FV variants in the liver and venom gland [21]. On the other hand, our findings indicate that the truncated B-domain FV transcript was most abundant in liver tissue from the two viperid snakes, which have not been reported to comprise FV as toxin in their venom. At present, we have no explanation for this finding, other than that the Elapidae and Colubridae (including the families Psammophiidae and Homalopsidae, which were until recently considered colubrids) are evolutionarily closer (median distance of 50 million years) relative to the Viperidae (median distance of 57.5 million years to both Elapidae and Colubridae) [24]. We speculate that the Viperidae may have undergone a divergent molecular evolution, which could have resulted in different transcript profiles and abundances. However, clear evidence for this assumption is lacking thus far. Furthermore, recent studies into the venom toxins of the genus *Pseudonaja* have revealed an intricate link between venom FV expression and genus [33], geographic location [34], ontogenetic dietary shifts [35], and dietary niches [36]. A number of these factors might also affect the expression and alternative splicing of the liver FV transcript in *P. textilis* or possibly in other snake species. However, additional information on expression levels of blood coagulation factors in snakes is presently not available.

Recent studies have highlighted the significance of alternatively spliced human FV variants in the regulation of tissue factor pathway inhibitor (TFPI), a key regulatory plasma protein of the prothrombinase complex. It was shown that a splice variant of human FV, known as FV-short in which part of the B-domain comprising the BR is spliced out, interacts with TFPI through the AR region in the FV B-domain [37-39]. As we have previously shown that the truncated B-domain FV variant from *P. textilis* displays full cofactor activity [40] and makes up ~25-30% of total FV in *P. textilis* (**Figure 2B**), this would suggest that approximately one third of circulating FV species exist in an active cofactor state in *P. textilis*. As such, our findings could allude to an alternative mode of FV regulation in snakes. In this respect, it is attractive to consider TFPI as a regulator of truncated B-domain FV, potentially by interacting with the highly acidic stretch of amino acids that forms the AR* [39]. However, it remains unclear whether the truncated B-domain snake FV transcript is translated into a plasma protein. Additional research is therefore required to confirm the physiological presence of FV species in snake plasma and to assess plasma levels of key regulatory proteins of FV, such as TFPI.

In summary, we have revealed the presence of two distinct FV transcripts in the liver transcriptome of three major families of the suborder Serpentes: a full-length B-domain transcript that includes all putative regulatory B-domain elements and a truncated B-domain transcript that lacks these essential B-domain sequences. Online database search tools show that alternative splicing of the full-length FV transcript likely accounts for the presence of the truncated FV transcript in liver

tissues. Overall, these findings suggest that the snake FV gene has undergone unique functional adaptations, potentially in response to the extreme physiological and phenotypic adaptations that are typical to snakes [16, 41].

References

1. Jiang, Y. and R.F. Doolittle, *The evolution of vertebrate blood coagulation as viewed from a comparison of puffer fish and sea squirt genomes.* Proc Natl Acad Sci U S A, 2003. **100**(13): p. 7527-32.
2. Davidson, C.J., et al., *Molecular evolution of the vertebrate blood coagulation network.* Thromb Haemost, 2003. **89**(3): p. 420-8.
3. Suzuki, K., B. Dahlback, and J. Stenflo, *Thrombin-catalyzed activation of human coagulation factor V.* J Biol Chem, 1982. **257**(11): p. 6556-64.
4. Jenny, R.J., et al., *Complete cDNA and derived amino acid sequence of human factor V.* Proc Natl Acad Sci U S A, 1987. **84**(14): p. 4846-50.
5. Corral-Rodriguez, M.A., et al., *Structural basis of thrombin-mediated factor V activation: the Glu666-Glu672 sequence is critical for processing at the heavy chain-B domain junction.* Blood, 2011. **117**(26): p. 7164-73.
6. Schuijt, T.J., et al., *Factor Xa activation of factor V is of paramount importance in initiating the coagulation system: lessons from a tick salivary protein.* Circulation, 2013. **128**(3): p. 254-66.
7. Bos, M.H. and R.M. Camire, *A bipartite autoinhibitory region within the B-domain suppresses function in factor V.* J Biol Chem, 2012. **287**(31): p. 26342-51.
8. Bunce, M.W., et al., *Restoring the procofactor state of factor Va-like variants by complementation with B-domain peptides.* J Biol Chem, 2013. **288**(42): p. 30151-60.
9. Mann, K.G., et al., *Surface-dependent reactions of the vitamin K-dependent enzyme complexes.* Blood, 1990. **76**(1): p. 1-16.
10. Rosing, J., et al., *The role of phospholipids and factor Va in the prothrombinase complex.* J Biol Chem, 1980. **255**(1): p. 274-83.
11. Rao, V.S. and R.M. Kini, *Pseutarin C, a prothrombin activator from Pseudonaja textilis venom: its structural and functional similarity to mammalian coagulation factor Xa-Va complex.* Thromb Haemost, 2002. **88**(4): p. 611-9.
12. Lechtenberg, B.C., et al., *Crystal structure of the prothrombinase complex from the venom of Pseudonaja textilis.* Blood, 2013. **122**(16): p. 2777-83.
13. Rao, V.S., S. Swarup, and R.M. Kini, *The nonenzymatic subunit of pseutarin C, a prothrombin activator from eastern brown snake (Pseudonaja textilis) venom, shows structural similarity to mammalian coagulation factor V.* Blood, 2003. **102**(4): p. 1347-54.
14. Bos, M.H., et al., *Venom factor V from the common brown snake escapes hemostatic regulation through procoagulant adaptations.* Blood, 2009. **114**(3): p. 686-92.
15. Minh Le, T.N., et al., *Gene duplication of coagulation factor V and origin of venom prothrombin activator in Pseudonaja textilis snake.* Thromb Haemost, 2005. **93**(3): p. 420-9.
16. Vonk, F.J., et al., *The king cobra genome reveals dynamic gene evolution and adaptation in the snake venom system.* Proc Natl Acad Sci U S A, 2013. **110**(51): p. 20651-6.

17. Livak, K.J. and T.D. Schmittgen, *Analysis of relative gene expression data using real-time quantitative PCR and the 2(-Delta Delta C(T)) Method.* Methods, 2001. **25**(4): p. 402-8.
18. Desmet, F.O., et al., *Human Splicing Finder: an online bioinformatics tool to predict splicing signals.* Nucleic Acids Res, 2009. **37**(9): p. e67.
19. Flicek, P., et al., *Ensembl 2013.* Nucleic Acids Res, 2013. **41**(Database issue): p. D48-55.
20. Wilkins, M.R., et al., *Protein identification and analysis tools in the ExPASy server.* Methods Mol Biol, 1999. **112**: p. 531-52.
21. Masci, P.P., A.N. Whitaker, and J. de Jersey, *Purification and characterization of a prothrombin activator from the venom of the Australian brown snake, Pseudonaja textilis textilis.* Biochem Int, 1988. **17**(5): p. 825-35.
22. Speijer, H., et al., *Prothrombin activation by an activator from the venom of Oxyuranus scutellatus (Taipan snake).* J Biol Chem, 1986. **261**(28): p. 13258-67.
23. Joseph, J.S., et al., *Amino acid sequence of trocarin, a prothrombin activator from Tropidechis carinatus venom: its structural similarity to coagulation factor Xa.* Blood, 1999. **94**(2): p. 621-31.
24. Kumar, S., et al., *TimeTree: A Resource for Timelines, Timetrees, and Divergence Times.* Mol Biol Evol, 2017. **34**(7): p. 1812-1819.
25. Kornalik, F. and B. Blomback, *Prothrombin activation induced by Ecarin - a prothrombin converting enzyme from Echis carinatus venom.* Thromb Res, 1975. **6**(1): p. 57-63.
26. Alfoldi, J., et al., *The genome of the green anole lizard and a comparative analysis with birds and mammals.* Nature, 2011. **477**(7366): p. 587-91.
27. Goren, A., et al., *Comparative analysis identifies exonic splicing regulatory sequences--The complex definition of enhancers and silencers.* Mol Cell, 2006. **22**(6): p. 769-81.
28. Lev-Maor, G., et al., *The "alternative" choice of constitutive exons throughout evolution.* PLoS Genet, 2007. **3**(11): p. e203.
29. Welton, R.E. and J.N. Burnell, *Full length nucleotide sequence of a factor V-like subunit of oscutarin from Oxyuranus scutellatus scutellatus (coastal Taipan).* Toxicon, 2005. **46**(3): p. 328-36.
30. St Pierre, L., et al., *Comparative analysis of prothrombin activators from the venom of Australian elapids.* Mol Biol Evol, 2005. **22**(9): p. 1853-64.
31. Viala, V.L., et al., *Venomics of the Australian eastern brown snake (Pseudonaja textilis): Detection of new venom proteins and splicing variants.* Toxicon, 2015. **107**(Pt B): p. 252-65.
32. Ogawa, T.a.S., H., *Venomics Study of Protobothrops flavoviridis Snake: How Venom Proteins Have Evolved and Diversified?* Medical Toxicology, 2020. DOI: 10.5772/intechopen.91960
33. Reeks, T., et al., *Deep venomics of the Pseudonaja genus reveals inter- and intra-specific variation.* J Proteomics, 2016. **133**: p. 20-32.
34. McCleary, R.J., et al., *Proteomic comparisons of venoms of long-term captive and recently wild-caught Eastern brown snakes (Pseudonaja textilis) indicate venom does not change due to captivity.* J Proteomics, 2016. **144**: p. 51-62.

35. Cipriani, V., et al., *Correlation between ontogenetic dietary shifts and venom variation in Australian brown snakes (Pseudonaja).* Comp Biochem Physiol C Toxicol Pharmacol, 2017. **197**: p. 53-60.
36. Skejic, J., *Venoms of related mammal-eating species of taipans (Oxyuranus) and brown snakes (Pseudonaja) differ in composition of toxins involved in mammal poisoning.* BioRxiv, 2018. DOI: 10.1101/378141
37. Vincent, L.M., et al., *Coagulation factor V(A2440G) causes east Texas bleeding disorder via TFPIalpha.* J Clin Invest, 2013. **123**(9): p. 3777-87.
38. Cunha, M.L., et al., *A novel mutation in the F5 gene (factor V Amsterdam) associated with bleeding independent of factor V procoagulant function.* Blood, 2015. **125**(11): p. 1822-5.
39. Wood, J.P., et al., *Tissue factor pathway inhibitor-alpha inhibits prothrombinase during the initiation of blood coagulation.* Proc Natl Acad Sci U S A, 2013. **110**(44): p. 17838-43.
40. Verhoef D., Y.X., Parthasarathy S., Reitsma P.H., Camire R.M., Bos M.H.A, *Functional implications of the unique disulfide bond in venom factor V from the Australian common brown snake Pseudonaja textilis.* Toxin Reviews, 2013. **33**(1-2): p. 37-41.
41. Castoe, T.A., et al., *The Burmese python genome reveals the molecular basis for extreme adaptation in snakes.* Proc Natl Acad Sci U S A, 2013. **110**(51): p. 20645-50.

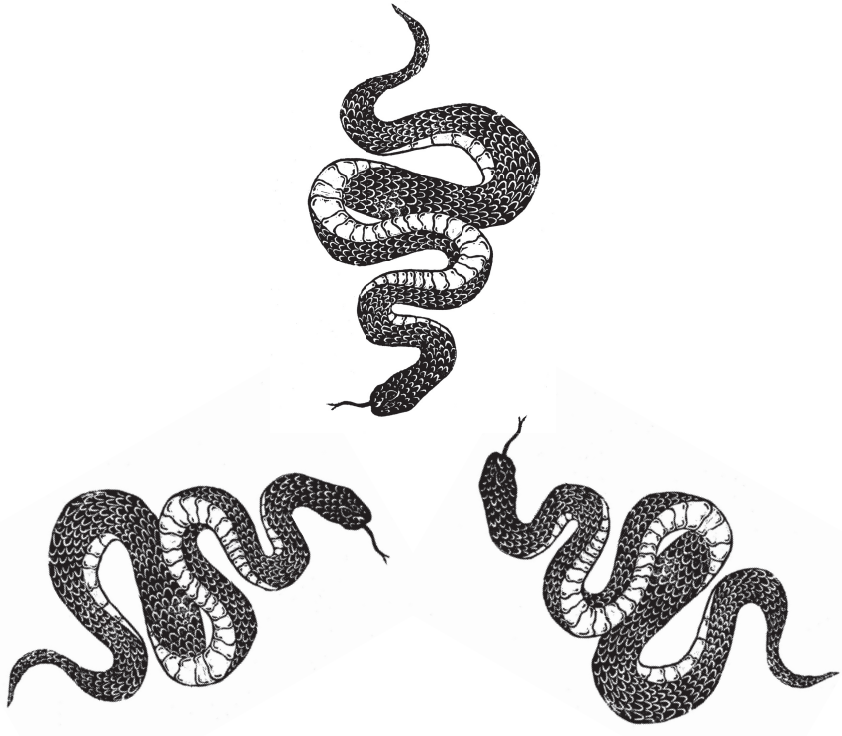

Chapter 3

Functional implications of the unique disulfide bond in venom factor V from the Australian common brown snake *Pseudonaja textilis*

Daniël Verhoef, Xiaoxun Yang, Sudarshan Parthasarathy, Pieter H. Reitsma, Rodney M. Camire, Mettine H.A. Bos.

Toxin Reviews, 2013. 33(1-2): p. 37-41

Abstract

The venom of the Australian brown snake *Pseudonaja textilis* contains a prothrombinase-like initiator of blood coagulation, which has evolved into a potent weapon through several gain-of-function adaptations. Here we examined the functional implications of a disulfide bond exclusively found in the factor (F)Va-like cofactor component, ptFV. We found that this remarkable structural feature is not required for the procoagulant properties of ptFV. The nearly identical liver-derived plasma ptFV that lacks this disulfide link displayed a similar procoagulant profile. Whether the unique disulfide bond imposes conformational constraints essential to other aspects of the venom FV life cycle remains to be determined.

Introduction

Many snake venoms contain toxins that disrupt the intricate balance between the pro- and anticoagulant mechanisms in blood (i.e. hemostasis), thereby effectively contributing to their lethal potency. One of these potent toxins that impacts hemostasis is the procoagulant prothrombin activator pseutarin C from the venom of the Australian common brown snake *Pseudonaja textilis* [1]. Consistent with the procoagulant nature of pseutarin C, *P. textilis* envenomation triggers venom-induced consumption coagulopathy, a rapid and systemic activation of blood coagulation resulting from uncontrolled turnover of prothrombin to thrombin that exhausts the coagulation system and can result in fatal bleedings [2, 3]. The prothrombin activating complex in *P. textilis* venom consists of a factor (F)Va- and FXa-like subunit, and structurally and functionally resembles the prothrombinase complex which is essential for thrombin formation during coagulation [4, 5].

The enzymatic activity of mammalian prothrombinase (FVa–FXa) is tightly controlled and follows from a sequential series of steps involving zymogen to protease and procofactor to cofactor transitions, and assembly of the macromolecular enzyme complex on a negatively charged phospholipid membrane surface [6, 7]. In contrast, the venom-derived prothrombinase-like complex, has escaped hemostatic control through several regulatory and structural modifications [1]. Making use of recombinant venom-derived *P. textilis* FV (ptFV), we have previously demonstrated that ptFV has uncoupled the preservation of the procofactor state and exists as a constitutively active cofactor through loss of B-domain sequences that autoinhibit FV cofactor function [8, 9]. We further uncovered that ptFV has bypassed the membrane-dependence of mammalian prothrombinase, as the *P.textilis* venom FV-FXa complex assembles and functions in solution [8]. Moreover, ptFV is functionally resistant to inhibition by the anticoagulant protease activated protein C (APC), despite APC-dependent proteolysis of its A2-domain [8]. These gain-of-function adaptations likely enable the enzyme to move unrestrained through the vasculature of the host and initiate indiscriminate clotting. Interestingly, since ptFV shares 99% sequence identity with its hemostatic counterpart that is expressed in the liver by a separate gene [10], this variant may comprise one or more of the features considered unique to ptFV.

Here we explore the functional linkage between the distinct procoagulant properties of ptFV and a disulfide bond covalently connecting its A2-A3 domains. This structural element is not conserved throughout vertebrate evolution, not even in liver ptFV, and is exclusive to ptFV [8]. Since the A2-A3 domains comprise binding regions for FXa and APC in human FV [11, 12], we examined the contribution of the disulfide bond to both the lipid-independent ptFVa-FXa activity and functional APC resistance of ptFV.

Material and Methods

Proteins

DAPA and human prothrombin, prethrombin-1, and APC were from Haematologic Technologies (Essex Junction, VT). Following synthesis (GenScript; Piscataway, NJ) of the base pairs encoding venom-derived *P. textilis* FXa (ptFXa) [13], recombinant ptFXa was prepared, purified, and characterized as described [14]. All functional assays were performed at 25°C in 20 mM Hepes, 0.15M NaCl, 5 mM $CaCl_2$, 0.1% polyethylene glycol 8000, pH 7.5.

Preparation of ptFV variants

Upon synthesis of the base pairs encoding venom-derived (ptFV) or liver-derived (ptFV-liver) P. textilis FV [10, 15], recombinant FV was prepared, purified and characterized [8]. The variants ptFV-SS and ptFV-liver-CC (**Figure 1A**) were generated employing mutagenic complementary oligonucleotides as described (Bos et al., 2009). Protein purity was assessed by SDS-PAGE using pre-cast 4%–12% gradient gels and the MOPS buffer system (Invitrogen; Carlsbad, CA). For pretreatment with thrombin, FV variants (1000 nM) were incubated at 37°C for 15 min with 50nM thrombin.

Macromolecular substrate activation

Steady-state initial velocities of macromolecular substrate cleavage were determined discontinuously at 25°C as described [14]. For progress curves of prethombin-1 activation, PCPS (50 μM; 75:25 w/w) [16], DAPA (10 μM), and prethrombin-1 (1.4 μM) were incubated with the various ptFV variants (1.0 nM), and the reaction was initiated with ptFXa (0.1 nM).

APC inactivation of ptFV variants

Inactivation of the various proteins (500 nM; ptFV, ptFV-SS, ptFV-liver or ptFV-liver-CC) in the presence of PCPS (50 μM) was initiated by APC (750 nM). Aliquots of the reaction mixture were withdrawn at the indicated time intervals and analyzed by SDS-PAGE and through assessment of the residual FV cofactor activity in prothrombin activation. Assay mixtures contained prothrombin (1.4 μM), PCPS (50 μM), DAPA (10 μM), FV (1.0 nM), ptFXa (0.1 nM), and prothrombin activation was determined as described under the section ''Macromolecular substrate activation''.

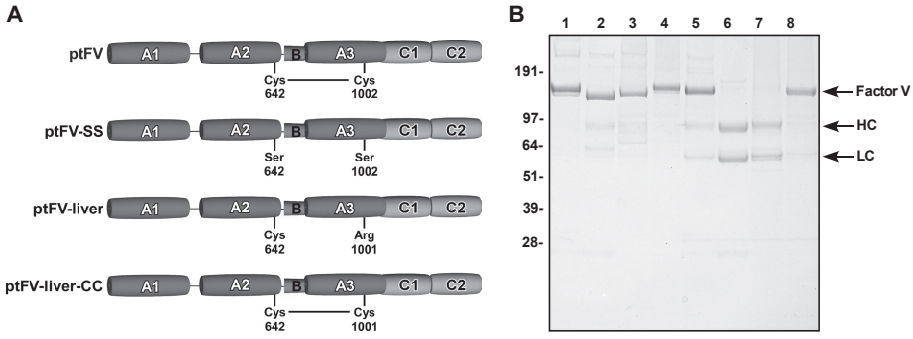

Figure 1. Schematic representation and SDS-PAGE analysis of rFV variants. (***A***) The common A1-A2-B-A3-C1-C2 domain structure of the recombinant *P. textilis* FV variants used in this study is shown schematically. Venom-derived *P. textilis* FV (ptFV) harbors a disulfide bond mediated by Cys642 and Cys1002 that covalently connects the A2 and A3 domains. In ptFV-SS, these Cys are substituted for Ser (Cys642Ser and Cys1002Ser). Liver-derived *P. textilis* FV (ptFV-liver) comprises an Arg at the position homologous to venom FV residue 1002, and in ptFV-liver-CC this region is modified to resemble venom FV (Arg1001Cys and Ala1002Glu). (***B***) Purified proteins (3µg/lane) were subjected to SDS-PAGE under nonreducing conditions and visualized by staining with Coomassie Brilliant Blue R-250. Lane 1, ptFV; lane 2, ptFV-SS; lane 3, ptFV-liver; lane 4, ptFV; lane 5, ptFV plus thrombin; lane 6, ptFV-SS plus thrombin; lane 7, ptFV-liver plus thrombin; lane 8, ptFV-liver-CC plus thrombin. The single-chain FV species ('factor V'), the heavy ('HC') and light ('LC') chains of the heterodimeric cofactor FVa, and the apparent molecular weights of the standards are indicated.

Results

SDS-PAGE analysis of ptFV variants

Recent crystallization of ptFV not only confirmed our earlier observation that the A2 and A3 domains are covalently linked via a Cys-Cys bond, but also disclosed the identity of the cysteines involved (Cys642-Cys1002) [17]. To assess the putative allosteric contribution of the A2-A3 link to the unique procoagulant features of ptFV, we eliminated this connection from ptFV by substituting the cysteines involved for serines (ptFV-SS; **Figure 1A**). In addition, we generated liver-expressed FV required for normal *P. textilis* hemostasis (ptFV-liver) that, despite being almost identical to ptFV, does not comprise a homologous A3-domain cysteine. The latter was introduced in ptFV-liver-CC to facilitate disulfide linkage similar to ptFV. Absence of the disulfide bond in ptFV-SS and ptFV-liver was confirmed by nonreducing SDS-PAGE analysis as demonstrated by the characteristic FVa heterodimer subsequent to thrombin activation, whereas ptFV and ptFV-liver-CC predominantly migrated as a single-chain species similar to the untreated molecules (**Figure 1B**).

Role of the disulfide bond in prethrombin-1 conversion

The ptFV variants were functionally assessed in the presence and absence of anionic phospholipids to examine whether the structural disulfide bond is linked to the remarkable ability of the venom-derived *P. textilis* FV-FXa complex to function in solution. To rule out the contribution of substrate-membrane binding to the rates of substrate conversion, we assayed activation of the prothrombin derivative prethrombin-1. Since prethrombin-1 lacks the membrane binding Gla and kringle-1 domains [18], lipid binding is not required for its efficient conversion to thrombin. All FV variants stimulated prethrombin-1 activation in an identical manner, irrespective of the availability of anionic membranes (**Table 1**). The apparent lack of loss- or gain-of-functions following either elimination or introduction of the Cys-Cys link suggests that the latter is not a functional requirement for the lipid-independent cofactor function of ptFV. Moreover, these data reveal that similar to venom FV, ptFV-liver exists as a constitutively active cofactor that is able to function in the absence of a lipid surface.

Table 1. Prethrombin-1 activation

Cofactor Species	**Initial Velocity [a] *+ PCPS***	**Initial Velocity [a] *- PCPS***
	nM IIα/min/ nM Enzyme	*nM IIα/min/ nM Enzyme*
ptFV	182 ± 19	197 ± 23
ptFV-SS	163 ± 1	220 ± 9
ptFV-liver	184 ± 35	181 ± 48
ptFV-liver-CC	166 ± 8	183 ± 5

[a] The initial velocity of thrombin generation (nM IIα/min/nM Enzyme) was determined as described in 'Materials and methods'. The mean values ± S.D. of at least two independent determinations are presented.

Role of the disulfide bond in functional APC resistance

We next determined whether removal of the unique disulfide bond in ptFV would affect its functional resistance to APC. Using high APC concentrations, all ptFV variants were proteolyzed at the previously identified APC cleavage sites Lys507 and Arg742, which are equivalent to the human Arg506 and Arg709 sites (**Figure 2A,C**) [8]. As anticipated, whereas the ptFV $A2_C$ and B-A3-C1-C2 fragments are held together by the A2-A3 connection, these proteolysis products are not covalently linked in the absence of the disulfide bond (**Figure 2A**). Interestingly, the $*A2_C$ fragment is lacking in APC-treated ptFV-liver, suggesting that the associated cleavage site is not available in this variant. To our surprise, full cofactor activity was retained following APC cleavage for all ptFV variants, including liver-derived ptFV (**Figure 2B**), even though hemostatic FV is generally assumed to be subject to APC-dependent downregulation *in vivo*. Further evaluation of the endogenous regulatory mechanisms is currently hampered by the lack of information on *P. textilis* APC. Overall, these findings indicate that not the covalent A2-A3 link, but noncovalent interactions likely stabilize the $A2_C$ fragment such that APC-treated *P. textilis* FV remains fully functional.

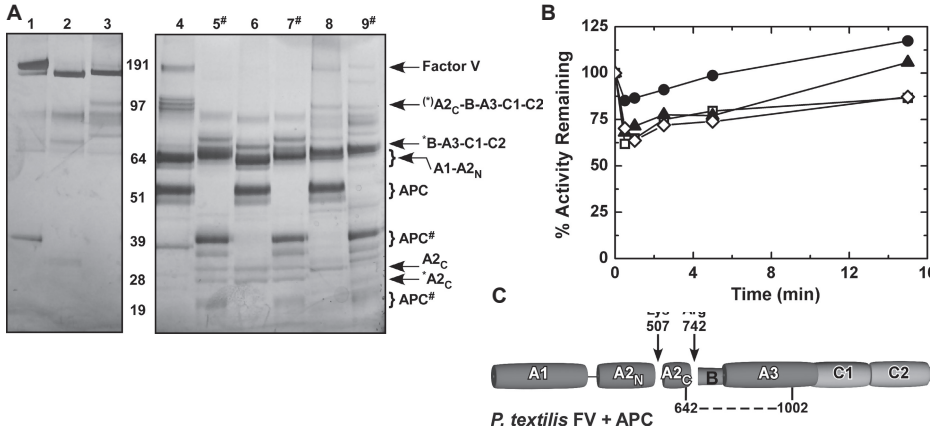

Figure 2. Inactivation of rFV variants by APC. Reaction mixtures containing 50 µM PCPS and 500 nM ptFV (-●-), ptFV-SS (-□-),ptFV-liver (-▲-), or ptFV-liver-CC (-◊-) were incubated with 750 nM APC. At selected time intervals, samples were removed for cofactor activity (***B***) or SDS-PAGE under nonreducing (lanes 1-4) or reducing (lanes 5-8) conditions and visualized by silver staining (1µg/lane; t=15min.; ***A***). Lanes 1,5, ptFV plus APC; lanes 2,6, ptFV-SS plus APC; lanes 3,7, ptFV-liver plus APC; lanes 4,8, ptFV-liver-CC plus APC. Protein bands are annotated according to the scheme in panel C: $A2_C$-B-A3-C1-C2, 508-1430; B-A3-C1-C2, 743-1430; A1-$A2_N$, 1-507; $A2_C$ 508-742. Fragments denoted by * comprise and additional cleavage site at their C-terminal ends. APC can be visualized under nonreducing an reducing conditions (#) as indicated. The functional measurements and gels are representative of two similar experiments.

Discussion

A hallmark of the macromolecular enzyme complexes involved in blood coagulation is their functional assembly on anionic membranes, which localizes the enzyme to a physiological cell surface and dramatically reduces the reaction dimensions and complexity of the assembly process (e.g. 1000-fold enhanced affinity for mammalian FVa-FXa) [19, 20]. Venom ptFV-FXa has escaped this regulatory requirement, which is likely induced through a variety of changes in the primary structure. Our functional assessment of the A2-A3 domain disulfide link unique to ptFV revealed that it is not at the basis of the lipid-independent cofactor function. This concurs with observations made in the human system suggesting that introduction of a homologous Cys-Cys link does not promote soluble FVa-FXa activity [21]. Functional analysis of other structural variations in ptFV or ptFXa may provide insight in this enigma [22].

Previously, we speculated that the ptFV disulfide bond stabilizes ptFV and prevents APC-mediated dissociation of the A2c fragment [8]. In the current study we showed that *P. textilis* FV variants either comprising or lacking this covalent link all proved functionally resistant to APC. This implies that a role for the disulfide bond in stabilization of the A2c fragment seems marginal at most. Whether the disulfide bond imposes conformational constraints essential to other aspects of the FV life cycle remains to be determined. Interestingly, sequence analysis revealed that a site homologous to the human APC cleavage site Arg306 is absent in both liver and venom *P. textilis* FV and is only preserved in mammals. In the mammalian system, cleavage at Arg506 results in partial (~80%) loss of cofactor activity while the A2C fragment is retained [23]. Following Arg306 cleavage, FVa activity is completely lost due to A2-domain dissociation. Our observations on *P. textilis* FV cleaved at the position homologous to residue 506 demonstrated no significant loss of FV cofactor activity, thereby indicating that the A2c fragment is stabilized within the A2-A3 domain structure. Thus far we can only speculate if this structural and functional integrity results from noncovalent interactions only, or whether binding of venom ptFXa may contribute as well.

Using liver-derived ptFV that is nearly identical to its venom counterpart but lacks the Cys-Cys link, we uncovered that this variant shares the remarkable procoagulant features initially observed for venom ptFV. Liver ptFV appears to circulate in an active, cofactor state, can function in solution when assayed with venom ptFXa, and is functionally resistant to APC. The implications for normal coagulation in P. textilis are unclear at this point, but considering that FV can only function in the presence of the liver-derived protease FXa that is assumed to require membrane binding for its activity, the likelihood of unregulated initiation of coagulation is minimal. To compensate for the apparent functional inconsequence

of APC, termination of clotting may be more dependent on coagulation inhibitors such as tissue factor pathway inhibitor-α which is modulated by FV in the human system [24]. Taken together, these findings invoke fundamental questions on the nature of the hemostatic regulatory processes in evolutionary distinct vertebrates.

References

1. Bos, M.H. and R.M. Camire, *Procoagulant adaptation of a blood coagulation prothrombinase-like enzyme complex in australian elapid venom.* Toxins (Basel), 2010. **2**(6): p. 1554-67.
2. Masci, P.P., A.N. Whitaker, and J. de Jersey, *Purification and characterization of a prothrombin activator from the venom of the Australian brown snake, Pseudonaja textilis textilis.* Biochem Int, 1988. **17**(5): p. 825-35.
3. Sutherland S, T.J., *Australian animal toxins: the creatures, their toxins and care of the poisoned patient.* . Melbourne, Australia: Oxford University Press, 2001.
4. Rao, V.S. and R.M. Kini, *Pseutarin C, a prothrombin activator from Pseudonaja textilis venom: its structural and functional similarity to mammalian coagulation factor Xa-Va complex.* Thromb Haemost, 2002. **88**(4): p. 611-9.
5. Speijer, H., et al., *Prothrombin activation by an activator from the venom of Oxyuranus scutellatus (Taipan snake).* J Biol Chem, 1986. **261**(28): p. 13258-67.
6. Krishnaswamy, S., *Prothrombinase complex assembly. Contributions of protein-protein and protein-membrane interactions toward complex formation.* J Biol Chem, 1990. **265**(7): p. 3708-18.
7. Camire, R.M. and M.H. Bos, *The molecular basis of factor V and VIII procofactor activation.* J Thromb Haemost, 2009. **7**(12): p. 1951-61.
8. Bos, M.H., et al., *Venom factor V from the common brown snake escapes hemostatic regulation through procoagulant adaptations.* Blood, 2009. **114**(3): p. 686-92.
9. Bos, M.H. and R.M. Camire, *A bipartite autoinhibitory region within the B-domain suppresses function in factor V.* J Biol Chem, 2012. **287**(31): p. 26342-51.
10. Minh Le, T.N., et al., *Gene duplication of coagulation factor V and origin of venom prothrombin activator in Pseudonaja textilis snake.* Thromb Haemost, 2005. **93**(3): p. 420-9.
11. Segers, K., et al., *Identification of surface epitopes of human coagulation factor Va that are important for interaction with activated protein C and heparin.* J Biol Chem, 2008. **283**(33): p. 22573-81.
12. Lee, C.J., S. Wu, and L.G. Pedersen, *A proposed ternary complex model of prothrombinase with prothrombin: protein-protein docking and molecular dynamics simulations.* J Thromb Haemost, 2011. **9**(10): p. 2123-6.
13. Rao, V.S., S. Swarup, and R. Manjunatha Kini, *The catalytic subunit of pseutarin C, a group C prothrombin activator from the venom of Pseudonaja textilis, is structurally similar to mammalian blood coagulation factor Xa.* Thromb Haemost, 2004. **92**(3): p. 509-21.
14. Camire, R.M., *Prothrombinase assembly and S1 site occupation restore the catalytic activity of FXa impaired by mutation at the sodium-binding site.* J Biol Chem, 2002. **277**(40): p. 37863-70.

15. Rao, V.S., S. Swarup, and R.M. Kini, *The nonenzymatic subunit of pseutarin C, a prothrombin activator from eastern brown snake (Pseudonaja textilis) venom, shows structural similarity to mammalian coagulation factor V.* Blood, 2003. **102**(4): p. 1347-54.
16. Higgins, D.L. and K.G. Mann, *The interaction of bovine factor V and factor V-derived peptides with phospholipid vesicles.* J Biol Chem, 1983. **258**(10): p. 6503-8.
17. Kumar S., S.S., Huntington JA., et al., *High resolution X-ray structure of snake venom factor V: evolution of a hemostatic cofactor to a toxin poised to inflict maximal damage to mammalian blood coagulation.* Blood (ASH 2011 Meeting Abstracts) 118:375., 2011.
18. KG., M., *Prothrombin.* Methods Enzymol, 45, 123-56., 1976.
19. Krishnaswamy, S., K.C. Jones, and K.G. Mann, *Prothrombinase complex assembly. Kinetic mechanism of enzyme assembly on phospholipid vesicles.* J Biol Chem, 1988. **263**(8): p. 3823-34.
20. Mann, K.G., et al., *Surface-dependent reactions of the vitamin K-dependent enzyme complexes.* Blood, 1990. **76**(1): p. 1-16.
21. Verhoef D., C.R.M., Reitsma P.H., Bos M.H.A., *Functional characterization of a structural element unique to venom factor V from the Australian common brown snake Pseudonaja textilis.* J Thromb Haemost (ISTH 2013 Meeting Abstracts) 11(S2):AS 36.3., 2013.
22. Lechtenberg, B.C., et al., *Crystal structure of the prothrombinase complex from the venom of Pseudonaja textilis.* Blood, 2013. **122**(16): p. 2777-83.
23. Mann, K.G., et al., *Activated protein C cleavage of factor Va leads to dissociation of the A2 domain.* J Biol Chem, 1997. **272**(33): p. 20678-83.
24. Duckers, C., et al., *Low plasma levels of tissue factor pathway inhibitor in patients with congenital factor V deficiency.* Blood, 2008. **112**(9): p. 3615-23.

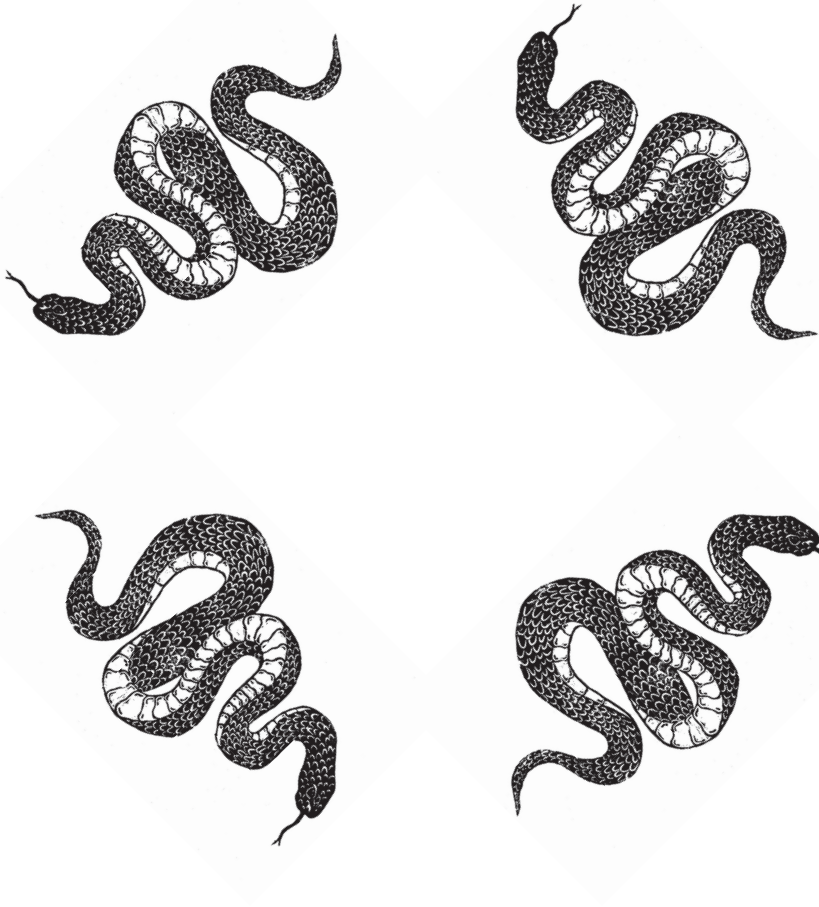

Chapter 4

Functional crosstalk between the A- and C-domains of blood coagulation factor V modulates phospholipid binding and cofactor stability

Daniël Verhoef, Gerry A.F. Nicolaes, Roy Schrijver, Pieter H. Reitsma, and Mettine H.A. Bos.

Manuscript in preparation

Abstract

Activated blood coagulation factor V (FVa) is an inherently unstable cofactor that is essential in the conversion of prothrombin to thrombin by factor Xa (FXa). In order to interact with FXa and prothrombin, FVa requires interaction with anionic phospholipid membranes via its two C-domains. Interestingly, the venom of the Australian snake *Pseudonaja textilis* contains a highly stable FVa-like homolog (ptFV) that is known to bind venom-derived FXa in the absence of a membrane surface. Moreover, ptFV has lost the ability to bind membranes, despite structural conservation of the C-domain pair. Here, we have explored the functional relationship between cofactor stability and phospholipid binding by exchanging the C-domains between constitutively active B-domainless human FV (hFV) and ptFV, and expressing, purifying and characterizing the chimeric variants hFV-ptC and ptFV-hC. Differential scanning calorimetry analysis and cofactor activity decay rate experiments revealed that the C-domain exchange adversely affected cofactor stability in ptFV-hC relative to ptFV, yet enhanced the stability of hFV-ptC relative to human FV. Furthermore, surface plasmon resonance analysis showed that the A-domains of human FV enabled phospholipid binding by the C-domains of ptFV. On the other hand, phospholipid binding by the human C-domains was reduced when linked to the A-domains of ptFV. In conclusion, our study has shown functional crosstalk between the A-domain trimer and C-domain pair of FV with regard to anionic phospholipid binding and cofactor stability. These findings provide novel insights into the multi-domain relationships that govern FVa cofactor function.

Introduction

Blood coagulation factor V (FV) is an essential cofactor in the conversion of prothrombin to thrombin, the latter converting soluble fibrinogen into insoluble strands of fibrin that serve to stabilize the platelet-based primary blood clot. The conversion of prothrombin is catalyzed by the prothrombinase complex, which is a macromolecular complex consisting of activated factor V (FVa) and activated factor X (FXa) that assembles on a negatively charged membrane surface in the presence of calcium ions [1]. FV circulates in blood as a 330 kDa single-chain inactive procofactor (domain organization A1-A2-B-A3-C1-C2) and is structurally homologous to blood coagulation factor VIII (FVIII) [2]. Activation of FV proceeds via limited proteolysis of its central B-domain by either (meizo)thrombin or FXa, which results in the removal of inhibitory sequences and exposure of the binding sites for FXa and prothrombin [3-6]. Once activated, the cofactor Va radically increases the catalytic rate of the serine protease FXa towards prothrombin [1].

Binding of FVa to an anionic phospholipid membrane is a prerequisite for productive interactions between the cofactor, FXa and prothrombin as it increases the binding affinity of FVa for FXa to a physiologically relevant concentration and facilitates docking of prothrombin onto the assembled prothrombinase complex [7, 8]. The discoidin-like C-domains of FVa coordinate binding to anionic phosphatidylserine (PS)-containing membranes through hydrophobic and electrostatic interactions between the net-negatively charged phospholipid membrane and the positively charged C-domains [9, 10]. It is generally acknowledged that FVa is anchored onto the phospholipid surface through dedicated phosphatidylserine-binding residues that are located on separate membrane binding loops, or so-called "spikes", which protrude from the base of each C-domain [10-15]. Additional studies indicate that the membrane-bound C-domain pair provides support for the three A-domains of FVa, which are arranged on top of the C-domains and engage with FXa and prothrombin [16-20]. Nevertheless, the exact structural arrangement of the C-domain pair relative to that of the A-domain trimer remains ambiguous [17, 18, 21]. In addition, it remains to be determined whether membrane binding is exclusively governed by the C-domains and/or whether the previously observed crosstalk between the C-domain pair and A-domain trimer may also affect the interaction of FV with an anionic surface [15].

The venom of the Australian snake *Pseudonaja textilis* (*P. textilis*) contains a weaponized homolog of FVa (ptFV) that is constitutively active and is able to bind a FXa homolog found in the same venom (ptFXa) with high affinity in the absence a phospholipid surface [22, 23], unlike any FVa species known to date. In addition, ptFV has been reported to display significantly reduced binding to phosphatidylserine-containing membranes [24]. The multi-domain structure of

ptFV is nonetheless identical to human FVa, as it consists of three A-domains and two C-domains that are organized in a configuration resembling membrane-bound FVa [18, 20, 22, 25]. Previously, we have reported that ptFV is functionally highly stable, as it retains cofactor activity upon extended proteolytic processing by the endogenous enzymatic regulator of FVa activity, activated protein C (APC) [23, 26]. Here we explored the functional relationship between the A-domain trimer and C-domain pair with regard to anionic phospholipid binding and functional cofactor stability. To do so, we swapped the C-domains of constitutively active B-domainless human FV (FV-810)[27] and ptFV and expressed, purified, and characterized the chimeric variants hFV-ptC and ptFV-hC. Our findings suggest that the conformational flexibility of the C-domain pair may be required for high affinity binding to procoagulant membranes, while stabilization of inter-domain contacts between the A-domain trimer and C-domain pair could impair membrane association.

Material and Methods

Materials and Reagents

The peptidyl substrate H-D-Phe-Pip-Arg-pNA (S2238) was obtained from Instrumentation Laboratories (Bedford, MA, USA). All cell culture reagents were from Life Technologies (Carlsbad, CA, USA) except insulin-transferrin-sodium selenite (ITS), which was from Roche (Basel, Switzerland). Small unilamellar phospholipid vesicles (PCPS) composed of 95% or 75% (w/w) hen egg L-phosphatidylcholine (PC) and 5% or 25% (w/w) porcine brain L-phosphatidylserine (PS) (Avanti Polar Lipids, Alabaster, AL, USA) were prepared and characterized as described previously [28]. FV-depleted human plasma and Neoplastine CI Plus 10 prothrombin time (PT) reagent were obtained from Diagnostica Stago (Paris, France). Normal pooled human plasma (NPP) was from Sanquin (Amsterdam, The Netherlands). All functional assays were performed in Hepes-buffered saline (HBS: 20 mM Hepes, 0.15 M NaCl, pH 7.5) supplemented with 5 mM $CaCl_2$, 0.1% PEG8000 and filtered over a 0.2 µm filter (assay buffer).

Proteins

Restriction endonucleases SnaBI, XmaI, and EcoRV were obtained from New England Biolabs (Ipswich, MA, USA). DAPA, human α-thrombin, human prothrombin, and human prethrombin-1 were from Haematologic Technologies (Essex Junction, VT, USA). Recombinant human FXa (hFXa) and venom-derived *Pseudonaja textilis* FXa (ptFXa) were prepared, purified, and characterized as described [26, 29]. Recombinant constitutively active B-domainless human factor V (FV810; hFV), venom-derived *P. texilis* FV (ptFV), and the variant ptFV-SS were prepared, purified, and characterized as described previously [23, 26, 27]. Molecular weights and extinction coefficients ($E_{0.1\%,\ 280\ nm}$) of the various proteins have been reported previously [23, 27]. The molecular weight and the extinction coefficient ($E_{0.1\%,\ 280\ nm}$) of the newly generated hFV-ptC and ptFV-hC chimeras were assumed to be similar to FV810 (216,000 kDa; 1.54) and ptFV (170,000 kDa; 1.25), respectively.

Construction of FV variants

The construction of pED-FV810 and pED-ptFV has previously been described [23, 27]. Constructs encoding for human FV (FV810) comprising the venom-derived *P. textilis* C-domains (ptFV sequence Cys1147-Phe1460; Uniprot: Q7SZN0), designated pED-hFV-ptC, and for ptFV comprising the human C-domain sequence (human full-length FV sequence Cys1907-Tyr2224; Uniprot: P12259), named pED-ptFV-hC, were generated employing splicing by overlap extension PCR. Specific oligonucleotides used to generate hFV-ptC were as follows: forward primer A, 5'-CCAGACCGTATTCTCTACATGCCC-3', encoding for human FV amino acid residues 1665-1673; complementary primer set reverse primer

B, 5-CCAGTCCCATTGGTAATTTACAGTCTCTGTCCATGATAAG-3', and forward primer C, 5'-CTTATCATGGACAGAGACTGTAAATTACCAATGGGACTGG-3', of which in the latter the first 22 bases correspond to human full-length FV cDNA, encoding for residues 1901-1907, and the last 18 bases to residues 1148-1154 in the ptFV cDNA; and reverse primer D, '5-CTTATTCCAAGCGGCTTCGGCCAG-3', encoding for pED-ptFV nucleotides 5654-5677. The resulting DNA fragment was TOPO-cloned (Invitrogen), digested with SnaBI and XmaI, gel-purified, and subcloned into pED-FV810 digested with the same enzymes. To ensure the absence of polymerase-induced errors, the entire modified cDNA was sequenced. The ptFV-hC construct was prepared using the same strategy with the following primers: forward primer A, 5'-GGCATTTGCTGAACATGGGTGGG-3', encoding for ptFV residues 1068-1075; complementary primer set reverse primer B' 5-GTCCCATTGGCATCCTACAATCTTTGTCAATGACAGTAAAG-3', and forward primer C, 5'-CTTTACTGTCATTGACAAAGATTGTAGGATGCCAATGGGAC-3', of which in the latter the first 22 bases correspond to ptFV cDNA, encoding for residues 1139-1146, and the last 19 bases to residues 1907-1913 in the human full-length FV cDNA; and reverse primer D, '5-CTTATTCCAAGCGGCTTCGGCCAG-3', encoding for pED-FV810 nucleotides 5918-5941, and restriction enzymes EcoRV and XmaI.

Expression and purification of FV variants

Transfection of the plasmids encoding FV constructs into baby hamster kidney cells, the selection of stable clones, and the expression and purification of FV810 and ptFV were performed as described previously [23, 27, 30]. The purification procedures of FV variants hFV-ptC and ptFV-hC were similar to those described for ptFV [23]. Protein purity was assessed by SDS-PAGE using pre-cast 4–12% gradient gels under nonreducing and reducing conditions (50mM DTT) using the MOPS buffer system (Thermo Scientific; Waltham, MA, USA) followed by staining with Coomassie Brilliant Blue R-250. For pretreatment with thrombin, FV variants (1000 nM) were incubated with 50 nM α-thrombin in assay buffer for 15 minutes at 37°C.

FV-specific Prothrombin Time (PT)-based clotting assay

The specific extrinsic clotting activity was determined using a modified FV-specific PT-based clotting assay. Purified FV samples were serially diluted in assay buffer supplemented with 0.1% bovine serum albumin (BSA). In a typical assay, 25 µl of FV-depleted plasma was mixed with an equal volume of sample, followed by a 60 second incubation period at 37°C. Coagulation was initiated after the addition of 50 µl PT reagent, and the coagulation time was monitored using a Start4 coagulation instrument (Diagnostica Stago). Reference curves consisted of serial dilutions of normal pooled plasma, and one unit of FV activity corresponds to the amount of FV in 1 ml of normal plasma (~8 µg).

Macromolecular substrate activation

Steady-state initial velocities of macromolecular substrate cleavage were determined discontinuously at 25 °C in assay buffer as described [31]. Briefly, progress curves of prothrombin and prethrombin-1 activation were obtained by incubating phospholipids (75:25 PCPS, 50 μM), DAPA (10 μM), and prothrombin or prethrombin-1 (1.4 μM) with recombinant FV variants (20 nM), and the reaction was initiated with 0.1–1.0 nM of hFXa or ptFXa. The rate of prothrombin or prethrombin-1 conversion was measured as described [32]. Additionally, prothrombin conversion was assayed in the presence of 95:5 PCPS (450 nM –1000 μM final) or 75:25 PCPS (10 nM – 100 μM final) phospholipid vesicles for hFV and hFV-ptC.

Differential Scanning Calorimetry (DSC)

DSC was performed on a Nano DSC instrument (TA Instruments, New Castle, DE, USA). FV protein solutions (0.2 mg/ml) were prepared in HBS and degassed. The volume of both the sample and reference cell was 0.3 ml, and the reference cell contained degassed HBS only. The cells were heated from 10°C to 110°C at a rate of 1°C per minute under a pressure of 3 atmospheres. Evaluation of the DSC curves was performed employing the NanoAnalyze 3.6 software pack (TA instruments).

Thermal FVa cofactor activity decay

Thermal denaturation experiments were essentially performed as described previously [33]. In brief, activation of FV variants (450 nM) with α-thrombin (50 nM) was carried out in assay buffer supplemented with 0.1% BSA for 15 minutes at 37°C. Following the inhibition of α-thrombin by the addition of hirudin (60 nM), the sample was equilibrated at ambient temperature for 15 minutes. Subsequently, the activated FV variants (20 nM) were incubated for 3–30 minutes at 52°C, upon which the thermal reaction was terminated by cooling in ice water. The cofactor activities of hFVa and hFVa-ptC aliquots were assessed at 250, 125, 63, and 31 pM FVa in FV-depleted plasma using the modified FV-specific PT-based clotting assay. Cofactor activities of ptFVa and ptFVa-hC were assessed at concentrations of 5.0, 2.5, 1.3, and 0.6 nM. The dataset was analyzed using the Graphpad Prism 7 software suite.

Surface Plasmon Resonance Analysis

Association and dissociation of FV variants to phospholipid vesicles was assessed by Surface Plasmon Resonance (SPR) analysis employing a Biacore T200 biosensor and a L1 sensor chip (GE Healthcare Life Sciences, Chicago, IL, USA) [34]. Biosensor experiments were performed in freshly prepared HBS that was filtered over an 0.2 μm filter. Phospholipids composed of 100% PC, or PC with either 5%, 10% or 25% (w/w) PS were dried under constant nitrogen flow, dissolved in HBS, sonicated for 5 minutes and homogenized by passing the mix fifteen times over a disposable polycarbonate membrane (pore size 0.1 μm) using an

extruder (Avestin Inc, Ottawa, Canada) as described [35]. L1 sensor chip cleaning, lipid coating, lipid stabilization, and lipid surface equilibration was performed as recommended by the manufacturer. Recombinant FV variants (20–2000 nM) were passed over an 100% PC reference surface (channel 1) and PC surfaces containing 5%, 10%, and 25% PS (channels 2, 3, and 4) in HBS at 18°C with a flow rate of 5 µl/min for 300 seconds. Subsequently, dissociation was monitored for 120 seconds. After each incubation, the lipid surfaces were regenerated three times with 50 mM NaOH for 60 seconds at flowrate of 10 µl/min, followed by HBS for 180 seconds, upon which the lipid surfaces were equilibrated with 1 mg/ml BSA in HBS for 60 seconds. Biosensor curves were corrected for binding to the 100% PC reference channel and corrected for the HBS signal. In addition, baseline values were subtracted prior to analysis. Following each series of FV variant incubations (nine concentrations per variant), the lipid surface of the L1-chip was replaced. The apparent dissociation constant ($K_{d,app}$) for the interaction between FV variants and the anionic phospholipid surface was obtained from the dependence of the steady state binding response (defined as binding at the onset of dissociation) on the concentrations of the FV species using nonlinear regression analysis via the Biacore software package.

Sequence alignment and superposition

Amino acid sequences of human FV (Uniprot: P12259) and *P. textilis* venom FV (Uniprot: Q7SZN0) were aligned employing the ClustalW algorithm for multiple sequence alignment (Vector NTI 11.5 Advance software suite, Thermo Scientific, Waltham, MA, USA). The C-domains were super positioned using the PyMOL Molecular Graphics System (Schrödinger, LLC). The isoelectric point was calculated with the ProtParam tool on the ExPASy server [36].

Results

The C-domains of human and *Pseudonaja textilis* venom-derived FV

Alignment of hFV and ptFV polypeptide amino acid sequences revealed that the C-domains share 59% sequence identity and 73% sequence similarity (**Supplementary Figure 1**). Superposition of the human and ptFV C-domains showed structural conservation of the characteristic discoidin-like fold of the C-domain pair and conservation of all three β-hairpin phospholipid binding loops at the base of each C-domain (**Supplementary Figure 2**) [10, 11, 25]. However, several positively charged residues are non-conserved in the ptFV C1-domain, resulting in a significantly lower isoelectric point for the ptFV C1-domain (pI: 6.77) compared to that of hFV (pI: 9.17). Furthermore, polar amino acid substitutions have occurred at six positions within the ptFV C2-domain, resulting in an increased hydrophilic character of ptFV C2 relative to hFV. Additional clusters of amino acids substitutions are found within some of the ptFV phospholipid binding loops and within two elongated loops (hFV: Ser^{1971}-Val^{1987} and Ser^{2130}-Val^{2146}) that cover the crest of the C1- and C2-domains. These latter structures are considered to form an extended surface that faces the A-domain trimer when FVa is bound to a membrane surface [18, 20, 25]. Taken together, the ptFV C-domain pair is relatively similar to that of hFV, yet marked differences occur within specific regions that have been shown to interact with the A-domain trimer or to contribute to phospholipid binding.

Construction and characterization of chimeric FV variants

To investigate whether the C-domains of ptFV convey enhanced cofactor stability and/or altered phospholipid binding affinities, we exchanged the C-domain coding regions of constitutively active B-domainless human FV (hFV, or FV-810) with those of ptFV, thereby generating the chimeric cofactors hFV-ptC and ptFV-hC (**Figure 1A**). SDS-PAGE analysis demonstrated that the purified chimeric variants hFV-ptC and ptFV-hC migrate similar to hFV and ptFV, respectively (**Figure 1B**, **Supplementary Figure 3**). In addition, both ptFV and ptFV-hC migrated as single chain species under non-reducing conditions upon incubation with thrombin, indicating that the unique A2-A3 domain disulfide linker in ptFV is maintained in ptFV-hC (**Figure 1B**) [23, 26]. Cofactor function was evaluated employing a purified prothrombinase assay using recombinant human FXa (hFXa) in the presence of a saturating concentration of phospholipid vesicles (PCPS, 50 μM), resulting in comparable rates of prothrombin activation for both hFV and hFV-ptC (**Figure 1C**). In contrast, the rate of prothrombin activation was approximately 40-fold lower using ptFV as cofactor for hFXa. This is consistent with previous findings and in part relates to the reduced affinity of ptFV for membrane-bound human FXa [23, 37]. Conversely, cofactor function of ptFV improved 3-fold by exchanging the ptFV C-domains for those of hFV.

We next aimed to establish whether the C-domains of ptFV drive its lipid-independent cofactor function and, if so, can sustain this unique property in the setting of human FV. Cofactor function was therefore assayed in the presence or absence of saturating concentrations of anionic phospholipid vesicles using the lipid-independent substrate prethrombin-1 [23, 26]. When using hFXa and lipids, replacing the human C-domains for those of ptFV reduced prethrombin-1 activation by almost 2-fold, relative to hFV (**Table 1**). On the other hand, prethrombin-1 conversion was significantly enhanced following exchange of the ptFV C-domains for those of hFV. These results show that C-domain-targeted humanization of ptFV cofactor improves its cofactor function towards hFXa. Interestingly, with lipids and ptFXa as protease, no prethrombin-1 activation was observed for hFV, whereas replacement of the human C-domains for those of ptFV resulted in detectable thrombin formation (**Table 1**). In the absence of lipids though, the hFV-ptC chimera did not display cofactor activity for either hFXa or ptFXa. Correspondingly, ptFV displayed no or hardly any loss of cofactor function for ptFXa following introduction of the human C-domains in the presence or absence of lipids (**Table 1**). Furthermore, no gain of function towards hFXa was observed for ptFV-hC. Taken together, these findings indicate that the C-domains affect overall cofactor activity towards human or venom-derived FXa in a lipid-dependent manner, but do not drive lipid-independent cofactor function.

Table 1. Prethrombin-1 Activation

Cofactor Species	**Initial Velocity^**	**Initial Velocity**	**Initial Velocity**	**Initial Velocity**
	hFXa	***ptFXa***	***hFXa***	***ptFXa***
	+ PCPS	***+ PCPS***	***- PCPS***	***- PCPS***
	nM IIα/min/ nM Enzyme	*nM IIα/min/ nM Enzyme*	*nM IIα/min/ nM Enzyme*	*nM IIα/min/ nM Enzyme*
hFV (FV-810)	**78 ± 11**	**0**	**0**	**0**
hFV-ptC	**46 ± 8**	**6 ± 6**	**0**	**0**
ptFV-hC	**14 ± 5**	**191 ± 16**	**0**	**174 ± 34**
ptFV	**2 ± 0**	**215 ± 14**	**0**	**237 ± 28**

The initial velocity of thrombin generation (nM IIα/min/nM Enzyme) was determined as described in 'Materials and Methods'. The mean values ± S.D. of two independent determinations are presented.

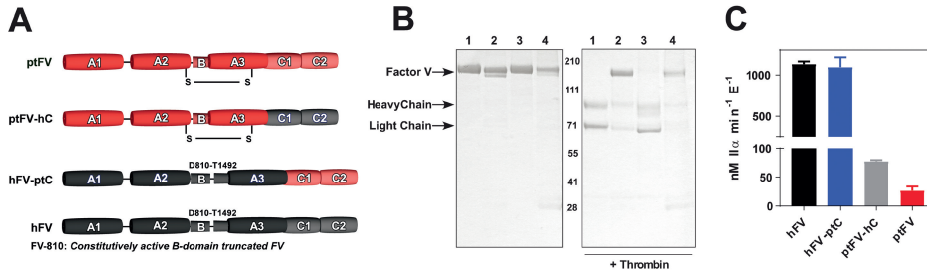

Figure 1. Chimeric FV variants. (***A***) The recombinant FV variants used in this study are shown schematically (ptFV, ptFV-hC, hFV-ptC, and hFV or FV-810); B-domain residues deleted in the human FV variants are indicated. hFV regions are indicated in black and ptFV regions in red. (***B***) Purified proteins (5 µg/lane) were subjected to SDS-PAGE before (left panel) and after treatment with thrombin (right panel) under non-reducing conditions and visualized by staining with Coomassie Brilliant Blue R-250. Lane 1: FV-810; lane 2: ptFV; lane 3: hFV-ptC; lane 4: ptFV-hC. The apparent molecular weights of the standards are indicated. (***C***) Reaction mixtures containing 50 µM PCPS, 10 µM DAPA, 1.4 µM prothrombin, and 20 nM FV variant (hFV or FV-810, hFV-ptC, ptFV, or ptFV-hC) were incubated for 5 min. at 25°C. The reaction was initiated with 0.1 nM hFXa, and thrombin generation was monitored as described in 'Materials and Methods'. The data are the means ± S.D. of two independent experiments.

The C-domains of *P. textilis* FV support cofactor thermostability

To study the cofactor thermostability of each FV variant, we evaluated protein heat capacity by differential scanning calorimetry (DSC). Thermal transition midpoint (T_m) analysis of heat capacity curves revealed a single denaturation event for hFV at 54°C (**Figure 2**). In contrast, ptFV displayed two separate denaturation events, one at 60°C and another at 70°C, pointing to a different and overall higher protein stability compared to hFV (**Figure 2**). As the A2- and A3-domains of ptFV are covalently linked via a disulfide bond that is found in ptFV only [23], we also analyzed the protein heat capacity of a previously characterized ptFV variant that contained serine replacements of the disulfide-forming cysteine pair (ptFV-SS) [26]. While ptFV-SS lacks the A2-A3 connecting disulfide link, we also observed two similar denaturation events, with the second denaturation event occurring at 67°C. This implies that the two sequential denaturation events observed for ptFV and ptFV-SS correspond to separate unfolding events, of which the second event may involve unfolding of the A2-A3 domain region and/or A-domain trimer (**Figure 2**). Interestingly, heat capacity analysis of the chimeric variant hFV-ptC revealed a single denaturation event at 58°C, indicating that the C-domains of ptFV increased cofactor stability when linked to the A-domains of hFV (**Figure 2**). In addition, the thermal transition midpoint of hFV-ptC was preceded by an extended denaturation lag phase, suggesting mitigation of protein unfolding in hFV-ptC. Heat capacity analysis of the chimeric variant that comprised the A-domains of ptFV and the C-domains of hFV did not produce curves that were amenable for thermal transition midpoint analysis.

In order to examine thermal stability of each cofactor in a functional context, we assessed cofactor activity decay rates after incubation at 52°C using a PT-based clotting assay. The central B-domain was removed prior to incubation using thrombin in order to exclude any possible contribution of the B-domain sequence to cofactor stability. By doing so, we were able to confirm the high stability and extended half-life of ptFVa (K <0.001 min^{-1}) relative to human hFVa (K 0.39 ± 0.04 min^{-1}) (**Figure 3**). Similar to the DSC results, hFVa-ptC (K 0.13 ± 0.04 min^{-1}) displayed improved stability and demonstrated a 3-fold prolonged half-life compared to hFVa. On the other hand, the C-domain exchange adversely affected the stability of ptFVa (ptFVa-hC: K 0.73 ± 0.25 min^{-1}), resulting in a more than 30-fold reduced *in vitro* half-life at 52°C relative to ptFVa (**Figure 3**). These findings confirm that the C-domains of ptFV improve cofactor stability in the setting of the human FV A-domains. Conversely, introduction of the human C-domain pair attenuates the thermostability of the ptFV A-domains.

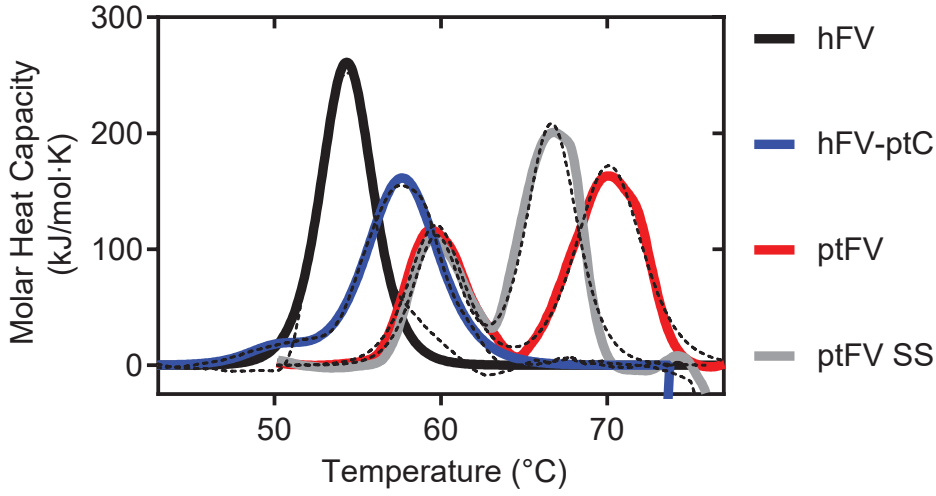

Figure 2. Differential scanning calorimetry. Heat capacity was monitored as described in 'Materials and Methods'. The data were fitted to a two-state model scaled for protein concentration after subtraction of the buffer baseline using the NanoAnalyze software from TA instruments. The derived molar heat capacity is shown for hFV (FV-810, *black*), hFV-ptC (*blue*), ptFV (*red*), or ptFV-SS (*grey*); intermitted lines display raw data curves. The total heat of unfolding (ΔH) was 856 kJ/mol for hFV, 1072 kJ/mol for hFV-ptC, 1569 kJ/mol for ptFV, and 1907 kJ/mol for ptFV-SS. All curves are representative of two similar experiments.

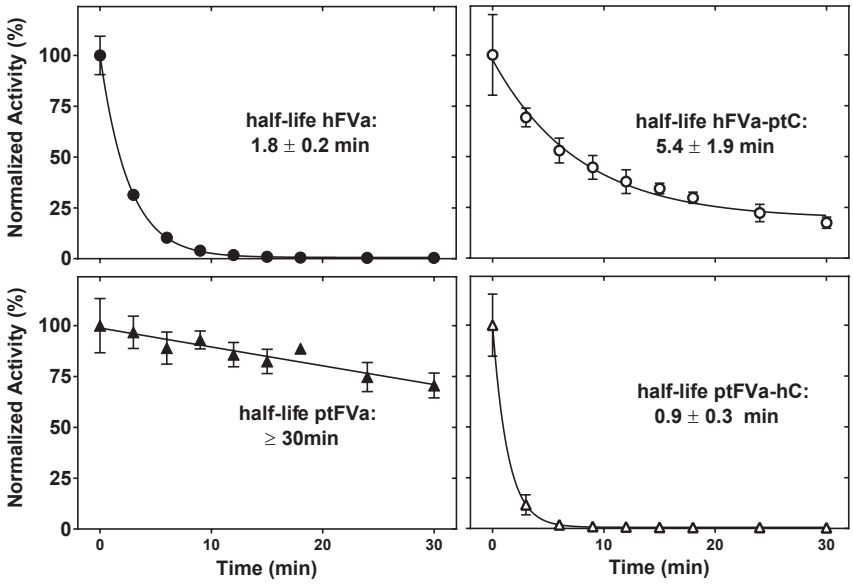

Figure 3. Thermal FVa cofactor stability. Thrombin-activated hFV (FV-810, *closed circles*), hFV-ptC (*open circles*), ptFV (*closed triangles*), or ptFV-hC (*open triangles*) (20 nM) was incubated at 52°C. At the indicated time points, aliquots were processed as described in 'Materials and Methods' and analyzed for FV-specific PT-based clotting activity. The data were normalized to the cofactor activity assessed at the start of the incubation. The cofactor decay rate constants (*K*) were determined by fitting the data to a one-phase decay function by non-linear regression, resulting in the following decay rate constants: hFVa: 0.39 ± 0.04 min^{-1}, hFVa-ptC: 0.13 ± 0.04 min^{-1}, ptFVa: <0.001 min^{-1}, ptFVa-hC: 0.73 ± 0.25 min^{-1}. The corresponding half-lives are indicated in each graph. The data are the normalized means ± S.D. of three independent experiments.

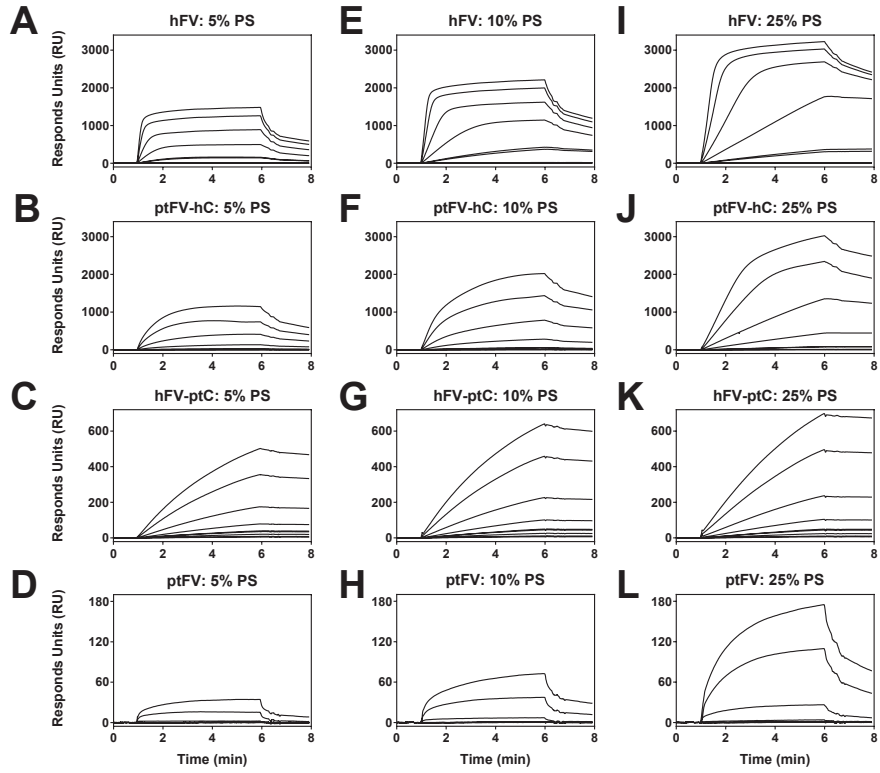

Figure 4. Binding of FV to anionic phospholipid vesicles. The association and dissociation of FV variants (0.02 - 2 μM) to PC phospholipid vesicles containing either 5% PS (***A-D***), 10% PS (***E-H***), or 25% PS content (***I-L***) for hFV (FV-810, ***A-E-I***), ptFV-hC (***B-F-J***), hFV-ptC (***C-G-K***), or ptFV (***D-H-L***) was assessed by SPR as described in 'Materials and Methods'. Cofactor injection started at t = 1 minute and was discontinued at t = 6 minutes. The binding curves were corrected for binding to a control channel coated with 100% PC vesicles (see Supporting **Figure 4)**.

The A-domains of human FV confer lipid binding to the ptFV C-domains

To assess binding of FV to negatively charged phospholipid vesicles, we performed surface plasmon resonance analyses using an L1 chip coated with phospholipid vesicles containing 5%, 10%, or 25% PS (**Figure 4**). Fitting of the phospholipid binding affinity at steady state of hFV revealed an apparent K_d of 1.0 μM for an anionic membrane surface with 5% PS content, and an apparent K_d of 0.5 μM for surfaces with 10% or 25% PS content (**Figure 5**). Binding curves of hFV-ptC, ptFV-hC and ptFV did not display saturation of the binding response at high ligand concentrations (**Figure 4**), precluding regular fitting of the binding constant at steady state. Estimation of their respective binding affinities nonetheless revealed micromolar affinities for both ptFV-hC and hFV-ptC, and millimolar affinities for ptFV (**Figure 5**). While these estimates indicated that ptFV-hC may display an increased affinity towards membranes comprising a higher PS content, this was not observed for hFV-ptC, suggesting reduced phosphatidylserine binding affinity for the ptFV C-domains. These results corroborate the C-domains as the main driving force in the interaction with anionic phospholipids, and confirm that the C-domains of ptFV display reduced lipid binding [24]. Intriguingly, our data also points to a role for the A-domains in mediating phospholipid binding by the C-domains, as the A-domains of human FV enhanced phospholipid binding by the C-domains of ptFV.

The affinity of hFV or hFV-ptC for phospholipid vesicles containing PS was further examined in a functional context by employing a purified prothrombinase assay with hFXa and increasing phospholipid concentrations. Both hFV and hFV-ptC displayed similar prothrombin activation rates in the presence of 25 - 100 μM of phospholipids containing 25% PS (**Figure 1C**). However, hFV-ptC required a 6-fold higher lipid concentration in order to produce half maximal prothrombin conversion rates (**Figure 6A**). Similar findings were obtained at 5% PS content, as hFV-ptC required an approximate 50-fold higher phospholipid concentration in order to generate prothrombin activation rates that were comparable to that of hFV (**Figure 6B**). These results confirmed that the ptFV C-domains displayed reduced affinity towards PS-containing membranes. Nevertheless, the ptFV C-domain pair has re-established the ability to bind to phospholipids in a manner that is conducive to cofactor function when paired with the human A-domain trimer.

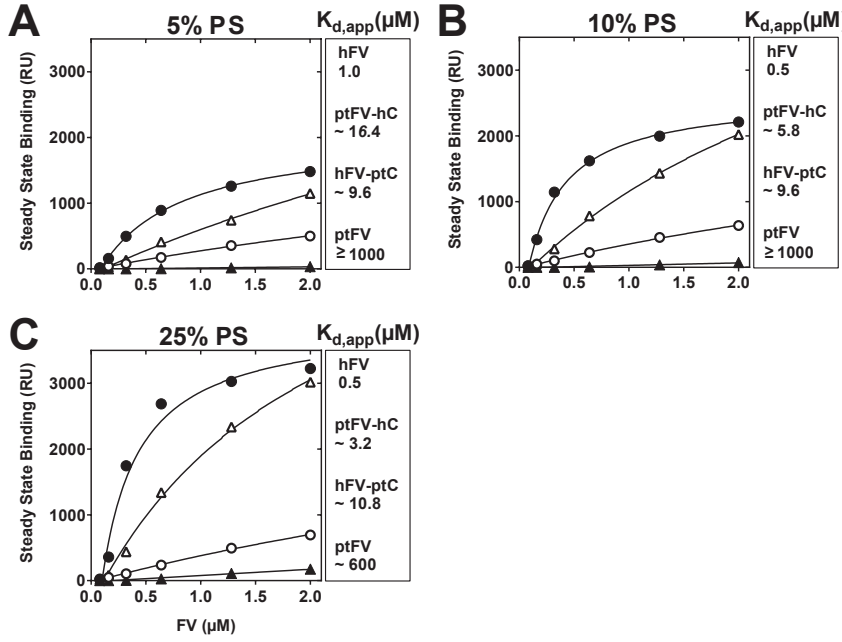

Figure 5. Steady state anionic phospholipid binding affinity. From the anionic phospholipid-FV binding data (**Figure 4)**, the binding response units (RU) at the onset of dissociation were plotted versus the concentrations (0.020-2 μM) of FV. The FV species were hFV (FV-810, *closed circles*), hFV-ptC (*open circles*), ptFV (*closed triangles*) or ptFV-hC (*open triangles*), and the interaction with phospholipid vesicles containing either 5% PS (**A**), 10% PS (**B**) or 25% PS content (**C**) that were coated to an L1 chip was studied employing SPR as described in 'Materials and Methods'. The apparent dissociation constants ($K_{d,app}$) were obtained following nonlinear regression analysis and are presented in the right-hand panels; numbers preceded by the operator (~) indicate estimated affinities; the operator (≥) indicates a low-end estimate.

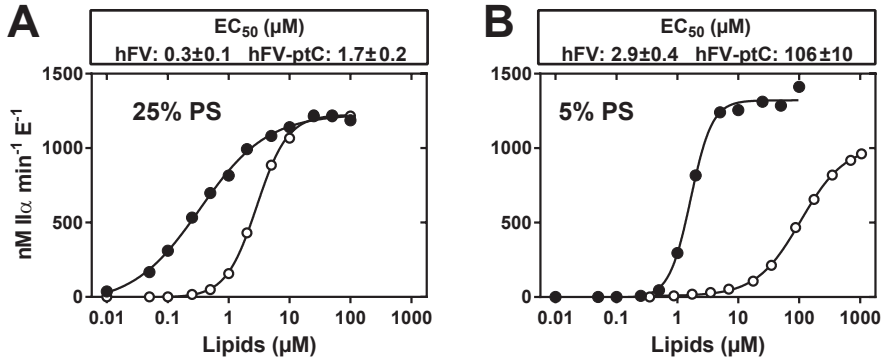

Figure 6. Phospholipid-dependent prothrombin activation. The initial velocity of thrombin generation (nM IIα/min/nM Enzyme) was determined in the presence of 0.1 nM FXa, 1.4 μM prothrombin, 10 μM DAPA and 20 nM hFV (FV-810, closed circles) or hFV-ptC (open circles) at increasing concentrations of phospholipid vesicles containing either 25% PS (***A***) or 5% PS (***B***) as described in 'Materials and Methods'. Lines represent best-fit EC_{50} curves. Insets: best-fit EC_{50} concentrations ± S.D. of the induced fit. All data points represent the means of two independent experiments.

Discussion

Over the past twenty years, the arrangement of the C-domain pair relative to that of the A-domain trimer of FVa and its possible implications to phospholipid binding and cofactor function have been studied systematically [10, 11, 17, 18, 21, 38, 39]. Here, we established the presence of functional crosstalk between the A-domains and C-domains by analyzing chimeric variants of FV that comprise either the A-domains of human FV and the C-domains of ptFV, or vice versa. Specifically, we were able to show that the C-domains of ptFV conferred cofactor stability when linked to the A-domains of human FV while, in turn, the A-domains of human FV improved phospholipid binding by the C-domains of ptFV. However, the absence of a complete and up-to-date crystal structure or NMR ensemble of human FVa restricts a comprehensive rationalization for the observed functional crosstalk between the A-domain trimer and its C-domain pair. Nevertheless, essential clues on the intricate multi-domain relationships that govern cofactor function can be gathered from structural studies on FV and its homolog FVIII.

The first models of the tertiary FV C1/C2 domain structure were generated by Pellequer et al who used the binding domain of galactose oxidase [PDB ID: 1GOF] as structural homolog [38, 40]. These models showed that the C-domains of FV were able to dimerize in a linear or 'head-to-head' fashion to form an extended structure [38]. This configuration was found to be energetically favorable in solution, as hydrophobic residues at the C1/C2 domain interface were buried due to the joining of the two homologous loops that cover the crest of the C1- and C2-domain, here termed apical C1 loop (Ser1971-Val1987) and apical C2 loop (Ser2130-Val2146) (**Supporting Figure 2**). The crystal structures of ceruloplasmin and the FV C2-domain have subsequently been used to construct a multi-domain model of human FVa [10, 39, 41]. This model also includes a linear C-domain arrangement that is connected to the A-domain trimer via a flexible linker connecting the A3 and C1 domains [39]. The crystal structure of APC-inactivated bovine FVa (domain organization A1-A3-C1-C2; FVa_i) was the first to feature a juxtaposed or 'side-by-side' conformation of the C-domains [11]. This arrangement appears to be stabilized by burial of hydrophobic residues at the A3/C1 interface and via extensive electrostatic interactions between the apical C1 loop and the N-terminal β-barrel of the A3-domain [11]. Collectively, depending on the relative orientation of the C-domain pair, the apical C1 loop may associate with the apical C2 loop [39] or the A3-domain [11] (**Supporting Figure 5**). An ensuing Cryo-EM study has shown that the juxtaposed C-domain arrangement represents the FVa-phospholipid binding pose [18]. However, the exact orientation of the membrane-bound C-domain pair relative to that of the A-domain trimer has remained elusive [17, 18]. More recently, Chaves et al applied atomic force microscopy to study activated FV in solution and revealed that the C-domains are, in fact, highly flexible

and able to adopt juxtaposed, linear, and otherwise extended configurations [21]. In other words, the C-domains seem to be in a constant state of rearrangement when FVa resides in solution.

In our current study we have established that the phospholipid binding affinity is inversely correlated to cofactor stability in ptFV. For instance, both DCS and thermal decay experiments clearly showed ptFV to be highly resistant to thermal denaturation, even upon removal of its unique disulfide bond linking the A2 and A3-domains (**Figures 2**,**3**) [26]. On the other hand, SPR experiments revealed that ptFV, of all FV variants tested, displayed the lowest binding affinity for anionic membrane surfaces (**Figures 4**,**5**). Although the ptFV-phospholipid binding was significantly enhanced following exchange of its C-domain pair for that of human FV, this chimeric variant displayed also a significantly shortened half-life during thermal decay experiments, indicating that cofactor stability and membrane binding are mutually exclusive in ptFV. Kinetic analyses have further shown that the ptFV C-domains are of little relevance to its lipid-independent cofactor function, as the chimera ptFV-hC was able to support cofactor function in the absence of phospholipids (**Table 1**). Taken together, these results show that anionic phospholipid binding has been uncoupled from cofactor function in ptFV. This is also reflected by the physical properties of the ptFV C-domains, as membrane binding affinity is potentially attenuated by the neutral isoelectric point of the C1-domain and the more hydrophilic nature of the C2-domain [9, 10, 12-15]. Importantly, sequence alignment revealed a disproportionally high number of amino acid substitutions within sequences that encompass the apical C1 and C2 loops in ptFV (**Supporting Figure 1**). We propose that these alterations serve to restrict dynamical variation in ptFV, effectively stabilizing the cofactor and preventing high affinity phospholipid binding. The full-length structure of ptFV has nevertheless been shown to adopt a juxtaposed C-domain configuration that resembles the human FVa membrane binding pose [18, 20, 25]. We therefore hypothesize that the impaired phospholipid binding affinity of ptFV stems from an inability to arrange its C-domain pair in linear or more extended arrangements, possibly due to reduced avidity between the apical C1/C2 loops and/or enhanced avidity between the A3-domain and the apical C1 loop.

The multi-domain structure of human FVa is recognized as inherently unstable and prone to spontaneous disassociation in the absence of calcium ions. Even so, of all FV variants studied here, hFV (FV-810) displayed the highest overall phospholipid binding affinity following SPR analysis. Interestingly, by linking the ptFV C-domain pair to the human FV A-domain trimer we were able to enhance cofactor stability and simultaneously preserve phospholipid binding (**Figures 2 - 6**). However, the hFV-ptC chimera exhibited significantly slower phospholipid association and dissociation rates, irrespective of vesicle PS content (**Figure 4**) and required 6- to

50-fold higher PS concentrations to achieve maximal prothrombin activation rates (**Figure 6**). These results confirm that the ptFV C-domains are relatively insensitive to PS and potentially less prone to adopt a phospholipid binding pose. In addition, the ptFV C-domains appear to be more stable than their human counterparts. For example, during DSC, we observed a higher thermal transient midpoint for the ptFV C-domain pair at 60°C, while denaturation of the complete hFV cofactor occurred at 54°C. Moreover, both DSC and thermal half-life experiments showed increased stability for both ptFV C-domain comprising cofactors (ptFV, hFV-ptC) relative to the human C-domain comprising cofactors (hFV, ptFV-hC) (**Figures 2**,**3**). Taken together, our observations potentially indicate that the ptFV C-domain pair is less flexible than its human counterpart and could therefore impede multi-domain rearrangements that would otherwise facilitate membrane association and dissociation (**Figure 4**) [15, 21]. Furthermore, our data seem to indicate that the human A-domain trimer can induce C-domain orientations that are conducive to membrane tethering, potentially by enabling the ptFV C-domains to sample more extended configurations. In contrast, the ptFV A-domain trimer was not able to fully support anionic phospholipid binding by the human C-domain pair since the steady state phospholipid binding affinity was reduced for ptFV-hC compared to hFV (**Figures 4**,**5**). Based on these observations we hypothesize that the human A-domain trimer is able to organize its C-domain pair to support selectivity for procoagulant membranes, potentially by reinforcing conformational flexibility of the C-domain pair via allosteric crosstalk between the A-domain trimer and the apical C1 and C2 loops. However, additional biophysical studies are required to substantiate this hypothesis.

Interestingly, conformational flexibility of the C-domain pair appears to be likewise required for high affinity membrane binding in the homologous cofactor VIIIa. For example, computational studies have indicated that flexibility of the FVIII C-domains may be required for the step-wise insertion of the phospholipid binding spikes into procoagulant membrane surfaces [42, 43]. In addition, the relative orientations of C1 and C2, as well as their specific membrane binding properties, have been reported to differ between FV and FVIII [44-47]. As the half-life of FVIIIa is notoriously short, even in comparison to FVa, several studies have been undertaken to improve half-life by introducing covalent links or by increasing hydrophobicity at the A3/C1 or A2/C1 interface [33, 48]. These studies have successfully increased cofactor thermostability, but invariably at the cost of FVIIIa clotting activity [33, 48]. A similar discrepancy was also observed in our study, as the stabile hFV-ptC chimera displayed reduced specific clotting activity while the unstable ptFV-hC chimera displayed increased clotting activity (data not shown). Similarly, a recent study reported decreased cofactor activity and impaired phospholipid binding of a FVIIIa variant that comprised the C1 domain of FV [49]. Conversely, the FV C1-domain was shown to associate more tightly with the A3-

domain of FVIIIa [49], implicating enhanced cofactor stability. In summary, these studies indicate that stabilization of the A3/C1 domain interface may obstruct high affinity phospholipid binding, both in FVIII and FV. Remarkably, sequence conservation of the apical C1 and C2 loop is poor between FV and FVIII, which may imply that these structures might have been molecularly customized to balance cofactor activity versus cofactor half-life during the evolution of the mammalian coagulome.

In conclusion, our study has shown that the A-domain trimer and C-domain pair of FV are functionally linked with regard to anionic phospholipid binding and cofactor stability. These findings provide novel insights into the multi-domain relationships that govern FVa cofactor function and will help to guide future protein engineering strategies.

References

1. Mann, K.G., et al., *Surface-dependent reactions of the vitamin K-dependent enzyme complexes.* Blood, 1990. **76**(1): p. 1-16.
2. Kane, W.H. and E.W. Davie, *Blood coagulation factors V and VIII: structural and functional similarities and their relationship to hemorrhagic and thrombotic disorders.* Blood, 1988. **71**(3): p. 539-55.
3. Suzuki, K., B. Dahlback, and J. Stenflo, *Thrombin-catalyzed activation of human coagulation factor V.* J Biol Chem, 1982. **257**(11): p. 6556-64.
4. Bos, M.H. and R.M. Camire, *A bipartite autoinhibitory region within the B-domain suppresses function in factor V.* J Biol Chem, 2012. **287**(31): p. 26342-51.
5. Schuijt, T.J., et al., *Factor Xa activation of factor V is of paramount importance in initiating the coagulation system: lessons from a tick salivary protein.* Circulation, 2013. **128**(3): p. 254-66.
6. Camire, R.M. and M.H. Bos, *The molecular basis of factor V and VIII procofactor activation.* J Thromb Haemost, 2009. **7**(12): p. 1951-61.
7. Mann, K.G., R.J. Jenny, and S. Krishnaswamy, *Cofactor proteins in the assembly and expression of blood clotting enzyme complexes.* Annu Rev Biochem, 1988. **57**: p. 915-56.
8. Bradford, H.N., S.J. Orcutt, and S. Krishnaswamy, *Membrane binding by prothrombin mediates its constrained presentation to prothrombinase for cleavage.* J Biol Chem, 2013. **288**(39): p. 27789-800.
9. Isaacs, B.S., et al., *A-domain of membrane-bound blood coagulation factor Va is located far from the phospholipid surface. A fluorescence energy transfer measurement.* Biochemistry, 1986. **25**(17): p. 4958-69.
10. Macedo-Ribeiro, S., et al., *Crystal structures of the membrane-binding C2 domain of human coagulation factor V.* Nature, 1999. **402**(6760): p. 434-9.
11. Adams, T.E., et al., *The crystal structure of activated protein C-inactivated bovine factor Va: Implications for cofactor function.* Proc Natl Acad Sci U S A, 2004. **101**(24): p. 8918-23.
12. Nicolaes, G.A., B.O. Villoutreix, and B. Dahlback, *Mutations in a potential phospholipid binding loop in the C2 domain of factor V affecting the assembly of the prothrombinase complex.* Blood Coagul Fibrinolysis, 2000. **11**(1): p. 89-100.
13. Saleh, M., et al., *The factor V C1 domain is involved in membrane binding: identification of functionally important amino acid residues within the C1 domain of factor V using alanine scanning mutagenesis.* Thromb Haemost, 2004. **91**(1): p. 16-27.
14. Peng, W., M.A. Quinn-Allen, and W.H. Kane, *Mutation of hydrophobic residues in the factor Va C1 and C2 domains blocks membrane-dependent prothrombin activation.* J Thromb Haemost, 2005. **3**(2): p. 351-4.
15. Majumder, R., et al., *A phosphatidylserine binding site in factor Va C1 domain regulates both assembly and activity of the prothrombinase complex.* Blood, 2008. **112**(7): p. 2795-802.

16. Autin, L., et al., *Proposed structural models of the prothrombinase (FXa-FVa) complex.* Proteins, 2006. **63**(3): p. 440-50.
17. Lee, C.J., et al., *Proposed structural models of human factor Va and prothrombinase.* J Thromb Haemost, 2008. **6**(1): p. 83-9.
18. Stoilova-McPhie, S., et al., *Defining the structure of membrane-bound human blood coagulation factor Va.* J Thromb Haemost, 2008. **6**(1): p. 76-82.
19. Lee, C.J., S. Wu, and L.G. Pedersen, *A proposed ternary complex model of prothrombinase with prothrombin: protein-protein docking and molecular dynamics simulations.* J Thromb Haemost, 2011. **9**(10): p. 2123-6.
20. Pomowski, A., F.I. Ustok, and J.A. Huntington, *Homology model of human prothrombinase based on the crystal structure of Pseutarin C.* Biol Chem, 2014. **395**(10): p. 1233-41.
21. Chaves, R.C., et al., *Factor Va alternative conformation reconstruction using atomic force microscopy.* Thromb Haemost, 2014. **112**(6): p. 1167-73.
22. Rao, V.S., S. Swarup, and R.M. Kini, *The nonenzymatic subunit of pseutarin C, a prothrombin activator from eastern brown snake (Pseudonaja textilis) venom, shows structural similarity to mammalian coagulation factor V.* Blood, 2003. **102**(4): p. 1347-54.
23. Bos, M.H., et al., *Venom factor V from the common brown snake escapes hemostatic regulation through procoagulant adaptations.* Blood, 2009. **114**(3): p. 686-92.
24. Kumar, S., Stayrook S., Huntington, J.A., Camire, R.M., Krishnaswamy, S., *New Structural Insights into High Affinity Membrane Binding By Coagulation Factor V/Va* Blood, 2014. **124**(21): p. 4216.
25. Lechtenberg, B.C., et al., *Crystal structure of the prothrombinase complex from the venom of Pseudonaja textilis.* Blood, 2013. **122**(16): p. 2777-83.
26. Verhoef D., Y.X., Parthasarathy S., Reitsma P.H., Camire R.M., Bos M.H.A, *Functional implications of the unique disulfide bond in venom factor V from the Australian common brown snake Pseudonaja textilis.* Toxin Reviews, 2013. **33**(1-2): p. 37-41.
27. Toso, R. and R.M. Camire, *Removal of B-domain sequences from factor V rather than specific proteolysis underlies the mechanism by which cofactor function is realized.* J Biol Chem, 2004. **279**(20): p. 21643-50.
28. Higgins, D.L. and K.G. Mann, *The interaction of bovine factor V and factor V-derived peptides with phospholipid vesicles.* J Biol Chem, 1983. **258**(10): p. 6503-8.
29. Verhoef, D., et al., *Engineered factor Xa variants retain procoagulant activity independent of direct factor Xa inhibitors.* Nat Commun, 2017. **8**(1): p. 528.
30. Bradford, H.N., J.A. Micucci, and S. Krishnaswamy, *Regulated cleavage of prothrombin by prothrombinase: repositioning a cleavage site reveals the unique kinetic behavior of the action of prothrombinase on its compound substrate.* J Biol Chem, 2010. **285**(1): p. 328-38.
31. Camire, R.M., *Prothrombinase assembly and S1 site occupation restore the catalytic activity of FXa impaired by mutation at the sodium-binding site.* J Biol Chem, 2002. **277**(40): p. 37863-70.

32. Krishnaswamy, S. and R.K. Walker, *Contribution of the prothrombin fragment 2 domain to the function of factor Va in the prothrombinase complex.* Biochemistry, 1997. **36**(11): p. 3319-30.
33. Wakabayashi, H., A.E. Griffiths, and P.J. Fay, *Increasing hydrophobicity or disulfide bridging at the factor VIII A1 and C2 domain interface enhances procofactor stability.* J Biol Chem, 2011. **286**(29): p. 25748-55.
34. Hodnik, V. and G. Anderluh, *Capture of intact liposomes on biacore sensor chips for protein-membrane interaction studies.* Methods Mol Biol, 2010. **627**: p. 201-11.
35. Wikstrom, A. and J. Deinum, *Probing the interaction of coagulation factors with phospholipid vesicle surfaces by surface plasma resonance.* Anal Biochem, 2007. **362**(1): p. 98-107.
36. Wilkins, M.R., et al., *Protein identification and analysis tools in the ExPASy server.* Methods Mol Biol, 1999. **112**: p. 531-52.
37. Speijer, H., et al., *Prothrombin activation by an activator from the venom of Oxyuranus scutellatus (Taipan snake).* J Biol Chem, 1986. **261**(28): p. 13258-67.
38. Pellequer, J.L., et al., *Homology models of the C-domains of blood coagulation factors V and VIII: a proposed membrane binding mode for FV and FVIII C2 domains.* Blood Cells Mol Dis, 1998. **24**(4): p. 448-61.
39. Pellequer, J.L., et al., *Three-dimensional model of coagulation factor Va bound to activated protein C.* Thromb Haemost, 2000. **84**(5): p. 849-57.
40. Ito, N., et al., *Crystal structure of a free radical enzyme, galactose oxidase.* J Mol Biol, 1994. **238**(5): p. 794-814.
41. Zaitseva I., Z.V., Card G., Moshkov K., Bax B., Ralph A., Lindley P., *The X-ray structure of human serum ceruloplasmin at 3.1 Å: nature of the copper centres.* J Biol Inorg Chem, 1996(1): p. 15-23.
42. Du, J., et al., *Molecular simulation studies of human coagulation factor VIII C-domain-mediated membrane binding.* Thromb Haemost, 2015. **113**(2): p. 373-84.
43. Madsen, J.J., et al., *Membrane Interaction of the Factor VIIIa Discoidin Domains in Atomistic Detail.* Biochemistry, 2015. **54**(39): p. 6123-31.
44. Parmenter, C.D., et al., *Cryo-electron microscopy of coagulation Factor VIII bound to lipid nanotubes.* Biochem Biophys Res Commun, 2008. **366**(2): p. 288-93.
45. Ngo, J.C., et al., *Crystal structure of human factor VIII: implications for the formation of the factor IXa-factor VIIIa complex.* Structure, 2008. **16**(4): p. 597-606.
46. Shen, B.W., et al., *The tertiary structure and domain organization of coagulation factor VIII.* Blood, 2008. **111**(3): p. 1240-7.
47. Gilbert, G.E., et al., *Conservative mutations in the C2 domains of factor VIII and factor V alter phospholipid binding and cofactor activity.* Blood, 2012. **120**(9): p. 1923-32.
48. Wakabayashi, H. and P.J. Fay, *Modification of interdomain interfaces within the A3C1C2 subunit of factor VIII affects its stability and activity.* Biochemistry, 2013. **52**(22): p. 3921-9.
49. Ebberink, E.H., et al., *Factor VIII/V C-domain swaps reveal discrete C-domain roles in factor VIII function and intracellular trafficking.* Haematologica, 2017. **102**(4): p. 686-694.

Supplementary information

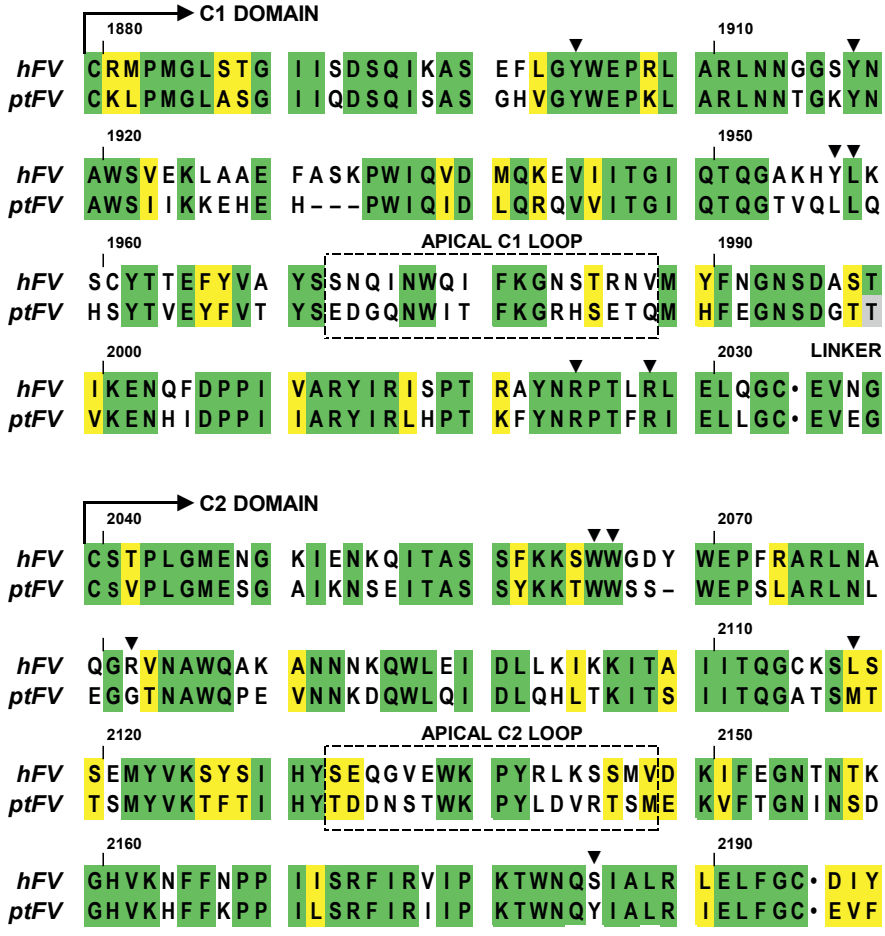

Supplementary Figure 1. Sequence alignment of the C1- and C2-domains of human and ptFV. Alignment of human FV (C^{1879}-Y^{2196}) and ptFV (C^{1117}-F^{1430}) polypeptide chains was performed using the Clustal W algorithm. Color coding: conserved residues (*green*), sequence similarity (*yellow*), non-conserved residues (*clear*). Black triangles denote residues that have been experimentally or structurally implicated in lipid binding [11-15], boxed sequences highlight the apical C1 and C2 loops, the dot indicates the end of the C-domain, and 'LINKER' represents the four residue linker connecting the C1- and C2-domains. Amino acid numbering corresponds to hFV (Uniprot P12259) after subtraction of the 28-residue signal peptide.

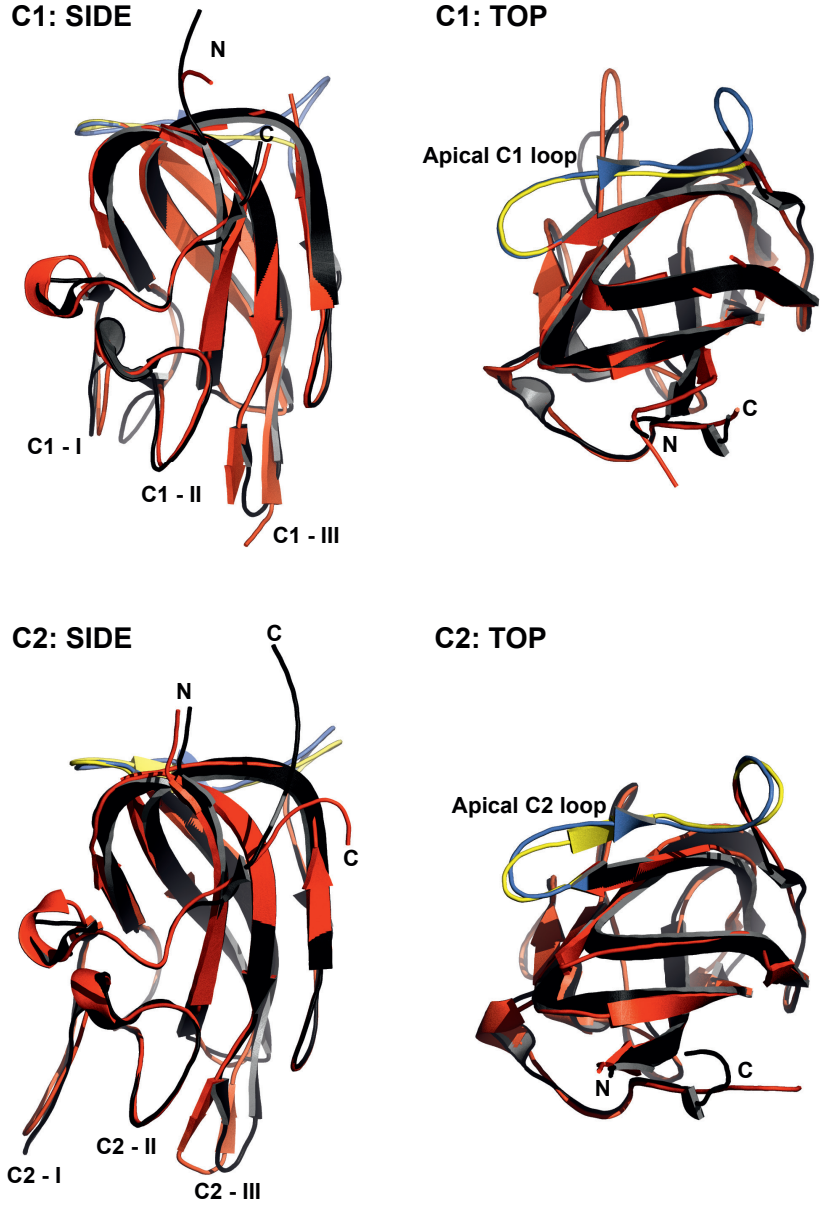

Supplementary Figure 2. Superposition of human FV and ptFV C-domains. The human C-domains (PDB ID 1FV4) and ptFV C-domains (PDB ID 4BXW) [25, 39] were superposed by aligning the structures exclusively to conserved residues. Roman numerals highlight the phospholipid binding spikes. Color coding: hFV (*black*), ptFV (*red*), human apical C1 or C2 loop (*blue*) and ptFV apical C1 or C2 loop (*yellow*). Note: the ptFV apical C1 loop sequence 'R^{1221}-HSET' is not sufficiently resolved in the ptFV crystal structure and is not included in the figure. Visualization and superposition was performed using PyMOL (Schrödinger).

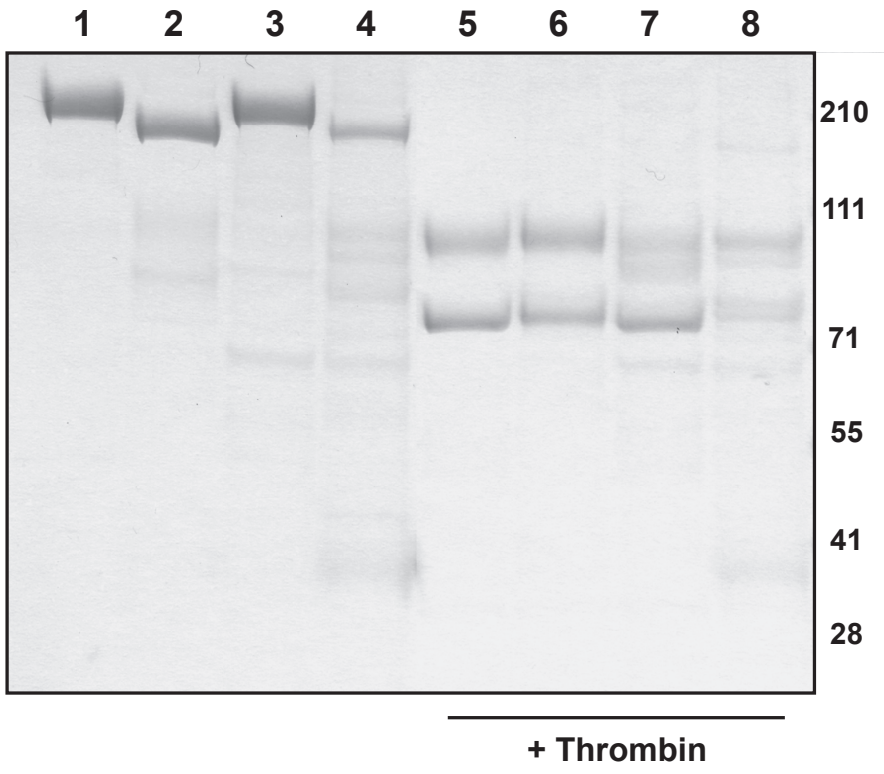

Supplementary Figure 3. Chimeric FV variants. SDS-PAGE analysis of purified proteins (5 µg/lane) before (lanes 1-4) and after treatment with thrombin (lanes 5-8) were subjected to SDS-PAGE under reducing conditions and visualized by staining with Coomassie Brilliant Blue R-250. Lanes 1,5: hFV (FV-810); lanes 2,6: ptFV; lanes 3,7: hFV-ptC; lanes 4,8: ptFV-hC. The apparent molecular weights of the standards are indicated.

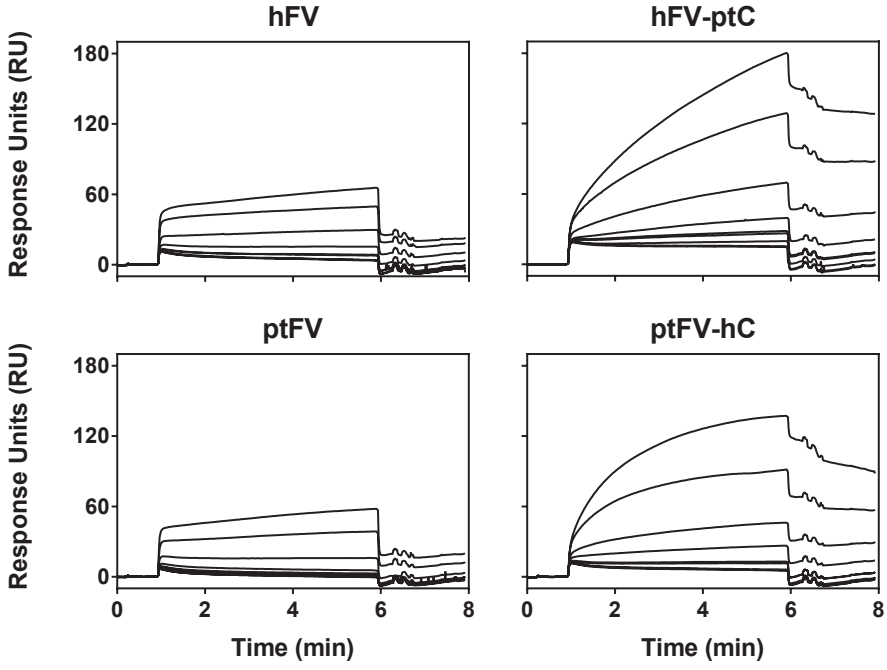

Supplementary Figure 4. Binding of FV to phosphatidylcholine vesicles. Reference association and dissociation phase SPR curves for hFV (FV-810), hFV-ptC, ptFV and pt-FV-hC to an L1 chip coated with phospholipid vesicles containing 100% PC was assessed by SPR as described in 'Materials and Methods'. Cofactor injection started at t = 1 minute and was discontinued at t = 6 minutes. Non-specific binding of FV to 100% PC showed up to 65 response units (RU) of binding at the maximal hFV concentration assessed, 180 RU for hFV-ptC; 140 RU for ptFV-hC, and 40 RU for ptFV.

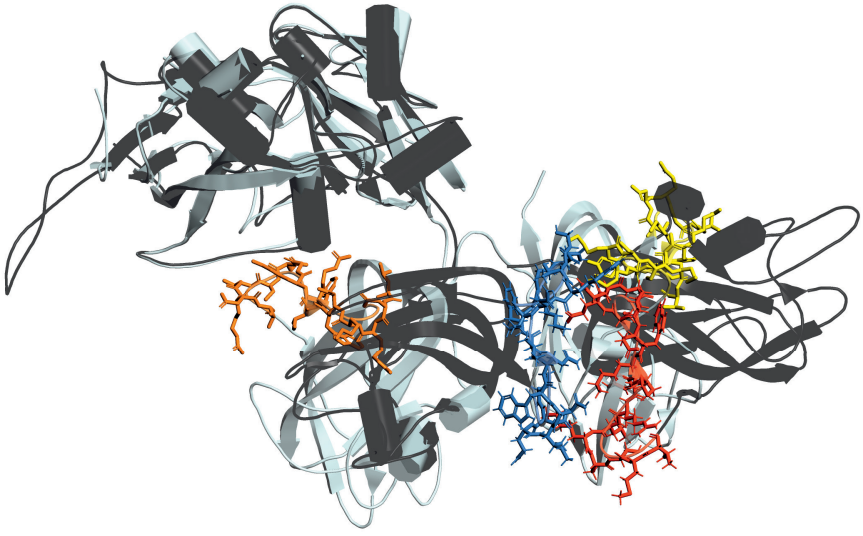

Supplementary Figure 5. The human FVa and bovine FVa$_i$ apical C1 and C2 loops. Superposition of human FVa and bovine FVa$_i$ structures was performed by exclusive alignment of conserved A3-domain residues. The linear C-domain configuration is represented by the model for human FVa (pdb: 1FV4, *dark grey*) [39], and the juxtaposed C-domain configuration is represented by the model for bovine FVa$_i$ (pdb: 1SDD, *light grey*) [11]. The human apical C1 loop (S1971-V1987, *blue*) and apical C2 loop (S2130-V2146, *red*) are highlighted and shown in sticks, the homologous bFVa$_i$ apical C1 loop (*orange*) and apical C2 loop (*yellow*) are shown in sticks as well. The apical C1 and C2 loops are in direct contact with each other while arranged in a linear C-domain configuration (human FVa). In contrast, the apical C1 and C2 loops are spaced apart while arranged in the juxtaposed C-domain configuration (bovine FVa$_i$). Visualization and superposition was performed using PyMOL.


4

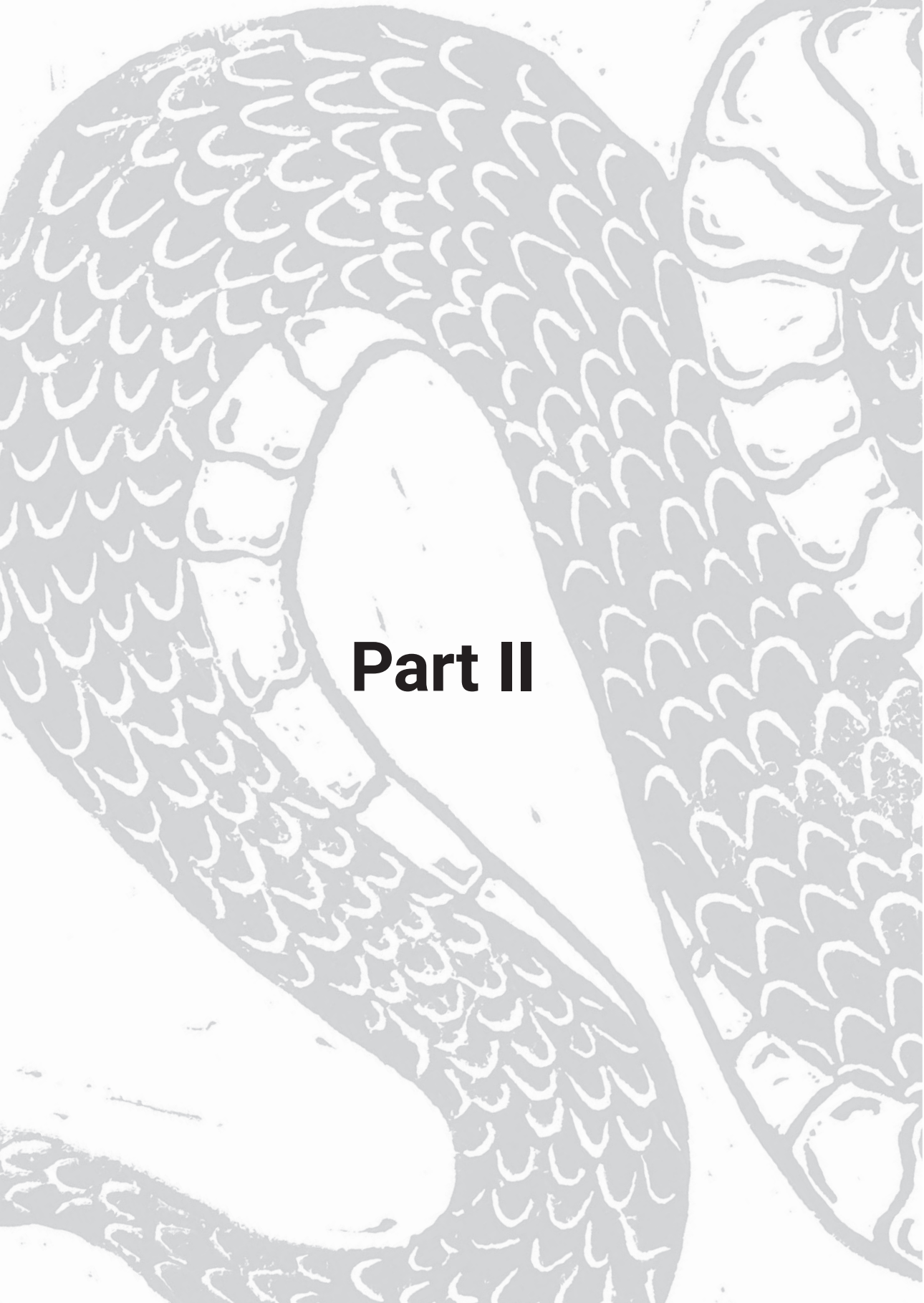

Part II

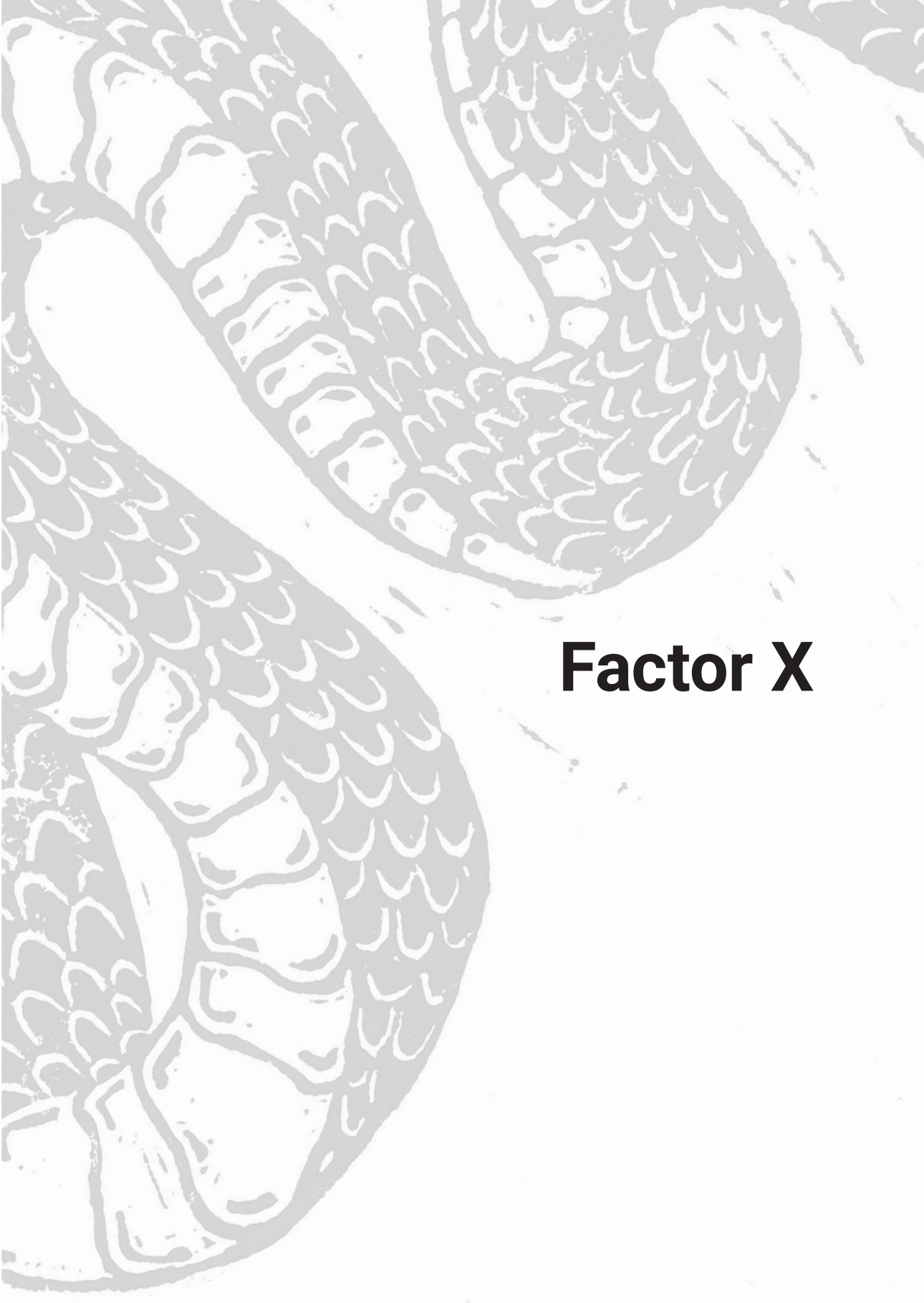

Factor X

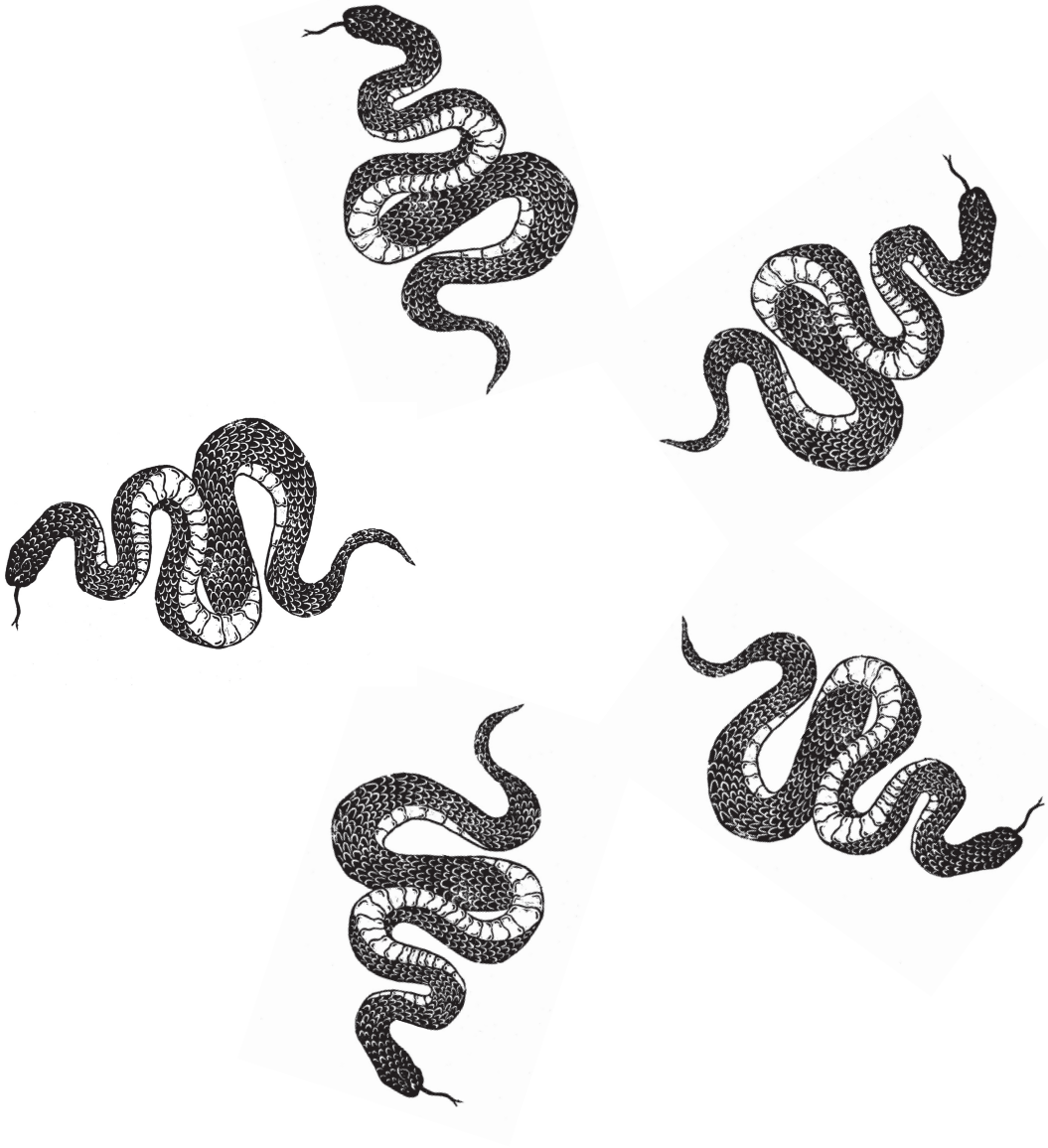

Chapter 5

Engineered factor Xa variants retain procoagulant activity independent of direct factor Xa Inhibitors

Daniël Verhoef, Koen M. Visscher, C. Ruben Vosmeer, Ka Lei Cheung, Pieter H. Reitsma, Daan P. Geerke and Mettine H.A. Bos.

Nature Communications, 2017. 8(1): p. 528.

Abstract

The absence of an adequate reversal strategy to prevent and stop potential life-threatening bleeding complications is a major drawback to the clinical use of the direct oral inhibitors of blood coagulation factor Xa (FXa). Here we show that specific modifications of the substrate binding aromatic S4 subpocket within the FXa active site disrupt high affinity engagement of the direct FXa inhibitors. These modifications either entail amino acid substitution of S4 subsite residues Tyr99 and/or Phe174 (chymotrypsinogen numbering), or extension of the 99-loop that borders the S4 subsite. The latter modifications led to the engineering of a FXa variant that is able to support coagulation in human plasma spiked with (supra-) physiological concentrations of direct FXa inhibitors. As such, this FXa variant has the potential to be employed to bypass the direct FXa inhibitor-mediated anticoagulation in patients that require restoration of blood coagulation.

Introduction

The human hemostatic system protects against thrombosis and bleeding by balancing pro- and anticoagulant stimuli through an intricate network of enzymatic reactions governed by (pro)enzymes, (pro)cofactors, and inhibitors, collectively known as the coagulation cascade. Blood coagulation factor X (FX) plays a pivotal role in this system as it, once activated and assembled into the prothrombinase complex, converts prothrombin to thrombin. Thrombin is the key regulatory enzyme of the coagulation cascade and, among others, converts soluble fibrinogen to insoluble fibrin strands, which serve to stabilize the platelet-based primary blood clot. The spatiotemporal assembly of the prothrombinase complex is tightly regulated and occurs exclusively on negatively charged membrane surfaces (of activated cells or platelets), where activated factor X (FXa) assembles with its cofactor activated factor V (FVa) in the presence of calcium ions [1]. This process is initiated through the activation of FX by the extrinsic (tissue factor (TF)-factor VIIa (FVIIa)-mediated) or intrinsic (factor VIIIa (FVIIIa)-factor IXa (FIXa)-mediated) pathways of coagulation. Once activated, FXa also propagates coagulation by activating other factors [2], including plasma FV in a phospholipid-dependent manner [3]. The interaction of FXa with its cofactor FVa is essential as it results in physiologically relevant catalytic rates of prothrombin activation [1, 4].

The (chymo)trypsin-like serine protease FXa circulates in plasma as a 59 kDa zymogen glycoprotein and consists of two chains that are covalently linked by a disulphide bond. The N-terminal light chain contains a vitamin K-dependent gamma-carboxyglutamic acid-rich (GLA-) domain and two epidermal growth factor-like (EGF) domains; the C-terminal heavy chain consists of an activation peptide and a serine protease domain. The FXa serine protease domain adopts the classical two β-barrel fold of chymotrypsin-like serine proteases, with the catalytic triad residues His57, Asp102, and Ser195 (chymotrypsinogen numbering) situated in the active site cleft that is located between the two β-barrels [5]. While the catalytic triad in conjunction with the oxyanion hole residues regulate substrate cleavage, the active site subpockets S1-S4 control substrate recognition and binding. In the S1 subsite, this interaction is facilitated through a salt bridge between Asp189 and a positively charged side chain/moiety from the substrate/ligand. The aromatic S4 subpocket, which is formed by residues Tyr99, Phe174, and Trp215, contributes via hydrophobic interactions. The macromolecular substrate specificity and affinity are primarily directed through exosite binding [6], which involves surface regions in the serine protease domain that are distinct from the active site [7]. Proteolytic removal of the FX activation peptide induces maturation of the serine protease domain through conformational rearrangements, resulting in proper alignment that allows for engagement of the exosite and active site regions [8, 9]. Apart from substrate binding, the mature active site also readily

interacts with the naturally occurring inhibitors of coagulation. Tissue factor pathway inhibitor (TFPI) tightly binds both the TF-FVIIa-FXa complex as well as free FXa [10]. The principal inhibitor of freely circulating FXa is the irreversible serine protease inhibitor antithrombin (AT) [11].

Active site inhibition of procoagulant serine proteases including FXa has been the focus of anticoagulant drug discovery for over a decade [12]. This has led to the clinical approval of several orally active, synthetic inhibitors of FXa for the prophylactic management of stroke in atrial fibrillation and prevention and treatment of venous thrombosis. These so-called direct oral anticoagulants (DOACs) currently include the direct FXa inhibitors rivaroxaban [13], apixaban [14], and edoxaban [15]. By reversibly engaging the active site of FXa with high affinity, the small molecules effectively block the catalytic activity of both free and prothrombinase-assembled FXa. However, a major drawback to their use is the absence of an adequate reversal strategy to prevent and stop potential life-threatening bleeding complications associated with anticoagulant therapy. Here we present human FXa variants that display a reduced sensitivity to inhibition by the direct FXa inhibitors due to modifications in the active site region, which are based on exceptional structural adaptations found in FX variants that are expressed in the venom of specific Elapid snakes. Using a combined computational and biochemistry approach, we have uncovered the mechanistic basis of the FXa inhibitor-sensitivity of these variants, and demonstrate their effectiveness as potential bypassing agents in plasma containing direct FXa inhibitors.

Materials and Methods

Materials and Reagents

Rivaroxaban, apixaban, and edoxaban were obtained from Alsachim (Illkirch, France) or Adooq Bioscience (Irvine, CA, USA), and weighted and dissolved in vehicle (10% EtOH (vol/vol), 10% Glycerol (vol/vol), 10% PEG400 (vol/vol) (Sigma) and 70% Dextrose (5% solution) (vol/vol)) and stored at -20°C. The peptidyl substrate methoxycarbonylcyclohexylglycylglycyl-Arg-pNA (SpecXa) was obtained from Sekisui Diagnostics (Stamford, CT, USA), the peptidyl substrates H-D-Phe-Pip-Arg-pNA (S2238) and N-α-benzyloxycarbonyl-D-Arg-Gly-Arg-pNA (S2765) were obtained from Instrumentation Laboratories (Bedford, MA, USA). All tissue culture reagents were from Life Technologies (Carlsbad, CA, USA) except insulin-transferrin-sodium selenite (ITS), which was from Roche (Basel, Switzerland). Small unilamellar phospholipid vesicles (PCPS) composed of 75% (w/w) hen egg L-phosphatidylcholine and 25% (w/w) porcine brain L-phosphatidylserine (Avanti Polar Lipids, Alabaster, AL) were prepared and characterized as described previously [16]. Calibrator and fluorescent substrate (FluCa) were from Thrombinoscope (Maastricht, the Netherlands). FX-depleted human plasma, Neoplastine CI Plus 10 prothrombin time (PT) reagent, and Triniclot automated activated partial thromboplastin time (APTT) reagent were obtained from Diagnostica Stago (Paris, France). Normal pooled plasma (NPP) was obtained from Sanquin (Amsterdam, the Netherlands). Unfractionated Heparin (UFH) was obtained from LEO Pharma (Ballerup, Denmark). Polybrene was obtained from Sigma Aldrich (St. Louis, Mo, US). All functional assays were performed in HEPES buffered Saline (HBS: 20 mM Hepes, 0.15 M NaCl, pH 7.5) supplemented with 5 mM CaCl2 and 0.1% PEG8000 (assay buffer). Mammalian expression vector pcDNA3.1 carrying recombinant human FX or recombinant *P. textilis* venom FX and the pcDNA3.1 vector carrying Furin proprotein convertase were generous gifts from Rodney Camire (Children's Hospital of Philadelphia). HEK293 cells were obtained from ATCC (Manassas, VA, USA). Cell lines were monthly checked for mycoplasma contamination employing the Venor®*GeM* mycoplasma detection kit (Minerva Biolabs, Berlin, Germany), and mycoplasma contamination was eliminated using Plasmacure™ and Plasmocin™ as prescribed by the supplier (InvivoGen, San Diego, CA, USA).

Proteins

Human recombinant factor V-810 (FV-810) was prepared, purified, and characterized as described previously [17]. Plasma-derived human factor Xa (pd-FXa), DAPA, corn trypsin inhibitor (CTI), antithrombin (AT), and human prothrombin were from Haematologic Technologies (Essex Junction, VT, USA). Tissue factor (TF, Innovin) was obtained from Siemens (Newark, NY, USA). RVV-X activator was obtained from Diagnostica Stago (Paris, France). Paired antibodies to determine factor X antigen were obtained from Cedarlane (Burlington, Canada). The Q5 site-

directed mutagenesis kit and restriction endonucleases, BglIII, HindIII, and ApaI were obtained from New England Biolabs (Ipswich, MA, USA). T4-DNA ligase was obtained from Roche. Recombinant tick anticoagulant protein (rTAP) was a generous gift from Sriram Krishnaswamy (Children's Hospital of Philadelphia). Molecular weights and extinction coefficients ($E_{0.1\%}$, 280 nm) of the various proteins have been reported previously [9, 23]. For the FX(a) variants, all values for the human protein were used.

Construction and expression of recombinant FX

DNA constructs encoding FX variants comprising the Tyr99Ala, Phe174Ala, or both substitutions were prepared from the pcDNA3.1 vector carrying wild-type human FX by site-directed mutagenesis and sequenced for consistency. DNA constructs encoding *P. textilis* isoform and liver FX paralogs, and inserts coding for chimeric FX variants (FX-A, FX-B, and FX-C), were synthesized by Genscript (Piscataway, NJ, USA), subcloned into pcDNA3.1-FX expression vector using either BglII and HindIII (FX paralogs) or ApaI (chimeric FX) and T4-DNA ligase and sequenced for consistency. HEK293 cell lines stably expressing wild-type recombinant human FX, (chimeric) variants of FX, or *P .textilis* paralogs of FX were obtained as described previously [18]. HEK293 cells were co-transfected with pcDNA3.1-FX and -Furin vectors by Lipofectamine2000 according to the manufacturer's instructions. FX expression of transfectants was assessed by conditioning individual clones on expression media for 24 hours and subsequently measuring the FX-specific PT/APTT clotting activity in a modified one-step assay by mixing conditioned media with FX-depleted human plasma in a 1:1 ratio. A reference curve of normal pooled plasma serially diluted in either assay buffer with 0.1% bovine serum albumin (BSA; for PT) or Owren-Koller diluent (for APTT), mixed in a 1:1 ratio with FX-depleted human plasma, was used to calculate the equivalent FX Units per ml plasma. Transfectants with the highest expression were expanded into a 6320 cm^2 cell factory (Thermo Scientific, Waltham, MA USA) and conditioned for 24 hours on expression media (DMEM-F12 nutrient mixture without phenol red supplemented with: penicillin/streptomycin/fungizone, 2 mM L-glutamine, 10 µg/ml ITS, 100 µg/ml Geneticin-418 sulphate, and 6 µg/ml Vit.K). Conditioned media was collected on 10 consecutive days, centrifuged at 4.000*g* to remove cellular debris, filtered over an 0.45 µm membrane, and supplemented with 1 mM benzamidine prior to storage at -20°C.

Purification of FX(a)

Recombinant FX was prepared, purified, and characterized as described previously [19], with the exception that the immunoaffinity purification was replaced by a calcium gradient (0-60 mM) purification of FX on a POROS HQ20-sepharose column (Applied Biosystems, CA, USA). The typical yield of fully γ-carboxylated recombinant FX was 0.9 mg/liter conditioned medium. Purified recombinant FX

was activated with RVV-X (0.1 U/mg FX), isolated by size-exclusion chromatography on a Sephacryl S200 HR column (V_t 460ml), and stored at -20°C in HBS containing 50% (vol/vol) glycerol. Purified products were visualized by Coomassie Brilliant Blue staining employing SDS-PAGE analysis.

Specific clotting activity

The specific extrinsic clotting activity was determined using a modified FX-specific PT-based clotting assay. Purified FX samples were serially diluted to less than 170 nM in assay buffer with 0.1% BSA. In a typical assay, 25 µl of FX-depleted plasma was mixed with an equal volume of sample, followed by a 60 second incubation period at 37°C. Coagulation was initiated after the addition of 50 µl PT reagent, and the coagulation time was monitored using a Start4 coagulation instrument (Diagnostica Stago). The specific intrinsic clotting activity was determined using a modified FX-specific APTT-based clotting assay. FX samples were serially diluted to less than 170 nM in Owren-Koller diluent. FX-depleted plasma (25 µl) was mixed with sample (25 µl) and APTT reagent (50 µl), followed by a 180 second incubation period at 37°C. Coagulation was initiated after the addition of 50 µl of 25 mM CaCl2, upon which the coagulation time was monitored. Reference curves consisted of serial dilutions of normal pooled plasma.

Macromolecular substrate activation

Steady-state initial velocities of macromolecular substrate cleavage were determined discontinuously at 25°C in assay buffer as described [8]. Briefly, progress curves of prothrombin activation were obtained by incubating PCPS (50 µM), DAPA (10 µM), and prothrombin (1.4 µM) with human recombinant FV-810 (20 nM; B-domain truncated, constitutively active FV [20]), and the reaction was initiated with 0.1 – 1 nM of pd-FXa, wt-FXa, FXa-A, FXa-B, or FXa-C. The rate of prothrombin conversion was measured as described [21]. The reported kinetic parameters and equilibrium binding constants for prothrombin (k_{cat}, K_m) and cofactor Va ($K_{d,\ app}$) by pd-FXa and wt-FXa correspond to previous reported values [20]. Prothrombin conversion was assayed in the absence or presence of direct FXa inhibitors apixaban or edoxaban (0.001 µM – 100 µM final) in order to determine IC_{50} concentrations for each (recombinant) FXa variant. Activation of FX variants by the intrinsic FVIIIa/FIXa tenase complex was performed as described [22]. Briefly, 40 nM FVIII (Aafact) was activated by 100 nM of thrombin and blocked after 30 seconds by adding 150 nM hirudin. Progress curves of FX activation were obtained by incubating FIXa (0.5 nM), PCPS (20 µM) and FX (13 – 2200 nM), and the reaction was initiated with FVIIIa (5 nM). The reaction was quenched in assay buffer with 50 mM EDTA at different time points, and the rate of FX conversion was measured as described. The FXa generated was quantified using a standard curve of wt-FXa or FXa-C.

Chromogenic substrate hydrolysis

The kinetics of peptidyl substrate hydrolysis (SpecXa and S2765) were measured in assay buffer using increasing concentrations of substrate (10 – 800 μM) and initiated with free FXa (2 – 5nM) or assembled into prothrombinase using the following conditions: PCPS (50 μM) and FVa (20 nM).

Inhibition of FXa by antithrombin

The rate of inactivation of FXa by AT was measured in assay buffer under pseudo-first order rate conditions at ambient temperatures as described previously [23]. Briefly, un-catalyzed reactions were prepared in assay buffer containing 0.2 – 1.0 μM AT with 7.5 nM FXa. After 0 – 110 minutes, residual enzyme activity remaining as a function of time was determined after the addition of 250 μM SpecXa and monitoring the initial steady state increase in absorbance at 405 nm. Catalyzed reactions were prepared in assay buffer containing 1 – 8 nM UFH, 0.5 μM AT, and initiated with 5.0 nM FXa. After 0.5 – 5.0 minutes, residual enzyme activity remaining as a function of time was determined after the addition of 250 μM SpecXa supplemented with 1 mg/ml polybrene. The rate of AT inhibition was determined by fitting the obtained values to an exponential decay function (k_1) and subsequent analysis by linear regression (k_2) using the GraphPad Prism software suite.

Inhibition of FXa by TFPI and rTAP

The overall dissociation constants (K_i) for TFPIα or rTAP binding to FXa were inferred from measurements of residual enzyme amidolytic activity. For TFPIα, reactions were prepared in assay buffer containing 5 nM FXa and 2 – 40 nM TFPIα. After incubation for 3 hours at ambient temperatures, residual enzyme activity was determined after the addition of 250 μM SpecXa and monitoring the initial steady state increase in absorbance at 405 nm. For rTAP, reactions were prepared in assay buffer containing 1 nM FXa and 0.5 – 100 nM rTAP. After incubation for 30 minutes at ambient temperatures, residual enzyme activity was determined after the addition of 250 μM SpecXa and monitoring the initial steady state increase in absorbance at 405 nm. The dissociation constants were determined by fitting the obtained values to the Morrison equation for tight binding using the GraphPad Prism software suite. The equation was constrained for the concentration of enzyme, substrate, and SpecXa Michaelis-Menten constant (K_m: pd-FXa 138 μM; wt-FXa 135 μM; FXa-A 645 μM; FXa-B 658 μM; FXa-C 659 μM).

Calibrated automated thrombography analysis

Thrombin generation was adapted from protocols earlier described [24]. Briefly, thrombin generation curves were obtained by supplementing FX-depleted plasma with TF (2 pM final), CTI (70 μg/ml), PCPS (20 μM), and 1 U/ml (prothrombin time FX clotting activity) of wt-FX (7 μg/ml) or chimeric FX-C (15 μg/ml) in the absence

or presence of apixaban. Alternatively, thrombin generation curves were obtained by supplementing NPP with TF (2 or 6 pM final), CTI (70 µg/ml), PCPS (20 µM), and 10 – 40 µg/ml of wt-FX or FX-C in the absence or presence of apixaban. Thrombin formation was initiated by adding substrate buffer (FluCa) to the plasma. FXa-initiated thrombin generation curves were obtained by supplementing FX-depleted plasma with CTI (70 µg/ml) and PCPS (20 µM). Thrombin formation was initiated by the addition of FXa premixed with apixaban in assay buffer without calcium, and supplemented with a thrombin fluorogenic substrate in $CaCl_2$ containing buffer (FluCa). The final reaction volume was 120 µl, of which 80 µl was plasma. Thrombin formation was determined every 20 s for 30 – 60 minutes and corrected for the calibrator using Thrombinoscope software. The lag time, mean endogenous thrombin potential (ETP, the area under the thrombin generation curve), time to peak, peak thrombin generation, and velocity index were calculated from at least three individual experiments.

Molecular Dynamics simulations

Molecular Dynamics (MD) simulations were performed using GROMACS version 5.1.4 [25], starting from the crystal structure with PDB ID 2P16 [14] for apixaban in complex with wt-FXa, or from the structure obtained by docking apixaban in the substrate binding cleft of isoform FXa (using the 4BXW PDB structure of isoform FXa [26]). To prevent steric hindrance between apixaban and the side chain of Glu192, its chi-1 dihedral was adapted from -147.66° to 54.41°, before docking, in order to open up the binding cleft and representing the orientation in human FXa. Docking was performed using the PLANTS software [27]. The center of the binding site was set to the corresponding center of geometry of apixaban in the wt-FXa structure with a search radius of 1.1 nm. The docking algorithm was ran under speed setting 1 and the resulting models were scored using CHEMPLP [27]. The third ranked structure was selected based on binding pose similarity to the wt-FXa in complex with apixaban.

During MD simulations, the protein was described using the GROMOS 54A7 [28] force field and the system was numerically integrated with a time step of 2 fs, using a leap-frog integrator [29]. After initial energy minimization, the protein was solvated in a periodic dodecahedral box with a minimum distance of 1.4 nm between the solute and the box edges. The system was neutralized by simulating the system in a 150 mM sodium chloride solution. After additional energy minimization, atomic velocities were randomly assigned according to Maxwell-Boltzmann statistics using different seeds for different simulations. The system was equilibrated in four subsequent 1 ns NVT simulations, where the temperature was raised from an initial 100 K to 200 K, and two simulations at a final temperature of 300 K. During the heating steps, protein heavy-atom positional restraining force constants were applied and gradually lowered (from 10000 kJ mol^{-1} nm^{-2} to 5000 kJ mol^{-1} nm^{-2},

50 kJ mol^{-1} nm^{-2}, and 0 kJ mol^{-1} nm^{-2}, respectively). After 5 ns unrestrained pre-equilibration, production simulations were run for 750 ns under NpT conditions in which the temperature was coupled weakly by velocity-rescaling [30] to an external bath at 300 K using a coupling constant of 0.1 ps. The pressure of the system was kept constant at a reference pressure of 1 bar, in an isotropic manner by coupling to a Berendsen barostat [31] using a coupling constant of 0.5 ps and a compressibility of 4.5 * 10^{-5} bar^{-1}. All bond lengths were constrained during simulation using the LINCS algorithm [32] with a single iteration and a highest order of 4 in the constraint coupling matrix. Pairwise interactions were monitored using a Verlet neighbor list [33] with a buffer tolerance of 0.005 kJ mol^{-1} ps^{-1}. Short-range electrostatic and van der Waals interactions up to a cutoff of 1.4 nm were evaluated every time step, and long range electrostatic interactions were computed using a PME scheme [34] with cubic interpolation and a fourier grid spacing of 0.125 nm. Center of mass motion was removed every 100 steps.

Simulation data were written out every 50 ps for further analyses, and minimal atomic distances were monitored using the GROMACS analysis tool g_mindist, where minimal interatomic distances were calculated every 1 ns between residue side-chain and apixaban atoms. For each residue in the protein we calculated a distribution of these distances over the complete production run, and we subsequently sorted the residues by the distribution median. Root-mean-square deviations (RMSD) during simulation of apixaban atomic positions were calculated after conformational fitting on the MD starting structure with respect to backbone atoms of the protein. Averaging over 10 ns intervals generated block-averaged time series for the analyzed data, and subsequently standard deviations were computed.

Statistical analysis

All in vitro data are presented as mean ± 1 standard deviation and are the result of at least three experiments, unless otherwise stated.

Data and code availability

All data supporting the findings of this study and code are available within the article and its Supplementary Materials or from the corresponding author upon reasonable request.

Results

Disruption of ligand-S4 subsite anchoring mediates resistance to direct FXa inhibitors

Comparison of crystal structures of human FXa in complex with the direct FXa inhibitors apixaban (Protein Data Bank (PDB) ID 2P16) or rivaroxaban (PDB ID 2W26) revealed highly similar ligand binding configurations, as both inhibitors occupy the FXa substrate binding S1 and S4 subsites through interactions with an almost identical set of amino acids [13, 14]. The X-ray structures further revealed that occupation of the S4 subsite is mediated, in part, by nonpolar stacking interactions, in which the P4-ring of the inhibitors is sandwiched between the aromatic side chains of Tyr99 and Phe174 (chymotrypsinogen numbering). To assess the molecular requirements for direct FXa inhibitor binding in more detail, we performed 750 ns Molecular Dynamics (MD) simulations of the FXa-apixaban complex (starting from the 2P16 crystal structure). During MD, apixaban adopted a stable position in the active site cleft of FXa, as reflected by the low minimal interaction distances (≤ 0.5 nm) between apixaban and many side chains of the residues lining the binding pocket, such as Phe174, Trp215, Gln192, Ser195 and Tyr99 (*cf.* **Figure 1A**). The narrow distribution of close range contacts between apixaban and the side chain atoms of the S4 pocket residues Tyr99 and Phe174 confirmed stabilization of apixaban in the S4 subsite.

The contribution of S4 residues Tyr99 and Phe174 to apixaban binding was assessed *in vitro* by generating human FXa variants comprising either Tyr99Ala, Phe174Ala, or both mutations. While the single amino acid substitutions resulted in a moderate reduction in apixaban inhibition (± 8-fold enhanced IC_{50}), introducing both mutations increased the IC_{50} of FXa inhibition by apixaban more than 100-fold (**Figure 1B**). These results indicate that modifying the S4 subsite destabilizes binding of apixaban into the FXa active site. In addition, upon mutating Tyr99 to Alanine, the FX specific clotting activity was drastically reduced (5% and 1% residual PT and APTT activity, respectively) and was essentially lost in combination with the Phe174Ala replacement (**Figure 1C**). These findings suggest that whereas both Tyr99 and Phe174 contribute to apixaban binding, Tyr99 is of key importance to both the active site conformation and function of FXa. This is consistent with the fact that Tyr99 is not only evolutionary conserved in a wide range of FX species (**Supplementary Figure 1**), but also essential to active site maturation in the homologous blood coagulation serine protease factor IXa [35, 36]. Alternatively, modifications targeting other amino acids that coordinate apixaban binding (**Figure 1A**) may potentially disrupt docking of apixaban into the active site while preserving clotting activity.Sequence analysis of FX species further revealed that FX paralogs found in various Elapid snakes comprise a heterologous insertion directly N-terminal to Tyr99 (between Thr95 and Lys96; **Supplementary Figure 1**)

[37]. These insertions result in an extended 99-loop (His91-Asp102) that borders the S4 subsite. Surprisingly, characterization of recombinantly prepared FXa paralogs from the Elapid snake *Pseudonaja textilis* showed that both the venom and isoform proteases, unlike any FXa species known to date, are highly insensitive to direct FXa inhibitors. This was demonstrated by a minimal 10,000-fold increase in the IC_{50} of FXa inhibition by apixaban or rivaroxaban (**Figure 2A,B**). While venom FXa is uniquely expressed in the venom gland [38], isoform FXa is both expressed in the liver and venom gland and represents an intermediate between *P. textilis* venom and liver FXa [39, 40]. In contrast, *P. textilis* liver FXa, which comprises a shorter 99-loop (**Supplementary Figure 1**), is efficiently inhibited by submicromolar concentrations of apixaban (**Figure 2B**). These results suggest that an extended 99-loop mediates a reduced sensitivity towards direct FXa inhibitors.

To elucidate the molecular mechanism that is at the basis of the apixaban resistance in *P. textilis* isoform FXa, we performed MD simulations using the crystal structure of isoform FXa (PDB ID 4BXW) [26]. Initial docking of apixaban showed that isoform FXa is able to accommodate apixaban in the active site in an orientation similar to that observed for human FXa (**Supplementary Figure 2**). This is consistent with the observation that the conformation of the S4 subsite is conserved in both FXa variants (**Supplementary Figure 2**). In isoform FXa, the 99-loop adopts an elongated and helical conformation (**Supplementary Figure 2**) with high structural flexibility. The latter is demonstrated by the relatively high B-factors of the 99-loop obtained from 750 ns MD simulations of apixaban-bound and unbound isoform FXa (**Supplementary Figure 3**). Five MD simulations of the isoform FXa-apixaban complex were independently performed, each initiated from an identical conformation but with different atomic starting velocities. During these 750 ns MD simulations we observed displacement of the isoform FXa 99-loop, as reflected by its RMSD values of ≥0.4 nm (**Supplementary Figure 3A-E**). In addition, the following events were observed: a) apixaban displacement from the S1 subsite, combined with a repositioning within the S4 subsite relative to its starting configuration (**Figure 3A**, **Supplementary Figure 4A**), b) apixaban displacement from its initial docked conformation, partial dissociation from the S1 subsite and repositioning within the S4 subsite (**Figure 3B-D**, **Supplementary Figure 4B-D**), or c) a stable apixaban binding conformation in the S1 and S4 subsites that mirrors the initial docking pose of apixaban (**Figure 3E**, **Supplementary Figure 4E**) and is similar to the apixaban configuration in the crystallized human FXa-apixaban complex (**Supplementary Figure 2**). Interestingly, this anchoring of apixaban in the S1 site was accompanied by the lowest flexibility in the displaced 99-loop (**Supplementary Figure 3E**). In the other four isoform FXa-apixaban simulations, we observed substantial movement of the 99-loop (**Supplementary Figure 3A-D**), similar to the simulations of unbound isoform FXa (**Supplementary Figure 3F-J**). This indicates significant mobility of the 99-loop in both the apixaban-bound and

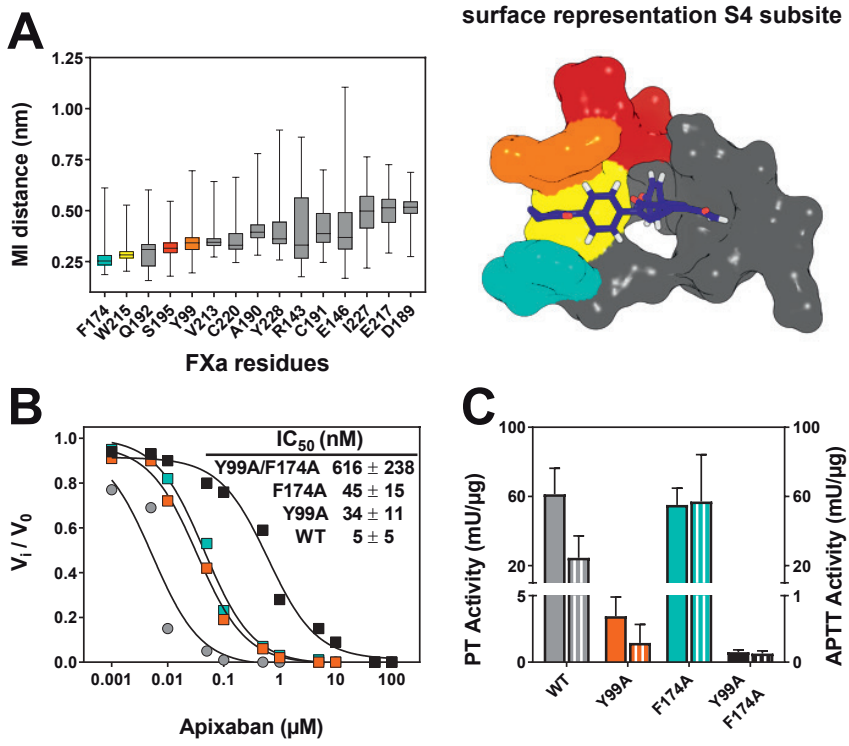

Figure 1. The S4 subsite of factor Xa coordinates apixaban binding and inhibition. (***A***) The minimal interatomic (MI) distances from the side chains of FXa residues to apixaban were calculated every nanosecond during a 750 ns MD simulation of apixaban-bound human FXa. Box plots (with whiskers from minimum to maximum) display the distribution of the observed MI distances for each of the 15 FXa residues with the shortest side chain to apixaban MI distance (sorted by average). The surface representation (inset) depicts the FXa-bound apixaban (blue) configuration throughout the MD simulation. Color coding (corresponding to box plots): S4 subsite residues Tyr99 (orange), Phe174 (cyan), and Trp215 (yellow), catalytic residue Ser195 (red), and others (grey). (***B***) The rate of peptidyl substrate conversion by 5 nM of RVV-X-activated wild-type (grey circles, WT), Tyr99Ala (orange squares, Y99A), Phe174Ala (cyan squares, F174A), or double mutant (black squares, Y99A/F174A) FX was determined with saturating amounts of the cofactor FV-810 (30 nM) and anionic phospholipid vesicles (PCPS, 50 μM) in the absence (V_0) or presence (V_i) of increasing apixaban concentrations (0.001–100 μM). The lines were drawn following nonlinear regression analysis of the data sets, and the fitted parameters for IC_{50} ± 1 standard deviation of the induced fit are shown in the inset. The data are the means of two similar experiments. (***C***) The specific extrinsic (PT Activity) or intrinsic (APTT Activity) clotting activity of wild-type (WT), Tyr99Ala (Y99A), Phe174Ala (F174A), or double mutant (Y99A/F174A) FX from conditioned media was determined as described in 'Materials' by dividing the PT or APTT clotting activity over the FX antigen concentration. Data represent the average ± 1 standard deviation of three representative high-producing stable cell lines per FX variant.

unbound states. The displacement of the 99-loop and the rapid displacement of apixaban observed for most MD simulations are indicative of steric hindrance between apixaban and the structurally flexible isoform FXa 99-loop, impairing apixaban binding. This could explain why isoform FXa is practically insensitive towards direct FXa inhibitors. This is further supported by MD simulations of apixaban binding to human FXa that lacks the extended 99-loop typical to isoform FXa. During these simulations (**Figure 3F-I**, **Supplementary Figure 4F-I**), partial dissociation of apixaban from the S1 subsite was observed in a single simulation only (at 600 ns; **Figure 3F**). Furthermore, apixaban repositioning from the S4 subsite occurred during another single simulation, but in a reversible manner (at 400 ns; **Figure 3G**). Other than these two displacement events, apixaban maintained its original orientation in human FXa during our 750 ns MD simulations

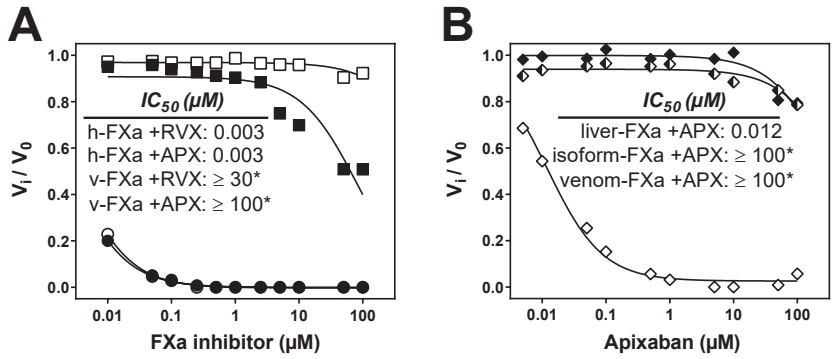

Figure 2. Functional characterization of the effect of the direct factor Xa inhibitors on factor Xa paralogs. (***A***) The rate of peptidyl substrate conversion by purified recombinant *P. textilis* venom FXa (10 nM; squares) or plasma-derived human FXa (2 nM, circles) was determined in the absence (V_0) or presence (V_i) of increasing concentrations (0.01 – 100 μM) of apixaban (APX; open symbols) or rivaroxaban (RVX; closed symbols). (*b*). The rate of peptidyl substrate conversion by RVV-X activated *P. textilis* venom FX (closed squares), isoform FX (semi-closed diamonds), or liver FX (open diamonds) was determined in the absence (V_0) or presence (V_i) of increasing apixaban concentrations (0.01 – 100 μM). (***A,B***) The lines were drawn following nonlinear regression analysis of the data sets, and the fitted parameters for IC_{50} are shown in the inset. The data are the means of two similar experiments. *For these experiments FXa inhibition was inefficient, precluding an accurate assessment of the IC_{50} values.

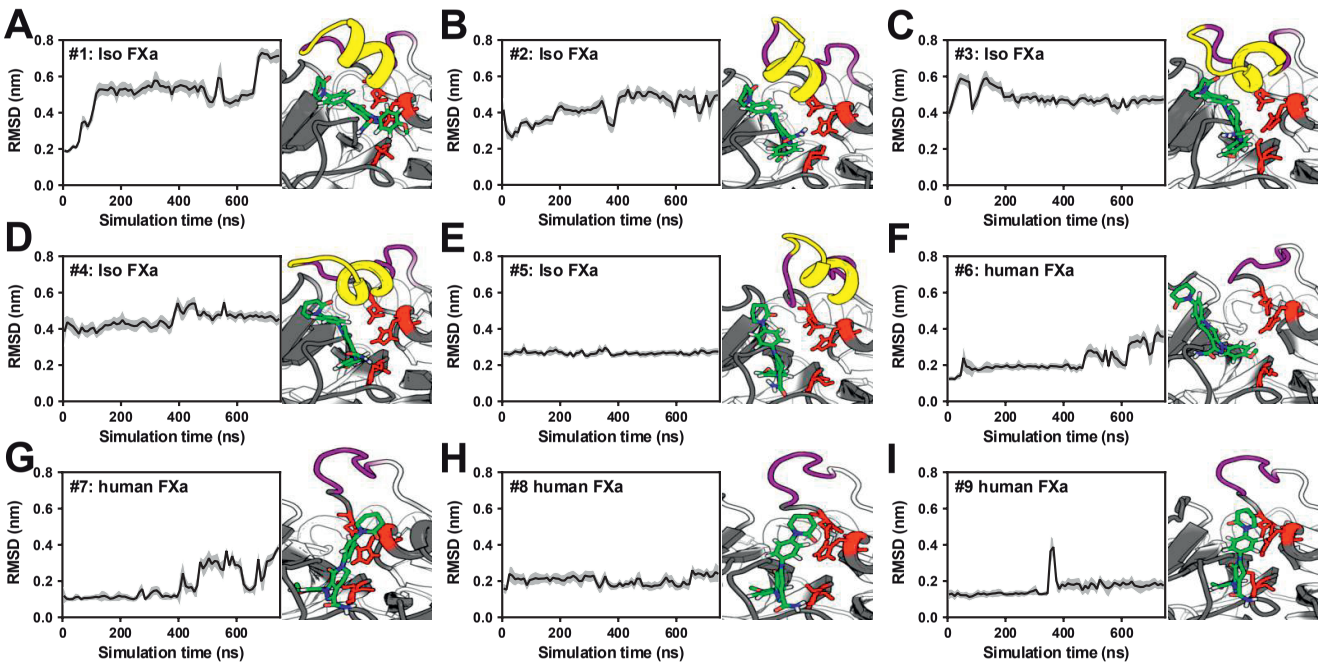

Figure 3. Molecular Dynamics simulations of apixaban bound to factor Xa variants. Root-mean-square deviations (RMSD) of atomic positions of the apixaban ligand during independent 750 ns MD simulations of apixaban binding to either *P. textilis* isoform FXa (Iso FXa; ***A-E***) or to human FXa (***F-I***) are presented as block averages over 10 ns intervals. The corresponding single standard deviation interval is indicated (grey density). For each independent simulation the molecular configurations at 750 ns are depicted, in which apixaban (green), the 99-loop (magenta), the isoform FXa extended 99-loop region PQKAYKFDL (yellow), and the catalytic triad residues (red) are highlighted. Molecular configurations at 250 ns and 500 ns are of each simulation are compared with those at 750 ns in **Supplementary Figure 4.**

Characterization of chimeric FXa

We next aimed to investigate whether insertions within the 99-loop similar to those found in snake FX (**Supplementary Figure 1**) reduce the sensitivity of human FXa towards direct FXa inhibitors. To this end, human-snake FX chimeras were constructed in which the human sequence His91-Tyr99 was replaced with the homologous region of venom (FX-A) or isoform (FX-C) *P. textilis* FX, or of *Tropidechus carinatus* venom FX (FX-B) (**Figure 4A**). Following stable FX expression in HEK293 cells, purified chimeric FXa variants were subjected to SDS-PAGE analysis, which showed all FXa variants to migrate similar to plasma-derived (pd-FXa) and recombinant wild-type FXa (wt-FXa) (**Figure 4B**).

Evaluation of the kinetics of prothrombin conversion in the presence of saturating amounts of the FVa-like cofactor FV-810 [20] and anionic phospholipids revealed that the rate of prothrombin activation by the chimeric variants was 3- to 10-fold reduced (**Table 1**), which may be indicative of a modified active site conformation. Nonetheless, the FXa variants displayed an up to 3-fold enhanced affinity for prothrombin as compared to wt-FXa and an apparent affinity for the cofactor Va that was similar to that of human FXa (**Table 1**). This shows that all chimeric variants are able to efficiently assemble into the prothrombinase complex and engage with the macromolecular substrate prothrombin.

Table 1. Kinetic constants for macromolecular or peptidyl substrate cleavage and prothrombinase assembly.

	Prothrombin*	**Prothrombin***	**Cofactor Va***	**S2765***	**S2765***	**S2765†**	**S2765†**
	K_m, μM	k_{cat}, min^{-1}	$K_{d,app}$, nM	K_m, μM	k_{cat}, s^{-1}	K_m, μM	k_{cat}, s^{-1}
pd-FXa	0.31 ± 0.07	1880 ± 136	0.41 ± 0.05	59 ± 19	47 ± 4	29 ± 8	36 ± 3
wt-FXa	0.41 ± 0.08	1243 ± 089	1.44 ± 0.41	33 ± 7	27 ± 2	26 ± 8	21 ± 2
FXa-A	0.14 ± 0.04	0122 ± 008	0.81 ± 0.26	39 ± 7	09 ± 1	243 ± 50	11 ± 1
FXa-B	0.25 ± 0.07	0239 ± 020	0.85 ± 0.28	49 ± 8	10 ± 1	249 ± 29	15 ± 1
FXa-C	0.22 ± 0.04	0370 ± 019	0.57 ± 0.06	60 ± 11	17 ± 1	216 ± 28	21 ± 1

The kinetic constants for the enzyme *prothrombinase or †FXa were obtained as described in 'Materials'. Fitted values ±1 standard deviation of the induced fit are representative of two to three individual experiments.

Extension of the FXa 99-loop impairs active site binding

Analysis of the direct FXa inhibitor-dependent inhibition of prothrombin activation revealed a dramatic increase in half-maximum inhibition for all FXa variants. Apixaban or edoxaban inhibition of FXa assembled into prothrombinase was least efficient for variants B and C, as we observed an up to ~700-fold increase in IC_{50}, while the inhibition of variant A was approximately 10- to 90-fold impaired as compared to human FXa (**Table 2**). These data indicate that, consistent with the MD simulations (**Figure 3A-E**), insertion of the snake venom His91-Tyr99 regions results in impaired binding of the S4 subsite in human FXa. As the cofactor FVa may also affect active site binding by apixaban, we assayed apixaban-inhibition of FXa-C in the presence and absence of FVa. Interestingly, we observed a 2-fold higher IC_{50} in the presence of factor Va and anionic phospholipids (**Supplementary Figure 5**) These findings indicate that prothrombinase-assembled FXa-C may be more resistant to inhibition by apixaban to some extent, which could result from structural constraints imposed by the interaction of FXa with FVa.

To further explore the effect of the insertions on the FXa active site, the binding and cleavage of the peptidyl substrate S2765 was examined. We observed an up to 9-fold increase in K_m and 2-fold reduced k_{cat} for the uncomplexed FXa variants compared to wt-FXa (**Table 1**). This further confirms that the FXa variants have a slightly altered activity and a modified active site. We next assessed the second-order rate constants of FXa inhibition by the active site-directed inhibitor AT [36]. Inhibition of FXa variant A proceeded at a 33-fold reduced rate relative to wt-FXa, whereas that of variants B and C was 10- and 4-fold decreased, respectively (**Table 2**). The impaired AT inhibition was restored upon the addition of unfractionated heparin (UFH), resulting in similar rates of AT inhibition for all FXa species, consistent with previous reports [42]. This shows that, unlike the FXa active site,

Table 2. Kinetic parameters for the inhibition of factor Xa variants.

	Antithrombin $k_{2,\ uncatalysed}$ $M^{-1}\ s^{-1} x\ 10^3$	**Antithrombin** $k_{2,\ UFH}$ $M^{-1}\ s^{-1} x\ 10^6$	**TFPIα** K_i, *nM*	**rTAP** K_i, *nM*	**Apixaban** IC_{50}, *nM*	**Edoxaban** IC_{50}, *nM*
pd-FXa	1.55 ± 0.13	3.59 ± 0.39	ND	0.87 ± 0.18	2 ± 0.2	3 ± 2
wt-FXa	4.07 ± 0.20	3.09 ± 0.64	1.62 ± 0.25	0.70 ± 0.04	1 ± 0.2	2 ± 1
FXa-A	0.12 ± 0.02	1.55 ± 0.46	4.35 ± 1.32	26.30 ± 8.45	93 ± 23	23 ± 14
FXa-B	0.41 ± 0.03	1.02 ± 0.40	4.41 ± 1.89	7.92 ± 1.88	652 ± 200	218 ± 31
FXa-C	0.95 ± 0.11	6.73 ± 3.61	6.46 ± 1.63	20.24 ± 6.56	716 ± 247	375 ± 215

Fitted values ± 1 standard deviation of the induced fit are representative of two to three individual experiments. ND: not determined.

the heparin-binding exosite in FXa [43] is not affected by insertion of the snake venom His91-Tyr99 regions. In addition, we investigated the binding affinities (K_i) of the active site inhibitors TFPIα and recombinant tick saliva anticoagulant protein (rTAP) [44] towards the chimeric FXa variants. Essentially, binding constants for both TFPIα and rTAP were perturbed, as rTAP binding was at least 11-fold reduced while TFPIα inhibition was at most 4-fold reduced in the chimeric FXa variants (**Table 2**). The difference between the binding constants of TFPIα and rTAP towards chimeric FXa corroborates structural data that reports a more extensive buried surface area between TFPIα-FXa (>1700 $Å^2$) [45] compared to rTAP-FXa (~900 $Å^2$) [46]. Moreover, inhibition of FXa by rTAP involves S4 subsite occupation [46], while inhibition of FXa by the Kunitz-II domain of TFPIα entails reorganization of the active site cleft through Tyr99 side chain reorientation [45]. Collectively, the attenuated inhibition of the FXa chimeras by AT, TFPIα, and rTAP is in agreement with the notion that extension of the 99-loop impairs active site engagement. Assessment of the catalytic efficiency of the FXa variants towards the macromolecular and peptidyl substrates suggests that this may be modulated by the length and/or composition of the region between His91-Tyr99. When comparing all FXa derivatives, variant FXa-C that comprises the shortest His91-Tyr99 sequence (**Figure 4A**) retained the highest k_{cat} towards both substrates (**Table 1**). The same trend was observed for AT inhibition in the absence of UFH (**Table 2**). From this we conclude that all of the sequences inserted between His91-Tyr99 negatively affect active site engagement. The relatively short amino acid insertion in variant C is derived from isoform FXa in which it adopts a helical conformation (**Supplementary Figure 2**) [26]. We speculate that this conformation may be maintained in FXa-C, resulting in a more structured 99-loop which compromises FXa catalytic activity least. Whether this results from a relatively limited extension over the active site and/or a different effect on overall protein motion and subpocket S4 flexibility between the FXa variants remains to be determined [47]. The relation between 99-loop architecture and substrate specificity has also been made clear in structural and biochemical studies on kallikreins. These trypsin-like serine proteases comprise 99-loops that vary greatly in length and can range from 2 to up to 22 additional residues between His91 and Tyr99, the latter concerns a kallikrein-like salivary toxin (BLTX) from the North American shrew [48, 49]. In general, variation of 99-loop length has significantly impacted enzymatic diversification in kallikreins. For example, the elongated 99-loop of human kallikrein-related peptidase-2 has been shown to extend over the active site and function as a regulator of enzyme activity through zinc-binding [50]. Alternatively, the BLTX 99-loop has been implicated to contribute to an increased catalytic efficiency *in silico* [51]. The elongated 99-loops of the venom FXa paralogs [18] may therefore be viewed in a broader perspective that highlights the general significance of 99-loop architecture in enzymatic diversification of trypsin-like serine proteases.

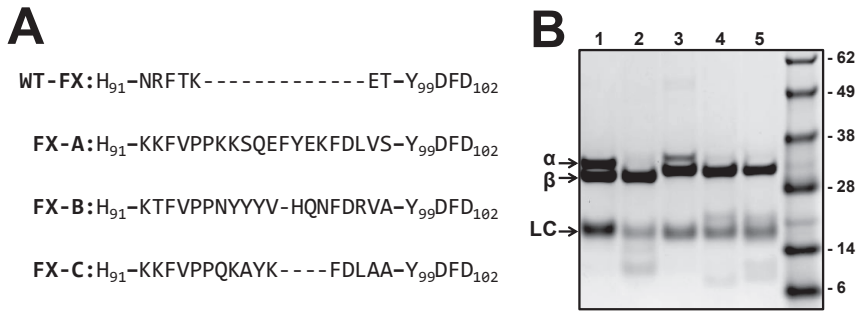

Figure 4. Snake-human factor X(a) variants. (***A***) An alignment of region His91-Asp102 in human FX (WT-FX) and FX variants A (FX-A), B (FX-B), and C (FX-C) is shown. The sequences inserted between His91-Tyr99 originate from *P. textilis* venom FX (FX-A), from *T. carinatus* venom FX (FX-B), or from *P. textilis* isoform FX (FX-C). (***B***) Proteins (3 µg/lane) were subjected to SDS-PAGE under reducing conditions and visualized by staining with Coomassie Brilliant Blue. Lane 1: plasma-derived FXa, lane 2: recombinant wild-type FXa, lane 3: FXa variant A, lane 4: FXa variant B, lane 5: FXa variant C. The protein bands corresponding to the heavy chain derived from α or β FXa (α/β), the FXa light chain (LC), and the apparent molecular weights (kDa) of the standards are indicated. While autoproteolytic excision of the C-terminal portion of FXa-α (residues 436–447) yields the β form of FXa, both isoforms are functionally similar with respect to prothrombinase assembly, prothrombin activation, antithrombin recognition, and peptidyl substrate conversion [41]. The purified products of wt-FXa and FXa variants B and C migrate predominantly as FXa-β; FXa variant A migrates as a 50/50 mixture of α and β FXa.

Chimeric FX(a) as hemostatic bypassing agent

The ability to activate prothrombin in the presence of physiological concentrations of direct FXa inhibitor potentially enables chimeric FXa to restore hemostasis in plasma inhibited by such anticoagulants. Functionality of the chimeric variants was therefore assessed by calibrated automated thrombography in plasma spiked with direct FXa inhibitors [24]. To do so, we first assessed FXa-initiated thrombin generation (TG) in FX-depleted plasma in the absence of FXa inhibitors. Thrombin generation initiated by FXa variant C resulted in a thrombin peak height and endogenous thrombin potential (ETP) similar to wt-FXa-initiated TG, while these parameters were modestly reduced following initiation with variant A or B (**Supplementary Table 1**). As expected, addition of a physiological concentration of apixaban (2 μM) significantly impaired wt-FXa-initiated TG. In contrast, the TG parameters were not affected upon initiation with FXa variant C (**Supplementary Table 1**). As FXa-C displayed superior TG parameters, we consequently investigated whether the zymogen form of variant C (FX-C) would be able to restore the apixaban-dependent defect in TG. To assess this, thrombin generation was initiated with a limiting tissue factor concentration (TF, 2 pM) in FX-depleted plasma supplemented with plasma concentrations of zymogen FX. Other than a 1.4-fold delay in time to peak with FX-C present (**Supplementary Table 2)**, comparable TG curves and parameters were obtained following supplementation with FX-C or wt-FX in the absence of inhibitor (**Figure 5A)**. Consistent with previous observations, FX-C-dependent TG was fully sustained both in the presence of physiological (2 μM) and supra-physiological (6 μM) concentrations of apixaban (**Figure 5A)** or edoxaban (**Figure 5B)**, while the TG parameters were severely impaired following wt-FX supplementation **(Supplementary Table 2)**.

The ability of FX-C to restore TG in the presence of apixaban was also examined in normal pooled plasma (NPP) from healthy individuals. Similar to previous findings, apixaban almost fully inhibited thrombin generation in NPP **(Figure 5C-D)**. Addition of increasing concentrations of zymogen FX-C to NPP restored TG both under conditions of a limited TF-trigger **(Figure 5C)** and upon initiation with a high TF concentration **(Figure 5D)**. This was demonstrated by a normalization of the peak height in the presence of 20 – 40 μg/ml FX-C, while the time to peak was 1.3- to 1.6-fold prolonged **(Supplementary Table 3)**. Assessment of TG upon addition of 40 μg/ml FX-C in the absence of apixaban indicated that no significant surplus of thrombin was generated as all TG parameters were within the range of those of NPP (**Supplementary Table 3**).

As the zymogen form of variant C typically displayed a TF-dependent delay in time to peak thrombin formed, we investigated whether activation of FV by variant FXa was perturbed. The FXa-dependent activation of FV is essential for the early phase of TG, thereby mediating the subsequent burst of thrombin formed [3].

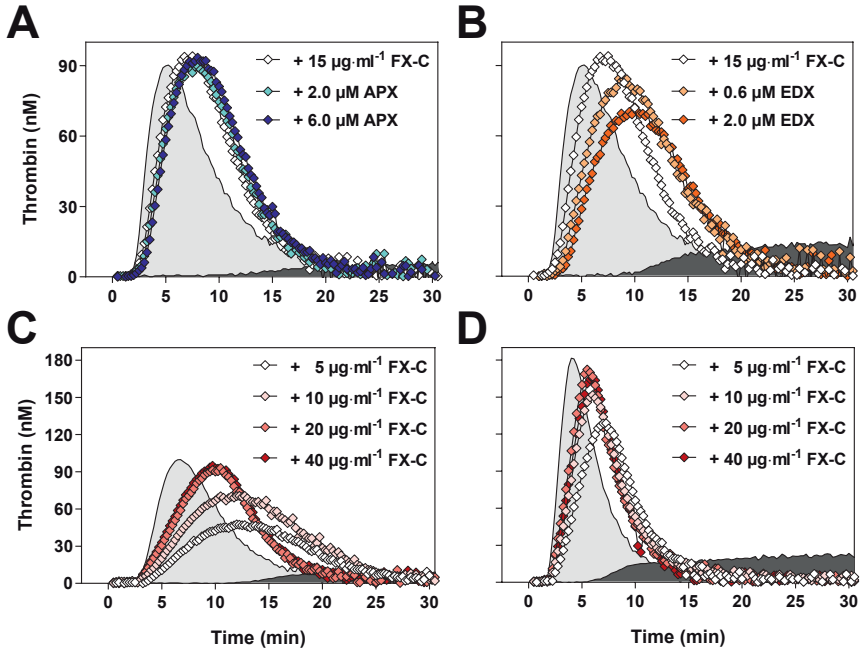

Figure 5. Zymogen factor X-C corrects thrombin generation in plasma spiked with apixaban. (***A,B***) Thrombin generation (TG) was measured for 30 minutes at 37°C in FX-depleted plasma supplemented with 1 U/ml FX-C (15 µg/ml) in the absence (open symbols) or presence of 2 µM or 6 µM apixaban (***A***, APX, blue symbols) or 0.6 µM or 2 µM edoxaban (***B***, EDX, orange symbols) with 2 pM tissue factor (TF) and 20 µM PCPS. Thrombin generation was initiated with $CaCl_2$ and a thrombin fluorogenic substrate as detailed in 'Materials'. The TG profiles of FX-depleted plasma supplemented with 1 U/ml (7 µg/ml) wt-FX in the absence (light grey area under the curve) or presence (dark grey area under the curve) of 2 µM apixaban (***A***) or 0.6 µM edoxaban (***B***) are shown. (***C,D***) Thrombin generation was measured for 30 minutes at 37°C in normal pooled plasma in the presence of 2 pM (***C***) or 6 pM (***D***) TF, supplemented with increasing concentrations FX-C (5 – 40 µg/ml), 2 µM apixaban, and 20 µM PCPS. The TG profiles of normal pooled plasma in the absence (light grey area under the curve) or presence (dark grey area under the curve) of 2 µM apixaban are shown. All curves are representatives of 3 to 6 similar experiments.

Proteolysis of full-length plasma-derived FV by FXa-C appears to involve one or more cleavage sites that are distinct from cleavage by wt-FXa, indicated by a differential fragmentation profile (**Supplementary Figure 6**). Nevertheless, FXa-C was also capable of generating the FVa heavy chain and light chain activation products, similar to wt-FXa. Furthermore, the delay in time to peak was not due to a defect in activation by the intrinsic tenase complex [22], as the kinetic parameters for FX-C activation by the intrinsic (FVIIIa/FIXa) tenase complex were unperturbed (**Supplementary Figure 7**). Another explanation could lay in the notion that activation of FX-C by the extrinsic or intrinsic tenase results in a partly zymogen-like conformation of the FXa active site. Given that assembly of FXa into the prothrombinase complex at least partially corrects an impaired active site [8, 9, 52, 53], we examined the affinity of the chimeric FXa variants towards the peptidyl substrate S2765 in the presence of saturating amounts of the cofactor Va and anionic phospholipids. Indeed, prothrombinase complex assembly of the FXa variants almost fully corrected the defective peptidyl substrate binding while the k_{cat} values were not significantly altered (**Table 1**). These results indicate that the delay in time to peak observed for chimeric FX-C in the TG assays reflect the additional time that is required by FX-C to engage FVa and become fully active. Importantly, studies on the protease-zymogen equilibrium of trypsin-like proteases have shown that the S4 subsite is involved in stabilization of the protease state [47, 54, 55]. Since the 99-loop is allosterically linked to the S4 subsite, insertions within the 99-loop may indeed shift the protease equilibrium towards a more zymogen-like state in the chimeric FXa variants.

Discussion

Through a combined computational and biochemical approach we have successfully pioneered the engineering of direct FXa inhibitor insensitivity in FX(a). Active site inhibition of FXa by direct FXa inhibitors requires binding of the ligand's P4 moiety into the S4 subsite through apolar stacking interactions with residues Tyr99 and Phe174. Our data has shown that disruption of apixaban binding is achieved by either replacing S4 subsite residues Tyr99 and/or Phe174 with Alanine, or by extension of the 99-loop which forms part of the S4 subsite. By replacement of the wild-type FXa 99-loop sequence with that of the *P. textilis* isoform FXa paralog, we obtained a FXa variant (FX(a)-C) that was highly resistant to the direct FXa inhibitors (apixaban IC_{50}: ~715 nM; edoxaban IC_{50}: ~375 nM). This variant was also able to restore thrombin generation in apixaban-spiked human plasma when added at a 2- to 4-fold plasma concentration (20 – 40 µg/ml). In addition, FX-C was capable of restoring thrombin generation at supra-physiological concentrations of apixaban or edoxaban. Finally, FX-C induced no in vitro hypercoagulability when present at a 4-fold plasma concentration in the absence of FXa inhibitor. These properties therefore allow FX-C to function as a bypassing agent in human plasma in order to reverse direct FXa inhibitor anticoagulation.

Thus far, a specific and adequate reversal strategy for the treatment of serious and life-threatening bleeding complications associated with the FXa inhibitor-mediated anticoagulant therapy is not clinically available [56]. Consequently, semi-specific reversal strategies to overcome FXa inhibition have been developed [57-59], of which two are based on modified forms of FXa. Andexanet alfa is a GLA-domainless, catalytically inactive FXa variant that functions as a decoy by trapping the FXa inhibitors through stoichiometric binding [57]. Another reversal approach takes advantage of a zymogen-like FXa variant (FXa-I16L) that comprises an impaired active site, but displays full catalytic activity when assembled into prothrombinase [9]. The reversal strategies that are based on scavenging the inhibitory compounds from the circulation require a high dose of catalytically inactive FXa molecules (0.9 or 1.8 grams protein per patient) [57] or synthetic cationic molecules (≤300 mg per individual) [58]. Our approach of bypassing the action of FXa-specific DOACs through diminished FXa inhibitor binding could have several benefits over the scavenging strategies. First, restoring hemostasis with inhibitor-insensitive FX would require administration of milligrams rather than grams of protein to equal or double the FX plasma concentration (10 µg/ml) [2]. In addition, a single administration of inhibitor-insensitive FX could potentially be sufficient to completely restore hemostasis, as the circulatory half-life of FX (34 – 40 hours) exceeds that of the direct FXa inhibitors apixaban (~12 hours) and edoxaban (10-14 hours) [2, 60, 61]. Moreover, the ability of an inhibitor-insensitive form of FX to sustain thrombin generation in plasma irrespective of

the FXa inhibitor concentration should facilitate ease of dosing in patients with limited background information.

In summary, chimeric FX-C could have the potential to serve as rescue therapeutic agent to overcome the effect of synthetic FXa inhibitors in case of potentially life-threatening bleeding events or emergency surgical interventions. Further studies into FX-C dosing, half-life, and mitigation of FXa inhibitor-dependent bleeding will therefore be required to assess its in vivo potential.

References

1. Mann, K.G., et al., *Surface-dependent reactions of the vitamin K-dependent enzyme complexes.* Blood, 1990. **76**(1): p. 1-16.
2. Bos, M.H.A., van 't Veer C, Reitsma P.H, *Molecular Biology and biochemistry of the coagulation factors and pathways of hemostasis*, in *Williams Hematology*, L.M.A. Kaushansky K., Prchal J.T., Levi M.M., Press O.W., Burns L.J., Caligiuri M.A., Editor. 2015, McGraw-Hill Education: New York City. p. 1915-1948.
3. Schuijt, T.J., et al., *Factor Xa activation of factor V is of paramount importance in initiating the coagulation system: lessons from a tick salivary protein.* Circulation, 2013. **128**(3): p. 254-66.
4. Mann, K.G., R.J. Jenny, and S. Krishnaswamy, *Cofactor proteins in the assembly and expression of blood clotting enzyme complexes.* Annu Rev Biochem, 1988. **57**: p. 915-56.
5. Hedstrom, L., *Serine protease mechanism and specificity.* Chem Rev, 2002. **102**(12): p. 4501-24.
6. Krishnaswamy, S., *Exosite-driven substrate specificity and function in coagulation.* J Thromb Haemost, 2005. **3**(1): p. 54-67.
7. Furie, B., et al., *Computer-generated models of blood coagulation factor Xa, factor IXa, and thrombin based upon structural homology with other serine proteases.* J Biol Chem, 1982. **257**(7): p. 3875-82.
8. Camire, R.M., *Prothrombinase assembly and S1 site occupation restore the catalytic activity of FXa impaired by mutation at the sodium-binding site.* J Biol Chem, 2002. **277**(40): p. 37863-70.
9. Toso, R., H. Zhu, and R.M. Camire, *The conformational switch from the factor X zymogen to protease state mediates exosite expression and prothrombinase assembly.* J Biol Chem, 2008. **283**(27): p. 18627-35.
10. Girard, T.J., et al., *Functional significance of the Kunitz-type inhibitory domains of lipoprotein-associated coagulation inhibitor.* Nature, 1989. **338**(6215): p. 518-20.
11. Huntington, J.A., R.J. Read, and R.W. Carrell, *Structure of a serpin-protease complex shows inhibition by deformation.* Nature, 2000. **407**(6806): p. 923-6.
12. Pinto, D.J., et al., *Factor Xa inhibitors: next-generation antithrombotic agents.* J Med Chem, 2010. **53**(17): p. 6243-74.
13. Roehrig, S., et al., *Discovery of the novel antithrombotic agent 5-chloro-N-({(5S)-2-oxo-3-[4-(3-oxomorpholin-4-yl)phenyl]-1,3-oxazolidin-5-yl}methyl)thiophene- 2-carboxamide (BAY 59-7939): an oral, direct factor Xa inhibitor.* J Med Chem, 2005. **48**(19): p. 5900-8.
14. Pinto, D.J., et al., *Discovery of 1-(4-methoxyphenyl)-7-oxo-6-(4-(2-oxopiperidin-1-yl) phenyl)-4,5,6,7-tetrahydro-1H -pyrazolo[3,4-c]pyridine-3-carboxamide (apixaban, BMS-562247), a highly potent, selective, efficacious, and orally bioavailable inhibitor of blood coagulation factor Xa.* J Med Chem, 2007. **50**(22): p. 5339-56.

15. Haginoya, N., et al., *Synthesis and conformational analysis of a non-amidine factor Xa inhibitor that incorporates 5-methyl-4,5,6,7-tetrahydrothiazolo[5,4-c]pyridine as S4 binding element.* J Med Chem, 2004. **47**(21): p. 5167-82.
16. Higgins, D.L. and K.G. Mann, *The interaction of bovine factor V and factor V-derived peptides with phospholipid vesicles.* J Biol Chem, 1983. **258**(10): p. 6503-8.
17. Bos, M.H., et al., *Venom factor V from the common brown snake escapes hemostatic regulation through procoagulant adaptations.* Blood, 2009. **114**(3): p. 686-92.
18. Larson, P.J., et al., *Structure/function analyses of recombinant variants of human factor Xa: factor Xa incorporation into prothrombinase on the thrombin-activated platelet surface is not mimicked by synthetic phospholipid vesicles.* Biochemistry, 1998. **37**(14): p. 5029-38.
19. Camire, R.M., et al., *Enhanced gamma-carboxylation of recombinant factor X using a chimeric construct containing the prothrombin propeptide.* Biochemistry, 2000. **39**(46): p. 14322-9.
20. Toso, R. and R.M. Camire, *Removal of B-domain sequences from factor V rather than specific proteolysis underlies the mechanism by which cofactor function is realized.* J Biol Chem, 2004. **279**(20): p. 21643-50.
21. Krishnaswamy, S. and R.K. Walker, *Contribution of the prothrombin fragment 2 domain to the function of factor Va in the prothrombinase complex.* Biochemistry, 1997. **36**(11): p. 3319-30.
22. Baroni, M., et al., *Asymmetric processing of mutant factor X Arg386Cys reveals differences between intrinsic and extrinsic pathway activation.* Biochim Biophys Acta, 2015. **1854**(10 Pt A): p. 1351-6.
23. Olson, S.T., I. Bjork, and J.D. Shore, *Kinetic characterization of heparin-catalyzed and uncatalyzed inhibition of blood coagulation proteinases by antithrombin.* Methods Enzymol, 1993. **222**: p. 525-59.
24. Hemker, H.C., et al., *Calibrated automated thrombin generation measurement in clotting plasma.* Pathophysiol Haemost Thromb, 2003. **33**(1): p. 4-15.
25. Abraham, M.J., et al., *GROMACS: High performance molecular simulations through multi-level parallelism from laptops to supercomputers.* SoftwareX, 2015. **1-2**(September 2015): p. 19–25.
26. Lechtenberg, B.C., et al., *Crystal structure of the prothrombinase complex from the venom of Pseudonaja textilis.* Blood, 2013. **122**(16): p. 2777-83.
27. Korb, O., T. Stutzle, and T.E. Exner, *Empirical scoring functions for advanced protein-ligand docking with PLANTS.* J Chem Inf Model, 2009. **49**(1): p. 84-96.
28. Schmid, N., et al., *Definition and testing of the GROMOS force-field versions 54A7 and 54B7.* Eur Biophys J, 2011. **40**(7): p. 843-56.
29. Amini, M., J.W. Eastwood, and R.W. Hockney, *Time Integration in Particle Models.* Computer Physics Communications, 1987. **44**(1-2): p. 83-93.
30. Bussi, G., D. Donadio, and M. Parrinello, *Canonical sampling through velocity rescaling.* Journal of Chemical Physics, 2007. **126**(1).
31. Berendsen, H.J.C., et al., *Molecular-Dynamics with Coupling to an External Bath.* Journal of Chemical Physics, 1984. **81**(8): p. 3684-3690.

32. Hess, B., et al., *LINCS: A linear constraint solver for molecular simulations.* Journal of Computational Chemistry, 1997. **18**(12): p. 1463-1472.
33. Pall, S. and B. Hess, *A flexible algorithm for calculating pair interactions on SIMD architectures.* Computer Physics Communications, 2013. **184**(12): p. 2641-2650.
34. Darden, T.A. and L.G. Pedersen, *Molecular modeling: an experimental tool.* Environ Health Perspect, 1993. **101**(5): p. 410-2.
35. Hopfner, K.P., et al., *Coagulation factor IXa: the relaxed conformation of Tyr99 blocks substrate binding.* Structure, 1999. **7**(8): p. 989-96.
36. Johnson, D.J., J. Langdown, and J.A. Huntington, *Molecular basis of factor IXa recognition by heparin-activated antithrombin revealed by a 1.7-A structure of the ternary complex.* Proc Natl Acad Sci U S A, 2010. **107**(2): p. 645-50.
37. Bos, M.H. and R.M. Camire, *Procoagulant adaptation of a blood coagulation prothrombinase-like enzyme complex in australian elapid venom.* Toxins (Basel), 2010. **2**(6): p. 1554-67.
38. Rao, V.S., S. Swarup, and R. Manjunatha Kini, *The catalytic subunit of pseutarin C, a group C prothrombin activator from the venom of Pseudonaja textilis, is structurally similar to mammalian blood coagulation factor Xa.* Thromb Haemost, 2004. **92**(3): p. 509-21.
39. Reza, M.A., et al., *Molecular evolution caught in action: gene duplication and evolution of molecular isoforms of prothrombin activators in Pseudonaja textilis (brown snake).* J Thromb Haemost, 2006. **4**(6): p. 1346-53.
40. Skejic, J. and W.C. Hodgson, *Population divergence in venom bioactivities of elapid snake Pseudonaja textilis: role of procoagulant proteins in rapid rodent prey incapacitation.* PLoS One, 2013. **8**(5): p. e63988.
41. Pryzdial, E.L. and G.E. Kessler, *Kinetics of blood coagulation factor Xaalpha autoproteolytic conversion to factor Xabeta. Effect on inhibition by antithrombin, prothrombinase assembly, and enzyme activity.* J Biol Chem, 1996. **271**(28): p. 16621-6.
42. Olson, S.T., et al., *Accelerating ability of synthetic oligosaccharides on antithrombin inhibition of proteinases of the clotting and fibrinolytic systems. Comparison with heparin and low-molecular-weight heparin.* Thromb Haemost, 2004. **92**(5): p. 929-39.
43. Rezaie, A.R., *Heparin-binding exosite of factor Xa.* Trends Cardiovasc Med, 2000. **10**(8): p. 333-8.
44. Waxman, L., et al., *Tick anticoagulant peptide (TAP) is a novel inhibitor of blood coagulation factor Xa.* Science, 1990. **248**(4955): p. 593-6.
45. Burgering, M.J., et al., *The second Kunitz domain of human tissue factor pathway inhibitor: cloning, structure determination and interaction with factor Xa.* J Mol Biol, 1997. **269**(3): p. 395-407.
46. Wei, A., et al., *Unexpected binding mode of tick anticoagulant peptide complexed to bovine factor Xa.* J Mol Biol, 1998. **283**(1): p. 147-54.
47. Abdel-Azeim, S., et al., *Molecular dynamics characterization of five pathogenic Factor X mutants associated with decreased catalytic activity.* Biochemistry, 2014. **53**(44): p. 6992-7001.

48. Carvalho, A.L., et al., *Crystal structure of a prostate kallikrein isolated from stallion seminal plasma: a homologue of human PSA.* J Mol Biol, 2002. **322**(2): p. 325-37.
49. Kita, M., et al., *Blarina toxin, a mammalian lethal venom from the short-tailed shrew Blarina brevicauda: Isolation and characterization.* Proc Natl Acad Sci U S A, 2004. **101**(20): p. 7542-7.
50. Skala, W., et al., *Structure-function analyses of human kallikrein-related peptidase 2 establish the 99-loop as master regulator of activity.* J Biol Chem, 2014. **289**(49): p. 34267-83.
51. Aminetzach, Y.T., et al., *Convergent evolution of novel protein function in shrew and lizard venom.* Curr Biol, 2009. **19**(22): p. 1925-31.
52. Levigne, S., et al., *Role of the alpha-helix 163-170 in factor Xa catalytic activity.* J Biol Chem, 2007. **282**(43): p. 31569-79.
53. Ivanciu, L. and R.M. Camire, *Hemostatic agents of broad applicability produced by selective tuning of factor Xa zymogenicity.* Blood, 2015. **126**(1): p. 94-102.
54. Sorensen, A.B., et al., *Molecular Basis of Enhanced Activity in Factor VIIa-Trypsin Variants Conveys Insights into Tissue Factor-mediated Allosteric Regulation of Factor VIIa Activity.* J Biol Chem, 2016. **291**(9): p. 4671-83.
55. Gohara, D.W. and E. Di Cera, *Allostery in trypsin-like proteases suggests new therapeutic strategies.* Trends Biotechnol, 2011. **29**(11): p. 577-85.
56. Ruff, C.T., R.P. Giugliano, and E.M. Antman, *Management of Bleeding With Non-Vitamin K Antagonist Oral Anticoagulants in the Era of Specific Reversal Agents.* Circulation, 2016. **134**(3): p. 248-61.
57. Lu, G., et al., *A specific antidote for reversal of anticoagulation by direct and indirect inhibitors of coagulation factor Xa.* Nat Med, 2013. **19**(4): p. 446-51.
58. Ansell, J.E., et al., *Single-dose ciraparantag safely and completely reverses anticoagulant effects of edoxaban.* Thromb Haemost, 2016.
59. Thalji, N.K., et al., *A rapid pro-hemostatic approach to overcome direct oral anticoagulants.* Nat Med, 2016. **22**(8): p. 924-32.
60. Frost, C., et al., *Safety, pharmacokinetics and pharmacodynamics of multiple oral doses of apixaban, a factor Xa inhibitor, in healthy subjects.* Br J Clin Pharmacol, 2013. **76**(5): p. 776-86.
61. Lip, G.Y. and G. Agnelli, *Edoxaban: a focused review of its clinical pharmacology.* Eur Heart J, 2014. **35**(28): p. 1844-55.

Supplementary information

Supplementary Fig. 1. Alignment of factor X serine protease domain sequences. Serine protease domain regions of FX were aligned to corresponding FX regions from several selected vertebrates. The His91-Val231 sequence is shown with the non-conserved 99-loop residues specific for *P. textilis* isoform FX[1], *P. textilis* venom FX[2], and *T. carinatus* venom FX[3] in bold [37]. Residues with the shortest Minimal Interatomic distances from their side chain to apixaban as observed in the MD simulation of apixaban-bound human FXa and as indicated in **Fig. 1A** are numbered and indicated in bold.

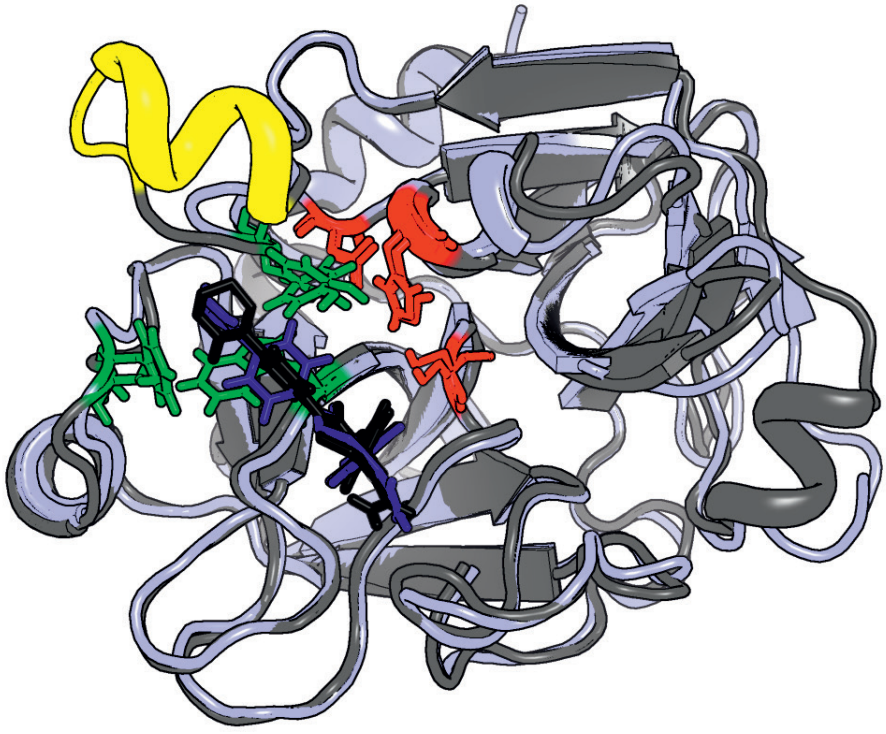

Supplementary Fig. 2. Apixaban binding orientation in human and snake factor Xa. Apixaban (blue sticks) bound to human FXa (light blue; PDB ID 2P16) was overlaid with apixaban (black sticks) docked into *P. textilis* isoform FXa (grey; PDB ID 4BXW). The isoform FXa insertion region PQKAYKFDL is highlighted in yellow, red residues indicate the position of the catalytic triad in both proteases, and green residues indicate the position of the S4 subsite residues Tyr99, Phe174, and Trp215.

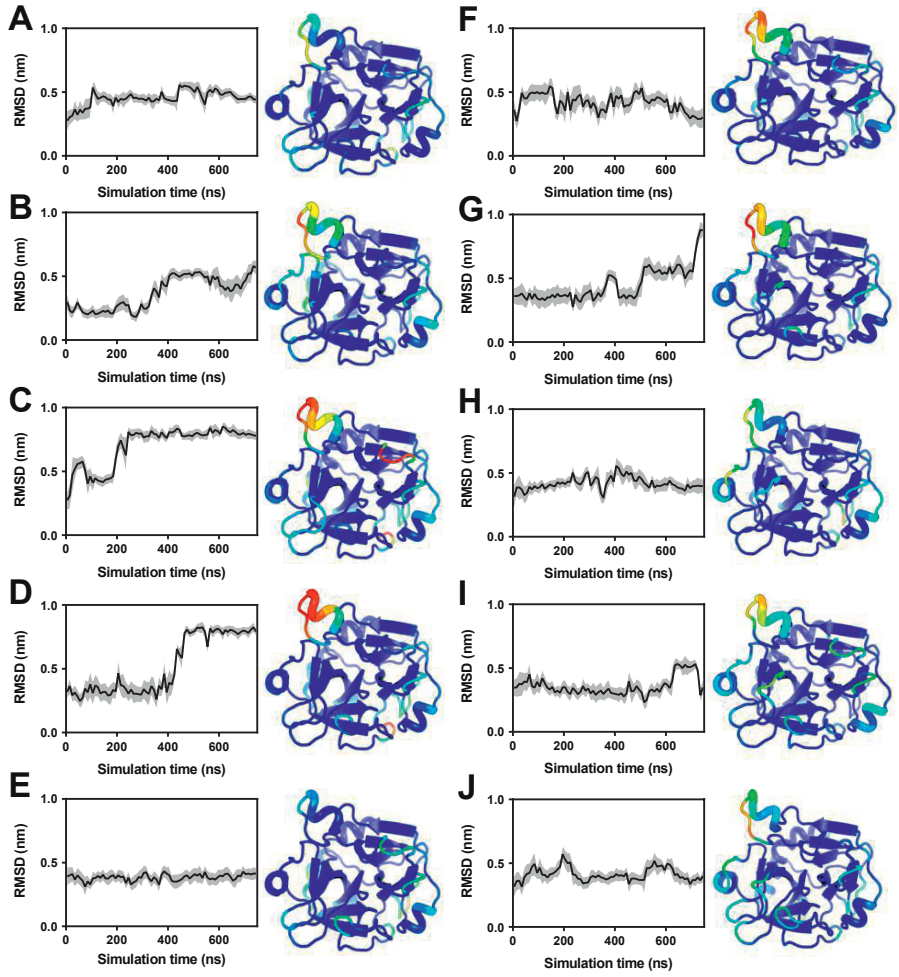

Supplementary Fig. 3. Molecular Dynamics simulations of apixaban-bound and unbound snake isoform factor Xa. Root-mean-square deviations **(**RMSD) of the backbone positions in the isoform FXa extended 99-loop region PQKAYKFDL during 750 ns MD simulations of apixaban-bound (APX bound) (***A-E***) or unbound (apo) (***F-J***) isoform FXa are presented as block averages over 10 ns intervals. The corresponding single standard deviation interval is indicated (grey density). The local flexibility of the *P. textilis* isoform FXa main-chain atoms was evaluated and calculated using GROMACS tool *g_rmsf* from atomic root-mean-square fluctuations. The resulting Debye-Waller factors (or B-factors) are projected onto the initial conformation of *P. textilis* isoform FXa (PDB ID 4BXW) as a blue-green-red gradient representing a ≤10 Å^2 to ≥300 Å^2 range of mobility. The B-factors are displayed for independent MD simulations starting from the same atomic coordinates but different randomly assigned velocities. The 750 ns MD simulations of apixaban-bound isoform FXa (***A-E***) correspond to simulations #1-5 in **Fig. 3A-E** and **Supplementary Fig. 4A-E**.

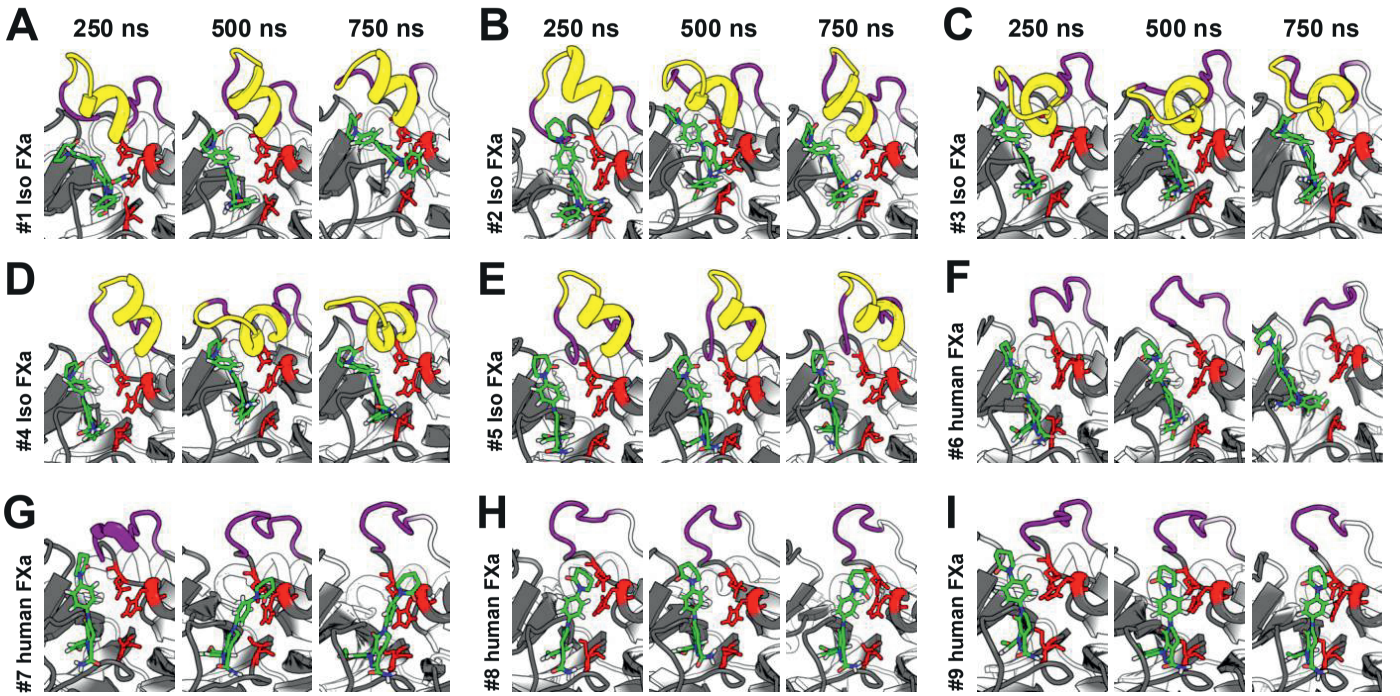

Supplementary Fig. 4. Factor Xa conformations during Molecular Dynamics simulations. The conformations of the isoform FXa-apixaban complex (simulations #1-5; ***A-E***) and human FXa (simulations #6-9; ***F-I***) at 250, 500, and 750 ns of MD simulations are depicted for each independent simulation. Apixaban (green), the 99-loop (magenta), the isoform FXa extended 99-loop region PQKAYKFDL (yellow), and the catalytic triad residues (red) are highlighted. The independent simulations of apixaban-bound isoform FXa (***A-E***) correspond to simulations #1-5 in **Fig. 3A-E** and **Supplementary Fig. 3A-E**. The independent simulations of human FXa (***F-I***) correspond to simulations #6-9 in **Fig. 3F-I**.

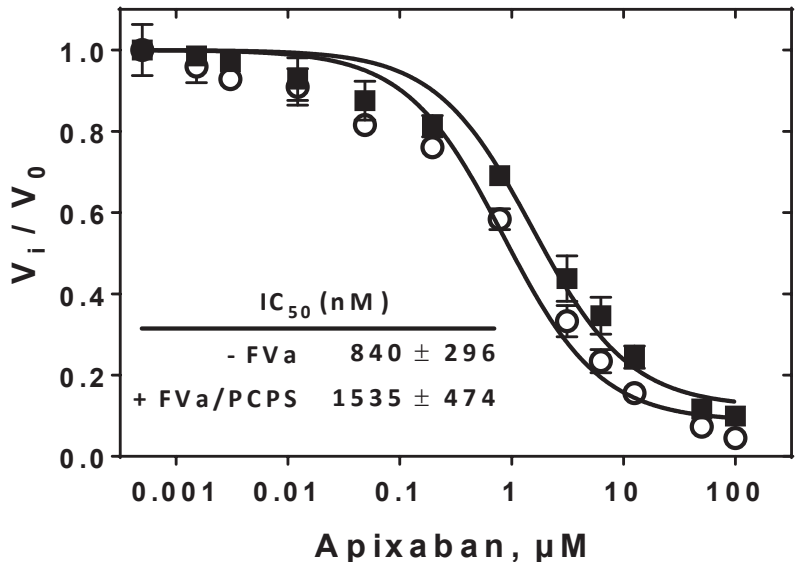

Supplementary Fig. 5. Inhibition of factor Xa-C by apixaban in the absence and presence of factor Va. The rate of peptidyl substrate conversion (250 µM SpecXa) by free (open circles) or prothrombinase-assembled (PCPS, 50 µM ; FVa, 30 nM; closed squares) purified recombinant human FXa-C (5 nM) was determined in the absence (V_0) or presence (V_i) of increasing concentrations (0.002 – 100 µM) of the inhibitor apixaban. The lines were drawn following nonlinear regression analysis of the data sets. The data are the means of three similar experiments, and are normalized for activity in the absence of inhibitor (V_0).

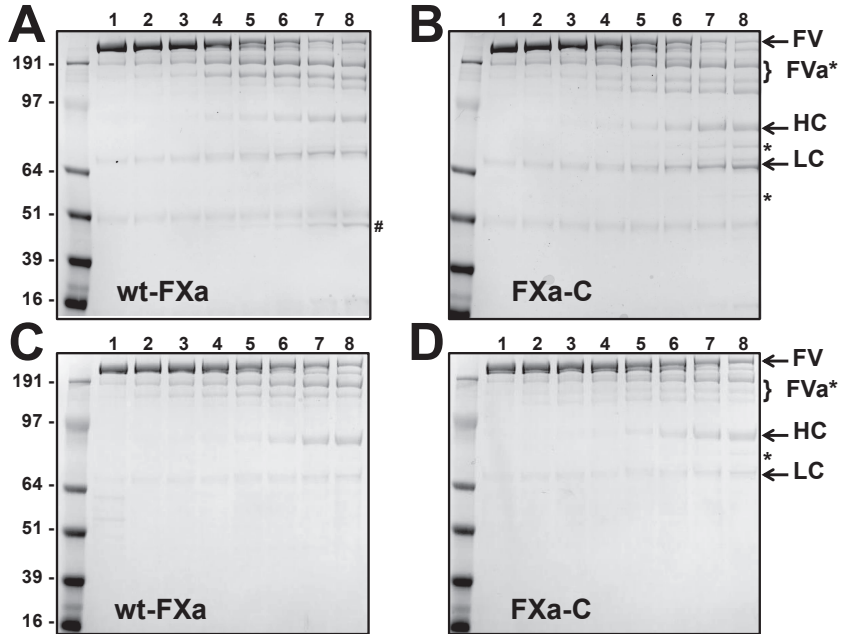

Supplementary Fig. 6. Activation of factor V by factor Xa variants. Plasma-derived (pd)-FV (400 nM) was incubated at 25°C either with increasing concentrations (0-100 nM) of wild-type FXa (wt-FXa) or FXa variant C (FXa-C) in the presence of 50 μM PCPS for 10 minutes (***A,B***) or with 5 nM wt-FXa or FXa-C in the presence of 25 μM PCPS for 1 – 60 minutes (***C,D***). Samples (3 μg/lane) were subjected to SDS-PAGE under reducing conditions using the MOPS buffer system and visualized by staining with Coomassie Brilliant Blue. (***A,B***) Lane 1: pd-FV, no FXa; lanes 2-8: pd-FV, wt-FXa or FXa-C at 0.5, 1, 5, 10, 20, 50, and 100 nM. (***C,D***) Lane 1: pd-FV, no FXa; lanes 2-8: pd-FV, incubated for 1, 2, 4, 10, 20, 40, and 60 minutes with wt-FXa or FXa-C. The protein bands indicative of single chain, uncleaved pd-FV (FV), partially activated FV (FVa*), FVa heavy chain (HC), and FVa light chain (LC) are indicated. The apparent molecular weights of the standards (kDa) are indicated. The data are representative of two similar experiments.

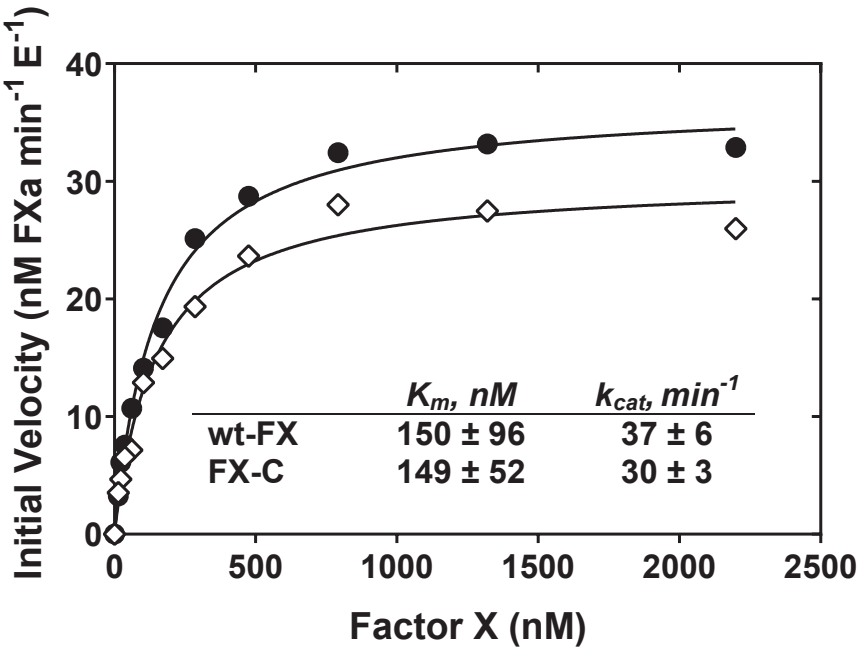

Supplementary Fig. 7. Activation of factor X variants via the intrinsic activation pathway. The rate of factor X (13 – 2200 nM) activation for wild-type (wt-FX; closed circles) or variant C (FX-C; open diamonds) by the intrinsic FVIIIa/FIXa tenase complex (PCPS, 20 μM; FIXa, 0.5 nM; FVIIIa 5 nM) was determined as described in 'Materials'. Individual data points represent the average of two independent experiments. The lines were drawn by fitting the data to the Michaelis-Menten equation using non-linear regression and the obtained values for K_m and k_{cat} ± 1 standard deviation of the induced fit are shown in the inset.

Supplementary Table 1. Factor Xa-initiated thrombin generation in factor X-depleted plasma in the absence or presence of apixaban.

	pd-FXa	wt-FXa	FXa-A	FXa-B	FXa-C
No inhibitor					
Lag time *(min)*	0.14 ± 0.05	0.33 ± 0.06	2.28 ± 0.77	1.85 ± 0.44	0.42 ± 0.08
Time to peak *(min)*	0.74 ± 0.05	1.03 ± 0.10	3.75 ± 1.15	3.57 ± 0.99	1.30 ± 0.09
Peak height *(nM)*	938 ± 121	836 ± 11	625 ± 144	512 ± 170	827 ± 29
Velocity index *(nM/min)*	1565 ± 201	1203 ± 97	473 ± 228	323 ± 156	937 ± 25
ETP *(nM•min)*	2573 ± 264	2667 ± 175	2313 ± 396	1979 ± 717	2792 ± 86
2 μM apixaban					
Lag time *(min)*	4.43 ± 1.71	5.22 ± 1.43	3.29 ± 2.08	2.02 ± 0.94	0.47 ± 0.12
Time to peak *(min)*	8.14 ± 2.63	8.82 ± 1.81	5.75 ± 3.41	4.07 ± 1.78	1.42 ± 0.20
Peak height *(nM)*	278 ± 128	272 ± 54	490 ± 214	435 ± 086	818 ± 40
Velocity index *(nM/min)*	87 ± 62	77 ± 22	289 ± 228	243 ± 113	868 ± 102
ETP *(nM•min)*	1845 ± 296	2031 ± 187	2059 ± 0375	1824 ± 0442	2823 ± 95

Thrombin generation was measured for 60 minutes at 37°C in FX-depleted plasma supplemented with 20 μM PCPS. Thrombin generation was initiated by the addition of 5 nM plasma-derived human FXa (pd-FXa), recombinant wild-type human FXa (wt-FXa), or chimeric FXa-A, FXa-B, or FXa-C premixed with HBS (no inhibitor) or apixaban (2 μM) and supplemented with $CaCl_2$ and a thrombin fluorogenic substrate as detailed in 'Materials'. All values represent averages ± 1 standard deviation obtained from at least three similar experiments.

Supplementary Table 2. Tissue factor-initiated thrombin generation in factor X-depleted plasma spiked with factor X variants.

	no inhibitor	2.0 µM APX	6.0 µM APX	0.6 µM EDX	2.0 µM EDX
wt-FX					
Lag time *(min)*	2.23 ± 0.27	10.59 ± 1.51	17.77 ± 4.05	11.95 ± 1.27	22.86 ± 5.54
Time to peak *(min)*	5.12 ± 0.65	49.57 ± 1.81	51.82 ± 0.52	37.14 ± 8.60	45.70 ± 9.59
Peak height *(nM)*	86 ± 25	8 ± 2	4 ± 1	13 ± 3	7 ± 2
Velocity index *(nM/min)*	31 ± 13	<1	<1	<1	<1
ETP *(nM•min)*	646 ± 088	NA	NA	NA	NA
FX-C					
Lag time *(min)*	2.98 ± 0.30	3.00 ± 0.22	3.25 ± 0.22	3.43 ± 0.30	4.16 ± 0.54
Time to peak *(min)*	7.32 ± 0.73	7.67 ± 0.50	8.17 ± 0.50	8.53 ± 0.86	10.34 ± 1.25
Peak height *(nM)*	93 ± 18	83 ± 12	86 ± 14	85 ± 22	62 ± 18
Velocity index *(nM/min)*	22 ± 6	18 ± 4	18 ± 4	17 ± 6	10 ± 4
ETP *(nM•min)*	806 ± 99	776 ± 30	789 ± 43	846 ± 131	722 ± 70

Thrombin generation (TG) was measured for 60 minutes at 37°C in FX-depleted plasma supplemented with 2 pM tissue factor (TF), 20 µM PCPS, and either 1 U/ml of wt-FX (7 µg/ml) or FX-C (15 µg/ml). Thrombin generation was initiated with $CaCl_2$ and a thrombin fluorogenic substrate as detailed in 'Materials'. Experimental data was obtained in the absence or presence of either 2 µM or 6 µM apixaban (APX), or 0.6 µM or 2 µM edoxaban (EDX). All values represent averages ± 1 standard deviation obtained from at least three similar experiments. NA, not applicable: for these experiments thrombin generation was insufficient, precluding an accurate assessment of the ETP.

Supplementary Table 3. Tissue factor-initiated thrombin generation parameters in normal pooled plasma spiked with factor X-C and apixaban

	NPP	**APX** *+ 5 µg/ml*	**APX** *+ 10 µg/ml*	**APX** *+ 20 µg/ml*	**APX** *+ 40 µg/ml*	*+ 40 µg/ml*
2 pM TF						
Lag time *(min)*	3.27 ± 0.16	4.45 ± 0.08	3.98 ± 0.06	3.69 ± 0.19	3.89 ± 0.20	3.25 ± 0.25
Time to peak *(min)*	6.65 ± 0.28	12.88 ± 0.38	11.44 ± 0.31	10.35 ± 0.63	10.35 ± 0.51	8.58 ± 0.63
Peak height *(nM)*	96 ± 22	50 ± 20	68 ± 17	77 ± 11	84 ± 11	87 ± 2
Velocity index *(nM/min)*	29 ± 6	6 ± 2	9 ± 2	12 ± 2	13 ± 3	16 ± 1
ETP *(nM•min)*	731 ± 127	719 ± 246	798 ± 191	740 ± 96	722 ± 45	696 ± 27
6 pM TF						
Lag time *(min)*	1.94 ± 0.15	3.04 ± 0.06	2.56 ± 0.10	2.35 ± 0.12	2.27 ± 0.04	2.08 ± 0.14
Time to peak *(min)*	4.10 ± 0.23	7.54 ± 0.56	6.10 ± 0.42	5.39 ± 0.30	5.35 ± 0.29	4.67 ± 0.14
Peak height *(nM)*	171 ± 23	120 ± 36	143 ± 26	168 ± 22	176 ± 16	190 ± 12
Velocity index *(nM/min)*	79 ± 9	27 ± 8	40 ± 8	55 ± 6	57 ± 6	74 ± 5
ETP *(nM•min)*	792 ± 100	864 ± 268	839 ± 204	849 ± 118	883 ± 86	868 ± 25

Thrombin generation (TG) was measured for 60 minutes at 37°C in normal pooled plasma (NPP) supplemented with 2 or 6 pM tissue factor (TF), 20 µM PCPS and 5 – 40 µg/ml FX-C in the presence of 2 µM apixaban (APX). Thrombin generation was initiated with $CaCl_2$ and a thrombin fluorogenic substrate as detailed in 'Materials'.
All values represent averages ± 1 standard deviation obtained from at least three similar experiments.


5

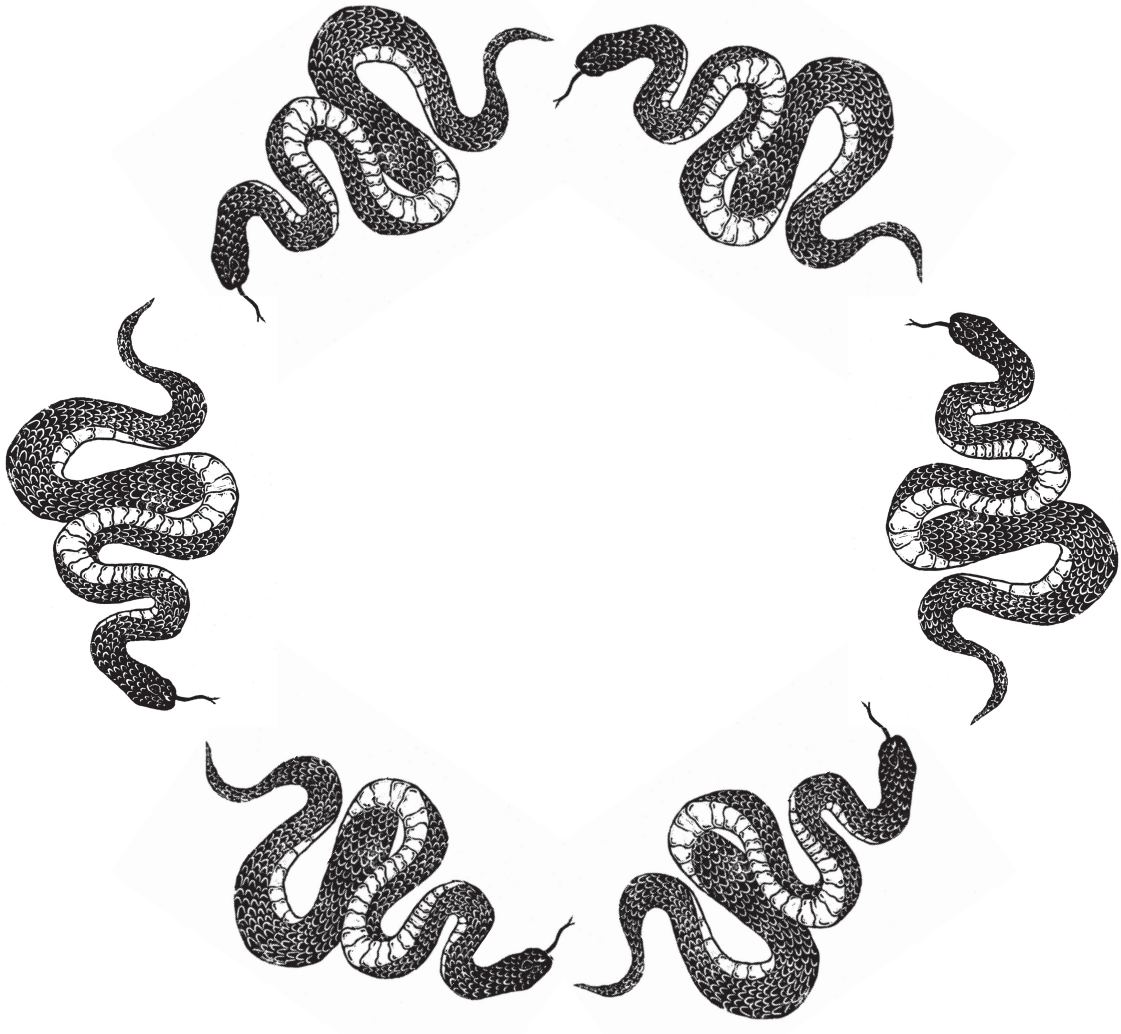

Chapter 6

Elevated anti-human factor Xa activity in rabbit and rodent plasma: implications for preclinical assessment of human factor X in animal models of hemostasis

Daniël Verhoef, Annabelle V. R. Tjalma, Ka Lei Cheung, Pieter H. Reitsma and Mettine H.A. Bos.

Thrombosis Research, 2021. 198: p. 154

Abstract

A wide variety of animal models on thrombosis and hemostasis are used in thrombosis and hemostasis research for the preclinical assessment of hemostatic agents. While the vertebrate coagulome is highly conserved, human and animal plasmas differ considerably when evaluated in coagulation assays such as prothrombin time (PT), activated partial thromboplastin time (APTT), and calibrated automated thrombography (CAT). Here, we have aimed to provide a reference framework for the evaluation of coagulation assays and inhibition of activated human FXa (hFXa) in various animal plasmas. To do so, a side-by-side evaluation of the extrinsic and intrinsic pathway of coagulation was performed by means of PT, APTT, and CAT measurements on (diluted) pooled plasmas from goats, pigs, rabbits, rats, mice, and humans. Plasma anti-FXa activity was assessed by determining the rate of recombinant hFXa inhibition through chromogenic activity analyses and immunoblotting. In general, rabbit, rat, and mouse plasmas exhibited robust clotting upon stimulation of both the extrinsic and intrinsic pathway, produced more thrombin during CAT upon plasma dilution, and displayed relatively high hFXa inhibitory activities. By comparison, goat, porcine, and human plasma displayed a similar profile in PT and APTT assays, produced less thrombin during CAT upon plasma dilution, and displayed comparable hFXa inhibitory activities. In conclusion, the observed differences in clotting parameters and anti-hFXa activity point to a higher anticoagulant threshold in plasma from rabbits, rats, and particularly in mice relative to human, goat, and porcine plasma. Finally, rat plasma was found to be more relevant to the preclinical assessment of human FX(a) in comparison to murine plasma.

Introduction

The vertebrate coagulome comprises a wide variety of (pro)enzymes, cofactors, and inhibitors that maintain an intricate balance between pro-, and anticoagulant pathways. While individual components of the coagulation cascade are highly conserved between mammals, large variations in response to various procoagulant stimuli have been reported [1-3]. For example, mouse and rabbit plasma have been observed to exhibit reduced rates of thrombin generation upon tissue factor-dependent activation of coagulation [4, 5]. While interspecies differences in coagulation factor levels that regulate thrombin formation may be fundamental to these observations, detailed comparisons between coagulation factor levels and coagulant activity across vertebrate species are sparse. Improved knowledge of global coagulation assays for rodent and non-rodent plasmas will facilitate the use and interpretation of animal models for studies in the field of thrombosis and hemostasis [6]. Moreover, the evaluation of specific coagulation parameters in various species will directly impact the selection of animal models for *in vivo* studies that are essential in the development of procoagulant therapeutics, such as for instance coagulation factor X (FX) and variants thereof [7-9].

Coagulation factor Xa (FXa) is an essential serine protease that plays a pivotal role in the initiation and propagation of the coagulation cascade [10, 11]. We recently developed a novel variant of human coagulation factor X (FX-C) that can propagate blood coagulation in the presence of direct FXa-inhibitors such as apixaban, edoxaban, or rivaroxaban [8]. FX-C is currently in preclinical development as a reversal agent for patients that use direct FXa-inhibitors and require restoration of blood coagulation. In order to identify a suitable animal model for the preclinical assessment of FX variants, we have evaluated the *in vitro* global clotting parameters of mouse, rat, rabbit, porcine, and goat plasma in a side-by-side comparison with human plasma, using assays and reagents designed for analysis of human proteins. In addition, the anticoagulant potential of these plasmas was examined by determining the rate of human FXa inhibition.

Material and Methods

Materials and Reagents

Unless stated otherwise, a single batch of platelet-poor pooled plasma per species was used for all experiments to avoid intra-assay variability. Mouse (wild-type C57BL/6, WT-A), rat (Sprague-Dawley), rabbit (New Zealand White), domestic pig, and goat (sub-species not defined) plasmas (3.2%(w/v) sodium citrate) were purchased from Innovative Research (Novi, MI, USA). Mouse, rat, and rabbit pooled plasmas were collected via jugular vein extraction, which is preferred over cardiac puncture extraction [12]. Domestic pig and goat pooled plasmas were obtained via arterial blood extraction. Mouse TFPI-low and wild-type C57BL/6 (WT-B) pooled plasmas were generous gifts from dr. George Broze (Washington University School of Medicine, St Louis, MO, USA) and dr. Cornelis van 't Veer (Amsterdam University Medical Centers, location Academic Medical Center, Amsterdam, The Netherlands). Antithrombin (AT)-low C57BL/6 pooled mouse plasma was a kind gift from dr. Bart van Vlijmen (LUMC, Leiden, The Netherlands) [13]. All procedures were approved by the individual institutional animal care and use committees (IACUC). Normal human platelet-poor pooled plasma (3.2%(w/v) sodium citrate) was from Sanquin (Amsterdam, The Netherlands). The peptidyl substrate SpectrozymeXa was obtained from Sekisui Diagnostics (Stamford, CT, USA). Small unilamellar phospholipid vesicles (PCPS) composed of 75% (w/w) hen egg L-phosphatidylcholine and 25% (w/w) porcine brain L-phosphatidylserine (Avanti Polar Lipids, Alabaster, AL, USA) were prepared and characterized as described previously [14]. Calibrator and fluorescent substrate (FluCa) were from Thrombinoscope (Maastricht, The Netherlands). Dade Innovin prothrombin time (PT) reagent (purified recombinant human tissue factor (TF) with synthetic phospholipids, calcium, buffers and stabilizers) was obtained from Siemens (Newark, NY, USA). Neoplastine CI Plus 10 PT reagent (lyophilized fresh rabbit brain thromboplastin hydrated with a calcium-containing solvent and heparin inhibitor), Triniclot automated activated partial thromboplastin time (APTT) reagent (containing platelet factor III from rabbit brain phospholipids and micronized silica as particulate activator) and CK Prest 5 APTT reagent (rabbit cephalin reagent with kaolin as particulate activator) were obtained from Diagnostica Stago (Paris, France). All functional assays were performed in HEPES-buffered saline (HBS: 20 mM HEPES, 0.15 M NaCl, pH 7.5) supplemented with 0.1% PEG 8000 (dilution buffer) and filtered over an 0.2 µm membrane.

Proteins

Plasma-derived human AT and corn trypsin inhibitor (CTI) were from Haematologic Technologies (Essex Junction, VT, USA). Recombinant tissue factor (TF, Innovin) was obtained from Siemens (Newark, NY, USA). RVV-X activator and the matched-pair antibody set for the enzyme-linked immunosorbent assay (ELISA) of murine

AT were obtained from Diagnostica Stago. Recombinant human FX (hFX) was prepared, purified, and characterized as described previously [8]. Purified hFX was activated with RVV-X (0.1 U/mg hFX), and hFXa was isolated by size-exclusion chromatography on a Sephacryl S200 HR column (V_t 460 ml) and stored at -20°C in HBS containing 50% (vol/vol) glycerol.

Coagulation assays

PT and APTT assays were performed on the Diagnostica Stago ST4 Coagulation Analyzer. PT samples were prepared by diluting plasma 2-, 6-, and 12-fold in dilution buffer supplemented with 0.1% bovine serum albumin (BSA). Samples (50 µl) were incubated for 60 seconds at 37°C, and coagulation was initiated by addition of 50 µl PT reagent at 37°C. APTT samples were prepared by diluting plasma 2-, 3- and 4-fold in Owren-Koller buffer (Diagnostica Stago). Samples (50 µl) were incubated for 180 seconds at 37°C with APTT reagent. Coagulation was initiated with 50 µl of 25 mM $CaCl_2$ at 37°C.

Calibrated automated thrombography analysis

Calibrated automated thrombography (CAT) was performed as described [15]. Briefly, thrombin generation curves were obtained by supplementing 80 µl (1.5-fold dilution) or 20 µl (3-fold dilution) of plasma with 20 µl of HBS containing TF (2, 6, or 20 pM final), CTI (70 µg/ml final), and PCPS (20 µM final) in 96-well round-bottom plates (Thermo Fisher Scientific, Waltham, MA, USA). Thrombin generation was initiated by adding 20 µl substrate buffer containing $CaCl_2$ supplemented with a thrombin fluorogenic substrate (FluCa). Thrombin formation was measured every 15 seconds for 60 minutes and corrected for the calibrator using Thrombinoscope software. For experiments with supra-physiological concentrations of AT, normal human pooled plasma was spiked with AT (0.625-2.5 µM; 125 – 200%) and assayed as described.

Inhibition of human FXa in pooled plasma

The rate of hFXa inhibition was essentially determined as previously described for AT inhibition in the absence of calcium [16]. Briefly, 25 µl of recombinant hFXa (10 nM) was added to 25 µl of plasma that was 2- to 100-fold diluted in dilution buffer, upon which the mixture was incubated for 5-60 minutes at ambient temperature. hFXa incubated in dilution buffer for 60 minutes at ambient temperature was used as reference. The residual enzyme activity as a function of time was determined after the addition of 50 µl SpecXa (500 µM) upon which the initial steady state increase in absorbance at 405 nm was monitored. The pseudo-first-order rate constants of hFXa inhibition (k_{obs}: nM s^{-1}) were determined by fitting the decrease in enzymatic activity to a single exponential function with a finite end-point as described [17]. Second order hFXa inhibition rate constants (k_2: nM s^{-1} dil^{-1}) were obtained by plotting k_{obs} against the plasma dilution and subsequent analysis by

linear regression using GraphPad Prism 7 (San Diego, CA, USA). Analysis of hFXa inhibition in wild-type (WT-A, WT-B), TFPI-low, or AT-low C57BL/6 mouse plasma was determined by incubating hFXa (10 nM) for 0-45 minutes in 25 µl of 4- to 200-fold diluted pooled plasma.

Immunoblotting of FXa-AT complexes

The rate of hFXa-AT complex formation was assessed by incubating 5 nM of hFXa in 12-fold diluted plasma for 1 – 90 minutes at ambient temperature. Samples were quenched by the addition of sample buffer with reducing agent (DTT; Invitrogen, Carlsbad, CA, USA), denatured for 10 minutes at 72°C, subjected to electrophoresis on pre-cast 4–12% Bis-Tris gels using the MOPS buffer system (Invitrogen, Carlsbad, CA, USA), and transferred to a nitrocellulose membrane using the Trans-Blot Turbo Transfer System (Bio-Rad, Hercules, CA, USA). The membrane was first probed with a polyclonal goat-anti-human FX antibody (Affinity Biologicals, Ancaster Canada), followed by an IRDye 680LT conjugated donkey-anti-goat polyclonal antibody (LI-COR Biotechnology, Lincoln, NE, USA) and detection at 700 nm using the Odyssey CLx Infrared Imaging System (LI-COR Biosciences). Relative band intensities of hFXa-AT were counted automatically, corrected for background, and analyzed by non-linear regression using GraphPad Prism 7 (San Diego, CA, USA) by fitting the data to a one-phase decay curve, whereby Y0 was constrained to zero.

Results

Rabbit, rat, and mouse plasma exhibit robust clotting parameters

The extrinsic pathway of coagulation was evaluated in pooled plasma from humans, goats, pigs, rabbits, rats, and mice employing PT-based clotting analyses. Previously, it has been demonstrated that the procoagulant response is more robust in diluted mouse plasma relative to undiluted plasma [4]. Therefore, clotting assessment was performed in serially diluted plasma using the electro-mechanical clot detection method (viscosity-based readout). In line with previous findings, we observed a shortening of the PT-based clotting time upon either 2- or 6-fold dilution of mouse and rabbit plasma compared to the undiluted samples (**Figure 1A**). Furthermore, undiluted rat plasma displayed an exceedingly prolonged clotting time (> 120 sec.), which was markedly shortened upon plasma dilution and close to previously reported values [2]. As expected, serial plasma dilutions resulted in a prolongation of the clotting time for all species. However, the extent to which the extrinsic clotting time was prolonged varied, with rabbit, rat, and mouse plasma displaying a similar profile that substantially differed from that observed for human, goat, and porcine plasma (**Figure 1A**). In case of the latter set of plasmas, the extrinsic clotting time of maximally diluted plasma (12-fold) was up to 5-fold prolonged relative to undiluted plasma (e.g. human plasma: 60.7 ± 6.9 sec. vs. 11.5 ± 0.4 sec., respectively). In contrast, extrinsic clotting was at most 2-fold prolonged in rabbit and mouse plasma upon maximal dilution (e.g. rabbit plasma: 27.4 ± 1.7 sec. vs. 16.4 ± 1.7 sec. for undiluted plasma). Similar trends in PT clotting times were observed using an alternative thromboplastin reagent (**Supplementary Figure 1A**). Collectively, these results suggest a consistently robust TF-induced fibrin clot formation in rabbit and mouse plasma.

To verify the observed relationship between plasma dilutions and clotting time, the intrinsic pathway of coagulation was evaluated employing APTT-based analyses. While human and goat plasma displayed prolonged APTT clotting times upon serial dilution, no substantial prolongation was observed following dilution of rat plasma (**Figure 1B**). However, analogous to previous reports we observed exceptionally short intrinsic clotting times in undiluted porcine plasma (17.1 ± 1.1 sec.) and mouse plasma (23.6 ± 1.4 sec.) [18, 19]. Furthermore, the APTT clotting times were more or less unperturbed upon serial dilutions of these plasmas. Similar trends in APTT clotting times of (diluted) rat and mouse plasma were observed using a contact activation reagent containing kaolin (**Supplementary Figure 1B**). Rabbit plasma, on the other hand, demonstrated a weak response of the intrinsic pathway (undiluted plasma: 122.0 ± 27.0 sec.). In contrast, rabbit plasma exhibited a very short clotting time (undiluted plasma: 23.8 ± 0.5 sec.) using the kaolin-based reagent. Subsequent dilution of rabbit plasma nonetheless resulted in a more prolonged clotting time relative to human plasma (**Supplementary Figure 1B**),

suggestive of a weaker intrinsic clotting pathway [2]. Overall, assessment of the intrinsic pathway of coagulation confirmed that mouse plasma displays relatively robust fibrin clot formation relative to human and goat plasma.

Dilution of rabbit, rat, and mouse plasmas enhances thrombin generation

To examine the effects of plasma dilution on TF-induced coagulation in more detail we assessed thrombin generation employing CAT analysis. The extrinsic pathway of coagulation was triggered using human recombinant TF [20], which was previously shown to be compatible with murine plasma [4, 21]. In addition, the use of human TF facilitated screening of clinically relevant animal plasma models for compatibility with reagents specific for human proteins. CAT analysis was performed using either a standard (80 µl plasma, 1.5-fold diluted) or reduced sample volume (20 µl plasma, 3-fold diluted), and thrombin generation was initiated with a low (2 pM) or high (6 pM) TF trigger [4, 22]. Interestingly, thrombin generation in 3-fold diluted rat and rabbit plasma displayed an increased thrombin peak, a shorter lag time and time to peak, and an enhanced velocity index relative to the parameters observed using 1.5-fold diluted plasma (**Table 1**). On the other hand, these parameters were either unaffected in 3-fold diluted goat plasma, or reduced (thrombin peak, velocity index) and prolonged (lag time, time to peak) in human and porcine plasma, irrespective of the TF concentration used. Remarkably, thrombin generation in mouse plasma was only observed following a 3-fold plasma dilution, as no detectable amounts of thrombin were observed for the 1.5-fold diluted plasma. Similar findings were obtained following initiation with 20 pM TF, consistent with previous reports [4]. Importantly, undiluted mouse plasma was shown to clot normally in the PT assay (**Figure 1A**), which uses excess amounts of TF to stimulate the extrinsic pathway. In contrast, in CAT analysis picomolar TF concentrations are used, which do not lead to detectable thrombin generated in all of the conditions employed. This apparent discrepancy between the PT and CAT assays suggests an elevated anti-coagulant threshold in mouse plasma that can be overcome by a robust extrinsic trigger. In conclusion, current observations demonstrate that serial dilution of rabbit, rat, and mouse plasma leads to enhanced thrombin generation. As such, plasma dilution increases the clotting potential in a manner that is independent and upstream from fibrin clot formation.

Plasma dilution mitigates antithrombin-dependent inhibition of thrombin generation

The anticoagulant serpin antithrombin (AT) is known to strongly regulate TF-induced thrombin generation and is the main plasma inhibitor of FXa [23, 24]. To investigate whether elevated plasma levels of AT may affect thrombin generation in diluted plasma, we analyzed normal pooled human plasma in the presence of increasing plasma concentrations of human AT. TF (6 pM) stimulation of 1.5-fold diluted plasma supplemented with 625 nM AT (125% final plasma concentration)

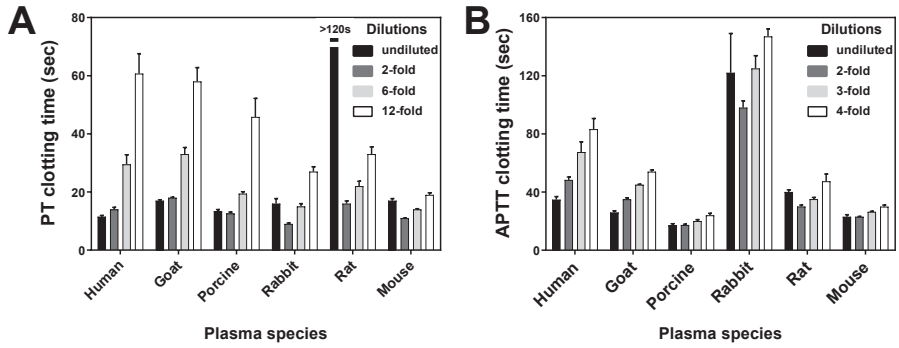

Figure 1. Analysis of the extrinsic and intrinsic pathways of coagulation in human and animal plasmas. (**A**) The extrinsic pathway of coagulation was assessed on undiluted and diluted (2-, 6-, and 12-fold) human, goat, porcine, rabbit, rat, or mouse plasma employing a PT-based clotting assay with a rabbit brain thromboplastin reagent (Neoplastine CI Plus) as described in 'Materials and Methods'. (**B)** The intrinsic pathway of coagulation was assessed on undiluted and diluted (2-, 3-, and 4-fold) human, goat, porcine, rabbit, rat, or mouse plasma using an APPT-based clotting assay with platelet factor III from rabbit brain phospholipids and micronized silica (TriniClot) as described in 'Materials and Methods'. Data analysis was performed with GraphPad Prism 7 and the coefficient of variation (CV = μ/σ) was calculated for all means. A mean CV of 10% or higher was observed for the PT or APTT clotting times of the following groups: PT of human plasma at 6- and 12-fold dilution and APTT at 3-fold dilution, PT of porcine plasma at 12-fold dilution, PT and APTT of undiluted rabbit plasma, PT of undiluted rat plasma, and APTT of 4-fold diluted rat plasma. The data represent the average clotting time ± 1 S.D. from six individual measurements.

typically displayed a 65% reduced thrombin peak (65 ± 8 nM) compared to that of 1.5-fold diluted plasma without additional AT (183 ± 12 nM) (**Figure 2**) [25]. However, employing similar conditions, thrombin generation in 3-fold diluted plasma resulted in a 15% reduced thrombin peak (70 ± 8 nM with 125% AT vs. 82 ± 8 nM with 100% AT). Further assessment of the thrombin peak and velocity index at AT plasma levels of up to 200% revealed a stronger procoagulant response in thrombin generation parameters of 3-fold diluted plasmas relative to the 1.5-fold dilution (**Figure 2**). Taken together, these results demonstrate that plasma dilution mitigates AT-mediated anticoagulation following TF-initiated thrombin formation. As such, these findings corroborate our observations on the enhanced extrinsic clotting potential in diluted plasmas (**Figure 1A; Table 1**). Furthermore, AT-mediated inhibition of FXa, and the reduction thereof upon plasma dilution, could potentially be at the basis of the attenuated thrombin formation observed for rabbit, rat, and mouse plasma.

Enhanced inhibition of human FXa in rabbit, rat, and mouse plasma

To assess anti-FXa activity in the various animal plasmas in more detail, we assayed the time-dependent inhibition of recombinant human FXa (hFXa, 5 nM) in a series of diluted plasmas (**Figure 3A,B**). Assessment of the second order rate constants (k_2) revealed similar rates of hFXa inhibition in human (k_2 9.2 ± 0.4 M s^{-1} dil^{-1}), porcine (k_2 8.2 ± 0.5 M s^{-1} dil^{-1}), and goat (k_2 9.6 ± 1.6 M s^{-1} dil^{-1}) plasma. Rat (k_2 22.2 ± 1.6 M s^{-1} dil^{-1}) and rabbit (k_2 24.9 ± 3.4 M s^{-1} dil^{-1}) plasma, on the other hand, displayed a 2- to 2.5-fold higher rate of hFXa inhibition relative to human plasma (**Figure 3C**). Notably, analysis of hFXa inhibition in mouse plasma required shortened hFXa incubations and higher plasma dilutions (**Figure 3B**), resulting in a hFXa inhibition that was over 13-fold higher compared to human plasma (WT-A, k_2 118 ± 5 M s^{-1} dil^{-1}; WT-B, k_2 119 ± 18 M s^{-1} dil^{-1}) (**Figure 3D**). These results show that inhibition of hFXa is enhanced in rabbit, rat, and particularly in mouse plasma.

As wild-type C57BL/6 mice are known to comprise 10- to 20-fold higher plasma levels of Tissue Factor Pathway Inhibitor (TFPI) relative to human plasma [26], a plasma pool of TFPI-low C57BL/6 mice was examined to assess the contribution of TFPI to hFXa inhibition [27]. Remarkably, no significant difference in hFXa inhibition rate was observed between TFPI-low plasma (k_2 125 ± 10 M s^{-1} dil^{-1}; 2-fold diluted PT 11.4 ± 0.4 sec; 2-fold diluted APTT 35.8 ± 1.1 sec) and a wild-type C57BL/6 plasma pool derived from the same breeding facility (WT-B, k_2 119 ± 18; PT 2-fold diluted 12.5 ± 0.8 sec; 2-fold diluted APTT 40.7 ± 1.8 sec) (**Figure 3D**). In addition, we studied the relative contribution of AT to hFXa inhibition in more detail in pooled plasma from C57BL/6 mice with AT plasma levels of 0.8-2% resulting from siRNA treatment that leads to knockdown of AT expression [13]. Remarkably, the rate of hFXa inhibition in AT-low plasma (k_2 78 ± 5) was only 1.5-

Human	Lag Time (min)	SD	Peak (nM)	SD	ttPeak (min)	SD	ETP (nM•min)	SD	Velocity (nM/min)	SD
2pM TF										
80µl	2.7	0.2	118.2	13.4	6.0	0.2	824.2	72.6	36.4	4.1
20µl	6.7	0.7	45.7	7.4	10.6	1.1	493.0	47.5	12.1	2.9
6 pM TF										
80µl	1.5	0.1	238.7	7.2	3.2	0.1	974.1	76.3	140.2	7.6
20µl	3.4	0.1	88.3	6.3	5.4	0.2	676.6	47.5	46.4	7.1
Goat										
2 pM TF										
80µl	2.7	0.2	26.9	8.9	7.1	0.8	231.3	61.7	6.0	1.0
20µl	3.8	0.3	31.8	3.5	9.3	0.3	338.6	47.4	5.9	0.7
6 pM TF										
80µl	1.6	0.3	84.2	6.8	4.2	0.4	495.1	54.8	32.8	4.2
20µl	1.9	0.1	84.8	2.8	4.4	0.2	569.2	39.6	35.0	1.7
Porcine										
2 pM TF										
80µl	1.4	0.1	98.1	7.5	2.6	0.1	247.5	8.1	85.2	15.0
20µl	2.9	0.3	52.4	5.7	4.6	0.4	257.0	20.9	31.6	4.9
6 pM TF										
80µl	0.9	0.1	113.7	4.4	2.0	0.1	251.4	7.7	106.4	16.8
20µl	1.6	0.1	67.5	4.6	3.1	0.1	289.6	15.3	46.6	5.7
Rabbit										
2 pM TF										
80µl	5.2	0.4	6.6	1.8	8.4	0.9	60.0	13.0	2.2	1.0
20µl	4.5	0.3	37.8	4.6	8.0	0.6	284.2	19.1	11.2	2.3
6 pM TF										
80µl	2.8	0.4	27.7	4.1	4.5	0.4	141.0	8.0	16.9	2.7
20µl	2.5	0.1	77.4	6.7	4.3	0.3	359.0	19.7	42.4	5.2
Rat										
2 pM TF										
80µl	1.8	0.3	36.2	3.9	5.3	0.4	380.0	15.9	10.5	1.6
20µl	1.5	0.1	68.1	4.4	3.2	0.1	380.2	46.8	41.0	1.9
6 pM TF										
80µl	1.3	0.1	48.4	11.5	4.0	0.1	393.9	38.6	18.2	5.8
20µl	1.0	0.1	76.9	5.8	2.5	0.1	387.8	53.4	53.6	2.2
Mouse										
2 pM TF										
80µl	0.0	0.0	0.0	0.0	0.0	0.0	0.0	0.0	0.0	0.0
20µl	1.8	0.6	42.7	19.1	3.5	1.5	244.3	43.0	24.0	19.2
6 pM TF										
80µl	0.0	0.0	0.0	0.0	0.0	0.0	0.0	0.0	0.0	0.0
20µl	0.8	0.1	82.5	7.1	1.9	0.2	212.7	19.8	71.1	6.9
20 pM TF										
80µl	0.0	0.0	0.0	0.0	0.0	0.0	0.0	0.0	0.0	0.0
20µl	0.4	0.1	83.7	0.7	1.3	0.1	174.3	14.0	104.6	7.7

Table 1. Calibrated automated thrombography parameters. Thrombin generation was measured in human, goat, porcine, rabbit, rat, or mouse (WT-A) plasma using a plasma volume of 80 µl (1.5-fold diluted plasma) or 20 µl (3-fold diluted plasma) following a 6 pM or 2 pM TF trigger. Thrombin generation was initiated with $CaCl_2$ and a thrombin fluorogenic substrate as detailed in 'Materials and Methods'. The lag time, thrombin peak, time to peak (ttpeak), and the velocity of thrombin generation were assessed. Values represent averages of three independent experiments ± 1 S.D.

fold lower relative to that of wild-type plasma (**Figure 3D**), which suggests that AT only partially accounts for the higher rates of hFXa inhibition in mouse plasma.

Mouse, rat, and rabbit plasma display distinct profiles of human FXa-antithrombin complex formation

The elevated rates of hFXa inhibition in rabbit and rodent plasma were investigated in more detail via immunoblotting of time-dependent hFXa incubations in diluted plasma using a polyclonal anti-human FX antibody. In addition, the relative rate of complex formation between hFXa and endogenous AT, thereby generating hFXa-AT, was assessed. As expected, incubation of hFXa in human plasma predominantly resulted in the formation of hFXa-AT complexes which differed in size according to FXa species (FXa-*α* 46 kDa, FXa-*β* 42 kDa) [28] and AT glycosylation status (AT*α* kDa 58, AT*β* 55 kDa) (**Figure 4A**) [29]. Furthermore, prolonged incubation (>10 minutes) also resulted in the appearance of minor amounts of high molecular weight species (HMWs, Mr >188 kDa) that are yet to be identified.

In line with the observations for human plasma, incubation of hFXa in mouse plasma led to the formation of hFXa-AT complexes with a similar distribution in apparent molecular weight (**Figure 4B**). However, the relative rate of hFXa-AT complex formation was 2.8-fold higher in mouse plasma relative to human plasma (**Figure 5A,B**), and consumption of hFXa was clearly observed (**Figure 4B**). Moreover, extensive formation of multiple HMWs over time was observed in mouse plasma. Furthermore, a hFXa-intermediate (hFXa-i) migrating at 62 kDa was apparent at the early time points and disappeared upon prolonged incubations of hFXa (**Figure 4B**). In contrast, the generation of hFXa-i and HWMs was rather limited upon incubation of hFXa in rat plasma (**Figure 4C**), while the relative rate of hFXa-AT complex formation was 2.1-fold higher relative to human plasma (**Figure 5C**). These findings highlight that the hFXa-AT complexation profile in rat plasma was more similar to that of human plasma. Finally, incubation of hFXa over time in rabbit plasma resulted in a persistent appearance of hFXa-i, notable consumption of hFXa, and a HMWs banding pattern that was distinct from mouse and rat plasma. In addition, the relative rate of hFXa-AT complex formation was 3.4-fold higher in rabbit plasma as compared to human plasma. Importantly, cross reactivity between the anti-human FX antibody and plasma FX native to mouse, rat, or rabbit was not observed. In summary, our observations indicate that the elevated rates of hFXa inhibition in rabbit and rodent plasma are partly mediated by enhanced hFXa-AT complex formation. In addition, the observed species-specific differences in the hFXa plasma absorption profile suggest the presence of unidentified hFXa binding components that are unique to each plasma.

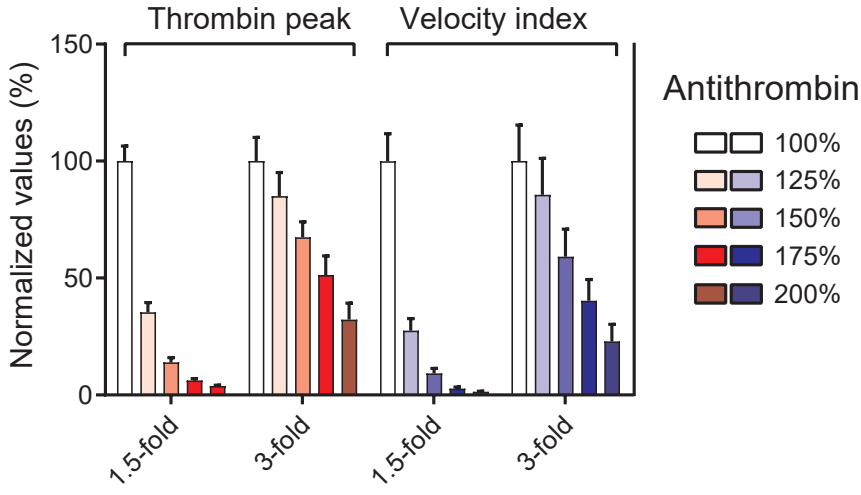

Figure 2. Calibrated automated thrombography of human plasma spiked with antithrombin. Thrombin generation was measured in either 1.5-fold (standard plasma volume of 80 µl) or 3-fold (plasma volume of 20 µl) diluted normal human plasma with 100-200% AT (final plasma concentrations) and 6 pM TF and 20 µM PCPS (final reaction concentrations). Thrombin generation was initiated with $CaCl_2$ and a thrombin fluorogenic substrate as detailed in 'Materials and Methods'. Percentages AT reflect final plasma concentrations of AT. The thrombin peak and the velocity index of thrombin formation were derived from individual experiments and normalized to conditions without 100% AT final plasma levels. Values represent the normalized averages ± 1 S.D. of three independent experiments.

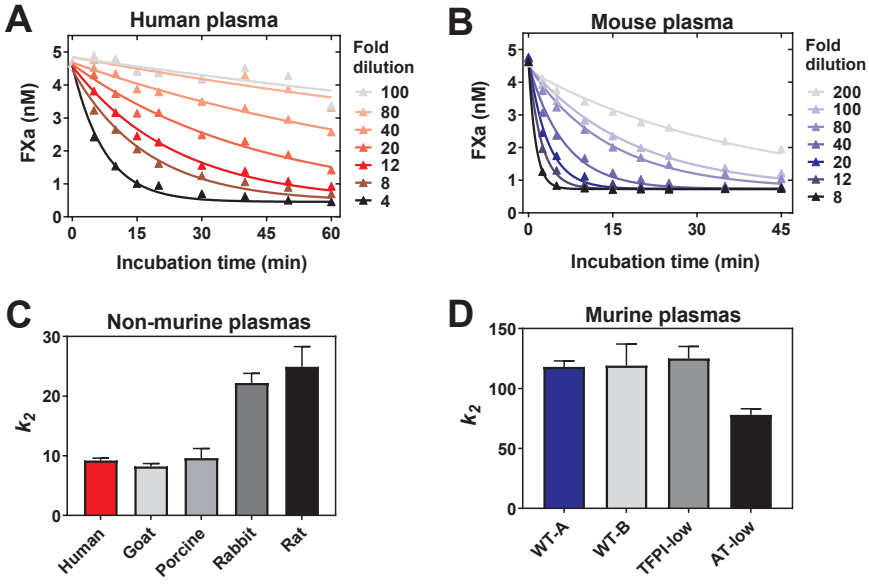

Figure 3. Inhibition of human FXa in human and animal plasmas. The rate of hFXa inhibition was measured under pseudo-first order conditions. hFXa (5 nM) was incubated in 4- to 100-fold diluted human plasma (**A**) or 8- to 200-fold diluted mouse plasma (**B**, WT-A) for up to 60 minutes at ambient temperature. At various time points, residual enzyme activity was measured using the chromogenic substrate SpecXa. The lines are drawn following analysis to equations detailed in 'Materials and Methods'. (**C,D**) hFXa (5 nM) was incubated in diluted human, goat, porcine, rabbit, or rat plasma (**C**, 4- to 100-fold diluted in dilution buffer) or in diluted murine WT-A, WT-B, TFPI-low, or AT-low plasma (**D**, 8- to 200-fold diluted in dilution buffer) for up to 60 minutes at ambient temperature. At various time points, residual enzyme activity was measured using the chromogenic substrate SpecXa, and the first order rates (k_{obs}, M s^{-1}) of hFXa inhibition were determined as detailed in 'Materials and Methods'. Second order rate constants of hFXa inhibition (k_2, M s^{-1} dil^{-1}) were obtained by plotting k_{obs} against the plasma dilution and subsequent analysis by linear regression. Values represent the average of three individual experiments ± 1 S.D.

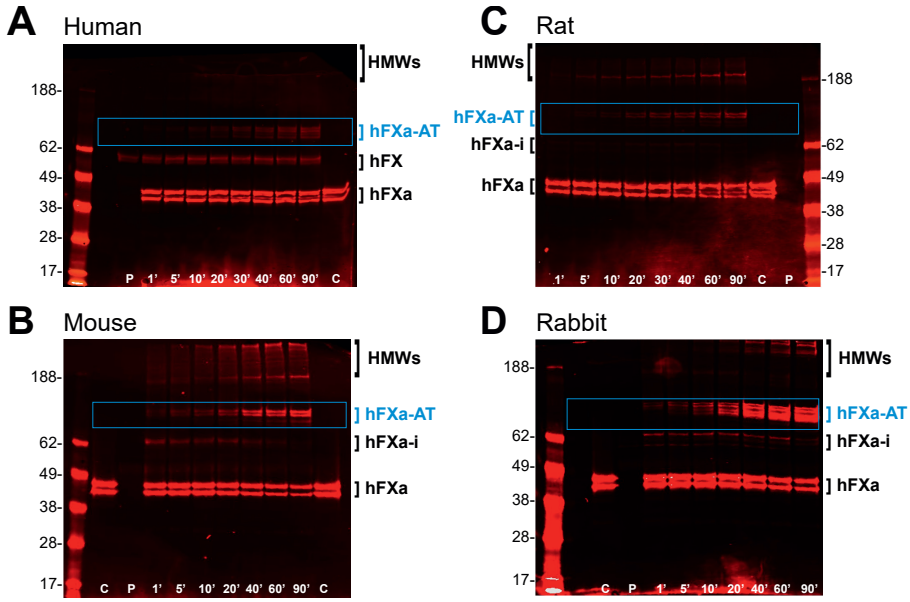

Figure 4: Immunoblotting of hFXa incubated in human, mouse, rat, or rabbit plasma. (**A**) hFXa (5 nM) was incubated in 12-fold diluted human plasma for 1 – 90 minutes at ambient temperature. Samples were taken at various time points, subjected to reducing SDS-PAGE analysis, blotted to a nitrocellulose membrane, and probed using a polyclonal goat-anti-human FX antibody as detailed in 'Materials and Methods'. The incubation time of hFXa (in minutes) is indicated at the bottom of the images; control lanes containing hFXa-αβ (hFXa, C) or plasma (P) only are indicated. (**B-D**) Similar to panel A, except hFXa was incubated in either 12-fold diluted mouse (**B**), rat (**C**) or rabbit (**D**) plasma. The protein bands corresponding to the hFXa-AT complexes (*blue*, boxed), High Molecular Weight species (HMWs), endogenous plasma derived human FX (hFX), hFXa intermediate (hFXa-i), recombinant human FXa (hFXa), and the apparent molecular weights (kDa) of the standards are indicated. Representative immunoblots of two independent experiments per species are shown.

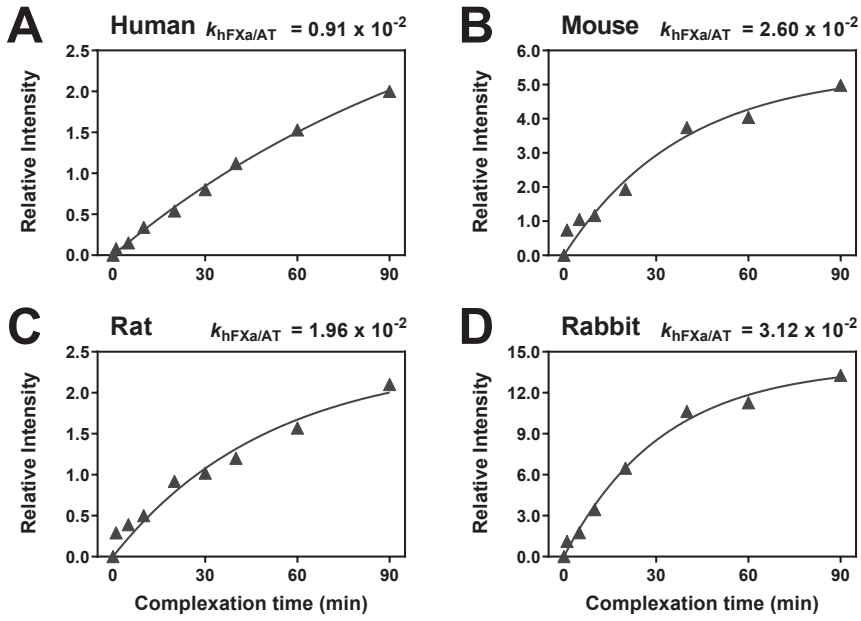

Figure 5. Rate of human FXa-antithrombin complex formation in human, mouse, rat, or rabbit plasma. The rate of hFXa-AT complex formation was assessed under pseudo-first order conditions. (**A-D**) hFXa (5 nM) was incubated over time in 12-fold diluted human, rabbit, rat, or mouse plasma, and hFXa-AT complex relative band intensities were quantified and analyzed via non-linear regression as described in 'Materials and Methods'. The rate of hFXa-AT complex formation ($k_{hFXa/AT}$, relative intensity per minute) is indicated. Datapoints represent averages of two independent experiments.

Discussion

Studies that serve to evaluate the procoagulant activity of human coagulation proteins build upon animal models and coagulation assays originally intended for human plasma. A relevant animal model will allow for reliable preclinical assessment and potential to extrapolate findings to the human system. As mouse, rat, rabbit, pig, and goat are frequently used in preclinical hemostasis ad thrombosis research [30, 31], we evaluated the coagulant characteristics of pooled plasmas from these species by means of extrinsic and intrinsic clotting analyses and CAT measurements. Side-by-side evaluation of standard PT and APTT clotting parameters revealed that of all species studied, goat plasma displayed a clotting profile comparable to human plasma, hallmarked by similarly prolonged clotting times following plasma dilution (**Figure 1**). CAT parameters obtained using human TF as extrinsic trigger demonstrated porcine plasma to behave in a manner analogous to human plasma, indicated by a diminished thrombin generating potential of diluted plasma (**Table 1**). In addition, both goat and rat plasma were able to effectively generate thrombin in this system. As such, these data indicate that thrombin formation in goat, porcine, and rat plasma is sensitive to human TF, an essential reagent specific to human FX.

Interestingly, plasma from mice, rat, and rabbit was characterized by an enhanced potential to generate thrombin after plasma dilution, whereas the opposite was observed for human and porcine plasma (**Table 1**). In line with these findings, plasma dilutions trended towards a potentiation of fibrin clot formation for smaller animals vs. a mostly dampened clot formation for larger animals (**Figure 1**). These differences in coagulation profile may in part be related to variations in the levels and/or inhibition kinetics of naturally occurring plasma inhibitors (e.g. AT, TFPI) that tightly control the procoagulant activity of serine proteases such as FXa in order to prevent runaway coagulation. Evidence of a role for interspecies differences in FXa inhibition that may be at the basis of this finding comes from our observation that mouse, rat, and rabbit plasma demonstrated fundamentally higher rates of hFXa inhibition (**Figure 3**). In contrast, the rate of hFXa inhibition in goat, porcine, and human plasma was nearly identical. Detailed plasma analysis by means of immunoblotting further revealed higher rates of hFXa-AT complex formation in rabbit, rat, and mouse plasma relative to human plasma (**Figure 5**). As such, we speculate that the distinctive coagulant profile observed for rabbit, rat, and mouse plasma results, at least in part, from enhanced FXa inhibition by AT. This may be the consequence of increased circulating levels of AT. Support for the latter comes from our observation that inhibition of thrombin generation by supra-physiological AT levels was mitigated upon dilution of human plasma (**Figure 2**). However, it is important to mention that information on AT levels in rabbit, rat, and mouse is scarce [32]. Summarizing, dilution of rabbit, rat, and mouse plasma increases the

clotting potential as a result, in part, of reduced endogenous AT plasma levels. As dilution is not expected to significantly impact the nanomolar amounts of AT-targeted coagulation factors generated in coagulation assays, lowering of the AT concentration will therefore impair efficient protease inactivation due to their intrinsically slow target inhibition rates in the absence of heparin-like saccharides [17]. As the rate of hFXa inhibition was only partially reduced in plasma from AT-low C57BL/6 mice (**Figure 3**), it seems likely that additional inhibitors contribute to the inhibition of FXa and as such to reduced clotting. TFPI may not play a substantial role to overall inhibition of hFXa, since under the conditions employed the rate of hFXa inhibition was comparable for plasma of wild-type and TFPI-low mice (**Figure 3**). Other FXa inhibitors endogenous to mouse plasma include protein Z-dependent protease inhibitor (ZPI) and alpha-2-macroglobulin [33-35]. The serpin ZPI circulates in complex with its cofactor protein Z, and this complex inhibits FXa in a calcium- and phospholipid-dependent manner [36]. Therefore, ZPI is not expected to contribute the kinetics of FXa inhibition under the conditions employed. The inhibitor α2-macroglobulin targets a broad spectrum of proteases in the circulation. Subsequent to binding and cleavage by the target protease, α2-macroglobulin undergoes an irreversible conformational change which traps the protein within a cage-like structure without directly blocking the protease active site [37, 38]. As such, α2-macroglobulin is not expected to impact the observed rate of FXa-inhibition. Finally, as knowledge on the spectrum and functionality of serpins implicated in murine hemostasis is limited, the involvement of an expanded set of serpin species including serpins from other clades, such as α1-antitrypsin variants or ovalbumin-like serpins [39, 40], cannot be ruled out. Whether the range and functional characteristics of naturally occurring plasma inhibitors is homologous for rabbit, rat, and mouse is unclear at this point.

The notion that multiple FXa-targeting inhibitors may circulate in mouse plasma agrees with our observation that hFXa interacted with several mouse proteins (**Figure 4**). Furthermore, Parng and colleagues corroborated our findings as they previously reported high plasma protein binding of catalytically active hFXa-I16L in mouse plasma, resulting in rapid plasma elimination of hFXa-I16L [41]. Moreover, they demonstrated that spiking of hFXa-I16L in mouse plasma leads to hFXa-I16L-HMW complexes, which were suggested to correspond to hFXa-I16L in complex with either a serpin or alpha-2-macroglobulin. An alternative explanation for the hFXa-HMW species observed may lie in the polymerization/aggregation of hFXa-AT complexes as described for human AT [42, 43]. While identification of the hFXa binding proteins was beyond the scope of this study, our immunoblotting strategy clearly underscores the intricate complexity of studying the procoagulant effects of human FXa in a non-human plasma environment.

A limitation of the current study is that additional data is required in order to substantiate claims towards our premise of elevated levels of circulating inhibitory proteins in rabbit, rat, and mouse plasma that would underpin some of the findings obtained here. More specifically, knowledge on the exact levels of coagulation proteins including factors X and VII, prothrombin, and AT, are necessary for a better understanding of the noted species differences. Unfortunately, evaluation of these parameters is hampered by the lack of species-specific reagents that would allow for these types of analyses. Other limitations are that the inhibition of species-specific FXa variants was not assessed, and the initiation of coagulation by rabbit- or rodent-derived proteins was not evaluated, nor that of the contribution of platelets. Examination of the above-mentioned elements is necessary to draw definitive conclusions regarding relative endogenous pro- or anticoagulant activity in these animals.

In conclusion, the current body of work serves as an informative standardization study in which selected species were compared with respect to coagulation assays and human FX(a). While it is difficult to find an animal model that fully mimics human physiology, we identified the rat plasma clotting system to be more relevant to preclinical studies that incorporate CAT, human TF, and human FXa as compared to murine plasma. The plasma clotting system of larger animals, such as goats or pigs, was however more similar to that of humans. Furthermore, it was uncovered that these differences are, in part, related to a fundamentally higher rate of FXa inhibition and FXa-inhibitor complex formation in rabbit, rat, and mouse plasma. These novel findings will help to further our understanding of non-human coagulation systems and will contribute to the extrapolation of experimental data during preclinical assessment of novel therapeutic strategies.

References

1. Gentry, P.A., *Comparative aspects of blood coagulation.* Veterinary Journal, 2004. **168**(3): p. 238-251.
2. Siller-Matula, J.M., et al., *Interspecies differences in coagulation profile.* Thrombosis and Haemostasis, 2008. **100**(3): p. 397-404.
3. Garcia-Manzano, A., et al., *Standardization of rat blood clotting tests with reagents used for humans.* Proc West Pharmacol Soc, 2001. **44**: p. 153-5.
4. Tchaikovski, S.N., et al., *Development of a calibrated automated thrombography based thrombin generation test in mouse plasma.* Journal of Thrombosis and Haemostasis, 2007. **5**(10): p. 2079-2086.
5. Tarandovskiy, I.D., et al., *Interspecies comparison of simultaneous thrombin and plasmin generation.* Sci Rep, 2020. **10**(1): p. 3885.
6. Lozier, J.N. and T.C. Nichols, *Animal Models of Hemophilia and Related Bleeding Disorders.* Seminars in Hematology, 2013. **50**(2): p. 175-184.
7. Thalji, N.K., et al., *A rapid pro-hemostatic approach to overcome direct oral anticoagulants.* Nat Med, 2016. **22**(8): p. 924-32.
8. Verhoef, D., et al., *Engineered factor Xa variants retain procoagulant activity independent of direct factor Xa inhibitors.* Nat Commun, 2017. **8**(1): p. 528.
9. Lu, G., et al., *A specific antidote for reversal of anticoagulation by direct and indirect inhibitors of coagulation factor Xa.* Nat Med, 2013. **19**(4): p. 446-51.
10. Schuijt, T.J., et al., *Factor Xa activation of factor V is of paramount importance in initiating the coagulation system: lessons from a tick salivary protein.* Circulation, 2013. **128**(3): p. 254-66.
11. Bos, M.H.A., van 't Veer C, Reitsma P.H, *Molecular Biology and biochemistry of the coagulation factors and pathways of hemostasis*, in *Williams Hematology*, L.M.A. Kaushansky K., Prchal J.T., Levi M.M., Press O.W., Burns L.J., Caligiuri M.A., Editor. 2015, McGraw-Hill Education: New York City. p. 1915-1948.
12. Huby, M.D., et al., *Establishment of Methods for Performing Thrombelastography and Calibrated Automated Thrombography in Rats.* Shock, 2014. **42**(1): p. 27-30.
13. Safdar, H., et al., *Acute and severe coagulopathy in adult mice following silencing of hepatic antithrombin and protein C production.* Blood, 2013. **121**(21): p. 4413-6.
14. Higgins, D.L. and K.G. Mann, *The interaction of bovine factor V and factor V-derived peptides with phospholipid vesicles.* J Biol Chem, 1983. **258**(10): p. 6503-8.
15. Hemker, H.C., et al., *Calibrated automated thrombin generation measurement in clotting plasma.* Pathophysiol Haemost Thromb, 2003. **33**(1): p. 4-15.
16. Olson, S.T., I. Bjork, and J.D. Shore, *Kinetic characterization of heparin-catalyzed and uncatalyzed inhibition of blood coagulation proteinases by antithrombin.* Methods Enzymol, 1993. **222**: p. 525-59.
17. Olson, S.T., et al., *Accelerating ability of synthetic oligosaccharides on antithrombin inhibition of proteinases of the clotting and fibrinolytic systems. Comparison with heparin and low-molecular-weight heparin.* Thromb Haemost, 2004. **92**(5): p. 929-39.

18. Munster, A.M.B., A.K. Olsen, and E.M. Bladbjerg, *Usefulness of human coagulation and fibrinolysis assays in domestic pigs.* Comparative Medicine, 2002. **52**(1): p. 39-43.
19. Nagashima, M., et al., *Thrombin-activatable fibrinolysis inhibitor (TAFI) deficient mice.* Frontiers in Bioscience, 2002. **7**: p. D556-D568.
20. Mackman, N., R.E. Tilley, and N.S. Key, *Role of the extrinsic pathway of blood coagulation in hemostasis and thrombosis.* Arterioscler Thromb Vasc Biol, 2007. **27**(8): p. 1687-93.
21. Petersen, L.C., et al., *Characterization of recombinant murine factor VIIa and recombinant murine tissue factor: a human-murine species compatibility study.* Thromb Res, 2005. **116**(1): p. 75-85.
22. Thomassen, M.C.L.G.D., et al., *Tissue factor-independent inhibition of thrombin generation by tissue factor pathway inhibitor-alpha.* Journal of Thrombosis and Haemostasis, 2015. **13**(1): p. 92-100.
23. Rietveld, I.M., et al., *Elevated coagulation factor levels affect the tissue factor-threshold in thrombin generation.* Thromb Res, 2018. **172**: p. 104-109.
24. van 't Veer, C. and K.G. Mann, *Regulation of tissue factor initiated thrombin generation by the stoichiometric inhibitors tissue factor pathway inhibitor, antithrombin-III, and heparin cofactor-II.* J Biol Chem, 1997. **272**(7): p. 4367-77.
25. Conard, J., et al., *Molar antithrombin concentration in normal human plasma.* Haemostasis, 1983. **13**(6): p. 363-8.
26. Maroney, S.A., et al., *Murine Hematopoietic Cell Tissue Factor Pathway Inhibitor Limits Thrombus Growth.* Arteriosclerosis Thrombosis and Vascular Biology, 2011. **31**(4): p. 821-826.
27. Huang, Z.F., et al., *Tissue factor pathway inhibitor gene disruption produces intrauterine lethality in mice.* Blood, 1997. **90**(3): p. 944-951.
28. Pryzdial, E.L. and G.E. Kessler, *Kinetics of blood coagulation factor Xaalpha autoproteolytic conversion to factor Xabeta. Effect on inhibition by antithrombin, prothrombinase assembly, and enzyme activity.* J Biol Chem, 1996. **271**(28): p. 16621-6.
29. Brennan, S.O., P.M. George, and R.E. Jordan, *Physiological variant of antithrombin-III lacks carbohydrate sidechain at Asn 135.* FEBS Lett, 1987. **219**(2): p. 431-6.
30. Honickel, M., et al., *Dose requirements for idarucizumab reversal of dabigatran in a lethal porcine trauma model with continuous bleeding.* Thromb Haemost, 2017. **117**(7): p. 1370-1378.
31. Spronk, H.M., et al., *Hypercoagulability causes atrial fibrosis and promotes atrial fibrillation.* Eur Heart J, 2017. **38**(1): p. 38-50.
32. Pichler, L., *Parameters of coagulation and fibrinolysis in different animal species - A literature based comparison.* Wiener Tierarztliche Monatsschrift, 2008. **95**(11-12): p. 282-295.
33. Meijers, J.C.M., P.N.M. Tijburg, and B.N. Bouma, *Inhibition of Human-Blood Coagulation Factor-Xa by Alpha-2-Macroglobulin.* Biochemistry, 1987. **26**(18): p. 5932-5937.

34. Han, X., R. Fiehler, and G.J. Broze, *Isolation of a protein Z-dependent plasma protease inhibitor.* Proceedings of the National Academy of Sciences of the United States of America, 1998. **95**(16): p. 9250-9255.
35. Hudson, N.W. and P.H. Koo, *Subunit and primary structure of a mouse alpha-macroglobulin, a human alpha 2-macroglobulin homologue.* Biochim Biophys Acta, 1982. **704**(2): p. 290-303.
36. Han, X., R. Fiehler, and G.J. Broze, Jr., *Characterization of the protein Z-dependent protease inhibitor.* Blood, 2000. **96**(9): p. 3049-55.
37. Qazi, U., et al., *The structure of the C949S mutant human alpha(2)-macroglobulin demonstrates the critical role of the internal thiol esters in its proteinase-entrapping structural transformation.* J Struct Biol, 2000. **131**(1): p. 19-26.
38. Rehman, A.A., H. Ahsan, and F.H. Khan, *alpha-2-Macroglobulin: a physiological guardian.* J Cell Physiol, 2013. **228**(8): p. 1665-75.
39. Owen, M.C., et al., *Mutation of antitrypsin to antithrombin. alpha 1-antitrypsin Pittsburgh (358 Met leads to Arg), a fatal bleeding disorder.* N Engl J Med, 1983. **309**(12): p. 694-8.
40. Heit, C., et al., *Update of the human and mouse SERPIN gene superfamily.* Human Genomics, 2013. **7**.
41. Parng, C., et al., *Preclinical Pharmacokinetics, Pharmacodynamics, Tissue Distribution, and Interspecies Scaling of Recombinant Human Coagulation Factor Xa(I16L).* J Pharm Sci, 2017. **106**(8): p. 2136-2143.
42. Marciniak, E. and G. Gora-Maslak, *High molecular weight forms of antithrombin III complexes in blood.* Thromb Haemost, 1983. **49**(1): p. 32-6.
43. Preissner, K.T., *Self-association of antithrombin III relates to multimer formation of thrombin-antithrombin III complexes.* Thromb Haemost, 1993. **69**(5): p. 422-9.

Supplementary information

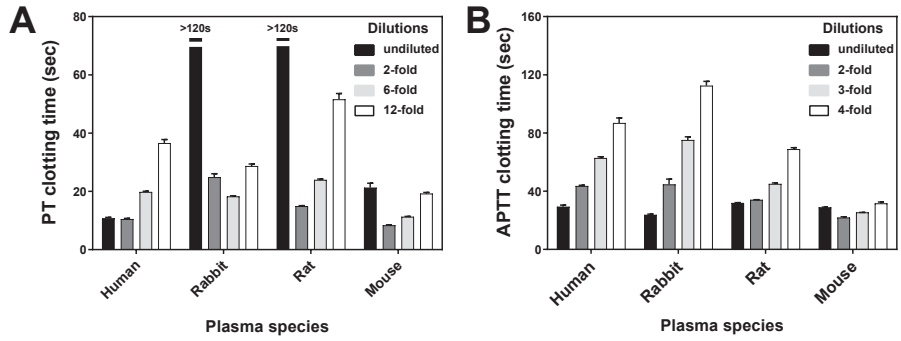

Supplemental Figure 1. Analysis of the extrinsic and intrinsic pathways of coagulation in human, rabbit, rat and mouse plasma using alternative reagents. (**A**) The extrinsic pathway of coagulation was assessed on undiluted and diluted (2-, 6-, and 12-fold) human, rabbit, rat, or mouse plasma employing a PT-based clotting assay with a recombinant human TF-based thromboplastin reagent (Dade Innovin) as described in 'Materials and Methods'. (**B)** The intrinsic pathway of coagulation was assessed with a rabbit brain cephalin APTT reagent containing kaolin as activator (CK Prest) on undiluted and diluted (2-, 3-, and 4-fold) human, rabbit, rat, or mouse plasma as described in 'Materials and Methods'. The data represent the average clotting time ± 1 S.D. from three individual measurements.

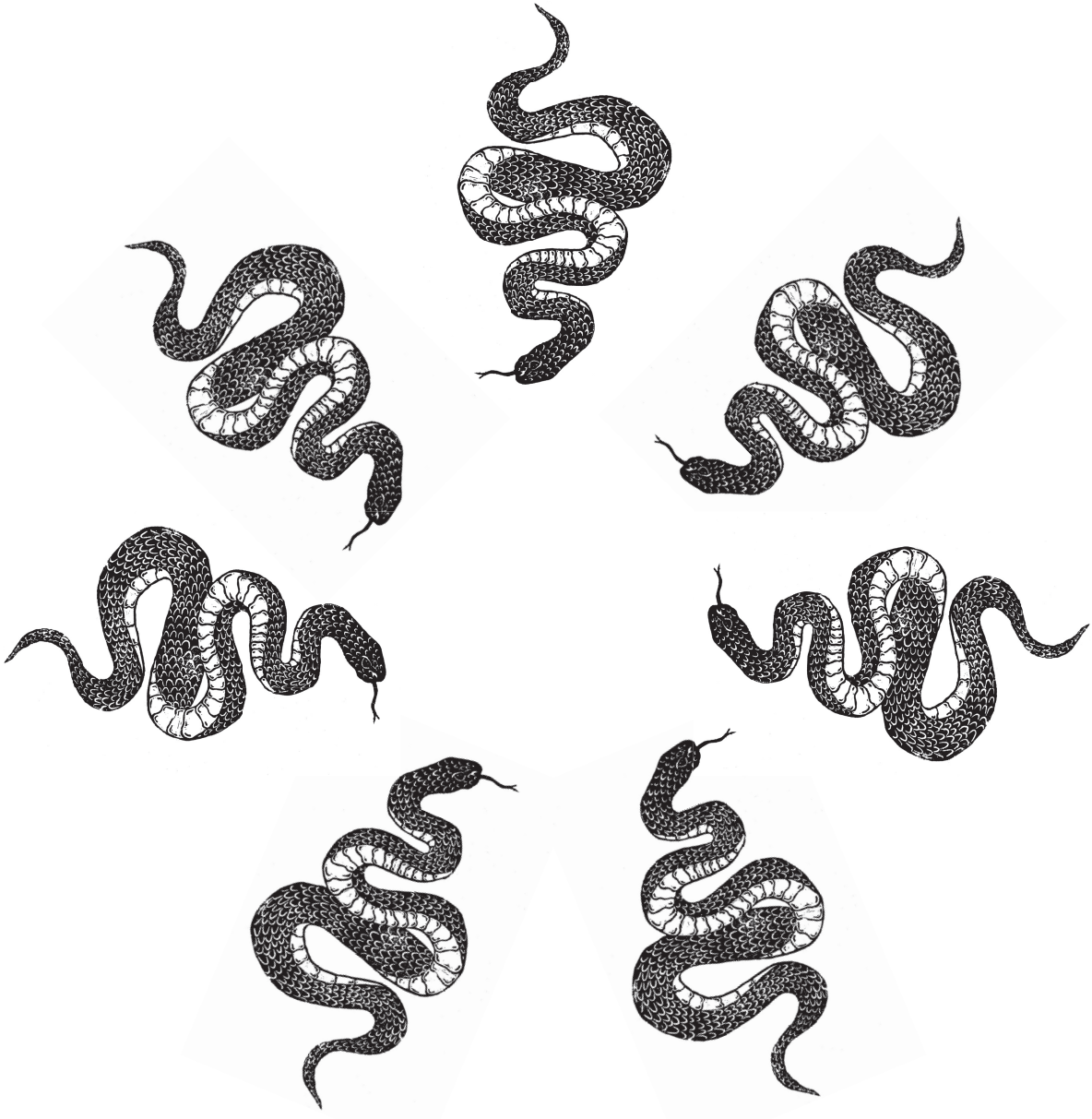

Chapter 7

General discussion and future directions

Circumventing the paradigm of prothrombinase assembly

The spatiotemporal assembly of the prothrombinase complex is tightly regulated and occurs exclusively on negatively charged membrane surfaces of activated cells or platelets, where activated factor X (FXa) assembles with its cofactor activated factor V (FVa) in the presence of calcium ions [1]. These molecular constraints are paramount to normal hemostasis as they serve to prevent fibrin clot formation at other sites away from the location of vascular injury. The venom of the Australian common brown snake *Pseudonaja textilis* contains a powerful prothrombin activator (Pseutarin C) that is structurally and functionally similar to the mammalian prothrombinase complex [2, 3]. However, both venom-derived FXa and FVa comprise unique molecular adaptations that serve to circumvent the conventional constraints of human FXa-FVa complex assembly [4-6]. For example, the venom-derived homolog of FVa (ptFV) is constitutively active due to the absence of a regulatory B-domain sequence [5] and is able to form a high affinity complex with venom-derived FXa (ptFXa) without the need for anionic phospholipid membranes or calcium ions [7]. In addition, both ptFV and ptFXa display prolonged procoagulant activity in circulation, as both proteins are insensitive to inhibition by their respective plasma regulators activated protein C (APC) [7] and antithrombin [8]. These gain-of-function adaptations enable the 'venom prothrombinase' to escape hemostatic regulation and to initiate indiscriminate clotting throughout the vasculature. The aim of this thesis has been to uncover the unique structural and functional relationships that govern the venom FXa-FVa complex assembly and function, with the intention to harness its potent procoagulant potential.

Part I - Factor V

Alternative splicing of the FV B-domain

In the first part of this thesis, we studied the genomic, structural and functional implications of several molecular modifications found in the *P. textilis* venom FV molecule. FV normally circulates in blood as an inactive procofactor (domain organization A1-A2-B-A3-C1-C2), and is only converted to its active form upon proteolytic removal of its central regulatory B-domain sequence [9, 10]. Previous studies have shown that venom FV is constitutively active due to the absence of a regulatory B-domain in both venom- and liver-derived *P. textilis* FV sequences [5, 7, 11]. In **chapter 2** of this thesis we have investigated whether absence of this B-domain sequence from liver-derived FV is unique to *P. textilis* physiology, or whether this trait is shared among other snakes. In contrast to previous studies [11, 12], we revealed that the liver transcriptome of *P. textilis* and other snake species included both full-length and B-domain deleted transcripts, suggesting unique functional diversification of the FV gene in members of the serpentes suborder. Additional data point to a conserved pre-mRNA exonic splicing enhancer (ESE) motif as potential regulator for alternative splicing of the full-length snake

B-domain transcript [13, 14]. As such, our findings constitute the first report of alternative splicing of the FV B-domain in a non-human species.

Thus far, alternative splicing of the FV B-domain has first been observed in patients that present with a rare bleeding disorder which is caused by supra-physiological plasma levels of Tissue Factor Pathway Inhibitor (TFPI) [15, 16]. In these patients, alternative splicing of the B-domain causes a FV variant known as FV-short to become a carrier protein for TFPI, potentially due to exposure of a high affinity binding site on the acidic region (AR) of the truncated B-domain sequence [17, 18]. Normally, the AR forms an essential part of the B-domain procofactor regulatory region (PRR) that, in conjunction with the B-domain basic region (BR), serves to stabilize the procofactor state of FV [19]. However, the essential BR is absent in FV-short due to activation of an alternative splice donor site and subsequent splicing. In a similar fashion, in **chapter 2** of this thesis we have shown that alternative splicing of the full-length snake FV B-domain also results in complete removal of the BR, leaving only a ~46 amino acid B-domain sequence that is distinctly acidic in nature. Potentially, this alternative acidic region could also function as a neo-epitope for TFPI binding by alternatively spliced snake FV. As TFPI is an essential inhibitor of prothrombinase activity and FXa [17, 20], high TFPI levels in snake plasma could possibly contribute to alternative regulation of prothrombinase activity. Additional research is therefore required to confirm the physiological presence of this alternative snake FV-short molecule in snake plasma, and to evaluate plasma levels of key anti-coagulant proteins such as antithrombin, protein C, and TFPI, as well as to assess the potential role of the truncated B-domain FV variant with regard to plasma TFPI regulation. These studies will undoubtedly provide new insights into the role of alternatively spliced FV molecules in hemostasis and their potential use in novel anti-thrombotic strategies.

Lipid-independent FVa cofactor function

The ability of ptFV to form a high affinity complex with ptFXa without the need for assembly on an anionic membrane surface has enabled Lechtenberg and co-workers to acquire an X-ray structure of the venom prothrombinase complex [21]. In addition to providing original insights into the potential conformation of the human prothrombinase complex, their model also uncovered structural features that were unique to venom ptFV-FXa. In **chapters 3 and 4** of this thesis we examined some of these distinct structural features in more detail and investigated their implications to prothrombinase complex assembly and function. In **chapter 3** we examined whether a non-conserved covalent link between the A2- and A3-domains of venom-derived ptFV induced potential conformational constraints that were essential to its lipid-independent cofactor function [7]. In addition, we investigated whether liver-derived ptFV was able to support lipid-independent prothrombin conversion by venom ptFXa as well. In short, both venom and liver

ptFV were found to support lipid-independent prothrombin conversion, irrespective of the presence or absence of a non-conserved covalent link between the A2- and A3-domain in either ptFV species. In addition, we established that this disulfide bond was not essential to cofactor function upon proteolytic degradation by APC. Moreover, liver ptFV was also functionally resistant to degradation by APC.

In **chapter 4** of this thesis we explored whether the venom C-domain pair was able to induce lipid-independent prothrombinase function by analyzing chimeric variants of FV that comprised either the A-domains of human FV and the C-domains of *P. textilis* venom FV, or vice versa. Functional analysis of these chimeras showed that the venom FV C-domains were of little relevance to its lipid-independent cofactor function, as the chimera comprising the venom A-domain trimer and human C-domain pair was also able to support cofactor function in the absence of phospholipids. In contrast, the chimera that comprised the human A-domain trimer and venom C-domain pair was not able to support lipid-independent cofactor function. These results show that high affinity binding of ptFV to venom ptFXa in solution is exclusively governed by the ptFV A-domain trimer. Additional functional analysis of structural features that are unique to the venom A-domain trimer are required to shed more light on the molecular requirements that govern lipid-independent cofactor function. One such feature includes the C-terminal part of the venom A2-domain which was shown to form an extended interaction interface with ptFXa in the crystallographic model of venom prothrombinase [21].

Functional crosstalk between the A and C-domains of FV

The multi-domain structure of the two chain molecule human FVa is recognized as inherently unstable and prone to spontaneous disassociation upon proteolytic removal of its central B-domain. Previously, we had reported that ptFV is functionally highly stable, as it retains cofactor activity upon extended proteolytic processing by the endogenous enzymatic regulator of FVa activity, APC [7, 22]. In addition, ptFV has been reported to display significantly reduced binding to phosphatidylserine-containing membranes [23]. As shown in **chapter 4**, the C-domains of ptFV confer cofactor stability when linked to the A-domains of human FV while, in turn, the A-domains of human FV improve phospholipid binding by the C-domains of ptFV. These unique findings imply functional crosstalk between the A-domain trimer and C-domain pair. We propose that such crosstalk is facilitated by transient interactions between the A-domain trimer and elongated loops (hFV: Ser1971-Val1987 and Ser2130-Val2146) that cover the crest of the C1- and C2-domains. Other studies have shown that, depending on the relative orientation of the C-domain pair, these elongated loops may potentially associate with each other [24], or alternatively with the A-domain trimer [25]. In addition, a more recent study used atomic force microscopy to show that the C-domains of FV undergo dynamic rearrangements while in solution, suggesting conformational

flexibility [26]. In **chapter 4**, we speculate that such conformational flexibility may be required for high affinity binding to procoagulant membranes. On the other hand, stabilization of inter-domain contacts between the A-domain trimer and C-domain pair may impair membrane association. However, additional engineering of FV is recommended to fully investigate the functional relationship between the elongated loop structures at the apex of the C1- and C2-domain and the A3-C1 domain interaction interface. Also, characterization of FV constructs by CD spectroscopy is suggested to survey the overall folding of the native and chimeric constructs.

The C-domains of ptFV bind phospholipids

It was previously reported that membrane association was abolished in the *P. textilis* venom-FV molecule [27]. However, in **chapter 4** we observed that the venom C-domains were able to bind phospholipid membranes when coupled to the A-domain trimer of hFV, albeit with a lower affinity and reduced phosphatidylserine sensitivity relative to the human C-domain pair. It is generally acknowledged that dedicated phosphatidylserine-binding residues facilitate membrane binding by FV. These residues are located on three separate membrane binding loops which protrude from the base of each C-domain [25, 28-32]. In the **4th chapter**, sequence analysis of these lipid-binding regions in ptFV revealed general sequence conservation of the first and second C1 membrane-binding loops [25]. The essential hydrophobic phospholipid binding pair [31, 32] on the third C1 loop is also partially conserved. However, most of the solvent exposed positively charged residues have been substituted in ptFV. Nonetheless, two essential phosphatidylserine-binding arginine residues remain in ptFV [30]. In addition, two essential aromatic phospholipid-binding residues on the first C2 phospholipid binding loop [29] are conserved as well. In contrast, the ptFV C2-domain displays poor amino acid conservation of the second membrane binding loop and moderate conservation of the third loop. In summary, several essential phospholipid binding features have been preserved in the C-domains of ptFV that could generally enable membrane anchoring, yet marked differences occur within specific phospholipid binding regions that may account for the reduced affinity to phosphatidylserine containing membranes in ptFV. In contrast to previous reports [23], we conclude that the ptFV C-domain pair has retained the ability to bind membrane surfaces, despite marked differences within specific phospholipid binding regions.

The venom A-domain trimer impedes phospholipid binding

In **chapter 4**, we show that the C-domains of ptFV can bind anionic phospholipids when coupled to the human A-domain trimer. Correspondingly, the chimeric variant that comprised the venom A-domain trimer and human C-domain pair displayed reduced phospholipid binding relative to hFV. This observation indicated that the venom A-domain trimer was less conducive to phospholipid binding. We

speculate that the unique disulfide bond between the A2- and A3-domain in ptFV may potentially constrain cofactor movement, impeding structural rearrangements required for phospholipid binding [23]. As removal of the disulfide bond from ptFV was shown to decrease overall thermal stability in **chapter 4**, we suspect that phospholipid binding might potentially be augmented in the variant lacking the covalent link between the A2- and A3-domain. Assessment of phospholipid binding by this variant is therefore recommended to investigate the role of this covalent link in ptFV with regard to phospholipid binding [22]. Efforts to introduce this covalent link in human FV have not been successful thus far, limiting our ability to study its effects on phospholipid binding and cofactor stability in the setting of human FV [33]. Implementation of dedicated protein modeling software, such as Molecular Operating Environment (MOE) [34], is recommended to improve disulfide bridging *in silico* before additional engineering strategies are attempted. Specifically, mutation of amino acids that surround a potential Cys-Cys pair may improve formation and stability of a disulfide bond [35, 36].

Part II - Factor X

Modulating inhibitor sensitivity in FXa

The second part of this thesis is focused on the structural and functional aspects of venom FX. In **chapter 5** of this thesis we discovered that venom derived FXa was highly insensitive to direct FXa inhibitors, unlike any FXa species known to date. This essential finding formed the basis of a new line of research that focused on developing a FX-based antidote against the direct FXa inhibitors. Inhibition of FXa by direct FXa inhibitors such as apixaban, rivaroxaban, or edoxaban is steadily becoming the mainstay of oral anticoagulant therapy due to their ease of dosing and relatively short half-life [37-41]. However, a major drawback to the use of direct FXa inhibitors is the absence of a safe and effective reversal strategy in the event of (trauma induced) bleeding [42-45]. Using a combined computational and biochemical approach we revealed that insertion of a heterologous segment into the 99-loop of venom FXa resulted in direct FXa inhibitor insensitivity in venom FXa. Introduction of similar structural features into the 99-loop of human FXa led to the engineering of FXa variants that were able to support coagulation in human plasma spiked with (supra-)pharmacologic concentrations of direct FXa inhibitors. As such, these FXa variants have the potential to be employed to bypass the direct FXa inhibitor-mediated anticoagulation in patients that require restoration of blood coagulation. The inhibitor-insensitive FXa variants have been patented [46], and are currently in (pre)clinical development as direct FXa inhibitor reversal agent. In addition to this work, we also applied insertional mutation of the 99-loop to successfully engineer inhibitor-insensitivity in thrombin. This work was also filed in a second patent on inhibitor-insensitive serine proteases [47]. Taken together, our findings highlight the general significance of 99-loop architecture in

modulating inhibitor insensitively in trypsin-like serine proteases and demonstrate the potential of studying natural homologs as a foundation for knowledge-based protein engineering.

Despite these evident successes, additional scientific work is still required to address a number of fundamental matters concerning chimeric FXa and thrombin variants. Essentially, we have not been able to clearly demonstrate how the length and amino acid composition of the 99-loop precisely modulates enzymatic activity and inhibitor insensitivity. For example, it is still unclear whether the inhibitor insensitivity can also result from steric hindrance by the 99-loop (potentially due to extension over the active site) as observed in kallikreins [48], in addition to an effect on overall protein motion and S4 subsite architecture [49, 50]. Furthermore, it is uncertain whether the 99-loop maintains a similar fold in chimeric FXa as that observed for the secondary structure of the 99-loop in venom derived FXa [21]. Structural and functional characterization of additional FX variants with 99-loop insertions varying in length and amino acid composition is therefore required to shed more light on these issues. Interestingly, a decreased sensitivity towards direct FXa inhibitors was also observed in FXa variants comprising substitutions at position Phe174 [51]. This amino acid forms part of the S4 subsite that is engaged by the direct FXa inhibitors [37, 39, 41]. Therefore, additional substitutions targeting the 174 position, as well as the amino acids immediately surrounding this position, should be investigated in more detail for their potential to modulate the sensitivity to the direct FXa inhibitors.

Differential inhibition of FXa in non-human plasmas

The discovery of inhibitor insensitive FXa variants had prompted us to categorically evaluate global clotting parameters in non-human plasma in order to facilitate the use and interpretation of animal models for the preclinical assessment of FX(a)-based bypassing agents. As outlined in **chapter 6** of this thesis, we assayed mouse, rat, rabbit, porcine, goat, and human pooled plasma using relevant coagulation assays such as the prothrombin time (PT), activated partial thromboplastin time (APTT), and calibrated automated thrombography (CAT). In short, we established that rabbit, rat, and mouse plasmas exhibited robust clotting pathways that differ distinctly from human, goat and porcine plasma when evaluated in clinical coagulation assays. In addition, we discovered fundamentally higher rates of FXa inhibition in rabbit, rat and mouse plasma, pointing to an overall higher anticoagulant threshold in these plasmas relative to human, goat, and porcine plasma. Overall, rat plasma was established as relevant small animal model for the preclinical assessment of human FX(a) variants. Apart from general implications on the selection preclinical models, it is thought-provoking to point out that higher FXa-inhibitory rates were observed in smaller mammals and vice versa, suggesting a potential link between species physiology, heart rate, and anticoagulation. On

another note, an association between physiology and coagulation has been found in human subjects also. For example, several studies have reported an increased thrombin generation potential in humans with a higher body mass index (BMI) [52-54]. On the other hand, a higher BMI may also be linked to induced coagulation through inflammatory pathways [55, 56]. In general, we advocate studying non-human coagulation systems in order to generate novel insights into the relationship between physiology and coagulation. With respect to the regulation of FXa, efforts should be made to assess the levels of FXa inhibitors such as TFPI, AT, protein Z-dependent protease inhibitor (ZPI), and alpha2-macroglobulin (a2M) in plasmas from larger and smaller mammals. Insights obtained from these types of studies are especially important, as the hemostatic system not only protects against thrombosis and bleeding, but is also intricately linked to systemic processes such as angiogenesis [57], inflammation [58], and innate immunity [59].

Conclusions

In this thesis, we have studied the functional and structural properties of the powerful prothrombin activator complex (ptFV-FX) from the venom of the Australian snake *P. textilis*. With respect to the non-catalytic subunit of this complex, we have found that 1) the absence of a regulatory B-domain in ptFV is most likely the result of a previously unidentified alternative splicing event. In addition, we have uncovered that 2) the unique disulfide bond in ptFV is not required for lipid-independent cofactor function. Furthermore, we have 3) established the presence of functional crosstalk between the A-domains and C-domains of FV by characterizing chimeras of human and ptFV. Therefore, by studying the venom-derived FV molecule we were able to shed new light on structural and functional relationships that govern FV function and prothrombinase complex assembly. With respect to the venom catalytic subunit ptFXa we have shown that 4) the elongated 99-loop mediates resistance to plasma-based FXa inhibitors and synthetic FXa inhibitors and that 5) introduction of this loop into human FXa enables protease function in plasma spiked with supra-physiological concentrations of direct oral FXa-inhibitors. As such, the ptFXa molecule proved to be an exceptional blueprint for the rational design of a unique gain-of-function adaptation to human FXa. In conclusion, our studies highlight the significance of studying the structural and functional aspects of venom-derived proteins for prospective protein engineering strategies.

References

1. Mann, K.G., et al., *Surface-dependent reactions of the vitamin K-dependent enzyme complexes.* Blood, 1990. **76**(1): p. 1-16.
2. Rao, V.S. and R.M. Kini, *Pseutarin C, a prothrombin activator from Pseudonaja textilis venom: its structural and functional similarity to mammalian coagulation factor Xa-Va complex.* Thromb Haemost, 2002. **88**(4): p. 611-9.
3. Masci, P.P., A.N. Whitaker, and J. de Jersey, *Purification and characterization of a prothrombin activator from the venom of the Australian brown snake, Pseudonaja textilis textilis.* Biochem Int, 1988. **17**(5): p. 825-35.
4. Rao, V.S., S. Swarup, and R. Manjunatha Kini, *The catalytic subunit of pseutarin C, a group C prothrombin activator from the venom of Pseudonaja textilis, is structurally similar to mammalian blood coagulation factor Xa.* Thromb Haemost, 2004. **92**(3): p. 509-21.
5. Rao, V.S., S. Swarup, and R.M. Kini, *The nonenzymatic subunit of pseutarin C, a prothrombin activator from eastern brown snake (Pseudonaja textilis) venom, shows structural similarity to mammalian coagulation factor V.* Blood, 2003. **102**(4): p. 1347-54.
6. Bos, M.H. and R.M. Camire, *Procoagulant adaptation of a blood coagulation prothrombinase-like enzyme complex in australian elapid venom.* Toxins (Basel), 2010. **2**(6): p. 1554-67.
7. Bos, M.H., et al., *Venom factor V from the common brown snake escapes hemostatic regulation through procoagulant adaptations.* Blood, 2009. **114**(3): p. 686-92.
8. Johnson DJ, H.J., *Pseudonaja textilis venom FXa is poorly inhibited by human antithrombin.* Abstracts of the XXIV congress of the International Society on Thrombosis and Haemostasis, 2013: p. PB 4.58-2.
9. Toso, R. and R.M. Camire, *Removal of B-domain sequences from factor V rather than specific proteolysis underlies the mechanism by which cofactor function is realized.* J Biol Chem, 2004. **279**(20): p. 21643-50.
10. Suzuki, K., B. Dahlback, and J. Stenflo, *Thrombin-catalyzed activation of human coagulation factor V.* J Biol Chem, 1982. **257**(11): p. 6556-64.
11. Minh Le, T.N., et al., *Gene duplication of coagulation factor V and origin of venom prothrombin activator in Pseudonaja textilis snake.* Thromb Haemost, 2005. **93**(3): p. 420-9.
12. Vonk, F.J., et al., *The king cobra genome reveals dynamic gene evolution and adaptation in the snake venom system.* Proc Natl Acad Sci U S A, 2013. **110**(51): p. 20651-6.
13. Goren, A., et al., *Comparative analysis identifies exonic splicing regulatory sequences--The complex definition of enhancers and silencers.* Mol Cell, 2006. **22**(6): p. 769-81.
14. Lev-Maor, G., et al., *The "alternative" choice of constitutive exons throughout evolution.* PLoS Genet, 2007. **3**(11): p. e203.
15. Vincent, L.M., et al., *Coagulation factor V(A2440G) causes east Texas bleeding disorder via TFPIalpha.* J Clin Invest, 2013. **123**(9): p. 3777-87.

16. Cunha, M.L., et al., *A novel mutation in the F5 gene (factor V Amsterdam) associated with bleeding independent of factor V procoagulant function.* Blood, 2015. **125**(11): p. 1822-5.
17. Wood, J.P., et al., *Tissue factor pathway inhibitor-alpha inhibits prothrombinase during the initiation of blood coagulation.* Proc Natl Acad Sci U S A, 2013. **110**(44): p. 17838-43.
18. Dahlback, B., *Novel insights into the regulation of coagulation by factor V isoforms, tissue factor pathway inhibitoralpha, and protein S.* J Thromb Haemost, 2017. **15**(7): p. 1241-1250.
19. Bos, M.H. and R.M. Camire, *A bipartite autoinhibitory region within the B-domain suppresses function in factor V.* J Biol Chem, 2012. **287**(31): p. 26342-51.
20. Thomassen, M.C.L.G.D., et al., *Tissue factor-independent inhibition of thrombin generation by tissue factor pathway inhibitor-alpha.* Journal of Thrombosis and Haemostasis, 2015. **13**(1): p. 92-100.
21. Lechtenberg, B.C., et al., *Crystal structure of the prothrombinase complex from the venom of Pseudonaja textilis.* Blood, 2013. **122**(16): p. 2777-83.
22. Verhoef D., Y.X., Parthasarathy S., Reitsma P.H., Camire R.M., Bos M.H.A, *Functional implications of the unique disulfide bond in venom factor V from the Australian common brown snake Pseudonaja textilis.* Toxin Reviews, 2013. **33**(1-2): p. 37-41.
23. Kumar, S., Stayrook S., Huntington, J.A., Camire, R.M., Krishnaswamy, S., *New Structural Insights into High Affinity Membrane Binding By Coagulation Factor V/Va* Blood, 2014. **124**(21): p. 4216.
24. Pellequer, J.L., et al., *Three-dimensional model of coagulation factor Va bound to activated protein C.* Thromb Haemost, 2000. **84**(5): p. 849-57.
25. Adams, T.E., et al., *The crystal structure of activated protein C-inactivated bovine factor Va: Implications for cofactor function.* Proc Natl Acad Sci U S A, 2004. **101**(24): p. 8918-23.
26. Chaves, R.C., et al., *Factor Va alternative conformation reconstruction using atomic force microscopy.* Thromb Haemost, 2014. **112**(6): p. 1167-73.
27. Kumar S., S.S., Huntington JA., et al., *High resolution X-ray structure of snake venom factor V: evolution of a hemostatic cofactor to a toxin poised to inflict maximal damage to mammalian blood coagulation.* Blood (ASH 2011 Meeting Abstracts) 118:375., 2011.
28. Macedo-Ribeiro, S., et al., *Crystal structures of the membrane-binding C2 domain of human coagulation factor V.* Nature, 1999. **402**(6760): p. 434-9.
29. Nicolaes, G.A., B.O. Villoutreix, and B. Dahlback, *Mutations in a potential phospholipid binding loop in the C2 domain of factor V affecting the assembly of the prothrombinase complex.* Blood Coagul Fibrinolysis, 2000. **11**(1): p. 89-100.
30. Saleh, M., et al., *The factor V C1 domain is involved in membrane binding: identification of functionally important amino acid residues within the C1 domain of factor V using alanine scanning mutagenesis.* Thromb Haemost, 2004. **91**(1): p. 16-27.
31. Peng, W., M.A. Quinn-Allen, and W.H. Kane, *Mutation of hydrophobic residues in the factor Va C1 and C2 domains blocks membrane-dependent prothrombin activation.* J Thromb Haemost, 2005. **3**(2): p. 351-4.

32. Majumder, R., et al., *A phosphatidylserine binding site in factor Va C1 domain regulates both assembly and activity of the prothrombinase complex.* Blood, 2008. **112**(7): p. 2795-802.
33. Verhoef D., C.R.M., Reitsma P.H., Bos M.H.A., *Functional characterization of a structural element unique to venom factor V from the Australian common brown snake Pseudonaja textilis.* J Thromb Haemost (ISTH 2013 Meeting Abstracts) 11(S2):AS 36.3., 2013.
34. *Molecular Operating Environment (MOE), Montreal, Quebec, Canada: Chemical Computing Group Inc.*
35. Marques, J.R., et al., *Amino acid patterns around disulfide bonds.* Int J Mol Sci, 2010. **11**(11): p. 4673-86.
36. Dombkowski, A.A., K.Z. Sultana, and D.B. Craig, *Protein disulfide engineering.* FEBS Lett, 2014. **588**(2): p. 206-12.
37. Pinto, D.J., et al., *Discovery of 1-(4-methoxyphenyl)-7-oxo-6-(4-(2-oxopiperidin-1-yl) phenyl)-4,5,6,7-tetrahydro-1H -pyrazolo[3,4-c]pyridine-3-carboxamide (apixaban, BMS-562247), a highly potent, selective, efficacious, and orally bioavailable inhibitor of blood coagulation factor Xa.* J Med Chem, 2007. **50**(22): p. 5339-56.
38. Frost, C., et al., *Safety, pharmacokinetics and pharmacodynamics of multiple oral doses of apixaban, a factor Xa inhibitor, in healthy subjects.* Br J Clin Pharmacol, 2013. **76**(5): p. 776-86.
39. Haginoya, N., et al., *Synthesis and conformational analysis of a non-amidine factor Xa inhibitor that incorporates 5-methyl-4,5,6,7-tetrahydrothiazolo[5,4-c]pyridine as S4 binding element.* J Med Chem, 2004. **47**(21): p. 5167-82.
40. Koretsune, Y., et al., *Short-Term Safety and Plasma Concentrations of Edoxaban in Japanese Patients With Non-Valvular Atrial Fibrillation and Severe Renal Impairment.* Circ J, 2015. **79**(7): p. 1486-95.
41. Roehrig, S., et al., *Discovery of the novel antithrombotic agent 5-chloro-N-({(5S)-2-oxo-3-[4-(3-oxomorpholin-4-yl)phenyl]-1,3-oxazolidin-5-yl}methyl)thiophene- 2-carboxamide (BAY 59-7939): an oral, direct factor Xa inhibitor.* J Med Chem, 2005. **48**(19): p. 5900-8.
42. Favresse, J., et al., *Andexanet alfa for the reversal of factor Xa inhibitors.* Expert Opin Biol Ther, 2019. **19**(5): p. 387-397.
43. Lu, G., et al., *A specific antidote for reversal of anticoagulation by direct and indirect inhibitors of coagulation factor Xa.* Nat Med, 2013. **19**(4): p. 446-51.
44. Ansell, J.E., et al., *Single-dose ciraparantag safely and completely reverses anticoagulant effects of edoxaban.* Thromb Haemost, 2016.
45. Thalji, N.K., et al., *A rapid pro-hemostatic approach to overcome direct oral anticoagulants.* Nat Med, 2016. **22**(8): p. 924-32.
46. Verhoef D., R.P.H., Bos M.H.A., *Prohemostatic proteins for the treatment of bleeding.* Patent application number: P104178EP00, 2015.
47. Verhoef D., R.P.H., Bos M.H.A., *Recombinant serine proteases.* Patent application number: P109970, 2016.

48. Skala, W., et al., *Structure-function analyses of human kallikrein-related peptidase 2 establish the 99-loop as master regulator of activity.* J Biol Chem, 2014. **289**(49): p. 34267-83.
49. Abdel-Azeim, S., et al., *Molecular dynamics characterization of five pathogenic Factor X mutants associated with decreased catalytic activity.* Biochemistry, 2014. **53**(44): p. 6992-7001.
50. Qu, S.Y., et al., *An Unexpected Dynamic Binding Mode between Coagulation Factor X and Rivaroxaban Reveals Importance of Flexibility in Drug Binding.* Chem Biol Drug Des, 2019. 94(3): p. 1664-1671.
51. Schreuder, M., Jourdi, G., Visscher, K.M., Cheung K., Poenou, G., Verhoef, D., Thomassen, S., Hackeng, T., Stepanian, A., Gaussem, P., Reitsma, P.H., Geerke, D.P., Siguret, V. and Bos, M.H.A., *F174-Substituted Human Factor X as Bypassing Agent for the Direct Factor Xa Inhibitors.* Manuscript in preparation.
52. Ay, L., et al., *Thrombin generation in morbid obesity: significant reduction after weight loss.* J Thromb Haemost, 2010. **8**(4): p. 759-65.
53. Beijers, H.J., et al., *Body composition as determinant of thrombin generation in plasma: the Hoorn study.* Arterioscler Thromb Vasc Biol, 2010. **30**(12): p. 2639-47.
54. Campello, E., et al., *Hypercoagulability in overweight and obese subjects who are asymptomatic for thrombotic events.* Thromb Haemost, 2015. **113**(1): p. 85-96.
55. Cleuren, A.C., et al., *Changes in Dietary Fat Content Rapidly Alters the Mouse Plasma Coagulation Profile without Affecting Relative Transcript Levels of Coagulation Factors.* PLoS One, 2015. **10**(7): p. e0131859.
56. de Mutsert, R., et al., *The Netherlands Epidemiology of Obesity (NEO) study: study design and data collection.* Eur J Epidemiol, 2013. **28**(6): p. 513-23.
57. Browder, T., J. Folkman, and S. Pirie-Shepherd, *The hemostatic system as a regulator of angiogenesis.* Journal of Biological Chemistry, 2000. **275**(3): p. 1521-1524.
58. Esmon, C.T., *Crosstalk between inflammation and thrombosis.* Maturitas, 2004. **47**(4): p. 305-314.
59. Delvaeye, M. and E.M. Conway, *Coagulation and innate immune responses: can we view them separately?* Blood, 2009. **114**(12): p. 2367-2374.


7

Chapter 8

English summary
Nederlandse samenvatting

English summary

Coagulation of the blood, or simply blood clotting, is a vital process in which blood congeals to form a protective barrier to prevent the loss of blood. Formation of a blood clot is usually triggered upon damage to endothelial cells that line the wall of a blood vessel. Exposure of subendothelial collagen prompts the activation of blood platelets which aggregate into a plug that blocks off the damaged vessel wall. The damaged endothelium and activated platelets also recruit blood clotting factors to the site of injury. These clotting factors reinforce the platelet plug by promoting the formation of a protective mesh of fibrin polymers in and around the primary platelet plug. These polymers are produced by the blood clotting enzyme thrombin by cleaving fibrinogen into fibrin strands that can self-associate to form an intricate network of fibrin polymers. Controlling the enzymatic action of thrombin is key to maintaining hemostasis. For example, if the activity of thrombin is not correctly contained to the site of injury it could lead to indiscriminate fibrin formation and ultimately to a pathological and life-threatening condition known as thrombosis. On the other hand, insufficient thrombin activity could result in poor fibrin deposition and clot instability, ultimately leading to recurrent bleeding and debilitating physiological complications.

Thrombin is maintained in the blood in a quiescent pro-enzyme or zymogen form known as prothrombin. The conversion of prothrombin into thrombin is governed by an enzymatic complex known as prothrombinase. This complex is formed by two essential clotting factors: activated factor V (five) and activated factor X (ten); FVa and FXa in short. Both clotting factors are also maintained in a quiescent form and are activated upon vascular damage. After activation, FVa and FXa are only able to form a complex on surfaces of activated platelets and damaged endothelial cells, thereby limiting the activation of thrombin to the site of injury. In addition, several anticoagulant proteins circulate in the blood that can limit the action of thrombin, FVa and FXa, thereby controlling blood coagulation. Interestingly, the venom of the Australian common brown snake *Pseudonaja textilis* is known to contain a powerful prothrombinase-like enzyme complex that can convert prothrombin in the absence of activated platelets or damaged endothelium. This enzyme complex consists of 'weaponized' FVa and FXa homologs, which are evolutionarily adapted to derail the hemostatic system of its prey, leading to runaway coagulation. In this thesis, I have studied the structural and functional properties of the *P. textilis* venom FXa-FVa complex with the intention to harness its potent procoagulant potential for medical use.

The first part of this thesis is centered around the relationship between molecular modifications unique to the *P. textilis* venom FV molecule (ptFV) and their implications to FVa function. Under normal circumstances, FVa is stored in the

blood as an inactive molecule (referred to as FV) until coagulation is initiated. In humans, this inactive FV form consists of six subunits, three so-called A-domains, a large B-domain that regulates activity and two C-domains. Activation of FV requires removal of the B-domain segment through the enzymatic action of either thrombin or FXa. Previous studies into the ptFV molecule have shown that the regulatory B-domain segment is absent in the cDNA sequence of ptFV, leading to the expression of a consistently active FVa molecule. In **chapter 2** it was investigated whether this genetic feature is unique to the cDNA sequence of venom ptFV, or whether it is a general hallmark of FV in snakes. To investigate this, cDNA was isolated from the liver of 13 different snake species and analyzed using DNA sequencing. Two separate FV cDNA transcripts were discovered in each of the 13 snake species that were studied: a transcript with a full-length B domain sequence and a considerably shorter second transcript lacking the B domain sequence. In addition, a conserved pre-RNA splicing site was identified in the full-length B-domain sequence among most of the studied snake species. This discovery suggests that the B-domain segment may be removed during processing of the snake FV mRNA in the liver via alternative splicing. Thus, although the B domain has been preserved as a potential regulator of FV activity in snakes, current findings also indicate that in some snake species the function of the FV molecule may be altered by alternative splicing of the B-domain.

In **chapter 3** the function of the venom ptFV protein was studied at the molecular level by constructing new variants of ptFV and testing these for their ability to support prothrombin conversion. As mentioned, the *P. textilis* venom FXa-FVa complex can convert prothrombin in the absence of a procoagulant cellular lipid surface such as activated platelets. This ability is referred to as lipid-independent FVa function and it specifically allows the venom molecule to initiate blood coagulation throughout the body. It was investigated whether lipid-independent ptFV function stemmed from the presence of a unique covalent link between the A2- and A3-domains in ptFV. Such a covalent link could potentially stabilize the molecule and thereby facilitate FVa function in the absence of a lipid surface. Interestingly, the ptFV molecule that is expressed in the liver of the snake does not include this covalent link. However, functional analysis revealed that both the venom- and liver-derived ptFV molecules were able to support prothrombin conversion in the absence of lipids, irrespective of the presence or absence of the covalent link between the A2- and A3-domains in both ptFV species. Furthermore, a previous study had shown that the ptFV is functionally resistant to degradation by activated protein C (APC), which is an essential anticoagulant enzyme. In the current study it was also established that the covalent link was not essential to ptFV function after degradation by the anticoagulant enzyme APC.

In **chapter 4**, additional functional aspects of the venom ptFV molecule were examined by engineering hybrid variants (chimeras) of ptFV and human FV. To this end, two FV chimeras were created in which the A-domains of human FV were linked to the C-domains of ptFV, or vice versa. Functional analysis of these chimeras showed that the ptFV C-domains were of little relevance to its lipid-independent FVa function, as the chimera comprising the ptFV A-domains and human C-domains was also able to support prothrombin conversion in the absence of a lipid surface. In contrast, the chimera that comprised the human A-domains and ptFV C-domains was not able to support prothrombin conversion under similar conditions. Chapter 4 also investigated the relationship between the stability of the FV molecule and its ability to bind to lipid surfaces. It was established that the C-domain exchange adversely affected protein stability in ptFV, yet enhanced stability in human FV. Moreover, we found that lipid binding by the ptFV C-domains was enhanced when these were linked to the A-domains of human FV. On the other hand, lipid binding was reduced when the human C-domains were linked to the A-domains of ptFV. These findings indicate that the ability of the C-domains to bind lipids is coupled to the molecular stability of the entire FV molecule.

In the second part of this thesis, the structural and functional properties of the FXa molecule from snake venom (ptFXa) were studied. In **chapter 5** new findings are presented which show that the ptFXa enzyme is insensitive to inhibition of its catalytic activity by small molecular inhibitors of FXa, such as apixaban, rivaroxaban, and edoxaban. These synthetic FXa inhibitors are often prescribed as anticoagulant drugs to prevent or treat thrombosis. However, these drugs may also cause severe bleeding as serious side effect. Previous research has shown that the molecular structure of ptFXa differs from human FXa in several ways. Most importantly, the polypeptide chain constituting the “99-loop” is significantly longer in the serine protease domain of ptFXa compared to the homologous region in human FXa. The 99-loop is part of the so-called “catalytic site” of the enzyme and is important for the recognition of other molecules involved in blood clotting. In chapter 5, three hybrid variants of human FXa were generated in which the original 99-loop was replaced with the 99-loop from three different snake venom FXa species. These hybrid FXa variants were all found to be significantly less sensitive to inhibition by the synthetic FXa inhibitors, but otherwise functioned almost similarly to human FXa. In theory, these hybrid variants would thus make it possible to restore blood coagulation in patients using synthetic FXa inhibitors as anticoagulant drugs. One of these three hybrid FX molecules, FX-C, now known as VMX-C001, is currently in preclinical development as a drug against FXa inhibitors for patients who need restoration of blood coagulation, for example in event of an internal bleeding or before immediate surgery.

In **chapter 6** some of the preclinical research is described that was conducted for the development of VMX-C001. To identify a suitable animal model for the preclinical development of our new FX molecule, several animal plasmas have been tested using routine and special coagulation assays. It was discovered that inhibition of activated human FX was enhanced in the plasma of rabbits, rats, and especially mice. These plasmas are therefore less suitable for research with human FX. However, these new findings also highlight that there are species-specific differences that may inadvertently influence the interpretation of coagulation tests. Nevertheless, small animals are usually selected for at least part of the preclinical research. In general, rats may serve as a relevant animal model for the preclinical evaluation of VMX-C001 due to the sensitivity of its plasma in most coagulation assay.

Nederlandse samenvatting

Bloedstolling is een essentieel proces waarbij het bloed stolt om een beschermende barrière te vormen ter vookoming van bloedverlies. De vorming van een bloedstolsel wordt normaal gesproken in gang gezet na schade aan de endotheelcellen van een bloedvat. Dit leidt vervolgens tot activering van bloedplaatjes welke ter plekke een bloedprop vormen waarmee de beschadigde vaatwand wordt afgedicht. Deze initieële prop is echter vrij zwak en moet verstevigd worden om goed op zijn plek te kunnen blijven. Het verstevigen van de bloedprop gebeurt met behulp van een aantal gespecialiseerde eiwitten uit het bloed. Deze eiwitten, ook wel stollingsfactoren genoemd, worden vanuit het bloed aangetrokken tot de beschadigde celmembranen van endotheelcellen en bloedplaatjes. Deze stollingsfactoren maken vervolgens in en om de bloedprop heen een verstevigend netwerk van polymeren aan. Deze polymeren worden geproduceerd door het bloedstollingsenzym trombine welke het stollingseiwit fibrinogeen omzet in fibrinepolymeren. De enzymatische werking van trombine moet echter uiterst nauwkeurig worden gecontroleerd om te voorkomen dat er geen fibrinepolymeren elders in het bloed kunnen ontstaan. Wanneer dit niet het geval is kan dit bijvoorbeeld leiden tot een pathologische en levensbedreigende aandoening genaamd trombose. Onvoldoende trombine-activiteit kan daarentegen resulteren in een verminderde afzetting van fibrine waardoor er een instabiel bloedstolsel ontstaat. Dit kan uiteindelijk leiden tot herhaaldelijk bloeden waardoor er gevaarlijke complicaties kunnen optreden.

Trombine wordt normaal gesproken in een inactieve pro-enzym vorm in het bloed gehandhaafd, deze vorm noemt men protrombine. De omzetting van protrombine in trombine wordt verricht door een enzymatisch complex genaamd protrombinase. Dit complex bestaat uit twee essentiële stollingsfactoren: geactiveerd factor V (vijf) en geactiveerd factor X (tien); FVa en FXa in het kort. Beide stollingsfactoren worden normaal gesproken alleen geactiveerd na schade aan de vaatwand. Normaal gesproken kunnen FVa en FXa uitsluitend een complex vormen op celmembranen, bijvoorbeeld op geactiveerde bloedplaatjes en beschadigd endotheel van de vaatwand. Zodanig vindt de omzetting van protrombine in trombine alleen plaats op plekken waar er sprake is van vaatschade. Ter voorkoming van trombose circuleren er bovendien verschillende antistollingseiwitten in het bloed welke de werking van trombine, FVa en FXa kunnen beperken. In deze context is het gif van de Australische gifslang *Pseudonaja textilis,* de 'common brown snake', zeer interessant. Het gif van deze slang bevat namelijk een krachtig enzymcomplex dat veel lijkt op het menselijke protrombinase, met als uitzondering dat het protrombine kan omzetten in afwezigheid van een beschadigd celmembraan. Het prothrombinase uit slangengif bestaat uit homologe FVa en FXa stollingseiwitten welke zeer efficiënt het bloedstollingsysteem van prooidieren kunnen ontregelen.

De FVa en FXa homologen uit slangengif zijn bovendien ongevoelig voor de beperkende werking van antistollingseiwitten. Een slangenbeet leidt zodanig tot een overactief stollingssysteem en het ontstaan van mirco-stolsels welke zeer grote schade aan weefsels en organen toebrengen. In dit proefschrift heb ik de moleculaire structuur en functionele eigenschappen van het *P. textilis* slangengif FXa-FVa-complex bestudeerd met als doel om het krachtige stollingspotentiaal hiervan te kunnen benutten voor toekomstig medisch gebruik.

In het eerste deel van dit proefschrift is de relatie onderzocht tussen verschillende moleculaire modificaties die uniek zijn voor het *P. textilis* gif FV molecuul (ptFV) en de uitzonderlijke functionele eigenschappen van dit molecuul. Onder normale omstandigheden wordt FVa in het bloed als niet-actief molecuul bewaard (aangeduid als FV) totdat er activatie van de stolling optreedt. Het niet-actieve FV molecuul bestaat uit zes subeenheden, drie zogenaamde A-domeinen, een groot B-domein welke de activiteit van het eiwit reguleert, en twee C-domeinen. Activering van FV vindt plaats nadat het B-domeinsegment is verwijderd door de enzymatische werking van trombine of FXa. Eerdere studies hebben aangetoond dat het B-domein vrijwel volledig afwezig is in de genetische code van ptFV, waardoor het molecuul in principe direct actief zou moeten zijn nadat het aangemaakt is. In **hoofdstuk 2** werd onderzocht of deze genetische eigenschap uniek is voor ptFV, of dat het een algemeen kenmerk is voor FV moleculen in slangen. Om dit te onderzoeken werd er cDNA uit de lever van 13 verschillende slangensoorten geïsoleerd en met behulp van DNA sequencing geanalyseerd. Elke slangensoort bleek twee afzonderlijke cDNA transcripten van FV te hebben: een lang transcript met een volledige B-domein sequentie en een aanzienlijk korter transcript zonder B-domein sequentie. Bij vrijwel alle slangensoorten werd in het lange transcript tevens een zogenaamde 'pre-RNA-splice site' teruggevonden. Deze ontdekking doet vermoeden dat de functie van het ptFV molecuul aangepast kan worden door het B-domein segment uit het RNA te verwijderen nog voordat het molecuul wordt aangemaakt. De belangrijkste vinding is echter dat het B-domein segment in het algemeen deel uitmaakt van slangen FV en mogelijk dus nog steeds functioneert als een potentiële regulator van FV activiteit.

In **hoofdstuk 3** zijn de functionele aspecten van het ptFV molecuul op moleculair niveau onderzocht door nieuwe varianten van dit eiwit te maken, en deze vervolgens te testen op hun vermogen om protrombine omzetting te ondersteunen. Zoals eerder vermeld kan het *P. textilis* gif FXa-FVa-complex protrombine omzetten in afwezigheid van een procoagulant celmembraan zoals dat van geactiveerde bloedplaatjes. Deze eigenschap wordt lipidenonafhankelijke FVa-functie genoemd. Deze specifieke functie stelt het gifmolecuul in staat om door het hele lichaam de bloedstolling te activeren. In hoofdstuk 3 is onderzocht of de lipidenonafhankelijke functie van ptFV is voortgekomen uit de aanwezigheid van een unieke covalente

verbinding tussen het A2- en A3-domein van ptFV. Een dergelijke covalente link zou mogelijk het gifmolecuul kunnen stabiliseren waardoor het beter in staat is om zijn functie uit te oefenen in afwezigheid van een lipidenoppervlak. Interesant genoeg ontbreek deze covalente verbinding in de ptFV variant die in de lever van de slang wordt aangemaakt. Echter, zowel de gif- en lever-ptFV bleken beiden in staat om lipidenonafhankelijke protrombineconversie te ondersteunen. Dit toont aan dat de covalente verbinding tussen het A2- en A3-domein geen rol speelt in de lipidenonafhankelijke functie van het ptFV gifmolecuul. In een eerdere studie werd daarnaast aangetoond dat de functie van het ptFV molecuul niet verstoord kon worden door geactiveerd proteïne C (APC), een belangrijk anti-stollings enzym dat FVa af kan breken. In hoofstuk 3 is tevens vastgesteld dat de covalente verbinding tussen het A2- en A3 domein ook niet betrokken is bij het behoud FVa functie na afbraak door APC.

In **hoofdstuk 4** zijn aanvullende functionele aspecten van het ptFV molecuul onderzocht door hybride varianten (chimera's) van ptFV en humaan FV te ontwerpen en te testen. Hiertoe zijn er twee chimera's van FV gemaakt waarbij de A-domeinen van menselijk FV werden gekoppeld aan de C-domeinen van het ptFV, of vice versa. Functionele analyse van deze chimeren toonde aan dat de ptFV C-domeinen niet relevant waren voor de lipidenonafhankelijke FVa-functie. Namelijk, de chimeer die de A-domeinen van ptFV omvatte in combinatie met de C-domeinen van humaan FV was goed in staat om protrombine omzetting te ondersteunen in afwezigheid van lipiden. De chimeer die de humane A-domeinen en de ptFV C-domeinen omvatte was daarentegen niet in staat om protrombine omzetting onder vergelijkbare omstandigheden te ondersteunen. In hoofdstuk 4 was ook de relatie tussen de stabiliteit van het FV molecuul en het vermogen om aan lipidenoppervlakken te binden onderzocht. De chimeer bestaande uit de humane A-domeinen en ptFV C-domeinen bleek een verbeterde stabiliteit te hebben, terwijl de chimeer bestaande uit de ptFV A-domeinen en humane C-domeinen een verslechterde stabiliteit had. Het vermogen om aan het lipidenoppervlak te binden was daarentegen juist verbeterd in deze chimeer. Tegelijkertijd bleek het vermogen om aan het lipidenoppervlak te binden afgenomen in de chimeer bestaande uit de A-domeinen van ptFV en C-domeinen van humaan FV. Deze bevindingen tonen aan dat het vermogen van de C-domeinen om het lipidenoppervlak te binden is gekoppeld aan de stabiliteit van het gehele FV molecuul.

In het tweede deel van dit proefschrift zijn de structurele en functionele eigenschappen van het FX molecuul uit slangengif nader onderzocht. In **hoofdstuk 5** werd aangetoond dat het ptFXa slangengif enzym ongevoelig is voor inhibitie van zijn katalytische activiteit door kleine moleculaire remmers van FXa, zoals apixaban, rivaroxaban en edoxaban. Deze synthetische FXa remmers worden vaak voorgeschreven als antistollingsmiddelen om trombose te voorkomen,

maar kunnen als bijwerking ook ernstige bloedingen veroorzaken. Uit eerder onderzoek is gebleken dat de moleculaire structuur van ptFXa op een belangrijk punt afwijkt van humaan FXa. Namelijk, in het serine protease domein van ptFXa is de polypeptide keten van de '99-loop' aanmerkelijk langer dan die van humaan FXa. Deze 99-loop maakt onderdeel uit van de zogenaamde 'katalytische site' van het enzym en is belangrijk voor de herkenning van andere moleculen die betrokken zijn bij de bloedstollling. In hoofdstuk 5 werden drie hybride varianten van het humane FXa gekarakteriseerd waarin de originele 99-loop was vervangen door de 99-loop uit drie verschillende slangengif FXa's. Deze hybride FXa varianten bleken allen aanzienlijk minder gevoelig te zijn voor inhibitie door synthetische FXa remmers, maar functioneerden verder nagenoeg gelijk aan humaan FXa. In theorie zouden deze hybride varianten het dus mogelijk maken om de bloedstolling te herstellen bij patiënten welke synthetische FXa remmers als antistollingsmiddelen gebruiken. Een van deze drie hybride FX moleculen, genaamd VMX-C001, is momenteel in preklinische ontwikkeling als medicijn tegen FXa remmers voor patiënten die herstel van de bloedstolling nodig hebben, bijvoorbeeld bij een inwendige bloeding of wanneer er onmiddellijk geopereerd moet worden.

In **hoofdstuk 6** is een deel van het preklinische onderzoek beschreven dat werd uitgevoerd ten behoeve van de ontwikkeling van VMX-C001. Om een geschikt diermodel te identificeren voor de preklinische ontwikkeling van VMX-C001 zijn er met behulp van routinematige en speciale stollingstesten verschillende dierenplasma's getest. Hierbij werd ontdekt dat geactiveerd humaan FX versneld wordt geremd in het plasma van konijnen, ratten en in het bijzonder muizen. Dit maakt deze plasma's minder geschikt voor onderzoek met humaan FX. Deze nieuwe bevindingen benadrukken echter ook dat er soortspecifieke verschillen zijn welke de interpretatie van stollinsgproeven kunnen beïnvloeden. Kleine dieren worden vaak gebruikt als experimenteel model in preklinisch onderzoek. Omdat het plasma van ratten gevoelig genoeg was voor veelgebruikte stollingsproeven kunnen deze dieren evenwel goed dienst doen als een relevant diermodel voor de preklinische evaluatie van VMX-C001.

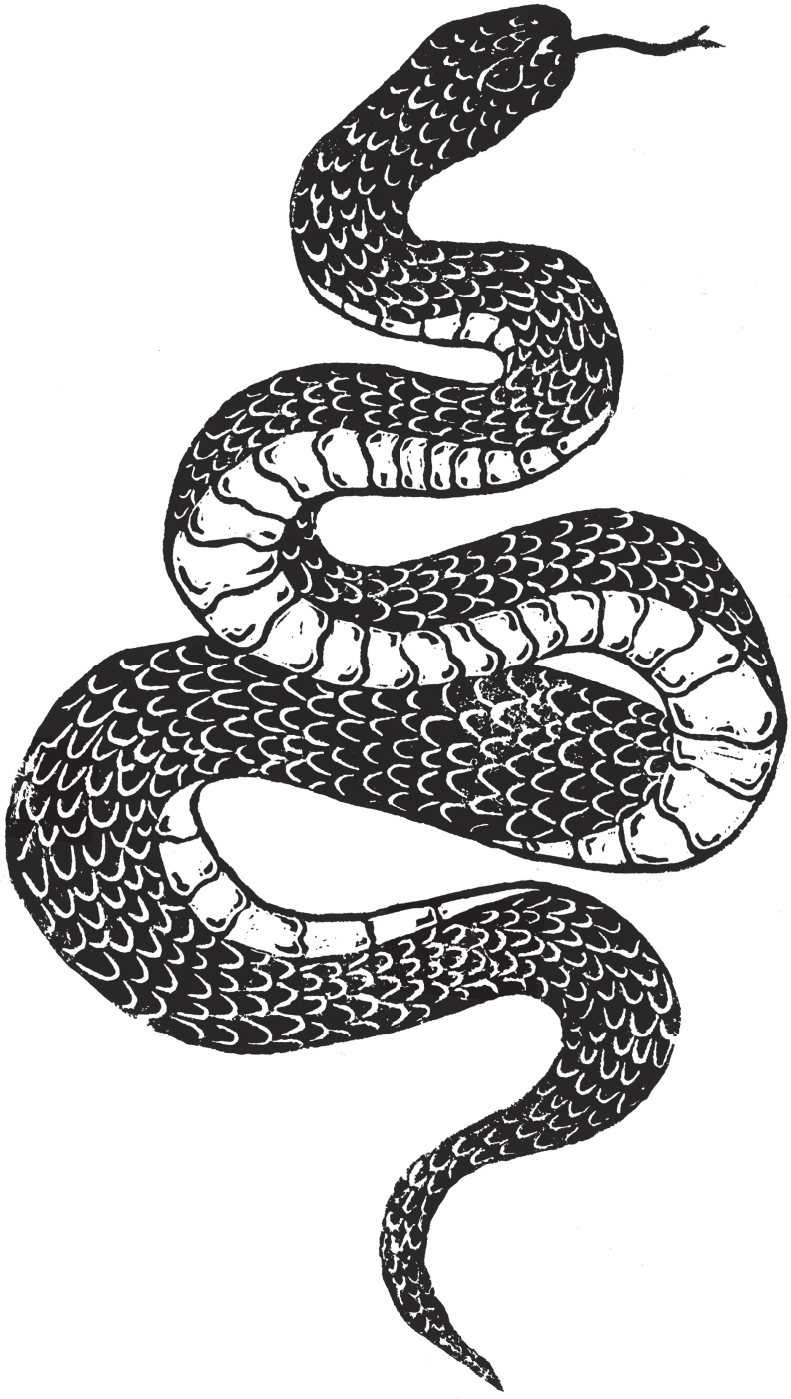

Appendices

Curriculum Vitae

Dankwoord

List of publications

Curriculum Vitae (English)

Daniël Verhoef was born on the 12th of November 1984 in the municipality of Haarlemmermeer as third child to Peter Verhoef and Quirina Pouw. His preparatory scientific education was followed at the Kaj Munk College in Hoofddorp between 1997 and 2003, with Nature & Health as final examination profile. Academic education commenced in 2003 at the Free University (VU) of Amsterdam where he studied Biomedical Sciences to become Bachelor of Science in 2008. Subsequently, he studied Biomolecular Sciences and Cell Biology to become Master of Science in 2011. Daniël supplemented his academic tuition with various extra-curricular activities such as: chairmanship to the mixed choir of the Free University, student member to the educational committee of the Biomolecular Sciences program and racer in the rowing eight at R.S.V.U. Okeanos. In addition, Daniël regularly tutored students on bachelor courses in biochemistry, microbiology, and life sciences.

Daniël enrolled at the Leiden University Medical Center Graduate School in the fall of 2011 to study the biochemistry of blood coagulation under the supervision of Prof. Dr. Pieter H. Reitsma and Dr. Mettine H.A. Bos at the section of Thrombosis and Hemostasis. During his doctoral training he collaborated with Dr. Daan Geerke on molecular modelling of factor Xa and with Dr. Gerry A.F. Nicolaes on biophysical characterization of factor V(a). His research findings were frequently selected for communication at scientific meetings such as those from the International Society on Thrombosis and Haemostasis (ISTH) and the American Society of Hematology (ASH). Intellectual property was claimed on two separate occasions: in 2014 a patent was submitted on 'Prohemostatic proteins for the treatment of bleeding', and in 2015 another patent was submitted on 'Recombinant serine proteases'. The doctoral research program was concluded in the spring of 2017 after an extension of one and a half years.

After his doctoral studies Daniël moved to the United Kingdom (UK) in 2017 to work on protein biochemistry and gene therapy at Freeline Therapeutics, plc. During his time at Freeline he worked closely together with Prof. Amit Nathwani, M.D. and Dr. Jonathan Foley on a range of genetic disorders amendable to gene therapy. In 2019, Daniël moved back to the Netherlands to continue his work on blood coagulation together with emeritus Prof. Dr. Pieter H. Reitsma at VarmX B.V., and Dr. Mettine H.A. Bos of the Leiden University Medical Center.

Curriculum Vitae (Nederlands)

Daniël Verhoef werd op 12 november 1984 in de gemeente Haarlemmermeer geboren als derde kind van Peter Verhoef en Quirina Pouw. Voorbereidend wetenschappelijk onderwijs werd tussen 1997 en 2003 gevolgd aan het Kaj Munk College te Hoofddorp, met Natuur & Gezondheid als eindexamenprofiel. Daniël begon in 2003 met zijn opleiding Biomedische Wetenschappen aan de Vrije Universiteit (VU) van Amsterdam en studeerde in 2008 af als Bachelor of Science. Vervolgens studeerde hij Biomoleculaire Wetenschappen en Celbiologie aan de VU om in 2011 als Master of Science af te studeren. Daniël vulde zijn academische opleiding aan met diverse extracurriculaire activiteiten zoals: voorzitterschap van het gemengd koor van de VU, studentlidmaatschap van de opleidingscommissie van zijn masteropleiding en als lid van de eerstejaars acht in het roeiteam van RSVU Okeanos. Daarnaast gaf Daniël regelmatig onderwijs aan bachelorstudenten in vakken als biochemie, microbiologie en levenswetenschappen.

In het najaar van 2011 begon Daniël aan zijn opleiding tot wetenschapper bij de Graduate School van het Leids Universitair Medisch Centrum, waar hij onder supervisie van Prof. Dr. Pieter H. Reitsma en Dr. Mettine H.A. Bos onderzoek verrichtte naar de biochemie van bloedstolling aan de afdeling Trombose en Hemostase. Tijdens zijn onderzoek werkte hij nauw samen met Dr. Daan Geerke aan computergestuurde modellering van het stollingseiwit factor Xa. In samenwerking met Dr. Gerry A.F. Nicolaes deed hij onderzoek naar de biofysische eigenschappen van het stollingseiwit factor Va. Daniëls onderzoek werd regelmatig uitgekozen voor mondelinge presentatie op wetenschappelijke bijeenkomsten zoals die van de International Society on Thrombosis and Haemostasis (ISTH) en de American Society of Hematology (ASH). Er zijn twee patenten ingediend op basis van de behaalde onderzoeksresultaten: in 2014 werd een patent ingediend op ‘Prohemostatische eiwitten voor de behandeling van bloedingen’ en in 2015 werd een patent ingediend op ‘Recombinante serine proteasen’. Het promotieonderzoek werd in het voorjaar van 2017 afgesloten nadat het met anderhalf jaar was verlengd.

Na zijn promotieonderzoek verhuisde Daniël in 2017 naar het Verenigd Koninkrijk (VK) om daar te werken aan eiwitbiochemie en gentherapie bij Freeline Therapeutics, plc. Gedurende zijn verblijf in het VK werkte hij nauw samen met Prof. Dr. Amit Nathwani, M.D. en Dr. Jonathan Foley in onderzoek naar genetische aandoeningen die met behulp van gentherapie kunnen worden behandeld. In 2019 verhuisde Daniël naar Nederland terug om samen met emeritus Prof. Dr. Pieter H.Reitsma zijn werk aan bloedstolling voort te zetten bij VarmX B.V., in samenwerking met Dr. Mettine H.A. Bos van het Leids Universitair Medisch Centrum

Dankwoord / Acknowledgements

Dit proefschrift zou nooit tot stand zijn gekomen zonder de hulp van vele collega's, vrienden en familieleden die mij onophoudelijk hebben gesteund met raad, daad en vriendschap.

In het bijzonder wil ik mijn promotor en co-promotor bedanken. Professor Pieter Reitsma, het was een voorrecht om mijn promotie onder jouw toezicht uit te voeren. Ik heb veel van je mogen leren en hoop nog lang met je samen te kunnen werken.

Doctor Mettine Bos, ik ben je zeer dankbaar voor de opleiding die je mij hebt gegeven, met jouw raad en daad heb ik de wetenschappelijke wereld leren navigeren. Ik kijk terug op veel leerzame werkbesprekingen, mooie congressen en waardevolle discussies.

Beste Ka Lei Cheung, sister in Faith, zonder goede analist ben je nergens. Jouw enthousiastme en onvermoeibare inzet hebben menig project doen slagen. Ik kan me mijn tijd bij T&H niet voorstellen zonder jou.

Mijn dank gaat verder ook uit naar alle fantastische promovendi en post-docs waarmee ik mijn promotietijd mocht doorbrengen. Lab-borrel, congres of late-night werk, wat heb ik veel met jullie mogen lachen, drinken, klagen, filosoferen en reizen. Het was een mooie tijd!

Ik wil ook graag alle huidige en oud-analisten van het stol-team, de niertjes en het epi-lab bedanken, jullie hulpvaardigheid was hartverwarmend en de koffie smaakte altijd goed dankzij al die heerlijke koekjes, taartjes en gebakjes.

All my love and kindness to those who I have worked with during my time at Freeline, it was a true pleasure. My sincere thanks to Professor Amit Nathwani and Doctor Jonathan Foley for taking me onboard and extending my horizon.

Promoveren is soms ook een eenzaam bestaan. Gelukkig waren er veel goede vrienden om mij heen die mij keer-op-keer uit de sleur wisten te halen. In het bijzonder wil ik de Hoofddorpers bedanken voor alle mooie feestjes, bierborrels en festivals, en EJZ11 voor de onvergetelijke tripjes en goede gesprekken.

Mijn dank gaat ook uit naar mijn familie. Lieve mama, dank je voor het geloof en vertrouwen dat je in me had. Ik mis je. Lieve Peter en Marieke, ik ben dankbaar dat jullie altijd onvoorwaardelijk voor me klaar staan, veel dank ook voor alle praktische hulp.

Ten slotte wil ik ook mijn lieve vrouw Marjolein bedanken voor de bere goede service tijdens alle ontelbare schrijfsessies. Zonder jouw steun was het proefschrift nooit af gekomen. Ik hou van je!

Publications

Daniël Verhoef, Annabelle V.R. Tjalma, Ka Lei Cheung, Pieter H. Reitsma and Mettine H.A. Bos. *Elevated anti-human factor Xa activity in rabbit and rodent plasma: Implications for preclinical assessment of human factor X in animal models of hemostasis. 2021. Thrombosis Research, 198: p. 154. DOI: https://doi.org/10.1016/j.thromres.2020.11.023*

Daniël Verhoef, Jonathan H. Foley, Andrew Goodale, Emma Macrae, Jenny McIntosh, Romuald Corbau, Keith Gomez, Anne Riddell, Amit C Nathwani. *A Novel Lysine to Arginine Substitution at Position 301 Enhances Activity of Factor IX. 2018. Blood, 132 (Supplement 1): 3772. DOI: https://doi.org/10.1182/blood-2018-99-112832.*

Daniël Verhoef, Koen M. Visscher, C. Ruben Vosmeer, Ka Lei Cheung, Pieter H. Reitsma, Daan P. Geerke and Mettine H.A. Bos. *Engineered Factor Xa Variants Retain Procoagulant Activity Independent of Direct Factor Xa Inhibitors. 2017. Nature Communications, 8(1): p. 528. DOI: 10.1038/s41467-017-00647-9.*

Daniël Verhoef, Mark Schreuder, Ka Lei Cheung, Pieter H. Reitsma and Mettine H.A. Bos. *Engineered Factor Xa Variants Retain Procoagulant Activity Independent of Direct Factor Xa-Inhibitors. 2015 Blood, 126 (23): 126. DOI: https://doi.org/10.1182/blood.V126.23.126.126*

Audrey C.A. Cleuren, Vicky T Blankevoort, Janna A. van Diepen, **Daniël Verhoef**, Peter J. Voshol, Pieter H. Reitsma, Bart J.M. van Vlijmen. *Changes in Dietary Fat Content Rapidly Alters the Mouse Plasma Coagulation Profile without Affecting Relative Transcript Levels of Coagulation Factors. 2015. PLoS ONE 10(7): e0131859. https://doi.org/10.1371/journal.pone.0131859.*

Daniël Verhoef, Xiaoxun Yang, Sudharsan Parthasarathy, Pieter H. Reitsma, Rodney M. Camire, and Mettine H.A. Bos. *Functional Implications of the Unique Disulfide Bond in Venom Factor V from the Australian Common Brown Snake Pseudonaja textilis. 2014. Toxin Reviews, 33:1-2, 37-41, DOI: 10.3109/15569543.2013.844712.*

Daniël Verhoef and Joen Luirink, *The 'Fts-Q-L-B' cell division protein complex; a three-piece puzzle of structure and function. 2011. MSc literature survey (intellectual property).*